

1997

ENHANCED SEDIMENT TRANSPORT NEAR SEAWALLS AND REFLECTIVE BEACHES

MILES, JONATHON RUPERT

<http://hdl.handle.net/10026.1/1901>

<http://dx.doi.org/10.24382/3518>

University of Plymouth

All content in PEARL is protected by copyright law. Author manuscripts are made available in accordance with publisher policies. Please cite only the published version using the details provided on the item record or document. In the absence of an open licence (e.g. Creative Commons), permissions for further reuse of content should be sought from the publisher or author.

**ENHANCED SEDIMENT TRANSPORT NEAR SEAWALLS AND
REFLECTIVE BEACHES**

by

JONATHON RUPERT MILES

**A thesis submitted to the University of Plymouth
in partial fulfilment for the degree of**

DOCTOR OF PHILOSOPHY

**Institute of Marine Studies
Faculty of Science**

October 1997

REFERENCE ONLY

UNIVERSITY OF PLYMOUTH	
Item No.	900 3419309
Date	- 6 NOV 1997 ^S
Class No.	T 551.36 MIL
Contl. No.	X 703-585761
LIBRARY SERVICES	

90 0341930 9



ABSTRACT

This thesis describes results of a field experiment to examine the effect of wave reflection on suspended sediment transport in front of a seawall. Two instrument rigs were set up on the beach at Teignmouth, South Devon, U.K., in June 1995. One rig (the seawall rig) was attached to a protruding section of seawall, positioning the instruments 1.2m seaward of the wall. The other rig (the beach rig) acted as a control and was positioned 135m downcoast where the seawall is set back so that conditions were those of a natural beach. At each rig high frequency measurements of wave elevation, current velocity and suspended sediment concentrations were made using pressure transducers (PTs), bi-axial electromagnetic current meters (EMCMs) and optical backscatter sensors (OBSs) respectively. Wave heights during the experiment were typically in the range $0.1 < H_0 < 0.3\text{m}$ in deep water outside the surf zone and incident wave periods were around 4 seconds. Measurements were made in a range of water depths from 0.5m to 2.5m.

At the natural beach, the reflection coefficient ($R = \text{reflected wave amplitude} / \text{incident wave amplitude}$) was found to be dependent on frequency, with low frequency waves ($f < 0.08\text{Hz}$) being preferentially reflected ($0.7 < R < 0.9$), while incident waves ($0.1 < f < 0.45\text{Hz}$) were dissipated ($0.1 < R < 0.2$). In front of the seawall the incident wave reflection coefficient was high ($0.75 < R < 0.9$), indicating only a small amount of dissipation and thus an effective doubling of energy over the sea bed. This was found to increase the suspended sediment concentrations in the water column. For similar water depths ($\sim 0.5\text{m}$), and instrument heights ($\sim 0.2\text{m}$) instantaneous maximum sediment concentrations in front of the wall reached 9kg/m^3 , compared with only 1.2kg/m^3 on the adjacent natural beach, despite similar incident wave conditions. Mean suspended sediment concentrations in front of the wall were also enhanced, ranging from 0.08kg/m^3 to 2.8kg/m^3 , while at the beach rig values were typically in the range 0.08kg/m^3 to 0.8kg/m^3 . At the seawall, mean and maximum suspended sediment concentrations were found to be dependent on water depth. Suspended sediment concentrations increased with decreasing depth.

Guza *et al.*'s (1984) time domain method for separating incoming and outgoing waves was adapted to allow the incoming and outgoing wave contributions to the cross-shore sediment transport to be analysed. Incoming waves transported sediment onshore in both beach and wall cases, with typical values of the oscillatory transport associated with the incoming waves being $0.0005 < u_{in}'c_s'_{beach} < 0.011\text{kg/m}^2/\text{s}$ and $0.0011 < u_{in}'c_s'_{wall} < 0.0187\text{kg/m}^2/\text{s}$. At the beach this resulted in a net onshore sediment transport by the waves, while in front of the wall offshore sediment transport associated with the reflected (outgoing) waves balanced the onshore sediment transport. Although the net cross-shore transport in front of the wall in this case was therefore reduced by wave reflection, the gross cross-shore transport was increased by a factor of two. Sediment accretion which was observed at the top of the natural beach was not observed in front of the wall, implying that the presence of the wall inhibited beach recovery in these accretionary conditions.

Mean cross-shore sediment transport rates were also larger at the wall than at the beach. Typical values were $\bar{u} \bar{c}_s'_{wall} = 0.05\text{kg/m}^2/\text{s}$ compared with $\bar{u} \bar{c}_s'_{beach} = 0.002\text{kg/m}^2/\text{s}$. This was attributed to the larger values of mean sediment concentration at the wall. Mean cross-shore sediment fluxes at the wall were directed onshore at the depth of the instruments, although this did not lead to accretion. It is suggested that sediment was prevented from settling by increased wave stirring, and was transported downcoast by enhanced longshore currents in front of the wall.

Both longshore currents and longshore sediment transport rates were found to be increased in front of the wall. Typical values of the mean longshore sediment flux were $0.0167 < \bar{v} \bar{c}_s'_{wall} < 0.320\text{kg/m}^2/\text{s}$, while at the beach typical values were $0.0001 < \bar{v} \bar{c}_s'_{beach} < 0.0142\text{kg/m}^2/\text{s}$ in 1m water depth. The enhanced longshore transport in front of the wall resulted in a bar forming downcoast from the end of the wall.

The seawall reflects incident waves back over the beach and this results in an increase in sediment suspension. The following were all found to be enhanced by the presence of the seawall: wave reflection, mean and instantaneous maximum suspended sediment concentrations, onshore transport by the incident waves, offshore transport by reflected waves, gross oscillatory cross-shore sediment transport, mean cross-shore sediment transport and mean longshore sediment transport rates.

CONTENTS

	page number
Copyright statement	i
Title page	ii
Abstract	iii
Contents	iv
List of figures	vii
List of tables	viii
List of plates	viii
List of symbols	ix
Acknowledgements	x
Author's declaration	xi
Relevant publications	xii
<u>Chapter 1. Introduction</u>	1
1.1 Introduction	1
1.2 Coastal defence engineering	2
1.3 Toe scour in front of the wall	2
1.4 The effect of the wall on the beach profile	3
1.5 Longshore transport	5
1.6 Beach process measurements approach	5
1.7 The present approach	6
<u>Chapter 2. Literature review</u>	7
2.1 Introduction to the review	7
2.2 Field investigations of sediment transport using high frequency measurements	9
2.3 Techniques to measure frequency dependent reflection	15
2.4 Laboratory tests of wave reflection, parameterisation of wave reflection	19
2.5 Field studies of wave reflection	23
2.6 Analytical models of wave reflection	27
2.7 Sediment dynamics associated with reflective structures. Physical and numerical models	31
2.8 Field investigations: low frequency measurements	38
2.9 Field investigations: high frequency measurements	43
2.10 Summary	46

<u>Chapter 3. Data collection</u>	48
3.1 Introduction	48
3.2 Instrumentation	49
3.2.1 Pressure transducers	49
3.2.2 Electromagnetic current meters	51
3.2.3 Optical backscatter sensors	53
3.3 Field experiment	57
3.3.1 Field site	57
3.3.2 Instrument layout	62
3.3.3 Wall rig	62
3.3.4 Beach rig	65
3.3.5 Data collection	66
3.3.6 Environmental information	74
3.3.7 Data processing	76
3.4 Summary	78
<u>Chapter 4. Data analysis techniques</u>	79
4.1 Introduction	79
4.2 Spectral analysis	80
4.3 Wave reflection analysis	88
4.3.1 Introduction	88
4.3.2 Time domain analysis	88
4.3.3 Frequency domain analysis	91
4.3.4 Principal component analysis	94
4.4 Wave reflection and sediment transport analysis	96
4.4.1 Time domain method	96
4.4.2 Frequency domain method	98
4.5 Data simulation	101
4.6 Summary	107
<u>Chapter 5. Results</u>	109
5.1 Introduction	109
5.2 Wave reflection analysis at the beach and wall	111
5.3 The nature of sediment suspension	115

5.4 The relationship between reflection and cross-shore sediment transport	120
5.5 Sediment transport by mean currents	125
5.6 Sediment transport: results from other days	128
5.6.1 Introduction	128
5.6.2 June 12th, PM tide analysis	129
5.6.3 June 13th, AM tide analysis	136
5.6.4 June 14th, AM tide analysis	141
5.7 Summary	146
<u>Chapter 6. Discussion</u>	148
6.1 Introduction	148
6.2 Wave reflection dynamics	149
6.2.1 Reflection coefficient calculation	149
6.2.2 Reflection estimates	151
6.3 Sediment dynamics	153
6.3.1 Sediment suspension	153
6.3.2 Cross-shore sediment transport	159
6.3.3 Longshore sediment transport	163
6.4 Morphology changes at Teignmouth	166
6.5 Further work	170
6.6 Summary	172
<u>Chapter 7. Conclusions</u>	174
Appendix: Instrument calibration graphs	177
References	182
Published conference papers	193

LIST OF FIGURES

	page number
1.4.1: Potential impacts of a seawall	4
2.1.1: Study areas contributing to present work	7
2.2.1: Co-spectrum obtained by Huntley and Hanes (1987)	12
2.5.1: Frequency dependent reflection coefficients (Tatavarti <i>et al.</i> , 1988)	24
2.6.1: Mass transport within standing waves	29
2.7.1.1: Scour patterns at vertical walls (Xie, 1981)	33
3.2.3.1: OBS beam pattern	55
3.3.1.1: Field site layout	57
3.3.1.2: Field site location	58
3.3.1.3: Beach profiles	59
3.3.1.4: Instrument positions in nodal structure	61
3.3.5.1: Cable layout	67
3.3.5.2: Filter characteristics	70
3.3.6.1: Weather chart	75
3.3.7.1: Data processing	76
4.2.1: Confidence intervals	84
4.5.1: Data simulation	101
4.5.2: Data simulation results	104
5.2.1: Beach FDRF, $h=1.28\text{m}$	111
5.2.2: Wall FDRF, $h=1.3\text{m}$	113
5.2.3: Wall FDRF, $h=2.27\text{m}$	114
5.3.1: Wall time series, $h=1.1\text{m}$	115
5.3.2: Beach time series, $h=1.0\text{m}$	115
5.3.3: Beach time series, $h=0.48\text{m}$	116
5.3.4: Wall time series, $h=0.6\text{m}$	117
5.3.5: Mean sediment concentrations, T136PM	118
5.3.6: Wall time series, $h=0.9\text{m}$	119
5.4.1: Wave reflection and co-spectra, $h=1.4\text{m}$	120
5.4.2: Wave reflection and co-spectra, $h=1.6\text{m}$	122
5.4.3: Wave reflection and co-spectra, $h=1.9\text{m}$	123
5.4.4: Wave reflection and co-spectra, $h=0.9\text{m}$	123
5.5.1: Mean velocities	126
5.5.2: Mean sediment fluxes	126
5.6.1.1: Wave elevation spectra	128
5.6.2.1: Mean sediment concentrations, T126PM	129
5.6.2.2: Vertical length scales and reference concentrations, T126PM	131
5.6.2.3: Wave reflection and co-spectra, $h=1.135\text{m}$, T126PM	132
5.6.2.4: Wave reflection and co-spectra, $h=1.55\text{m}$, T126PM	133
5.6.2.5: Wave reflection and co-spectra, $h=0.98\text{m}$, T126PM	134
5.6.2.6: Mean sediment fluxes, T126PM	134
5.6.3.1: Mean sediment concentrations, T136AM	136
5.6.3.2: Vertical length scales and reference concentrations, T136AM	137
5.6.3.3: Wave reflection and co-spectra, $h=1.5\text{m}$, T136AM	138
5.6.3.4: Wave reflection and co-spectra, $h=1.2\text{m}$, T136AM	138
5.6.3.5: Wave reflection and co-spectra, $h=0.9\text{m}$, T136AM	139

5.6.3.6: Mean sediment fluxes, T136AM	140
5.6.4.1: Mean sediment concentrations, T146AM	141
5.6.4.2: Vertical length scales and reference concentrations, T146AM	142
5.6.4.3: Wave reflection and co-spectra, h=0.6m, T146AM	143
5.6.4.4: Wave reflection and co-spectra, h=1m, T146AM	144
5.6.4.5: Wave reflection and co-spectra, h=1.5m, T146AM	144
6.3.1.1: Simulation of solitary wave reflection	157
6.3.1.2: Wall time series, run 5, T136PM	158
6.3.2.1: Three increased longshore current hypotheses	165
6.4.1: Beach morphology, June 13th	166
6.4.2: Beach morphology, June 16th	167
Appendix	
Spherical EMCM (9170) channel X calibration	177
Spherical EMCM (9170) channel Y calibration	177
Spherical EMCM (9171) channel X calibration	178
Spherical EMCM (9171) channel Y calibration	178
Annular EMCM channel X calibration	179
Annular EMCM channel Y calibration	179
Pressure transducer calibrations	180
OBS (1400) calibration	180
OBS (1401) calibration	181
OBS (1402) calibration	181

LIST OF TABLES

3.3.5.1: Instrument heights	71
3.3.5.2: Instrument channels	72
3.3.5.3: Mean water depths	73
3.3.6.1: Environmental information	74
4.2.1: Units of spectra	86
4.5.1: Data simulation inputs and outputs	103
5.5.1: Sediment fluxes, T136PM	127
5.6.2.1: Sediment fluxes, T126PM	135
5.6.3.1: Sediment fluxes, T136AM	140
5.6.4.1: Sediment fluxes, T146AM	145
6.3.2.1: Sediment fluxes, T126PM	160

LIST OF PLATES

3.1: Instruments on beach and wall rigs	63
3.2: Wall rig in action	64
6.3.1.1: Suspension by outgoing waves	155
6.4.1: The bar south of Sprey Point	168

LIST OF SYMBOLS

a	wave amplitude, or where specified: fourier constituent or reflection coefficient constant
b	fourier constituent, or where specified: reflection coefficient constant
c	wave celerity, or where specified: fourier constituent
c_s	sediment concentration
d	fourier constituent
e	fourier constituent
f	frequency
g	gravitational acceleration
h	water depth
i	$i = \sqrt{-1}$
k	wave number ($2\pi/\lambda$)
n	n th frequency
p	pressure
p_o	atmospheric pressure
t	time
u	horizontal cross-shore velocity
v	longshore velocity
w	vertical velocity
w_s	settling velocity
x	horizontal (cross-shore) co-ordinate
y	horizontal (longshore) co-ordinate (3D), vertical axis (2D).
z	vertical position. $z = 0$ at the surface, $z = -h$ at the bed
C_o	reference concentration
C_{xy}	coherence between x and y
E	energy
G	gain function
H	wave height
H_o	deep water wave height
H_b	wave height at break point
$H_{1/3}$	height of the highest third of waves
K_r	bulk reflection coefficient
L_s	vertical length scale
N_y	nyquist frequency
Q	attenuation
$R(f)$	frequency dependent reflection coefficient
S_{xx}	power spectrum of the time series of x
S_{xy}	cross spectrum of the time series of x and y
S_{ii}	power spectrum of incoming wave time series
S_{oo}	power spectrum of outgoing wave time series
SSP	surf similarity parameter
T	wave period
V	voltage
β	beach / structure slope
η	water surface elevation
θ	phase angle
λ	wavelength
λ_o	deep water wavelength
ξ	Iribarren number
π	pi
ρ	water density
σ	angular frequency ($2\pi/T$)
ϕ	velocity potential, or where specified: phase
ω	angular wave frequency
Ω	beach classification parameter
Δt	time step
in	denotes incoming wave
out	denotes outgoing wave
$\langle \rangle$	denotes time averaging

ACKNOWLEDGEMENTS

I would like to thank my supervisors, Dr Paul Russell and Professor David Huntley for their encouragement and support. I would also like to thank Dr Mark Davidson for his ideas and discussions which have assisted greatly in giving direction to the research. The academic interest of Dr Tim O'Hare is also gratefully acknowledged. I am also very grateful to Miss Rebecca King for her support and for proof reading the many versions of each chapter.

The technical support from the staff at the University of Plymouth was gratefully received. In particular, I would like to thank Mr Peter Ganderton for his diligent efforts to ensure that any instrumentation problems were smoothly sorted out during calibration and fieldwork phases of the project, and I would like to thank Mr Andy Prideaux for assistance in building the rig.

I would like to thank the many people who assisted with the field deployment, in particular: Mr Paul Fisher, Dr Karen Stapleton, Dr Lisa Redbourn, Dr David Simmonds, Mr Lee Copson and Mr Tony Davies. I am also very grateful to the Teignbridge District Council, in particular their Chief Engineer, Mr Tony Machin, for allowing us to use the site.

Finally I would like to thank my family and friends who made all this possible.

AUTHOR'S DECLARATION

At no time during the registration for the degree of Doctor of Philosophy has the author been registered for any other University award.

The project was funded by the Higher Education Funding Council through the University of Plymouth.

A variety of internal seminars were attended. Seminars were given by researchers from within the Institute of Marine Studies and from the Coastal Group of the Department of Civil and Structural Engineering in the University. The seminars covered a wide variety of oceanographic and coastal engineering issues. The author presented work at two internal seminars while at Plymouth and won the Institute of Marine Studies poster competition with a poster titled 'Sediment transport near seawalls' in 1995.

A short course in Coastal Engineering and Shoreline Management organised by the Civil Engineering Department of the University was attended in September 1995.

The material in this thesis has been presented by the author at several external conferences. These were: UK Oceanography, 1994 (Stirling); Royal Geographical Society meeting, 1995 (Teignmouth); Geological Society Marine Studies Group Meeting, 1996 (Southampton); 25th International Conference on Coastal Engineering, 1996 (Orlando, Florida), and the International Conference on Coastal Dynamics, 1997 (Plymouth).

Signed Jonathan R. Miles

Date 30/10/97

RELEVANT PUBLICATIONS

Miles, J.R., Russell, P.E. and Huntley, D.A., 1997. Suspended sediment response to wave reflection. *Proceedings of Coastal Dynamics '97*, (Plymouth), ASCE.

Miles, J.R., Russell, P.E. and Huntley, D.A., 1996. Sediment transport and wave reflection near a seawall. *Proceedings of the 25th International Conference on Coastal Engineering*, (Orlando, Florida), ASCE.

Miles, J.R., 1996. Field investigation of sediment suspension and transport in front of a seawall. *Abstract of Geological Society Marine Studies Group meeting*, (Southampton). Awarded prize for 'Best Oral Presentation'.

Miles, J.R., Russell, P.E. and Huntley, D.A., 1994. Enhanced sediment transport near seawalls and reflective beaches. *Abstract of UK Oceanography 94*, (Stirling).

CHAPTER 1: Introduction

1.1 Introduction

Recent estimates of sea level rise predict an increase in mean sea level of approximately 100mm over the next 20 years (Bray *et al.*, 1992). The Ministry of Agriculture, Fisheries and Food (MAFF) recommend an allowance of between 4mm per year to 6mm per year for the design or adaptation of coastal defences expected to last beyond the year 2030 (MAFF, 1991). Large areas of the coast of the United Kingdom are low lying, and it is estimated that that over 5% of the population of 60 million live below the 5m contour, land covering an area of 8000 km² (Palmer, 1996). Large areas of this land are in danger of flooding and inundation by the sea which would result from an increase in sea level. Many others live on or close to eroding cliffs and are therefore directly at risk from coastal erosion. With approximately 1486km of sea defences stretched along the coast of England and Wales¹ alone, it is vital that there is a good understanding of the effects of coastal defences on local coastal processes.

Seawalls are used as a method of coastal protection on many shorelines throughout the world, yet their effects on nearshore hydrodynamics and sedimentary processes remain surprisingly poorly understood (Kraus, 1988; Kraus and McDougal, 1996). Indeed, wave reflection from a seawall may even increase sediment transport in front of the wall and exacerbate the erosion problems (Silvester, 1977). This thesis presents the first field measurements of sediment transport processes in front of a seawall, with a view to gaining a better understanding of the complex relationship between wave reflection and sediment transport.

In this chapter the main issues of coastal engineering and coastal process research which have led to the present study are introduced. A more complete review of the literature is presented in chapter 2. There are a variety of coastal engineering solutions to erosion problems (1.2), although there have been specific problems associated with vertical walls. Examples of these problems are that: toe scour can develop at the bottom of the wall (1.3), the beach profile may be altered as a result of the wall (1.4) and the longshore transport regime may also be affected (1.5). In order to gain insight into the nature of sediment transport on natural beaches, various researchers have used high frequency measurements

¹ Source: Environment Agency, Kingfisher House, Goldhay Way, Orton Goldhay, Peterborough, PE2 5ZR.

of hydro- and sediment dynamic processes (1.6). This process orientated exploratory approach is adopted in the present study (1.7).

1.2 Coastal defence engineering

Many of the seawalls around the U.K. coastline were built by local authorities at the turn of the 19th century, often combining coastal defences with promenades for the expanding tourist industry. Seawalls are a 'hard engineering' solution to the problem of wave attack of the coast, and engineers have recognised for some years the benefit of a 'softer' approach to coastal defence. Modern coast protection schemes often use designs such as rubble mound breakwaters to protect the backshore. These are porous structures which dissipate the wave energy more effectively than a vertical wall. The waves are then not reflected seawards and so have less effect on the beach. The problems created by waves impacting directly on the structure are also reduced by this approach.

An alternative method of defending the coast is the use of beach nourishment schemes. The shallow slope of a man made beach dissipates wave energy effectively before it reaches the shore. This engineering solution is often preferred by coastal planners as it can be less costly than large structures, and the results appear more 'natural' (Carter, 1988). These solutions are not always possible however, and seawalls are still being built as a last line of defence against the sea, particularly in areas where the land behind is valuable. Coastal defence strategies around the world rely heavily on seawalls, and the processes driving the sediment transport in front of these structures are not well understood.

1.3 Toe scour in front of the wall

One of the reasons seawalls fail is that scour troughs develop in the sediment at the toe of the wall, and the foundations of the structure are undermined. Whilst toe protection has gone some way to dealing with this problem, the problem of scour remains as toe protection is often damaged during large storms. This scour may lead to failure of the wall (Oumeraci, 1994), and the results can be catastrophic in terms of land lost from behind the wall. Consequently, physical models have been aimed at understanding the development of scour troughs directly in front of vertical walls.

An early pioneering laboratory experiment into wave reflection driven scour was carried out by Dorland (1940). He concluded that:

'...the primary force of wave action alone does not cause scour in front of vertical walls. However, this force may place the material in suspension where it may easily be transported by currents which otherwise cause no damage...'

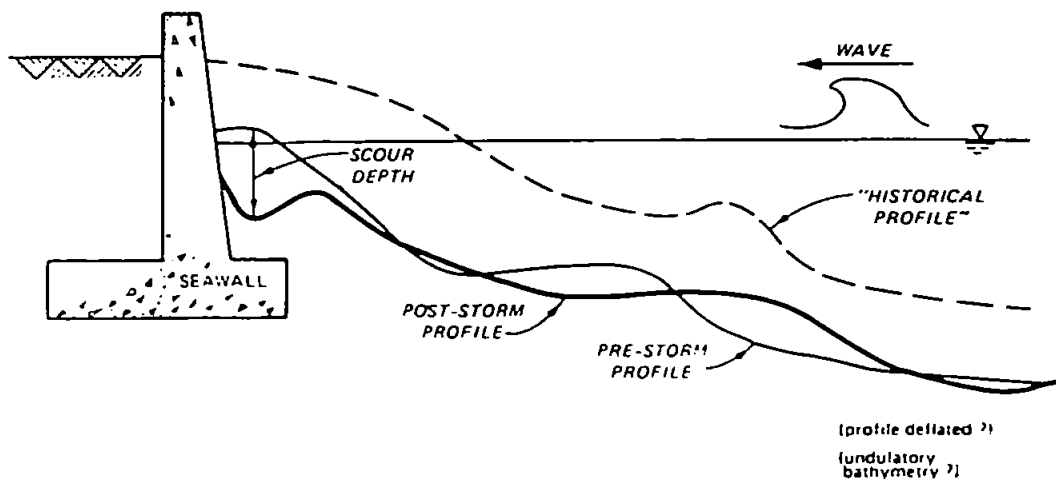
Numerous other researchers have carried out laboratory experiments investigating the relationship between wave reflection at a structure and the sediment response in order to determine the type and depth of scour which may occur (e.g. Chestnutt and Schiller, 1971; De Best and Bijker, 1971; Irie and Nadaoka, 1985; Xie, 1985; Hsu and Silvester, 1989; Hughes and Fowler, 1991). The observations suggest that an increase in reflection coefficient² of the armouring will lead to more scour at the toe of the structure (Sato *et al.*, 1969; Hayashi, 1987; Griggs and Tait, 1988).

1.4 The effect of the wall on the beach profile

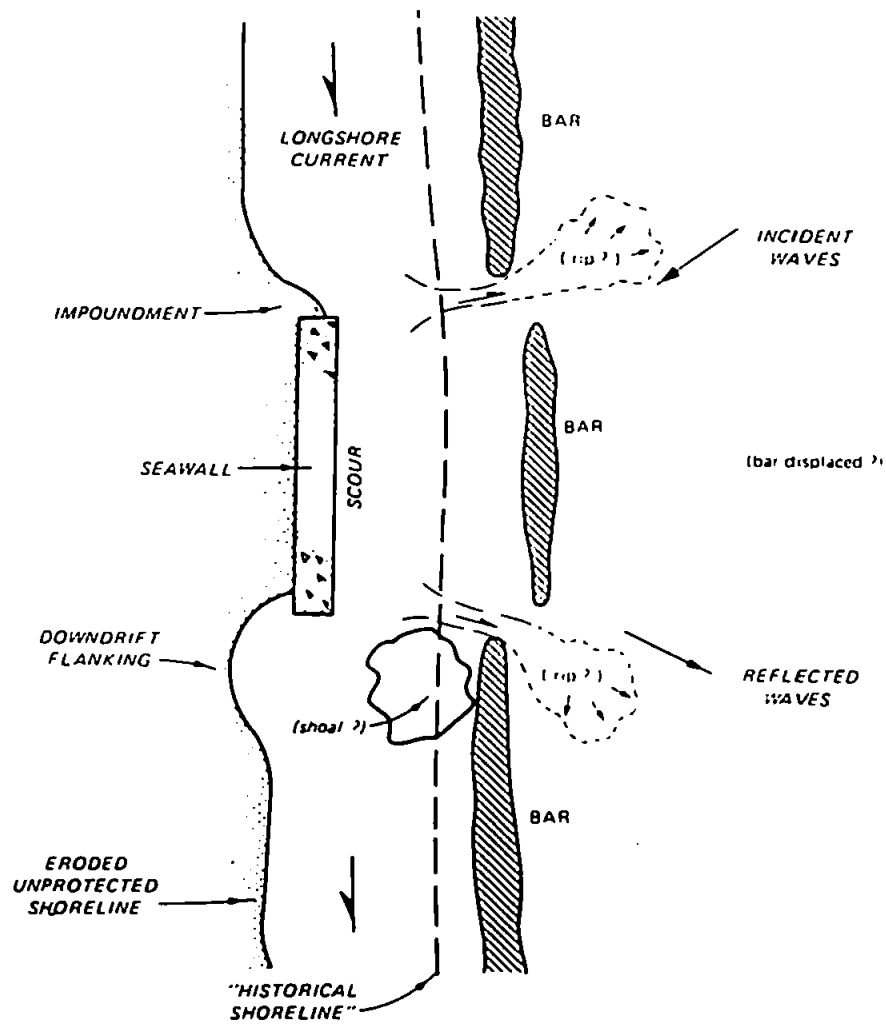
There is considerable debate over the detrimental effect of a wall on the beach profile (Baba and Thomas, 1987; McDougal *et al.*, 1987; Komar and McDougal, 1988; Terchunian, 1988; Tait and Griggs, 1990; Nakashima and Mossa, 1991; Kraus and McDougal, 1996; McDougal *et al.*, 1996). Field measurements using beach profile surveying techniques have been presented from a variety of cases: where the wall has apparently given rise to enhanced erosion of the beach (Pilkey and Wright, 1988; Fitzgerald *et al.*, 1994); where no difference has been found between protected and unprotected sections of coast during the passing of a storm (Nelson, 1991); and where the wall was completely destroyed in storms (Morton, 1988).

Kraus (1988) summarised the beach processes associated with seawalls and presented the potential impacts of a seawall on the beach profile and planform in two figures, based on a review of literature available up to 1988 (figure 1.4.1). On an eroding coastline where a wall is built, the profile schematic shows the effects of a storm on the beach in front of the wall. The bar may be displaced offshore, and toe scour may develop at the wall. The presence of a seawall has also been suggested to be responsible for a deflated profile (Dean and Mauermeyer, 1983; Dean, 1987a,b). A deflated profile results in a narrowing of the dry beach width, a feature which has been observed by Pilkey and Wright (1988). In plan view, Kraus suggests that the wall may give rise to upcoast sediment impoundment, leading to downdrift flanking and downcoast erosion of unprotected shorelines. The wall may also give rise to downdrift erosion through inhibited sediment supply or upcoast

² The reflection coefficient is the ratio of the incoming wave amplitude to the outgoing wave amplitude.



Profile view of potential impacts of seawalls.



Plan view of potential impacts of seawalls

figure 1.4.1: Potential impacts of a seawall as identified by Kraus (1988).

flanking from end reflections. These erosion features have been found by Walton and Sensabaugh (1979), McDougal *et al.* (1987) and Toue and Wang (1990).

The impacts of a seawall on the beach described above have all been observed using either laboratory models or surveying techniques. Surveying methods are useful as they provide a view of the overall effect of an event such as a tide or a storm. However, they are at best a tidal average and do not provide information on the processes driving the observed changes in beach profile. This information is vital if there is to be a better understanding of the mechanisms responsible for coastal morphology changes near seawalls.

1.5 Longshore transport

Silvester (1975, 1977) observed that the oblique reflection of wave energy at a wall leads to the re-application of energy over the bed and this in turn leads to extra suspension of sediment. The oblique wave attack drives a longshore current, and combined with an increase in sediment suspension this leads to an enhanced longshore sediment transport in front of the wall. Silvester's view is not universally accepted however, for example Ozasa and Brampton (1979) treat a wall which extends seaward of the surf zone as a groyne which inhibits the longshore transport of sediment.

The position of the wall relative to the surf zone and the nature of the incident waves will undoubtedly affect the longshore sediment transport regime in front of the wall, and not surprisingly, arguments have been given for both increased and decreased longshore transport rates in front of seawalls (Birkemeier, 1980; MacDonald and Patterson, 1985; Kraus, 1988; Uda, 1989; Johnson, 1992; Kamphius *et al.*, 1992).

1.6 Beach measurements approach

The most prominent feature of the investigations looking at the effects of the seawall on beach processes to date is the lack of process based field studies. There have been no attempts to investigate the sediment suspension and transport processes *in situ* (Kraus and McDougal, 1996). Therefore, this thesis presents the first results of this kind.

This approach to understanding the sediment transport processes has been used extensively on natural, undefended beaches. One of the more frequently used methods is to deploy pressure transducers (PTs), electromagnetic current meters (EMCMs) and optical backscatter sensors (OBSs) on the beach at low tide (Downing *et al.*, 1983). As the tide

covers the instruments, high frequency measurements of the waves and the associated water velocities can be made. Elevation and velocity values can be compared with measurements of suspended sediment concentrations also made at high frequency. In this way an understanding of the processes driving any change in beach profile can be measured and understood.

The British Beach and Nearshore Dynamics (B-BAND) programme (Russell *et al.*, 1991) was one such experiment. During the B-BAND programme a series of beach deployments of PTs, EMCs and OBSs were carried out on a range of macrotidal beaches from a morphodynamically dissipative site to a steeper reflective beach. The results show that variation in the steepness of the beach leads to different hydrodynamic and sediment dynamic processes.

The idea that a change in shoreline steepness will lead to a change in beach sediment transport dynamics is well documented. Sand transport processes have been examined on undefended dissipative, flat beaches (e.g. Jaffe *et al.*, 1984; Beach and Sternberg, 1988, 1992; Russell, 1993). Other workers have examined processes on steeper beaches (e.g. Huntley, 1975; Davidson *et al.*, 1993a,b; Osborne and Greenwood, 1992). In terms of the hydrodynamics, the increase in steepness of the shoreline is recognised to give an increase in wave reflection at the shoreline (Guza and Bowen, 1975; Guza and Inman, 1975; Wright *et al.*, 1988), and the existence of a seawall at the head of the beach represents the ultimate condition of complete wave reflection. The presence of the seawall is therefore expected to have considerable effects on the sediment dynamics directly in front of it.

1.7 The present approach

The present project focuses on the existence of the wall at the back of the beach. The central theme for the thesis is therefore the sediment response to the presence of wave reflection. To this end, PTs, EMCs and OBSs were deployed directly in front of the near-vertical Brunel seawall at Teignmouth in South Devon. Simultaneous measurements were made using identical instruments positioned on an adjacent natural beach 135m downcoast of the seawall, enabling a comparison of sediment suspension and transport processes at work in these two different environments. The method of deploying the instruments and gathering the data is discussed in depth in chapter 3. This is followed by a detailed description of analysis procedures in chapter 4. Results are presented in chapter 5 and discussed in chapter 6.

CHAPTER 2: Literature review

2.1 Introduction to the review

In this chapter, different aspects of research which are relevant to sediment transport near seawalls are reviewed. There have been a number of different approaches to understanding the nature of nearshore dynamics. Research areas relevant to the present study which are included in this review are summarised by figure 2.1.1.

Study areas contributing to the present investigation.

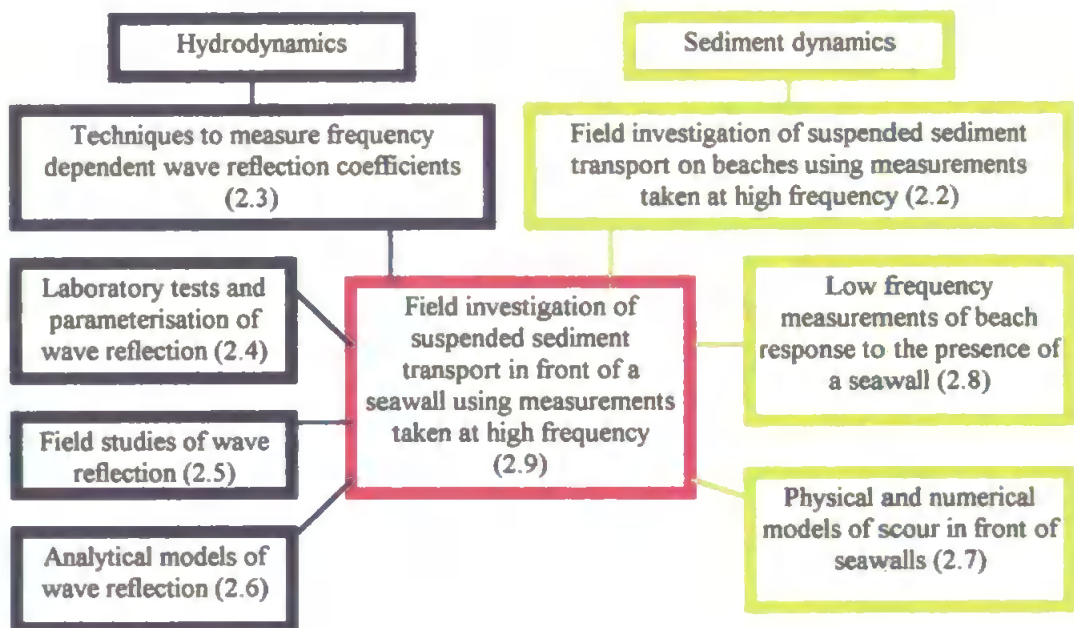


figure 2.1.1: Various study areas contribute to the present work. Research which has been carried out on the individual topics shown above is discussed in the literature review. Section numbers are shown in brackets.

Field observations of beach sediment dynamics on natural beaches are reviewed first (section 2.2). The researchers engaged in such observations have identified useful observation and analysis techniques, which can be extended to the case of a seawall at the head of the beach.

One of the most obvious effects on the hydrodynamics in front of the wall is the increase in wave reflection. It is essential that the frequency dependent reflection coefficient can be obtained if the effect of wave reflection on sediment transport is to be understood.

The next section (2.3) therefore looks at techniques which have been used to measure this wave reflection. The logical extension of this is to examine cases where such analyses have been used in the field, and examples in section 2.4 come from field experiments to measure wave reflection from both man made structures and natural beaches. Coastal engineers have employed slightly different techniques than the scientists to solve this problem, choosing wave tanks in the laboratory over field investigation. This usually results in some sort of parameterisation for a bulk reflection coefficient which can then be applied to other similar situations. Examples of such experiments are given in section 2.5. Of course the ultimate test of whether the physics are correctly understood is whether or not an accurate model can be made, and there have been attempts at this for the case of wave reflection. These are given in section 2.6.

To examine the effect of the hydrodynamics on the sediment there has been a similar three pronged approach. Physical and analytical/numerical models of the effects of seawalls on a fronting beach are covered next, (section 2.7). Whilst these observations provide useful insight into the processes at work, they are not backed up by field observations. Field investigations have almost exclusively used profiling and surveying techniques to investigate the effects of the seawall on the beach and the response of the beach to storms (section 2.8). There have been few attempts to document the effects of seawalls on sediment dynamics based on process measurements (section 2.9). There is a clear niche for the present study in that there have been no documented studies of sediment transport processes in front of seawalls utilising high frequency measurements of hydrodynamic and sediment dynamic processes. These measurements will help to clarify the relationship between wave reflection and sediment transport in front of coastal defence structures.

2.2 Field investigations of sediment transport using high frequency measurements

The investigation of sediment suspension and transport in front of a seawall is a natural extension to the research which has already taken place on natural beaches. Researchers have compared the dynamics of shallow sloping beaches to those of steeper beaches, comparing their reflectivity and the dominant modes of sediment transport on them according to wave frequency. The beach headed by a seawall represents a natural extension of this as the reflectivity at all frequencies is increased toward unity by the seawall, and thus the form of sediment suspension and transport in front of the wall will change. It is therefore important to examine the processes of sediment suspension and transport on natural beaches so that the effect of the presence of a seawall at the head of the beach can be considered in relation to these processes.

Fast response sediment sensors

To observe the process of sediment suspension it is necessary to make measurements of suspension at high frequency, otherwise the effects of individual waves and wave groups will be missed. There are currently two instruments capable of making such measurements which are suitable for the nearshore zone. The optical backscatter sensor (OBS) (Downing *et al.*, 1981; Downing, 1983) does so by sending out a pulse of infrared light and detecting the backscatter of this light from the water column. The output voltage is linearly related to the concentration of sediment in suspension, and the instrument can thus be calibrated using a sample of the beach sediment. The result is a time series of sediment concentration at the point where the OBS is deployed. The OBS is designed to be most sensitive to a certain particle size banding (see OBS manual), and the result of this is that while the OBS responds well to sediment, it does not respond to bubbles in the water column (these forward scatter light). Thus the OBS is well suited to the surf zone. Further discussion of the lack of response of the OBS to aeration in the water column is given in chapter 3.

The Acoustic Backscatter Sensor (ABS) (Vincent *et al.*, 1986) performs in a similar manner to the OBS, using much lower frequency energy. It is also calibrated for the sediment in suspension but can give information on the variation in concentration with depth. A problem arises in the surf zone with bubbles however, the ABS being sensitive to these. The ABS is thus suitable for work outside the surf zone.

Large scale experiments

Both sorts of instrument mentioned above provide the user with a large data set of sediment response to wave action, when used in conjunction with fast response current meters (e.g. electromagnetic current meters) and pressure transducers to measure surface elevation. The high initial costs of buying the instruments, together with the large effort required for a successful investigation means that fast response sensor deployment is often suited best to large scale multi institutional experiments. Such deployments may take place over a period of several days to several weeks, and analysis tasks are often spread between groups.

There have been several of these large scale investigations, and experimenters have deployed rigs in different conditions to obtain new results. Such experiments include the Nearshore Sediment Transport Study (NSTS) on the west coast of the USA (Seymour, 1989), the Natural Environment Research Council (NERC) project in Japan (Horikawa, 1987), the Canadian Coastal Sediment Transport Study (C²S²: Willis, 1987) and the British Beach and Nearshore Dynamics project (B-BAND: Russell *et al.*, 1991) examining the sediment transport processes on three macrotidal beaches of different steepness in the U.K.

There have also been a series of experiments at Duck in North Carolina on the east coast of the USA. These include DUCK82 (Mason *et al.*, 1984), SUPERDUCK86 (Martens and Thornton, 1987), DELILAH (Surf zone hydrodynamics based), DUCK94 and SANDYDUCK in 1997 (Birkemeier and Thornton, 1994). The CSTAB project (Coastal Sediment Transport Around Banks) is a more recent example from the U.K which involved funding from Europe, a field site in Belgium and collaboration between institutions in Liverpool, Plymouth, Southampton, and Spain (Simmonds *et al.*, 1995).

Frequency dependent sediment transport

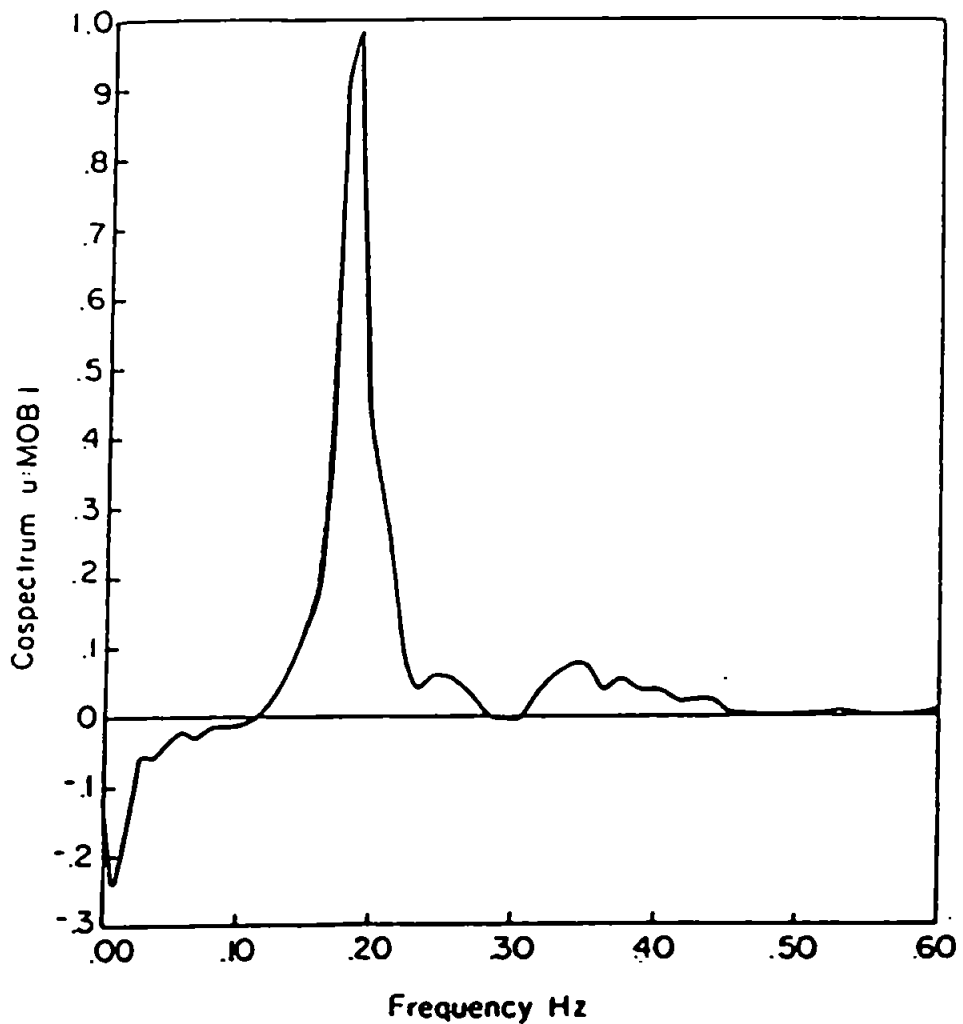
It is evident from the variety of wave frequencies incident on the shoreline, from tides through infragravity and gravity band energy to higher frequency turbulence, that sediment suspension and transport will take place at a variety of timescales. The particular timescale indicates the process which is most important in that region at that time or in those specific conditions. It is this approach of determining magnitude of sediment transport at a particular frequency which most experimenters use to tackle the problems of nearshore sediment dynamics.

Jaffe *et al.* (1984) documents field measurements of suspended sediment transport during a storm from the DUCK82 experiment. In an attempt to relate measured nearshore sediment transport rates to the change in beach morphology, Jaffe split the time series into mean and time varying components through the surf zone, and found that even though mean currents were directed offshore, the waves were able to bring sufficient sediment ashore to move the bar shorewards. This indicates the importance of separating the time series into its constituent frequencies.

In a similar way to the fourier separation of wave components from an elevation sensor record or current meter record, a fourier transform from the time domain to the frequency domain can be made of the suspended sediment time series. Cross spectral analysis of the sediment time series with the current meter data gives information on the direction and quantity of sediment flux. This is in fact given by the co-spectrum, the real part of the cross spectrum (Huntley and Hanes, 1987). By taking such a co-spectrum between sediment and cross-shore current data gathered from co-located gauges just outside the surf zone on a natural beach, Huntley and Hanes found onshore sediment transport at the frequency of the incident waves, and an offshore transport of sediment at a lower, infragravity frequency¹ - the frequency of surf beat (figure 2.2.1). Sediment is suspended by the larger waves in the groups. Long waves are in their offshore phase when incident waves are large, and transport sediment offshore, even though the incident waves move it onshore (Shi and Larsen, 1984). This offshore infragravity transport was relatively weak seaward of the surf zone in Huntley and Hanes's (1987) case.

Further inside the surf zone the lower frequency waves begin to dominate the spectrum, the level of infragravity energy grows towards the shoreline and is linearly related to the incident wave height (Holman, 1981). This trend is affected by beach slope, with the inner surf zones of dissipative beaches being dominated by infragravity oscillations while on more reflective beaches, incident wave energy contains a larger part of the energy (Davidson *et al.*, 1993a).

¹ Kinsman (1965) defined the infragravity frequency band as 0.0033-0.033 Hz and the incident (gravity) wave band as 0.033-1 Hz. In practice a trough in the spectrum between the two frequency bands can generally be observed.



Cospectrum of cross-shore velocity and suspended sediment concentration at MOB1. The units of the cospectral amplitude are $(g\ell^{-1})(ms^{-1})Hz^{-1}$.

figure 2.2.1: Huntley and Hanes (1987) produced a co-spectrum between the oscillatory velocity and the time series of sediment suspension. Suspension events which occur repeatedly in phase with the positive (onshore) velocity part of the waves give rise to a net shoreward sediment transport at the frequency of the incident waves. This is shown by the large positive peak in the co-spectrum. At a frequency lower than that of the incident waves there is a net offshore transport.

The dominance of the infragravity energy on dissipative beaches is known to increase during storms, and this has been observed to affect the sediment transport (Russell, 1993). In the inner surf zone during storms, levels of infragravity energy are particularly high, and this can give rise to a large amount of sediment suspension and transport at infragravity frequency (Beach and Sternberg, 1988). When combined with undertow this can result in a strong offshore sediment transport (Russell, 1993).

Greenwood *et al.* (1991) used the co-spectrum to examine data obtained from under both shoaling and breaking waves on barred and non barred shore faces (part of the Canadian Coastal Sediment Transport Programme: C-COAST). The net balance of sediment transport depended on the contributions of the individual components of the various components. Wind waves were found to transport sediment onshore (as Huntley and Hanes (1987) found), infragravity waves were found to give offshore transport at low frequencies over a barred shoreface, although the result was not as clear for the non-barred shoreface (see also Osborne and Greenwood, 1992a,b).

Huntley and Hanes's co-spectral result of onshore sediment transport at incident wave frequency and offshore sediment transport at infragravity frequency outside the surf zone may not apply well offshore of the surf zone, as indicated by Wright *et al.* (1991) who used OBSs deployed on a tripod in slightly deeper water (7-17m). They found incident waves to be the major source of shear stress on the bed, but found that they caused offshore transport as well as onshore. This reverse transport at incident wave frequency may be due to the presence of bedforms (c.f. Dingler and Inman, 1976). Low frequency sediment transport was also found to be shoreward as often as seaward. The effect of the tide, especially at macrotidal locations has also been found to alter this result. Davidson *et al.* (1993b) found a marked asymmetry in the sediment concentrations on either side of the tide, sediment concentrations being maximum on the ebb. Offshore sediment transport at incident wave (gravity band) frequency was found at high tide, and this was suggested to be due to the presence of bedforms (ripples). The destruction of the ripple field as the tide ebbs may result in the asymmetry observed.

Clearly, a large amount of effort has gone into examining the processes of sediment suspension and transport on natural beaches. The dominant modes of sediment transport are, in general, identifiable by frequency and they vary through the surf zone.

On shallow beaches with wide surf zones, the inner surf zone generally is where most of the sediment is suspended, and the dominance of infragravity energy in this region is evident. The sediment dynamics of steeper beaches with narrower shorefaces tends to be dominated by gravity band waves and their subharmonics. As reflectivity increases further with the presence of a seawall, it seems sensible that the dominant mode of transport will depend on the slope of beach fronting the wall, the incident wave characteristics and the nature of the wave reflection from the seawall. The observation of sediment dynamics in front of a seawall would thus be a very interesting next step for the science to take, not to mention the use of such observations that could be made by coastal engineers. The placing of OBSs in conjunction with current meters and pressure transducers in the immediate vicinity of a seawall remains undocumented to the authors knowledge.

2.3 Techniques to measure frequency dependent reflection

Coastal engineers now recognise the importance of wave reflection from coastal structures as an indicator of the level of energy not dissipated by or transmitted through the structure. The resulting hydrodynamics from the combination of reflected and incident waves has been thought to be responsible for scour in front of coastal defence structures, and investigations into the nature of the reflection coefficient have thus become important both for scientific interest and engineering applications. The aim of this section is to introduce the available techniques for measuring reflection coefficients.

There are a variety of techniques available for measuring the reflection coefficient of a structure or beach, and most are applicable both in laboratory wave tanks and in the field. Some use surface elevation records from a variety of points, and others use co-located current meters and surface elevation recorders combined. In fact what is required of the observations is a spectral estimation of the reflection coefficient, as the reflection coefficient is frequency dependent. The attempts to parameterise the reflection coefficient according to slope of reflector, frequency, wave height, water depth and other parameters are covered in a later section.

Kajima (1969) provided a method for decomposing incident and reflected wave spectra from surface elevation records taken at two points, although with only two spatial elevation measurements the technique suffers singularities where the sensors are an integer number of half wavelengths apart. Goda and Suzuki (1976) also presented a method where two elevation values give the reflection, and although this technique is commonly used it also suffers from singularities at critical frequencies and is sensitive to noise, non-linearities in the waves passing between the sensors and measurement errors. Gaillard *et al.* (1980) used three sensors to eliminate singularities, the autospectra from each sensor and the cross spectra between them determine the frequency dependent reflection coefficient. Mansard and Funke (1980) also used three elevation values to give the incident and reflected wave spectra and hence the reflection coefficient. In their case the wave spectra were calculated using a least squares method. Interestingly they noted that reliable results were only obtained if there was a high cross correlation between sensors, suggesting that coherence would be a good indicator of confidence in the estimates. Isobe and Kondo (1984) extended the three gauge method to estimate directional spectra in an incident and reflected wave field, although this requires additional sensors.

An important problem which applies to all these techniques, however, is that to use the method over locally varying topography, an assumption has to be made as to the wave response to depth variation, and this can result in inaccurate reflection estimates. Methods which use measurements from a single point avoid this problem. Such a method, involving the use of a current meter combined with a water elevation sensor (such as a pressure transducer) to separate the incident and reflected wave spectra was suggested by Guza *et al.* (1984). In this method the time series of the incoming and outgoing waves is obtained using shallow water wave theory and the spectra are taken from these time series. As it is only applicable in shallow water the technique lends itself to detecting infragravity wave reflection in the nearshore. It is also easy to programme and use, and hence lends itself to exploration of new ideas for data analysis (see chapter 4). Guza *et al.* (1984) stated that incoming and outgoing components of long waves could be decomposed using the following equations:

$$PC(t) = (\eta + (\frac{h}{g})^{1/2} u) / 2 \quad 2.3.1$$

$$MC(t) = (\eta - (\frac{h}{g})^{1/2} u) / 2 \quad 2.3.2$$

where PC(t) is the plus characteristic time series and MC(t) is the minus characteristic time series, u, η and h are velocity, elevation and water depth respectively. The origin of these equations is shown in chapter 4.

Noise in the data has the effect of making the reflection coefficient appear larger than it actually is (this is termed a 'bias' in the reflection coefficient estimate). The technique is thus suited only to data with good coherence.

To get around the noise problem two further techniques have been introduced (Tatavarti *et al.*, 1988). The first is a frequency domain method which uses the cross spectrum between the current meter and the elevation in the reflection estimate. This has the effect of extracting the coherent parts of the signal, and thus the effect of noise is minimised. Tatavarti *et al.* (1988) also introduces a further frequency domain method which uses principal component analysis (PCA) to extract the correlated parts of the signal thereby reducing the bias on the reflection coefficient which results from noise in the data. Huntley *et al.* (1995) used simulated data to test Guza *et al.*'s (1984) time domain method against two frequency domain methods and found that the time domain method over estimated the reflection coefficient while Tatavarti's frequency domain method under estimated it. The PCA method was found to be bias free except for very low coherence and reflection coefficients of close to one.

This last method (PCA) seems to be the most suitable for use with the present data as it: i) reduces the effect of noise in the data, ii) is least susceptible to low coherence between elevation and velocity, iii) can provide incoming and outgoing time series (theoretically). Both Tatavarti *et al.* (1988) and Huntley *et al.* (1995) have applied the frequency domain techniques to data from natural beaches, the results demonstrate the benefits of the PCA technique over the first frequency domain technique, which is shown to be less affected by noise than Guza *et al.*'s (1984) time domain method.

Various other interesting developments have taken place. Tatavarti (1987) presents a further method for decomposing the incident and reflected energy involving the use of the cepstrum, the spectrum of the log power spectrum. It requires special filters (filters applied in the frequency domain) however, and the technique has not been used on beaches as it requires definition of the point of reflection. Hughes (1993) also presents a method for estimating reflection using co-located gauges. The method is a frequency domain one and uses either elevation and cross-shore velocity measurements, or vertical and cross-shore velocity measurements. If proven in the field, this may allow a single bi-axial current meter to be used in the estimation of the frequency dependent reflection coefficient. The theory is tested in a tank for the case of complete reflection and is found to suffer the problem of reflection greater than unity when the coherence between signals drops. The technique is untested on field data. Frigaard and Borsen (1995) have shown how the incident and reflected wave trains can be separated in a time domain method using two elevation sensors. Previous methods (Goda and Suzuki, 1976; Mansard and Funke, 1980) used frequency domain calculations. The method splits the wave field in real time using digital features. This technique may be of great importance in determining wave impulses on walls and breakwaters. However, it is untested in the field.

The time domain technique of Guza *et al.* (1984) has advantages for ease of data analysis and has interesting possibilities for incorporating sediment \times velocity co-spectra. The frequency dependent analysis of Tatavarti *et al.* (1988) and the principle component analysis of Tatavarti *et al.* (1988) and Huntley *et al.* (1995) do provide less sensitivity to noise, however, and these are thus selected as the most suitable techniques to use and apply to the field data. It may be possible to inverse fast fourier transform the spectra resulting from the frequency domain method, providing phase information is kept from the initial fourier transform. This will allow a co-spectral analysis of incoming and outgoing time series with sediment, similar to a simpler method which can be carried out with the results of Guza *et al.* (1984).

The separation of incoming and outgoing waves using Guza *et al.*'s (1984) method has also been used to investigate the nature of the standing long wave pattern inside the surf zone (Masselink, 1995; Ruessink, 1995). Masselink (1995) gathered data from a macrotidal beach in Queensland, Northern Australia. Cross spectral and cross correlation analyses were applied to time series of incoming long waves, outgoing long waves and the wind-wave wave envelope. Masselink was able to determine that the incoming bound long wave was released at the break point, traverses the shoreline as a free wave and is reflected just seaward (5m) of the shoreline. This results in a standing wave pattern in the inner surf zone. Ruessink (1995) found similar results to these from data obtained on the Netherlands coast, where the beach was also dissipative, but in this case exhibited a multiple bar system.

2.4 Laboratory tests of wave reflection, parameterisation of wave reflection

Experimenters and engineers can use physical tests to determine the nature of wave response to coastal structures. The reflection coefficient is most often expressed as a function of structure slope, the wave steepness (the ratio of wave height to wavelength), wave period and the ratio of water depth to wavelength (Wiegel, 1964). One of the most important parameters which is universally used in predicting the nature of wave reflection at coastal structures is the Iribarren number (Iribarren and Nogales, 1949; Miche, 1951; Battjes, 1975; Shore Protection Manual, 1984). It is interesting to note that similar parameters have been used to describe the surf zone and its breaker characteristics (e.g. Galvin, 1968).

Iribarren and Nogales (1949) first combined the beach slope β and the deep water wave steepness (H/λ_0) to form a 'similarity parameter' of the form:

$$\xi = \frac{\tan \beta}{\sqrt{H / \lambda_0}} \quad 2.4.1$$

This was used to determine whether wave breaking would occur for waves approaching a plane sloping bed. By assuming that the wave would reach the limit of its stability when its amplitude equalled the water depth it was in, Iribarren predicted the value of ξ for which breaking would occur as $\xi=2.3$. This result was investigated using physical tests and it was suggested that such a value of ξ corresponded to a regime halfway between complete breaking and complete reflection.

To relate reflection to wave breaking Miche (1951) hypothesised that the reflected wave height was the maximum possible for a non breaking wave of a given period on a given slope. Thus the energy dissipated was assumed to be given by the proportion of wave height above the critical breaking height. In terms of wave steepness, this gives

$$K_r = \frac{(H_0 / \lambda_0)_c}{(H_0 / \lambda_0)} \quad \text{if } K_r < 1, \text{ else } K_r = 1 \quad 2.4.2$$

where $(H_0 / \lambda_0)_c$ is the critical steepness for the onset of breaking.

This can be expressed in terms of ξ (the Iribarren number) and ξ_c (the critical value of ξ for the onset of breaking) (Battjes, 1975):

$$K_r = \left(\frac{\xi}{\xi_c} \right)^2 \quad \text{if } K_r < 1, \text{ else } K_r = 1 \quad 2.4.3$$

This theoretical reflection coefficient based on Miche's hypothesis can be related to the real reflection coefficient using Iribarren and Nogales's breaking criteria. This results in an expression for the reflection coefficient in terms of ξ . At the onset of breaking, a typical value of the Iribarren number is $\xi_c=3$ (Battjes, 1975). Therefore

$$K_r \approx 0.1 \xi^2 \quad \text{if } K_r < 1, \text{ else } K_r = 1 \quad 2.4.4$$

The frequency dependent nature of wave reflection can therefore be determined as follows.

The Iribarren number can be expressed in terms of the wave period as:

$$\xi = \sqrt{\frac{gT^2}{2\pi H}} \tan\beta \quad 2.4.5$$

Equation 2.4.4 suggests that the reflection coefficient is proportional to ξ^2 , thereby implying a dependence on T^2 or f^{-2} .

The relationship between the reflection coefficient and wave period is regularly discussed in the literature by those who examine the frequency dependent reflection coefficients of structures and natural beaches. This is discussed further in section 2.5.

Galvin (1968) related a parameter similar to the Iribarren number to the way in which waves break. He identified an 'offshore parameter': (symbol G used here for clarity)

$$G = \frac{H_o}{\lambda_o} \tan^2 \beta \quad 2.4.6$$

where H_o is the offshore wave height and λ_o is the offshore wavelength, and β is the beach slope. He also defined an 'inshore parameter' :

$$G_b = \frac{H_b}{gT^2} \tan\beta \quad 2.4.7$$

where H_b is the wave height at breaking. It is possible to express the offshore parameter in terms of ξ , and this is in fact ξ_o^{-2} . The inshore parameter is not expressible in terms of ξ although Galvin's results could be reworked in terms of an inshore ξ (Battjes, 1975). Galvin's experiments show that for $G_b > 0.0688$ the waves were spilling, while for plunging and collapsing waves values were less than this ($G_b < 0.0688$).

The Iribarren number ξ is regularly used in the parameterisation of reflection coefficients obtained from laboratory experiments. By varying the parameters in the equation, empirical relationships can be found relating different shoreface slopes and incident wave

conditions. This method can also be extended for different types of reflective surfaces. For example, for a test on a rubble mound break water it has been found that:

$$K_r = a(1 - \exp(-b\xi)) \quad 2.4.8$$

where $a=0.503$ and $b=0.125$ (Giminez-Curto, 1979).

An alternative form was found by Seelig and Ahrens (1981) for a similar structure:

$$K_r = \frac{a\xi^2}{(b+\xi^2)} \quad 2.4.9$$

with $a=0.6$ and $b=6.6$. (Note: different values of a and b would apply to different structures).

Allsop (1990) gave a similar form of the equation to Seelig and Ahrens (1981) but found that for his case the coefficients were $a=0.64$ and $b=9.64$. A discussion of these is contained in Davidson *et al.* (1994), who also covers the estimates of Postma (1989).

Davidson *et al.* (1994) used field data to estimate the relationship between reflection coefficient and Iribarren number for a rock island breakwater. A parameterisation similar to Seelig and Ahrens was used. Different values of the coefficients a and b were found depending on the depth of water in front of the structure, and while the values of a were generally similar, Davidson's values of b were larger for a rock island breakwater (slope 1/1.1) ($25 < b < 80$). For a berm breakwater (slope 1/6). Davidson gave $a=0.42$ and $b=2$ for deeper water ($d > 3m$), while for shallower water the reflection coefficient was found to be insensitive to the Iribarren number. Davidson concluded that 'The reflection coefficient is directly related to the steepness of the incident waves unless a surf zone is fully developed...'

Hughes and Fowler (1995) arrived at a different form of parameterisation using irregular waves in a series of wave tank tests. They used a form of parameter similar to the Iribarren number and defined

$$\xi_h = \frac{\sqrt{h/gT^2}}{\tan \beta} \quad 2.4.10$$

They arrived at an equation of the form

$$K_r = \frac{a}{a + \xi_h^b} \quad 2.4.11$$

For smooth slopes Hughes and Fowler gave $a=0.1176$ and $b=2.6$, while for rubble mound slopes $a=0.1415$ and $b=0.804$. While no physical justification was given, their results agreed with the form of Seelig and Ahrens (1981), although they commented that Seelig and Ahren's equation for monochromatic waves would have underestimated the reflection coefficient for each of the individual wave components. Hughes and Fowler indicated that the reflection coefficient is higher for irregular waves than the monochromatic analysis would suggest.

They (Hughes and Fowler, 1995) also presented data on RMS velocities as a function of distance from the toe of structure. This ties in with their earlier work on scour (Hughes and Fowler, 1991). The RMS velocity envelope closely followed the bed profile for irregular waves (Xie, 1981). A parameterisation for this was not presented however. (Scour profiles and Xie's work is covered in section 2.7).

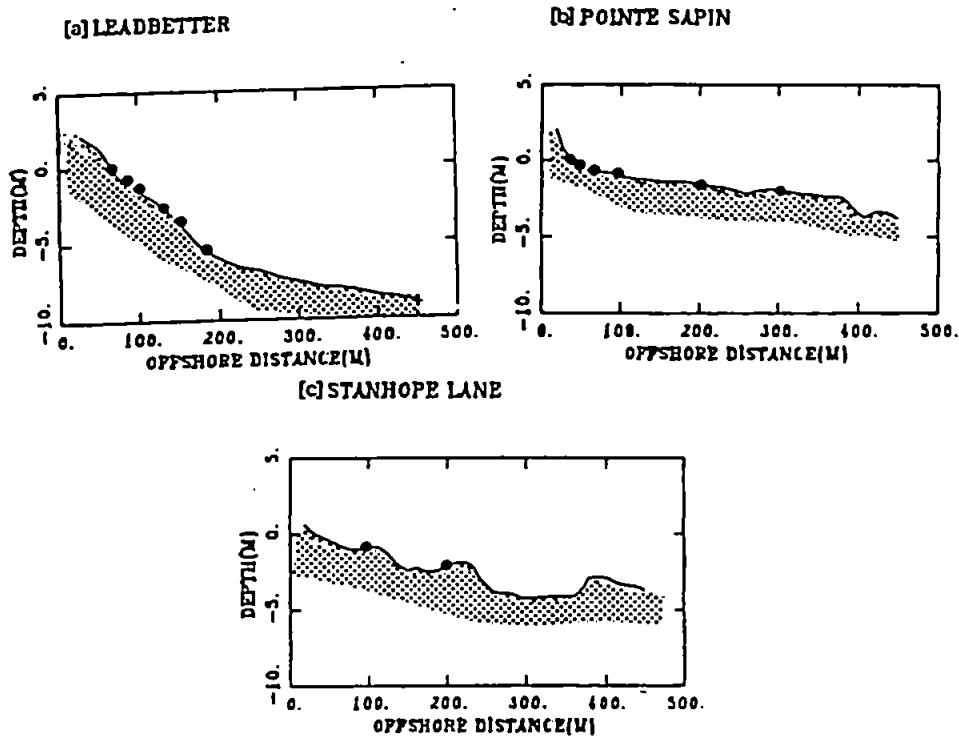
As can be seen by the above, researchers are converging to an empirical relationship between wave reflection and the physical parameters of the incident waves and the structure represented by the dimensionless parameters. It is encouraging that the field tests of workers such as Davidson provide relationships which are not too distant from those gained in the laboratory. While these observations are very useful for coastal engineers they are not absolute proofs based on physical processes, and there remains work to be done in this field. The implications for understanding sediment transport are important in that the suspension and transport of sediment in front of a reflective surface is governed by the hydrodynamics in the region. When the physical relationship between the sediment and wave reflection is better understood in this area, then attempts to parameterise the suspension processes in terms of the reflection may be forthcoming, and will provide a useful tool for coastal engineers.

2.5 Field studies of wave reflection

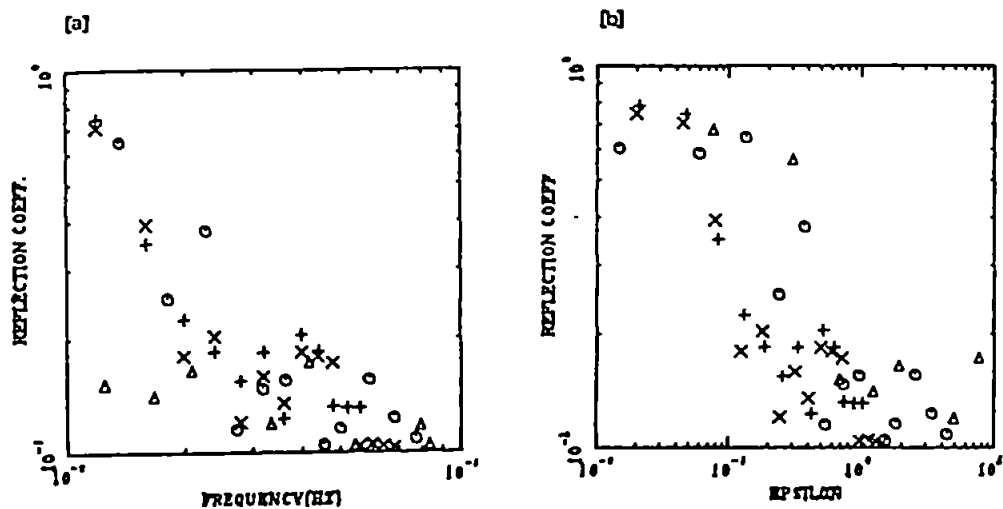
The measurement of wave reflection in the field is considered important as it allows the performance of coastal defence structures to be determined. Using such measurements, coastal engineers can validate physical and numerical models of wave dissipation and test the parameterisation of wave reflection. Field studies of wave reflection from natural beaches are also extremely valuable as the reflection of energy over the shoreface affects the morphodynamic processes taking place on the beach. The beach's ability to defend the coast therefore depends on the degree to which energy is either reflected or dissipated.

Field studies of wave reflections from both natural beaches and coastal structures require that wave monitoring devices are placed near the structure in appropriate places and measurements are made at high frequency, to the order of several hertz. The type and positioning of the instruments is a key factor in experimental design for such experiments as this determines the type of analysis that can be used. Developments in the analysis techniques are thus vital for such experiments as they control the quality of results available.

Tatavarti *et al.* (1988) used the techniques they developed for co-located current and elevation gauges to examine the reflection characteristics of a variety of beaches. They concluded that the shape of the reflection coefficient spectra depends on the shape of the beach, but that in all cases low frequency energy was reflected more easily than at higher frequencies. The data used from the NSTS and C²S² projects came from a variety of morphologically dissimilar sites. Leadbetter beach had a steep shoreface for half its tidal range with a shallow sloping low tide terrace. Pointe Sapin was almost exponential in profile while the Stanhope Lane site was a multibarred shore face. Examples of Tatavarti's results are shown in figure 2.5.1. The determination of a non dimensional parameter to describe the frequency dependent reflection coefficient for three beaches was not immediately forthcoming, even with the obvious advantages of their analysis techniques. Kubota *et al.* (1990) also used co-located current meter and elevation gauges to study wave reflection from the swash zone. They used Guza *et al.*'s (1984) method to separate the incoming and outgoing spectra but modified the method for quasi-linear wave theory.



Beach profiles and relative locations of the instrument stations for (a) Leadbetter, California (U.S.A), (b) Pointe Sapin, New Brunswick (Canada) and (c) Stanhope Lane, P.E.I., (Canada).



(a) Reflection coefficient as a function of the frequency for run PS62 (o), ST12 (Δ), LB7 (+), LB3 (x). (b) Reflection coefficient as a function of the non dimensional number ϵ for run PS62 (o), ST12 (Δ), LB7 (+), LB3 (x).

figure 2.5.1: Tatavarti *et al.* (1988) examined frequency dependent reflection coefficients from a variety of natural beaches. Their results show energy dissipation occurring at the frequency of the incident waves, while reflection occurs at lower (infragravity) frequencies.

In a study on wave reflection from an exposed dissipative beach, Nelson and Gonsalves (1990) used data from five spatially separated elevation gauges. They applied Mansard and Funke's (1980) three gauge technique for linear waves to this data to measure reflection in the infragravity band in the surf zone. The results indicate both a frequency dependence and a depth dependence to the reflection coefficient although no attempt is made at parameterisation in the style of Miche (1951).

Walton (1992) applied a frequency domain method to elevation and current meter data from a natural beach and found a small amount of reflection in the wind wave frequency but values greater than unity at low (infragravity) frequency. This could possibly be attributed to the low coherence problem as discussed by Mansard and Funke (1980) and Tatavarti *et al.* (1988). It may, on the other hand be a real phenomena, a result of non-linear interactions in the surf zone transferring energy from the incident band to lower frequencies.

Elgar *et al.* (1994) used an array of 24 elevation sensors to determine the reflection of waves from a natural beach. The beach was concave and they used the variety of slopes presented to the surf zone (defined by the region of swash excursion) during each tide, together with a frequency dependent analysis to examine Miche's parameterisation. The results are consistent with Miche's parameterisation, although infragravity band reflection was, in some cases, greater than unity. Like Walton's (1992) observations, this may be due to long wave amplification in the nearshore.

Bird *et al.* (1994), Davidson *et al.* (1994) and Dickson *et al.* (1995) have all examined wave reflection from natural breakwaters. There is considerable engineering interest in the parameterisation of reflection, and also there is interest in the performance of the structures in question. Bird *et al.* (1994) and Davidson *et al.* (1994) used an array of six pressure transducers near a variety of structures and these are described by Bird *et al.* (1994), including a rock island breakwater and a beach with a seawall. Bird *et al.* (1994) documented the use of a modified maximum likelihood method to obtain directional spectra in the region of the reflective structures, the method being based on Isobe and Kondo's (1984) technique.

Davidson *et al.* (1994) carried out further analysis using data from two of Bird's sites and accurately modelled the elevation variance distribution of the sea surface in the strongly

reflective wave field using shallow water linear wave theory. Davidson found that wave reflection was inversely proportional to wave steepness for waves breaking close to or on to the structure, and in the case of a fully developed surf zone, reflection decreased in the gravity frequency band.

The decrease in reflection with increasing frequency agrees with the findings of other authors (e.g. Dickson *et al.*, 1995). Dickson found an approximately linear relationship between the inverse of frequency and the reflection coefficient. Their study involved an array of wave gauges and used a directional spectrum approach. Their analysis gave results from a variety of wave angles up to 30 degrees from normally incident. Interestingly their linear relationship was not found by other authors, Miche's hypothesis suggesting an f^{-2} dependence for the reflection coefficient for monochromatic waves. Tatavarti *et al.* (1988) discussed reflection in terms of the Iribarren number but did not conclude a specific relationship between incident wave parameters and the reflection coefficient. They suggested that Miche's monochromatic case solution may not be appropriate to beaches due to the effects of wave shoaling and breaking which result in changes in wave amplitude. The majority of authors however, particularly those of engineering origin continue to attempt to obtain the best parameterisation for reflection, involving wave period, usually in terms of the Iribarren number.

2.6 Analytical models of wave reflection

It is clear that it is necessary to understand and achieve the ability to predict wave response to coastal features before an effective prediction of sediment transport can be made. In recent years researchers have had the luxury of being able to measure these processes *in situ*, however prior to having this capability investigators were limited to physical models and analytical models. Producing an analytical model from first principles requires a firm grasp of the processes involved, and the selection of suitable boundary conditions will determine the uses and the limitations of the model. Differences between the model and the real situation will arise if these processes and boundary conditions are not correctly understood. Thus models can also provide a check that processes are in fact properly understood when considered in relation to field observations.

The superposition of two monochromatic wave trains travelling in opposite directions in deep water forms the most simple model of a standing wave, however it is necessary to extend this model to understand more complicated situations. Linear theory provides a reasonable base for such an extension. The theory for a progressive wave of known frequency in a certain water depth was originally derived by Airy (1845). By obtaining a dispersion relation between wavelength, wave period and water depth, the necessary boundary conditions for the bed and the free surface can be solved, and an expression for the velocity potential obtained. From this the fluid velocity field can be obtained, as can the water pressure. To obtain the standing wave case, two opposing wave trains are added, and the solution runs in a similar fashion to the progressive wave case. When the waves shoal into shallower water, linear theory becomes less accurate, non-linear processes are at work moving energy to higher frequency harmonics and the Stokes solution for second, third and fourth order waves becomes a more appropriate model. On the shallow slopes of beaches, much energy is dissipated, and there are conditions when standing waves will not arise.

Carrier and Greenspan (1958) used the full non-linear, sloping bottom, shallow water equations to show that for a standing wave to be theoretically possible on a sloping beach:

$$r = \frac{a_i \omega_i^2}{g \tan^2 \beta} < 1 \quad \text{i denotes incident wave parameters.} \quad 2.6.1$$

This is the form of parameter that was later used by Galvin to classify breaker types. It has also been used by Guza and Inman (1975) as an indicator of conditions which may lead to the development of edge waves and beach cusps in reflective beach environments.

Opposing Stokes waves can be superimposed for a standing wave solution for the nearshore. These solutions do however rely on the bed being of constant level, and this is not usually the case in the nearshore zone. It is possible to solve the standing wave problem in the case of a sloping bed and this was done by Lamb (1932). The solution for the water surface takes the form of a Bessel function, the magnitude of oscillations decreasing with increasing water depth. This approach can be taken a stage further to a two component slope, although the solution is more complex (Suhayda 1974, Hotta *et al.*, 1981). Davidson *et al.* (1994) identified that using combinations of the flat bed solution and the sloping shoreface solution, solutions for more complex topography are possible. The solutions presented for the free surface show very good agreement with field data.

Hughes (1992) used a linear method to predict RMS velocities in the vicinity of a reflective structure in terms of the incident wave spectrum and the reflection coefficient of the structure. This solution was extended for sloping structures (Hughes and Fowler, 1995), although the structure is not defined as a boundary condition but enters the model directly as a reflection coefficient calculated using an inverted Iribarren type parameter. The results show good agreement with the laboratory data gathered. Interestingly, the envelope of the RMS solution is similar in appearance to Lamb's Bessel function solution.

Longuet Higgins (1953) also examined the difference between progressive waves and standing waves, and found a difference in the mass transport in the two cases. For progressive waves, the mass transport (i.e. mean current) in the boundary layer is in the direction of travel of the waves throughout the water column, while for standing waves the boundary layer transport is reversed relative to the rest of the water column, with convergence to the nodes. Above the boundary layer the transport is towards the antinodes (see figure 2.6.1). This raises an interesting point - if the transport is in one direction for $K_r=0$ (progressive waves) and in the opposing direction for $K_r=1$ (complete reflection leads to standing waves), there must be a value of the reflection coefficient for which reversal occurs. This has been found theoretically to occur for reflection values greater than 41.4% (Carter *et al.*, 1973) (i.e. $K_r>0.414$). Carter *et al.* also verified this experimentally in a physical model test.

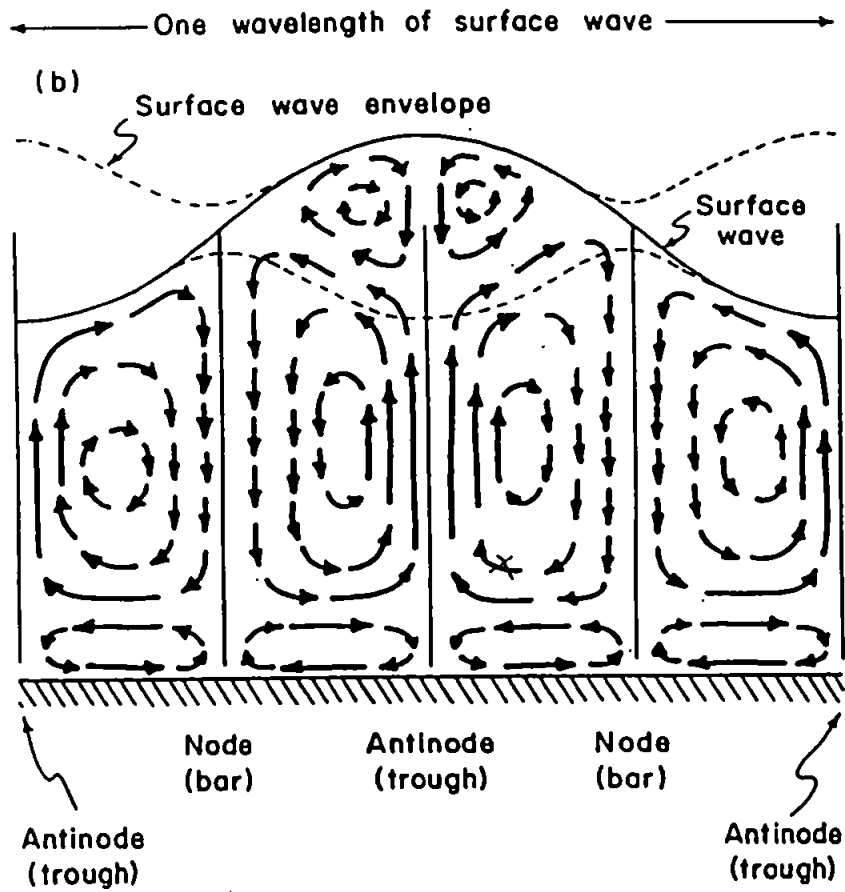


figure 2.6.1: Mass transport within standing waves (after Allen, 1981). The residual circulation in the standing wave is shown, as is the transport within the boundary layer as derived by Longuet Higgins (1953).

This result is obviously going to be important for more reflective structures as this provides a mechanism for sediment to be moved offshore from directly in front of the reflector out to the elevation node. It also indicates that more than 82% of the energy must be dissipated by a structure if it is not going to significantly effect the flow field. The solution for mass transport beneath a partially standing wave takes a similar form to that of the fully standing wave, with boundary layer convergence at the nodes and divergences in the antinodes (see Allen, 1981).

Of interest finally is the case of waves incident on a seawall at an angle. The dispersion relation for such waves has been found (Green, 1986) although the results are not verified in the field.

Considerable ground has obviously been covered in the theory of wave reflection, and in terms of modelling wave tank processes, the analytical and physical models appear to tie in well with each other. This is however a first step and there are complications for the models which are then applied to full scale situations. Non-linearities in shoaling waves approaching structures or the shoreline give one such problem. Irregular wave theory may provide some answers, as will the solutions for the full spectrum of waves as they evolve towards the shore and are then reflected away. While such solutions are not simple, linear theory has been shown to work reasonably well for the case of non broken waves in the nearshore, and this is encouraging as it allows the work of Longuet Higgins (1953) and Carter *et al.* (1973) to be considered in relation to suitable field data.

--

2.7 Sediment dynamics associated with reflective structures: physical and numerical models

To understand and measure scour in front of structures, coastal engineers use scaled down physical models. An alternative approach is to attempt to model the processes numerically or analytically, and these results can be compared to physical model tests. Few researchers have compared their results with field data.

2.7.1 Laboratory models

The earliest models of seawall beach interaction are those of Bagnold (1940; 1946), Dorland (1940) and Russell and Ingliss (1953). Dorland found that while the waves did not cause scour in front of the wall, material was placed in suspension which may then be transported by currents which would otherwise cause no damage. Kraus (1988) and Kraus and McDougal (1996) found no field measurements of suspended sediment concentrations at seawalls with which to verify this early hypothesis. Wave conditions in Dorland's experiment were accretionary according to the erosion/accretion criteria introduced by Dean (1973)², and this may be the reason for the lack of scour trough development (O'Brien, 1984).

Dean's (1986) 'approximate principle' suggests that in erosive conditions the scour trough immediately fronting the armouring will be 'less than or equal to that volume that would have been provided through erosion by that portion of the profile upland of the armouring if that armorings were not present'. This suggests that the erosion is passive and depends on the sediment source which is required. Other workers relate scour depth to the incident wave height (e.g. Russell and Ingliss, 1953; Sawaragi and Kawasaki, 1960; Sato, *et al.*, 1969; Chestnutt and Schiller, 1971; 1977; Xie, 1981; Irie *et al.*, 1986) although Kamphius, *et al.* (1992) have since suggested that the average local scour depth could not be related to deep water incident wave height. Fowler (1992) described an experiment which supported the rule of thumb that the limiting scour depth was approximately equal to the deep water wave height. Scour prediction results are reviewed by Fowler (1993).

The results of Xie (1981) and Irie *et al.* (1986) indicate that it is possible to estimate the depth of scour from the ratio of water depth to wavelength. In the case of monochromatic

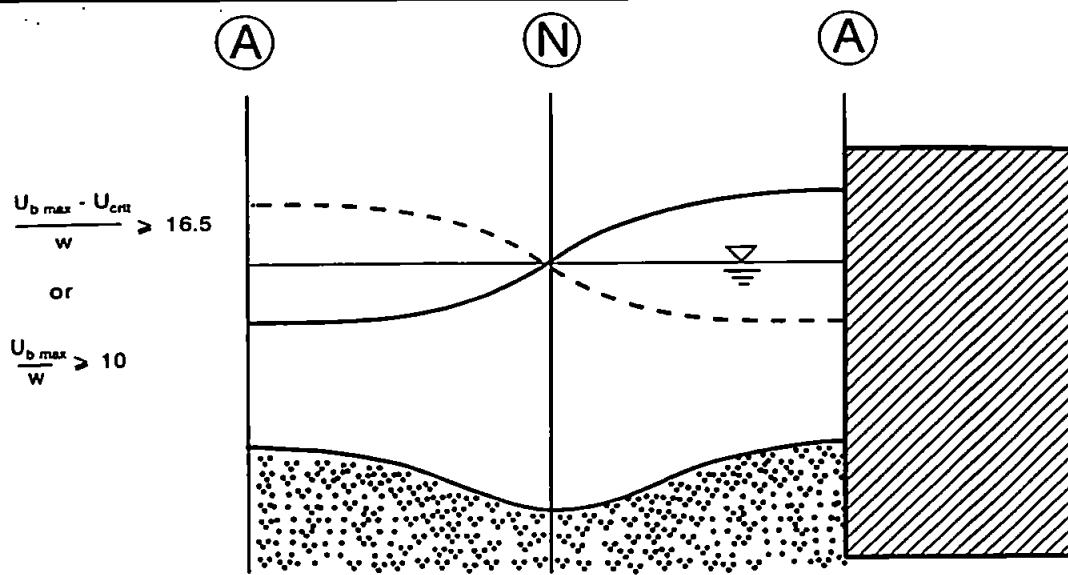
² Dean's criteria was based on small scale studies and has since been revised - see Kriebel *et al.* (1986) and Larson and Kraus (1989).

waves, normally incident on a structure, this can be done from wave period and water depth by solving the dispersion equation. Although scour can be considered in terms of the dimensionless parameter S/H (scour depth to wave height), in the surf zone the ratio of wave height to water depth can be considered constant, thus for this case it is possible to consider scour in terms of the ratio of scour depth to water depth (Goda, 1970). The centres of scour trenches are located at odd multiples of quarter wavelengths from the reflecting wall in the case of fine sand (Best *et al.*, 1971; Xie, 1981) i.e. at elevation nodes (velocity maximum) but for coarse sand troughs are located halfway between nodes and antinodes, (Xie, 1981 and Irie and Nadaoka, 1984). Xie's results are shown in figure 2.7.1.1.

The reason given for this is that in the case of coarse sand most of the transport is as bedload, while for finer sand the transport is dominated by suspended load. Xie (1981) identifies the importance of fall velocity, bed velocity and the critical bed velocity required for suspension in the determination of which case of the two cases will dominate, and suggests an empirical classification based on these parameters. Irie and Nadaoka (1984) suggest a similar criteria, also based on a laboratory study. However, such rhythmic cross-shore sedimentary structures have not been identified in the field (Kraus, 1988; Kraus and McDougal 1996).

Hsu and Silvester (1989) consider the case of waves approaching a reflector at an angle. They verify that waves normally incident to a structure in laboratory conditions can give rise to mounds at half wavelength spacing from it with troughs in between. The wave field resulting from angled wave reflection initially gave rise to trenches, but then led to erosion all over the bed. A test by Tanaka *et al.* (1972) shows sediment being transported in a longshore direction by the reflected wave field, resulting in sediment erosion upcoast and sediment accretion down wave and down coast. Lin *et al.* (1987) found that breaking wave heights in an obliquely reflected short crested wave field were greater than predicted for simple progressive waves, and this indicated that the scour may be more severe. Silvester (1975, 1977) also suggested that wave reflection would re-apply the energy over the bed, providing extra energy for sediment suspension. In Silvester's concise words:

'Reflection of waves from walls obliquely doubly applies energy to a sedimentary bed and hence expedites the transmission of material down coast' (Silvester, 1977).

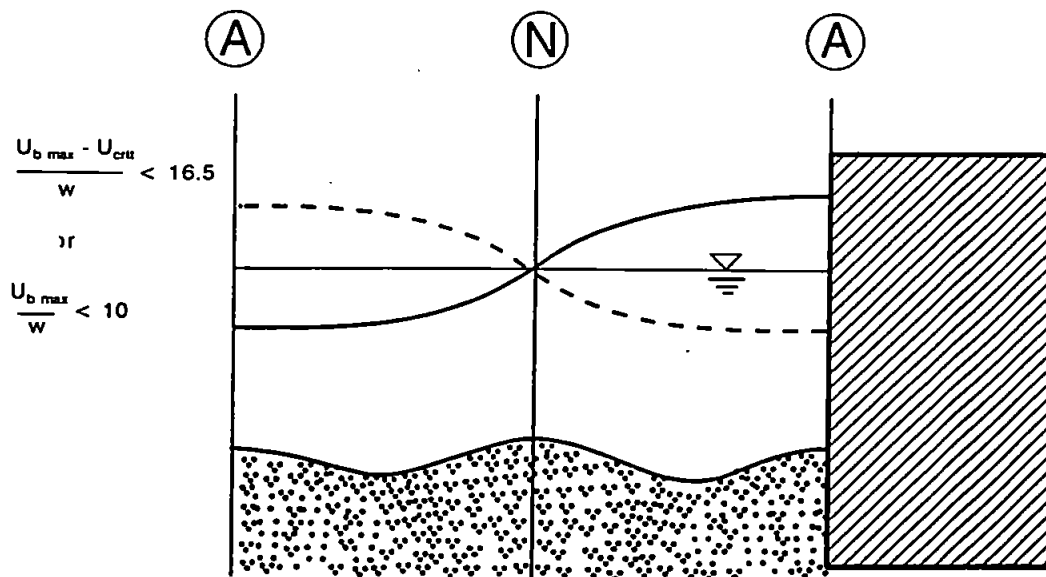


(a) RELATIVELY FINE SAND (Suspension)

- relatively fine sand (suspension)

XIE-Criterion : $(U_{b\max} - U_{crit}) / w \geq 16.5$

IRIE-Criterion: $(U_{b\max} / w) \geq 10$



(b) RELATIVELY COARSE SAND (Bed load)

SCOUR PATTERN BENEATH STANDING WAVES

- relatively coarse sand (bed load)

XIE-Criterion : $(U_{b\max} - U_{crit}) / w < 16.5$

IRIE-Criterion: $(U_{b\max} / w) < 10$

figure 2.7.1.1: Depending on the size of sediment, Xie (1981) found two basic types of scouring pattern for standing waves normally incident on a vertical wall. Xie (1981) offers a parameterisation for when each will occur, as does Irie and Nadaoka (1984). The boundary layer mass transport in the standing wave case is used to explain the differences. A large number of waves are required before such a system becomes fully developed.

Various authors have considered the effect of irregular waves normally incident on a structure (Xie, 1981; 1985; Hsu and Silvester, 1989; Hughes and Fowler, 1991; Oumeraci, 1993). Xie (1981, 1985) performed moveable bed tests on scour, and produced a bedform which was rhythmic with decreasing amplitude further away from the structure. This structure is similar to the pattern of water velocities associated with irregular wave reflection. Hughes and Fowler (1991) give an expression for the RMS velocity at any distance from the structure in terms of the incident wave spectrum, and their laboratory investigations show that the positions of maximum velocity correspond to the positions of maximum scour. They go on to provide a predictive equation for the depth of scour for fine sediments which are moved in suspension. Interestingly, they point out that the magnitudes of scour are considerably less than the monochromatic result. Hsu and Silvester (1989) found that the use of spectral or irregular waves would slow the erosion process down, as positions of maximum disturbance would not remain in the same place for any length of time, irregular waves giving rise to a more uniform scour over the bed. In these scale experiments a long time (11 hours was insufficient) is required to reach equilibrium. This means that the results will only be applicable to structures in deeper water which will not dry out at mid to low water, especially in regions where wave climate changes rapidly.

McDougal *et al.* (1987) used a series of laboratory tests to examine the effect of structure length on down and up-coast erosion. They used monochromatic, normally incident waves on an equilibrium beach with a vertical structure placed at the still water line, and measured the effect of the structure on the beach contours. They gave empirical linear relationships between depth of flanking and seawall length, and the length of excess flanking with seawall length. The relationships suggest that both length and depth of flanking increase linearly with structure length. They compare results with the field results of Walton and Sensabaugh (1978), results which are published in Chiu (1977) and fit this field data to their empirical estimates. McDougal *et al.* (1987) also document their plans for further tests in a larger tank to bridge the gap between the laboratory and field data.

The most recently documented attempt to model the effects of seawalls on the beach has been carried out by McDougal, *et al.* (1996). A large scale laboratory experiment was carried out as part of the SUPERTANK laboratory data collection project (Kraus *et al.*, 1992) and the results were compared to a modified version of the SBEACH model (Larson and Kraus, 1989; McDougal *et al.*, 1994) which includes the effects of wave reflection at

the shoreline. They concluded that wave reflection was probably not a significant contributor to beach profile change or to scour in front of seawalls, and that while there were no longshore gradients, the reflected waves cause no more sand to be suspended than if there was no seawall present.

Clearly there is much dispute over the effects seawalls have on the beach. McDougal *et al.* (1996) were not the first to use numerical models in order to understand the interactions between the wall, hydrodynamics and sediment dynamics, and other mathematical modelling attempts are described in the next section.

2.7.2 Analytical and numerical models

Herbich and Ko (1969) developed an analytical model of scour in front of a seawall from first principles. Their model is based on an analysis of the force required to move a particle of sediment which is dependent on the local bed velocity. Using the equation of continuity between antinodes to solve for this velocity in the boundary layer, Herbich and Ko (1969) arrived at an equation for the ultimate scour depth under the antinodes of the wave envelope. They then compared the analytical model with physical tests and arrived at an agreement which they describe as 'reasonably good'. They also conclude that the length of scour is only a function of wavelength, and more interestingly found that although they expected that the scour would occur at the toe of the structure, in actual fact the first scour hole developed some distance seaward of the structure.

Dean (1991) considers the application of an equilibrium beach profile to a seawall backed beach. In an example case the model is run to examine the effect of rising sea level. The beach profile moves inshore and the wall is undermined. The model does not include wave reflection, however sediment is transported offshore as a result of the rise in sea level. Dean has also looked at the effect of a seawall on beach nourishment (Dean and Yoo, 1994). In this study they used analytical, numerical and physical models and deduced that the seawall's main effect is in increasing the rate of longshore transport of the nourished sediment. This was considered to be a result of the lack of sediment available as a source to replenish the nourishment. The spreading of the planform of the nourishment was not accelerated by the seawall.

A similar model to Dean and Yoo's was developed by Hanson and Kraus (1985) and implemented in the GENESIS shoreline change model (Hanson and Kraus, 1989). The

results produced are similar to those produced by Dean and Yoo's (1994) model (Kraus and Hanson, 1995).

McDougal *et al.* (1994, 1996) used a numerical profile change model to examine the effect of a seawall on beach profile. The SBEACH model was originally developed for open coasts (Larson and Kraus, 1989). Wave transformations are based on the model of Dally *et al.* (1984), cross-shore transport is based on Kriebel and Dean (1985). McDougal *et al.* (1996) modified SBEACH by adding in a reflected wave component from the seawall which in turn modifies the wave field by adding in a partial standing wave. This in turn alters the radiation stress, wave set-up and breaking. The model has three components: wave transformation, cross-shore sediment transport and profile change. The modified model results were compared to SUPERTANK data (see Kraus *et al.*, 1992; McDougal *et al.*, 1996) and the predicted scour depth at the seawall gave fair agreement with the tank results. This scour however was rather minor, even when exposed to large monochromatic waves. The development of troughs like Xie's were not observed, although a breakpoint bar did form. The model results were also compared to runs of SBEACH with no wave reflection terms. Conclusions included that the wave reflection did not significantly contribute to beach profile change, and that reflected waves result in no more sand being suspended than if reflection was not present (McDougal *et al.*, 1996). This is contrary to the conclusions of Kraus (1988), the notions of Silvester (1972, 1975, 1977) and the observations of Dorland (1940). The argument is more in line with the approximate principle argument of Dean (1986), in fact McDougal states 'During storms, the profile change for a beach with a wall has about the same general shape as for a beach without a wall, except near the wall where the profile tends to flatten and a trench may form'.

Rakha and Kamphius (1995) also use a numerical model to examine beach profiles with and without seawalls in the same incident wave conditions and compare their results to laboratory results. The results show profile lowering in the vicinity of the seawall, although they comment that the reflection coefficient only has a small effect on the beach profile development close to the seawall.

The attention which has been focused on the modelling of beach profile response to the presence of a seawall has resulted in a considerably better understanding of processes which drive changes in beach profile, and the numerical models therefore appear to be producing similar results to the laboratory tests. There have also been many field

measurements of beach profiles associated with seawalls, and these are covered in the next section. However, field measurements of suspension and sediment transport processes associated with reflection are absent from the literature.

2.8 Field investigations: low frequency measurements

There has been a considerable effort to record the effects of seawalls on the beach, with interest being directed particularly at the evolution of the beach profile before, during and after storms (e.g. Fitzgerald, 1980; Sexton and Moslow, 1981; Kriebel *et al.*, 1986; Kriebel, 1987; Davis and Andronaco, 1987; Sayre, 1987; Fitzgerald *et al.*, 1994) and the long term performance of coastal structures (e.g. Hiranandi and Gole, 1961; MacDonald and Patterson, 1985; Carter *et al.*, 1986; Dette and Gartner, 1987; Kraus *et al.*, 1988; Basco *et al.*, 1992). Most of those researchers making measurements of the beach do so using survey techniques. Some compare protected and unprotected shorelines (e.g. Birkemeier, 1980; Sexton and Moslow, 1981; Berrigan, 1985a,b; Zimmerman and Bokuniewicz, 1987), while others take surveys at regular intervals to establish patterns of evolution (e.g. Baba and Thomas, 1987; Griggs and Tait, 1988). In this section of the review an attempt has been made to follow the topics which are most important and discuss what has been done in each one.

Scour features

Scour troughs are usually observed in the field at the base of more reflective structures after storms or hurricanes (e.g. Sawaragi and Kawasaki, 1960; Sexton and Moslow, 1981; Morton, 1988). Morton (1988) used survey techniques at three sites before and after hurricanes and found that the scour troughs formed by storms rapidly filled in during recovery. Griggs *et al.* (1994) summarised seven years of survey data and found, surprisingly, that a scour trough was never observed in front of any of the seawalls studied.

Ridge and runnel features have been found in front of coastal structures (Davis and Andronaco, 1987) although these are rare (Dean, 1986). Kriebel *et al.* (1986) took profiles of a site at Sand Key, Florida and have observed a similar looking structure to a ridge and runnel, although they called it a 'swash bar'.

Uda (1989) examined scour at structures along the Japanese coast and concluded that scour was not produced solely by cross-shore transport processes. He suggested that sand was first moved from the foot of structures by longshore processes which resulted in a deflated profile. Subsequently, a combination of cross-shore and longshore processes gives rise to sufficient scour at the base of the structure to cause failure.

Beach recovery

As with Morton's observations, others have found that a beach backed by a wall is fully capable of recovery after a storm, although it may be at a slower rate than on an adjacent beach (Kriebel, 1987; Kriebel *et al.*, 1986). Nakashima and Mossa (1991) surveyed a section of beach for four years and found that after a hurricane, the beach recovered more quickly if no stabilisation was present than if it was present, and this was attributed to the fact that the sediment budget was expended re-filling the scour trough in front of the wall. Moody (1996) on the other hand found recovery to be essentially the same on walled and un-walled beaches in a physical model experiment.

Baba and Thomas (1988) used profile studies to investigate the effect of the monsoon season on a defended section of the southwest coast of India. They found that in the calmer season the beach remained steep with a berm, but during the monsoon when waves were steeper, an offshore bar formed which removed a lot of energy from the incident waves.

Deflated Profile

A scour trough does not always form in front of the wall. Griggs and Tait (1988) surveyed sections of defended and undefended coastline in Monterey bay in California before and after a storm and found no such scour trough at any time. The seawall was however not a vertical one. They found the profile deflated on both wall and natural beach sections during the storm, although the berm in front of the stabilised sections eroded more quickly than the undefended sections. Drowned erosion, attributed to end reflections, persisted for 150m down coast of the wall. Hall and Pilkey (1991) used aerial photographs to monitor stabilised and unstabilised coasts in New Jersey. The stabilised ones had significantly narrower beach faces and long term erosion was thought to be the problem in this case. Pilkey and Wright (1988) also suggested that long term erosion was more likely to be the cause of such erosion than short term, storm events.

Birkemeier *et al.* (1991) obtained profiles of a South Carolina beach before and after Hurricane Hugo (Hurricane Hugo struck in 1989, see Finkl and Pilkey (1991)). Many of the walls along the beach front were submerged during the storm surge, and the dunes behind were consequently eroded substantially. Profiles were lowered in front of walled sections by up to 1.5m. Kraus and McDougal (1996) commented that this lowering of the

profile was 'in a manner typically consistent with Dean's approximate principle' (Dean, 1986).

Nelson (1991) also surveyed the effects of Hurricane Hugo. Nelson obtained survey lines from in front of the seawall and adjacent to the seawall before and after the storm at locations comparable with previously obtained survey data. Nelson concluded that the erosion was not increased in front of seawalls or rip rap revetments, although erosion troughs were observed at many rip rap armoured beaches in the study area.

End Flanking

Morton (1988) found that the greatest flanking erosion was downcoast, possibly due to the interruption of the sediment transport budget. Sexton and Moslow (1981) also reported downcoast flanking, in their case the wall was damaged as a result. Chiu (1977) and Walton and Sensabaugh (1979) surveyed beaches backed by seawalls on the Gulf Coast of the United States. They were investigating the effects of a hurricane which struck in 1975. They noted increasing erosion with structure length, an observation which was tested later by McDougal *et al.* (1987) in tank tests. The presence of a seawall means that the upper part of the beach is unavailable as a sediment source during a storm. Thus longshore sediment transport from this region may be deficient in sediment during such storm events, resulting in downcoast erosion.

Other workers have come up with similar results and arguments, these including Birkemeier (1980) who found downcoast erosion on Lake Michigan as a result of an upcoast seawall. He also noted that scour was present on the downdrift side of the wall. Griggs and Tait (1988) found similar results for a seawall in Monterey Bay. Kriebel *et al.* (1986) and Kriebel (1987) took profiles of a site at Sand Key, Florida to examine the effects of Hurricane Elena (1985). They however found no downdrift flanking, a profile only 30m downcoast of the wall showed no difference to those up to thousands of meters away.

Sand Accretion (Groyne effect)

A further process is that of the seawall acting as a groyne. Seawalls which protrude from the shore can block the littoral drift of sediment. Such walls may result from beach retreat or profile deflation. Others may be built in this way to extend the shore seaward. Not only does this create a deficit in the sediment budget downcoast, it also can result in accretion

upcoast. Birkemeier (1980) observed a beach developing upcoast of a seawall where no beach had previously been, and discussed the effect of sand accretion.

Recovery phase

After a storm, the beach recovers by moving sand from offshore bars to the regions further inshore. In time, the berm is rebuilt and a 'summer' profile is re-established. The presence of a seawall at the head of the beach may not always delay the recovery of the beach (e.g. Davis and Andronaco, 1987; Kriebel, 1987; Griggs and Tait, 1988) although it has been observed to do so (Sayre, 1987). Sayre (1987) surveyed protected and unprotected beaches on the west coast of Florida before and after Hurricane Elena (1985), and while the unstabilised sections recovered, the stabilised sections were still not completely recovered after 15 months, and required nourishment.

Summary of low frequency measurements

Many researchers have used surveying techniques to monitor the effects of seawalls on the beach, and considerable effort has gone into documenting the effect of storms on the beaches fronting these structures. As a result there is now a reasonable qualitative understanding of most of the longer term processes at work in this region and the effects of storms on the profile evolution. Profiles in tidal water are at best obtained once every 12 hours, a time scale which represents a long time average over which to determine the nature of processes driving sediment transport.

To move on from this position it will be necessary to home in on individual hydrodynamic processes in the field and examine their contributions to sediment transport. The current debate by laboratory investigators into the effects of wave reflection on sediment transport indicates that this is one such process which is in need of field investigation. Measurements of hydrodynamics and sediment dynamics made at high frequency in the reflective environment will facilitate this investigation and lead to a better understanding of how seawalls affect beach profile change. Care must be taken when considering the results of all the investigations as the nature of the interaction between the wall and the beach is different in many cases. Rubble mound seawalls placed above the high tide mark as a storm defence mechanism are likely to have far less effect on the coastal morphodynamics than a solid vertical wall placed at the mid tide level. In answering the popular question 'What is the effect of the seawall on the beach?' (Kraus, 1988; Kraus and McDougal, 1996) and other questions such as 'Can seawalls and beaches coexist'

(Terchunian, 1988) great care must be taken in identifying the nature of the system and the type of armouring used. The literature is clear in suggesting that there is a great diversity in possible effects of different seawalls in different situations. A better understanding of processes associated with the simpler cases is required.

2.9 Field investigations: high frequency measurements

Whilst there have been many surveys of the effects of a seawall backed beach made using profiling techniques, few investigators have made measurements of incident wave conditions and the sediment response to these conditions. The two papers below are two attempts to examine the hydrodynamic effects, one using a pressure gauge mounted on a nearby pier as an indication of incident wave conditions, the other making visual observations of swash oscillations. No reference to other works which document high frequency measurements from in front of a seawall has been found, and the use of current meters and sediment sensors in front of a wall, logging at high frequency is undocumented (Kraus, 1988; Kraus and McDougal, 1996). The use of such instruments will provide valuable insight into the sediment transport processes associated with wave reflection.

Baba and Thomas (1987) studied a beach backed by a rubble mound seawall in India for six years. They used profile information from beach surveys to discern long term processes. A wave recorder ('pressure-type wave recorder') located on a nearby pier was used to examine wave statistics including wave height, wave steepness and wave spectra. Wave heights varied from 0.4 to 6m, with 60 to 80% being larger than 2.5m during the monsoon period June to September. Wave periods were typically in the range 5 to 18 secs, with lower values (<10 secs) occurring during the monsoon (i.e. large, steep waves are predominant). Neutrally buoyant floats were used to examine nearshore currents and wave directions were recorded from visual observations.

Baba and Thomas found that during fair weather periods, a berm developed seawards of the wall and the beach face became steep. During the monsoon period the beach changed shape. The berm eroded and the sediment was deposited in a longshore bar which acted as a submerged breakwater and dissipated a most of the wave energy. The damage to the seawall at the back of the beach was thus minimal. This observation prompted Baba and Thomas to recommend that a wide beach is maintained in front of the wall to act as a buffer to the waves during the monsoon periods. They found that the berm eroded in this way when the wave steepness exceeded 0.03 (c.f. Dean, 1973; Kriebel *et al.*, 1986). When the wave steepness dropped beneath this value, the longshore bar migrated back to the beach and reformed a berm. Their study was on a microtidal beach, the tidal range being less than 1m. During the monsoon period, when the bar was present, waves were found to break and dissipate on this bar, thus waves reaching the wall would have significantly less energy.

Baba and Thomas did not mention the effects of wave reflection, presumably the rubble mound breakwater dissipated the remainder of the energy that got to the top of the beach.

Plant and Griggs (1992) documented short term effects of a seawall on nearshore hydrodynamic processes and the resultant beach morphology. They made visual observations of the swash interacting with a seawall, measured the groundwater elevation in front of a seawall and on a natural beach, made profile measurements and measured longshore velocities using a dye tracer at a site in Monterey bay in California. The reflection of the swash from the seawall was observed to increase the backwash duration compared to a natural beach. The advancing swash was in the form of a white water bore, the backwash in the form of seaward flowing sheet flow. Reflected waves were found to propagate seawards 2-3 seconds after impact. This delay occurred because the seawall has a rubble mound toe through which the water propagated before impacting the concrete behind.

The ground water results showed that both the beach fronting the wall and the natural beach exhibited an asymmetrical response to the tide, taking longer to drain than to flood. Results from the upper part of the profile showed the groundwater response of the upper beach lagged the lower beach and was more asymmetric in response in both wall and beach cases. The presence of the wall accelerated the rise of the water table, and this was attributed to the presence of rock armouring under the sand. The rate of drop of the water table depended on cross-shore position. Just in front of the seawall, the drop in water column lagged the natural beach, but dropped at a similar rate. Lower down the beach in front of the wall, the water table again lagged the natural beach but dropped more quickly than on the natural beach. Further investigation would be necessary if these results were to be tied in to profile variation.

Plant and Griggs (1992) also showed how the effluent line (the landward limit of saturated sand) was displaced in front of the wall. This line is shown to be further seaward in front of the wall at low tide, and hence incoming waves would reach drier sand sooner in this region. This may assist accretion on the lower profile in front of the wall. At high tide however, the effluent line was deflected towards the wall (meeting the base of the wall). This could impede accretion during the latter parts of the flood tide.

Plant and Griggs's profile results suggest that the seawall may displace patterns of variability offshore, more importantly they concluded that while the seawall affected short-term beach variability, it had no affect on the seasonal erosion-recovery cycle.

Clearly the approach of relating incident wave conditions to change in beach morphology is essential for coastal engineers so that well informed decisions can be made about coastal defence strategies. The process orientated studies to date have not used the full array of techniques available that have been developed by researchers into natural beach processes and it is this direction of investigation which is likely to lead to further understanding of the processes involved.

2.10 Conclusion / Summary

This chapter has reviewed literature related to the problems associated with wave reflection and sediment transport on beaches in front of seawalls. A variety of approaches have been used to investigate the effect of a wall on the beach, including the use of physical models, numerical models and field measurements. However there have been no high frequency measurements of sediment suspension and transport made in front of seawalls until now. Without high frequency measurements, the processes which drive the lower frequency beach changes cannot be quantified, and discussion of such processes remains speculative. Such an experiment can derive its analysis techniques from those used to look at natural beaches as similar instruments would be used. The experiment design is covered in a later section, but the basis of it comes from this review.

The physical model tests indicate that wave reflection is a dominant hydrodynamic process in front of a wall. It is possible to obtain the frequency dependent reflection coefficient using the techniques developed by Guza *et al.* (1984) and Tatavarti *et al.* (1988). Further important parameters are the water depth at the wall and the wave period and height. Co-spectral analysis (Huntley and Hanes, 1987) will reveal more about the frequency dependent sediment transport processes in front of the wall. It will be necessary to ensure suitable comparisons can be made with a natural beach, so that the analysis routines can be verified according to accepted theories and processes. Used in conjunction with profiling techniques, this approach will give a considerable amount of information on the nature of sediment suspension and transport in front of a seawall, and this represents a significant step in understanding coastal processes.

Interestingly, similar observations on beaches have moved from looking at low energy conditions, outside the surf zone, through to deploying instruments and making observations of processes in a variety of different morphological conditions - flat beaches, steep beaches and beaches with bars. They have also been made in a variety of incident weather conditions from complete calm or local seas to storms. In a similar way, the observation of processes associated with a reflective structure fronted by a beach could be carried out for vertical walls, sloping revetments and rubble mound breakwaters, in conditions ranging from calm seas to storms. The benefit of doing this is that when this information is documented, engineers will be better able to apply different coastal defence strategies to local situations.

Unfortunately, observations take time to organise, are difficult and expensive to make, especially in high energy conditions, and the development of further suitable analysis techniques takes time. This study represents the first of the steps required, high frequency measurements of sediment response to wave action on a near vertical seawall in small wave conditions.

CHAPTER 3: Data collection

3.1 Introduction

The overall aim of the experiment, according to the niche identified in the literature review, is to investigate the nature of sediment suspension and transport in front of a seawall. More specifically, the effect of wave reflection on the sediment dynamics will be examined using *in situ* measurements taken at high frequency. This chapter describes the field experiment which was used to investigate these processes.

Two rigs of instruments were deployed at Teignmouth in South Devon in June 1995. One was positioned directly in front of a seawall to measure the sediment response to wave reflection. The other was installed on an adjacent natural beach and provided control data. Instrumentation is covered first in section 3.2. Following this is a description of the field site and experiment at Teignmouth in South Devon (section 3.3). The description is split up into sections as follows. First a field site was identified (section 3.3.1), and the desired instrument layout considered (3.3.2). Rigs to hold the instruments in position were designed and built (3.3.3 and 3.3.4) and this allowed data to be collected in the appropriate manner (3.4.5). Environmental information including topographic surveys and weather maps were obtained (3.4.6) during the experiment. The data could then be processed into a form ready for analysis using a personal computer (3.4.7). The analysis of the data from the instruments is covered in full in chapter 4.

3.2 Instrumentation

3.2.1 Pressure transducers

Pressure transducers (PTs) were required to obtain information on wave elevation, wave period and mean water depth at the position of the instruments. The PTs used in this experiment were Druck PTX164¹ models which use a piezo resistive strain gauge to relate water pressure on the head of the instrument with voltage across the gauge. At pressure, deformation of a diaphragm in the head of the instrument causes a change in the resistance of the strain gauge and this is recorded as a fluctuation in output voltage due to a change in the current which can pass through the resistor. In this experiment, this signal was transferred from the instrument to the logging station via a 200 meter cable. The instruments are cylindrical in shape, measuring 177mm long with a diameter of 25mm.

The hydrostatic pressure equation relating water pressure to depth gives:

$$p = p_0 - \rho g z \quad 3.2.1.1$$

where p is the pressure at some depth z ($z=0$ at the surface and -ve below the surface), p_0 is the atmospheric pressure, ρ is the density of water and g is the acceleration due to gravity. The relationship between hydrostatic water pressure (p) and water depth (z) is linear and the output voltage can thus be linearly calibrated against water depth. The presence of waves was determined using the hydrostatic pressure in shallow water where the assumption is made that:

$$-z = h + \eta \quad 3.2.1.2$$

where h is the mean water depth, η is the elevation of the water surface above the mean and z is the distance to the surface of the water. This assumption requires that the wave pressure does not diminish with depth as a result of attenuation, and the equation becomes:

$$p = p_0 + \rho g h + \rho g \eta \quad 3.2.1.3$$

The mean of the pressure signal is $p_0 + \rho g h$, from which the water depth can be obtained, while the $\rho g \eta$ term represents the hydrostatic pressure due to the waves. Attenuation of pressure increases with depth and increasing wave frequency. The relationship between them comes directly from linear theory as follows:

$$Q = \cosh(k(z+h))/\cosh(kh) \quad 3.2.1.4$$

where Q is the attenuation, k is the wave number, z is the depth of interest and h is the water depth.

¹ Sensors supplied by Druck Limited: Fir tree lane, Groby, Leicester, England, LE6 0GH.

In this case the attenuation was small because the incident waves were in a sufficiently shallow water depth and a linear relationship between surface elevation and pressure at the bed (i.e. at the pressure transducer) therefore remained valid. An applicable example is that of shallow water waves of amplitude 20cm, with a period of 5 seconds, in 1m deep water, passing over a PT mounted 10cm off the bed. In this case, the celerity $c=3.13\text{m/s}$, the wavelength is thus $\lambda=15.65\text{m}$, and so the wave number $k=0.4\text{m}^{-1}$ (thus $kh<1$). The resulting attenuation of pressure with depth given by the above equation is $Q=0.93$, i.e. the PT underestimates the wave height by 7%, and in this case the PT would measure the wave amplitude as 18.6cm. It was therefore considered reasonable to measure the surface elevation of the water in the presence of waves in the same way as the mean water depth, provided that the PT is close enough to the surface, or the waves are in a sufficiently shallow water depth. Ripples and higher frequency waves would obviously be filtered out by having the sensor in deeper water, however the more important incident and long period waves are relatively unaffected.

The instruments were calibrated for gain in a deep tank at the Royal Naval Engineering College at Manadon (Plymouth). The instruments were lowered through known water depths and the voltage output was logged using the same logging system as used in the field experiment. Both PTs were lowered in 30cm steps to a total depth of 3.6m. Calibration outputs for all instruments are given in an appendix. The result is an equation relating the output voltage of the instrument to water depth which was obtained using linear regression. The offset depends on the atmospheric pressure, and field offsets were obtained before and after each tide to account for changes in this.

The following equations give the gain and offset of the instruments obtained from the calibration runs in the tank at Manadon:

$$\text{PT1403: } d = 5.152 \times V - 15.36 \quad 3.2.1.5$$

$$\text{PT1404: } d = 5.1626 \times V - 15.185 \quad 3.2.1.6$$

Here d is the depth of water above the instrument resulting in an output voltage V . To convert this to actual water depth in the field, the instrument height above the bed on each day was added to d and the offset modified according to the field offset. While Druck give a non-linearity error band of 0.1%, the tank calibration was found to give maximum errors of $<\pm 0.3\%$. This translates to an error of $<\pm 1\text{cm}$ in 3m of water.

3.2.2 Electromagnetic current meters

The current meters used were Valeport model 800² two axis electromagnetic flow meters. Two spherical electromagnetic current meters (EMCMs) were used to measure water velocities in front of the seawall and one annular EMCM was used to measure water velocities on the beach. The two spherical EMCMs used comprise of a head of diameter of 5.5cm joined to the body of the instrument by a narrow stem. Four electrodes are positioned around the outside of this sphere. The annular sensor has a 17cm diameter open head, with electrodes on the inside of the head.

The principle of operation of the EMCM is based on Faraday's Law that a conductor moving in a magnetic field produces a voltage. In the case of the EMCM, the conducting fluid is water, the magnetic field is produced by a coil in the sensor head and the voltage is measured by the electrodes. By using two pairs of electrodes mounted orthogonally, two axis flow velocity measurements can be obtained from a single sensor.

The sampling volume for the spherical EMCMs is given by Valeport as a sphere with diameter of approximately 3 sensor diameters, while for the annular EMCM it a sphere of 10cm diameter. Care was thus taken when installing the instruments that no two sensors were positioned too close together, or too close to other ferromagnetic objects (i.e. placed at distances >18cm apart). Care was also taken to ensure that the flow in the vicinity of the sensor head was not disturbed by other instruments. The EMCMs were orientated using a level and compass to ensure that cross-shore and longshore currents were correctly measured.

The instruments were calibrated for gain in a tow tank at the Royal Naval Engineering College at Manadon (Plymouth). They were towed at speeds from -2.0 to +2.0 m/s in increments of 0.2 m/s using an identical electronics set up to that used in the field. During each complete calibration run the instruments were not removed from the water and remained powered up at all times. The velocity of the towing carriage was known and a linear calibration for the gain of the instruments was thus obtained. EMCM calibration graphs are given in the appendix.

² Sensors were supplied by Valeport Ltd., Townstal Industrial Estate, Dartmouth, Devon, TQ6 9LX, U.K.

The following calibration equations were deduced relating water velocity to voltage output of the instruments in the tank at Manadon:

Sensor 9169 (annular), channel 1300: $v(\text{m/s}) = 0.95 V - 0.26$ 3.2.2.1

Sensor 9169 (annular), channel 1301: $v(\text{m/s}) = 1.08 V - 0.23$ 3.2.2.2

Sensor 9170 (spherical), channel 1302: $v(\text{m/s}) = 1.26 V + 0.02$ 3.2.2.3

Sensor 9170 (spherical), channel 1303: $v(\text{m/s}) = 1.29 V + 0.18$ 3.2.2.4

Sensor 9171 (spherical), channel 1304: $v(\text{m/s}) = 1.05 V + 0.00$ 3.2.2.5

Sensor 9171 (spherical), channel 1305: $v(\text{m/s}) = 1.04 V + 0.00$ 3.2.2.6

Here v is the velocity in m/s for that particular channel and V is the output voltage of the instrument. Instrument offsets (zeros) were taken in the field before and after each run while the instruments were still powered up. This was done by placing the instruments in a large container of seawater and recording a short run. This container was cylindrical, had a diameter of 55cm and a depth of 60cm. EMCM electrodes were cleaned before and after each run. Laboratory gains and field offsets were applied to the data prior to analysis.

Having analysed EMCM performance in both steady (mean) and oscillatory flows, Cunningham *et al.* (1979) found them to have a relatively flat frequency response, and showed that they responded linearly to current speed variation. They found an uncertainty in the gain of the instruments of between 5 and 10% for a single gain applied over frequency. For mean flows, the generally accepted error in the measurement is ± 2 to 3 cm/s (Huntley and Hanes, 1987). Huntley and Hanes do comment however, that this can be improved by taking *in-situ* field offsets. No evidence was found to suggest that the sensors can predict significant flows of the wrong sign (Aubrey and Trowbridge, 1985; Guza, 1988). Having tested the instruments in a series of laboratory tests, Aubrey *et al.* (1984) and Aubrey (1989) reported errors of up to 2.5% for mean currents and up to 4% for oscillatory flows, while errors in gain of up to 10% were found for mean and oscillatory flows. Doering and Bowen (1987) also found maximum errors in this region, they give errors of 8 to 10% from comparisons of PT and EMCM data in the NSTS field experiments.

While the measurements described in the previous paragraph apply mostly to Marsh McBirney current meters, the Valeport ones used in this experiment operate on an identical principle. After testing the instruments for offset and gain stability, Valeport give a mean zero signal stability to less than 5mm/sec and a gain accuracy of better than 1% + 5mm/s of the reading for their instruments. This means that the EMCMs should be at most 1.5cm/s in error in a 1m/s flow for averaged readings, which represents a 1.5% error.

3.2.3 Optical backscatter sensors

Optical backscatter sensors³ were used to measure suspended sediment both in front of the seawall and on the beach. The optical backscatter sensor (OBS) was initially conceived and documented by Downing *et al.* (1981). It has since been widely used in the investigation of nearshore sediment dynamics (Jaffe *et al.*, 1984; Beach and Sternberg, 1988; 1991; Russell *et al.*, 1991; Wright *et al.*, 1991; Greenwood *et al.*, 1991; Osborne and Greenwood, 1992a,b; Huntley *et al.*, 1993; Davidson *et al.*, 1993a,b; Osborne and Greenwood, 1993; Russell, 1993; Aargard and Greenwood, 1994; 1995). The OBS3 was chosen over other sediment sensors because of its:

1. Small size and sample volume.
2. Linear response and wide dynamic range.
3. Insensitivity to bubbles and organic matter.
4. Ambient light rejection and low temperature coefficient.
5. Logging electronics can be connected using a 200m cable.

The OBS's small size makes it ideal for monitoring nearshore sediment dynamics while giving little impedance to the flow. The complete housing and sensor unit measures 181mm in length and has a maximum diameter of 31mm. The sensor head of the instrument has a diameter of 18mm, and a length of 40mm (further specifications are provided by the OBS1 and 3 manual, D&A instrument company).

The OBSs were carefully positioned several centimetres off the bed to ensure that they did not interfere directly with the bed or include the bed in their sampling volume. The recommended minimum height above the bed to prevent the OBS 'seeing' the bed is 2.7cm (OBS manual). However video analysis of *in-situ* OBSs has shown that the instruments need to be at least 5cm off the bed to prevent the flow diverging around the instrument, causing a 'rooster tail' of sediment to form down-stream of the instrument (Black and Rosenberg, 1991). Care was taken to make sure that the OBSs did not have any other structures in their view as this would also affect the results. They were positioned so that they pointed along the wave crest, into the expected mean longshore current so that preference was given to neither the front or the back of the wave, and also so that eddies containing sediment would not form by the instrument head.

³ Sensors were supplied by the D&A Instrument Company, 40-A Seton Road, Port Townsend, WA 98368.

Inside the head of an OBS is a high intensity infrared emitting diode (IRED) and four photo-diode detectors. The beam pattern is shown in figure 3.2.3.1. Light which hits small enough particles in the water column (i.e. sediment) is backscattered by them, and is sensed by the photo-diode detectors. The amount of sediment in the water column in this volume is found to be linearly related to the amount of backscatter. Thus the output voltage from the OBS can be calibrated for sediment concentration. The problem of one OBS seeing the light from a different OBS in the same vicinity is avoided by introducing a small time delay between the sensors taking their readings. The effects of this delay on process observation is negligible as the time delay is short (1 khz).

The instruments were calibrated in the laboratory using the technique advised by the OBS manual. Samples of sand from Teignmouth beach were sequentially added to a large container of seawater in which the OBSs were mounted. The sand was suspended using a paint stirrer driven by an electric drill. While the OBSs took their readings, a known volume of water and sediment was syphoned from inside the container from the same position as the OBSs. Sediment was filtered from the known water volume, dried and weighed. A time average of the concentration of sediment in the water next to the OBS at the time of logging was thus found. This technique was found to give an excellent linear relationship between voltage output of the OBS and sediment in suspension. (see calibration graphs in appendix). The following equations were found to relate the output voltage of the instrument and the amount of sediment in suspension during the calibration runs:

$$\text{OBS1 (1400) } c_s = 27.4 V - 27.99 \quad 3.2.3.1$$

$$\text{OBS2 (1401) } c_s = 25.94 V - 27.23 \quad 3.2.3.2$$

$$\text{OBS3 (1402) } c_s = 26.42 V - 27.49 \quad 3.2.3.3$$

In the above equations, c_s is the sediment concentration in g/l (this is equivalent to kg/m^3) and V is the output voltage of the instrument.

Instrument offset values were found using the method recommended by Downing (1983). Careful examination of the time series reveals a minimum value which is taken to be the voltage for which there is no sediment in suspension. This assumes that sediment suspension events take place episodically, and that at some time during the run all sediment falls out of suspension. This minimum value was removed from the data prior to analysis.

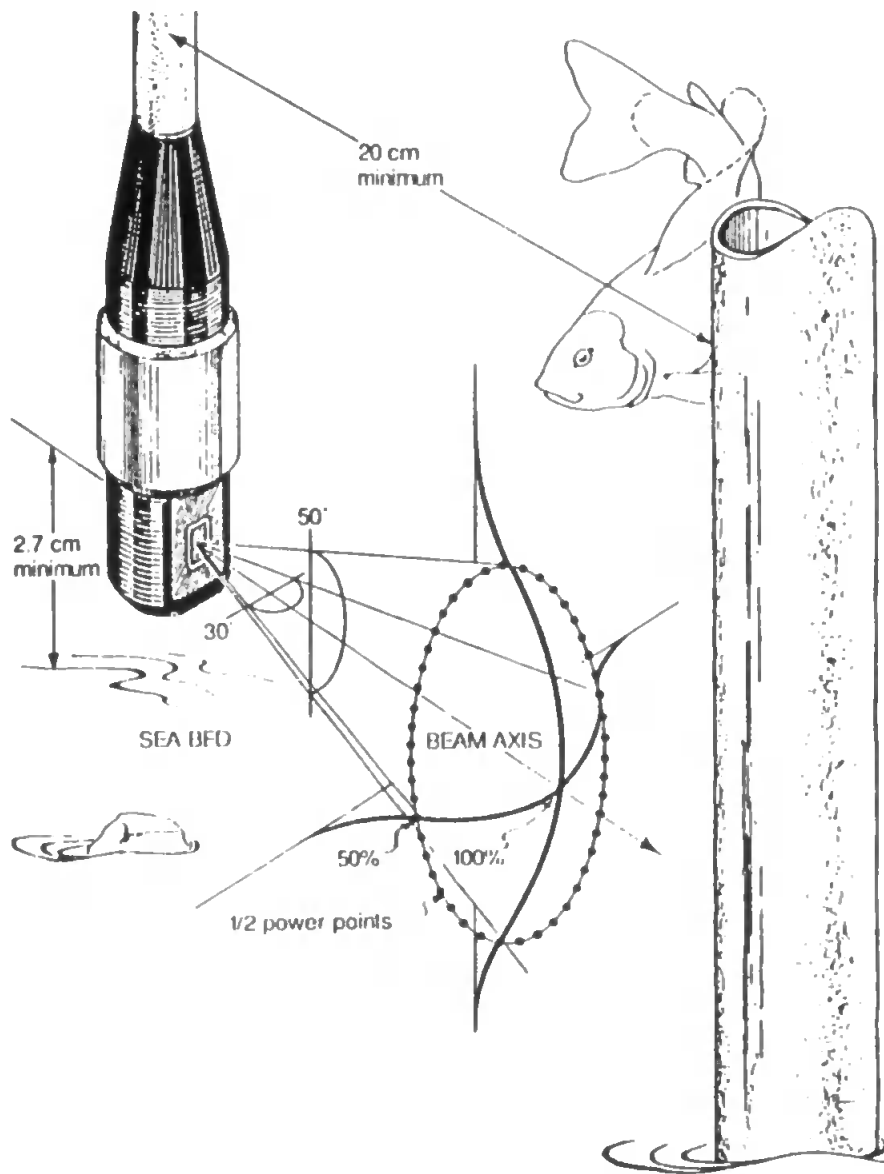


figure 3.2.3.1: OBS beam pattern (from D&A instrument company OBS 1&3 instruction manual).

While the removal of the offset value is important in the analysis of mean concentrations, it is not critical when the signal is analysed using spectral methods as the mean is removed prior to the signal being fast fourier transformed (Bendat and Piersol, 1986).

Discussion of the effect of aeration

One of the questions which was of concern is the effect of bubbles in the water column on the OBS. Although the OBS manual states that the OBS is relatively insensitive to bubbles, it is useful to consider the evidence for this so that there is confidence that the signal from the instrument does actually represent sediment and not aeration. The usual defence of the OBSs insensitivity to aeration is that the bubbles forward scatter the light which hits them while sediment backscatters the light. This explanation was questioned and discussed in depth by Huntley (1982) in a report for the Canadian Coastal Sediment Study.

Two further pieces of evidence are of interest in this area. The first relates to Downing's initial tests and calibrations of the instrument. During a calibration run he passed bubbles across the sensor instead of sediment. The OBSs showed a lack of sensitivity to the bubbles.⁴

The second piece of evidence is probably of most importance as it involves the use of the OBSs by Downing *et al.* (1981) in a dissipative surf zone. While the lower OBSs on their rig were reading suspension events in the surf zone, an OBS higher up (at 0.53cm in a mean depth of 1.5m in 1-1.5m bores) did not detect aeration and was above the level of the suspension events. In other words the OBSs were responding to sediment and not bubbles.

⁴ Note: this is not as conclusive as it first appears as the bubbles were in the size range 0.25 to 2mm, while the sediment had a mean grain size of 0.165mm.

3.3 Field experiment

3.3.1 Field site

The field site for the experiment was chosen as Sprey Point at Teignmouth in South Devon. The railway line joining Teignmouth to Dawlish runs along the coast at this location, and is supported by a seawall built by Brunel. At Sprey Point there is a protruding section of wall (figure 3.3.1.1) which is fronted by a sandy beach and flanked by beaches on each side. The position of the site is illustrated in figure 3.3.1.2.

To investigate the effect of wave reflection on the sediment dynamics, instruments were mounted on the seawall at Sprey Point. A second set of instruments was simultaneously deployed on the beach to the south to provide an experimental control.

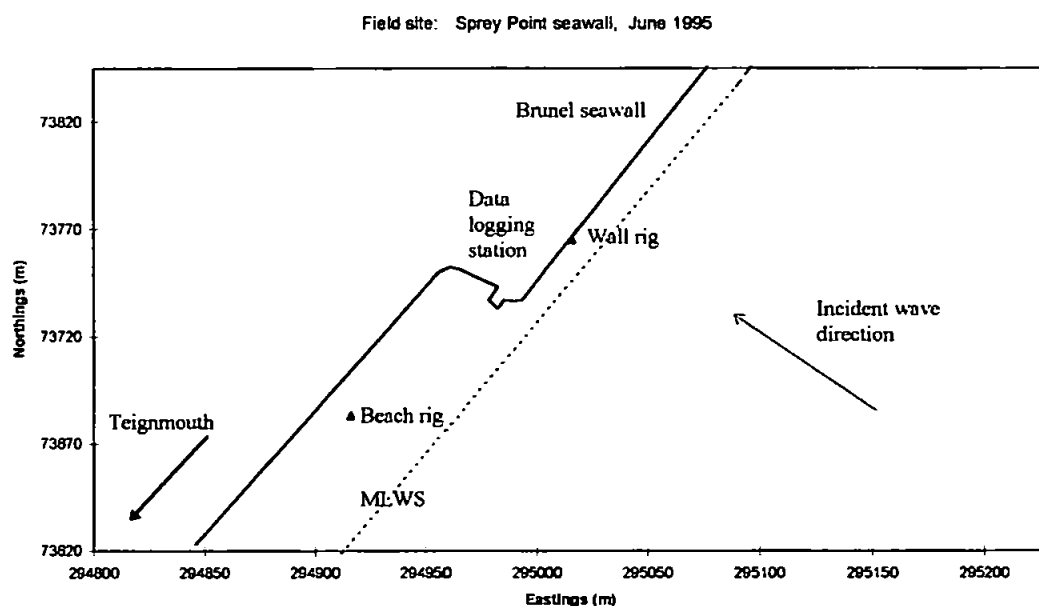


figure 3.3.1.1: Field site layout

Site description

The wall at Sprey Point is made of granite blocks, is approximately 7m high and the lower half of the wall slopes at an angle of 53° to the horizontal. The average beach gradient in front of the wall is approximately 2 in 35 which gives a beach slope of 3.27° (figure 3.3.1.3, Wall profile). The beach morphology exhibits an almost linear low tide terrace from 35m offshore of the wall to 15m offshore.



figure 3.3.1.2: Field site location.

The beach steepens between 5 and 15m from the wall and flattens again directly in front of the wall (0 to 5m). The steepening of the profile towards the wall may be expected on a natural beach, while the flattening of the profile in front of the wall is likely to be a result of wave interaction with the wall.

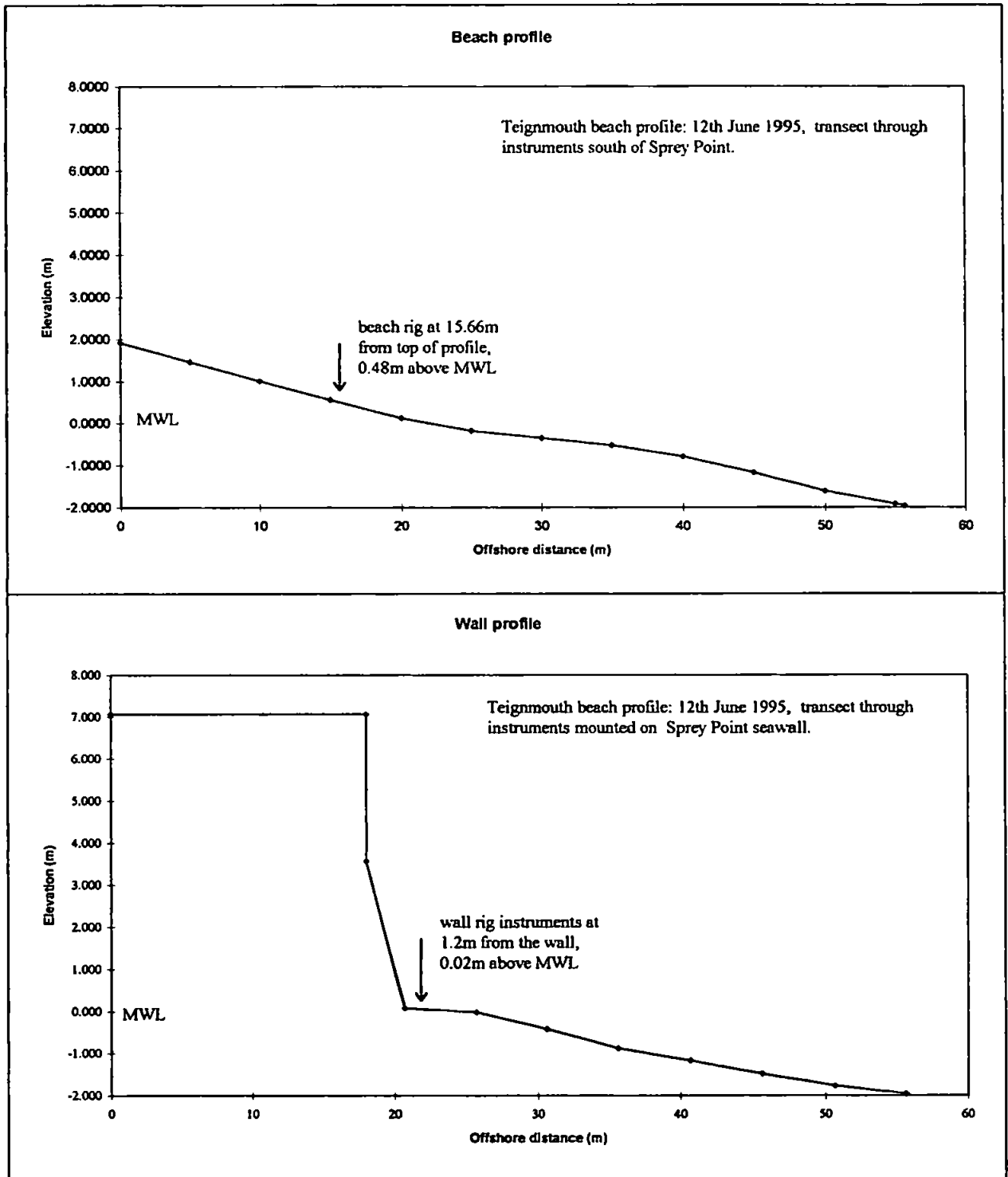


figure 3.3.1.3: Beach profiles at the wall and beach sites, Teignmouth, June 1995.

The beach to the south is of similar slope to the beach in front of the Sprey Point wall, having an average gradient of 3.8 in 55, which corresponds to a beach slope of 3.95° (figure 3.3.1.3, beach profile). This section of the beach is unaffected by the Brunel seawall except during the highest of tides. The cross section of this part of the beach shows an overall steepening of the profile from the low tide mark at 55m to the head of the beach at 0m, with a small bump in the profile between 25 and 35m. The grain size of the sand is in the range of medium quartz sand with $D_{50} = 0.24\text{mm}$.

This choice of site had several benefits.

1. At the point that the instruments are attached to the wall, there is sufficient tidal coverage to completely cover the instruments.
2. Wave reflections are strong in this region at high water.
3. The beach to the south of the site provides an excellent control site.
4. Access to the site is possible along the beach.

Beach classification at the site

The classification of the beach according to its reflectivity is indicated by the surf similarity parameter (Wright and Short, 1984). Typical values of breaker height (0.3m) and wave period (4 secs) give the surf similarity parameter a value of 15.8. This indicates that the beach has an intermediate beach classification. The surf similarity parameter (SSP) is of similar form to the Iribarren number and is as follows:

$$\text{SSP} = H_b (2\pi/T)^2 / g \tan^2 \beta \quad 3.3.1.1$$

SSP < 2.5 reflective; 2.5 to 20 intermediate, > 20 dissipative.

Increasing the slope of the beach to match that of the wall (53°) gives a lower SSP of 0.043 which, as expected, falls into the reflective category.

Wright and Short's (1984) classification delineated 6 categories of beaches based on the parameter $\Omega = H_b / w_s T$ (H_b is the breakpoint wave height, w_s is the sediment fall velocity, T is the wave period). Masselink and Short (1993) extended this parameterisation to include a description of beach morphology by introducing the 'relative tidal range' (relative tidal range = tidal range / H_b). With $H_b = 0.3\text{m}$, $w_s = 0.02\text{m/s}$, $T = 4\text{s}$, the parameter Ω has a value of 3.75. Again this indicates an intermediate beach. The tidal range was 5.2m (maximum) during the June 1995 experiment which took place during Spring tides and thus the relative tidal range was 17.67.

While Masselink and Short's model does not include this combination, it indicates that larger relative tidal ranges imply flatter, more featureless beaches. The large relative tidal range in this location may be a factor which tends to flatten the beach at Teignmouth.

Rig positions

Two rigs of instruments were installed at the site during June 1995. One rig was mounted on the wall, 35m north east of the southern corner of the Sprey Point wall protrusion. In this position the rig was just above the mean water level contour. The instruments on the wall rig were positioned 1.2m from the wall in order that they were approximately midway between the elevation antinode at the wall and the elevation node just offshore of the wall (estimated for wave periods between 3 seconds and 5 seconds). This position in the nodal structure was chosen to obtain the best coherence between elevation and velocity so that the reflection analysis would be as accurate as possible. A schematic of the instrument positions at the wall rig is given in figure 3.3.1.4.

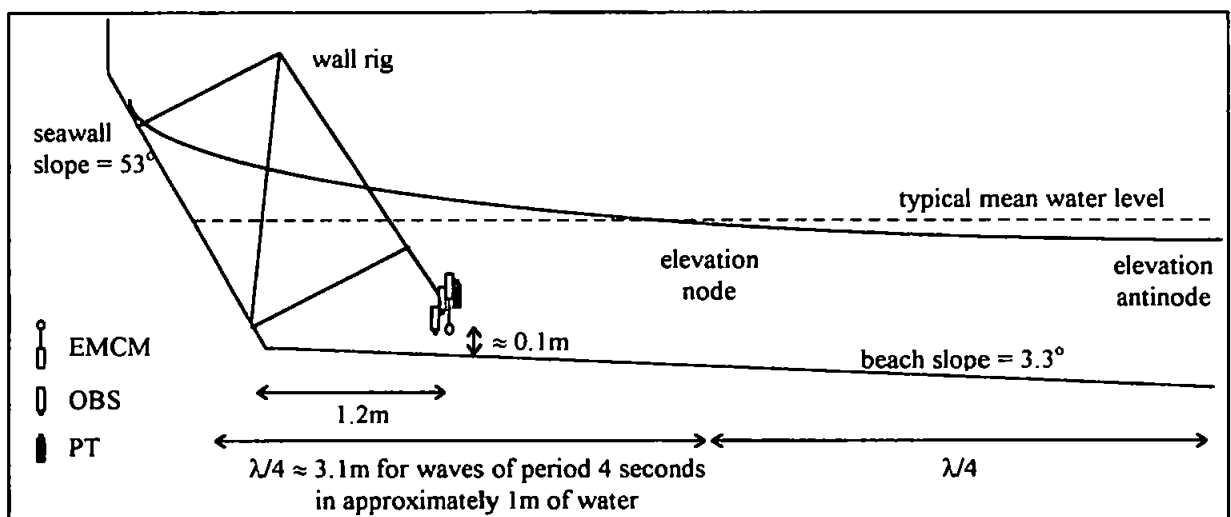


figure 3.3.1.4: Instrument positions relative to the position of nodes and antinodes.

The second rig was buried into the beach 135m south west of the wall rig on a beach contour 0.46m higher than the wall rig. It was not possible to locate the beach rig on the same contour as the wall rig because the water table remained sufficiently high as the tide ebbed. A high water table makes rig deployment particularly difficult due to the liquid nature of wet sand. The beach rig was located 15.6metres from the head of the beach. It would therefore be affected by wave reflections from the wall at the back of the beach when the water depth was greater than 1.52metres above it.

The beach rig was considered far enough away from the south corner of the Sprey Point wall that end effects of the wall would diminish before reaching the rig. Visual observations made during the experiment substantiated this.

3.3.2 Instrument layout

To measure frequency dependent wave reflection and frequency dependent sediment transport, a basic array of one pressure transducer (PT), a bi-axial electromagnetic current meter (EMCM) (measuring cross-shore and longshore velocities) and an optical backscatter sensor (OBS) were mounted on each of the two rigs. A further current meter was attached to the wall rig to obtain measurements in the vertical plane, and a second OBS was mounted above the first so that estimates of the time for the sediment to rise through the water column could be made. On both rigs, the PT and EMCM were co-located in the vertical longshore plane in order that they were the same distance from the reflector, beach or wall respectively. The EMCMs and OBSs were also co-located in the vertical (longshore) plane. EMCMs were carefully aligned using a magnetic compass and level so that cross-shore and longshore velocity measurements and sediment flux measurements could be made. The instrument layouts on the beach and wall rigs are shown in plate 3.1.

3.3.3 Wall rig

In previous experiments such as the B-BAND programme (Russell *et al.*, 1991) and the CSTAB project (Simmonds *et al.*, 1995) the approach taken to siting the instruments was to bury rigs, to which the instruments were attached, in the beach. However, during preliminary experiments at this location, rigs of this conventional style failed dramatically due to the extremely mobile nature of the sediment in front of the wall. The approach used to get around this problem was to suspend the instruments from the seawall itself. The structure designed to do this is shown in plate 3.2. The wall rig was constructed of 50×50×5mm angle iron, which was zinc coated to prevent corrosion. Sections were either welded or bolted together so that the rigs could be transported as a flat package. The rig was attached to the seawall using Hilti internally threaded anchors which were drilled into the wall and held in place using epoxy resin. The complete structure protruded 1.2m from the wall and was 3.2m high.

The wall rig was found to have the following benefits:

1. The instruments were held close enough to the bed to make the necessary measurements.
2. The instruments were mounted sufficiently far from the wall for valid estimates of reflection coefficient to be made.
3. The rig was extremely rigid and would not resonate.

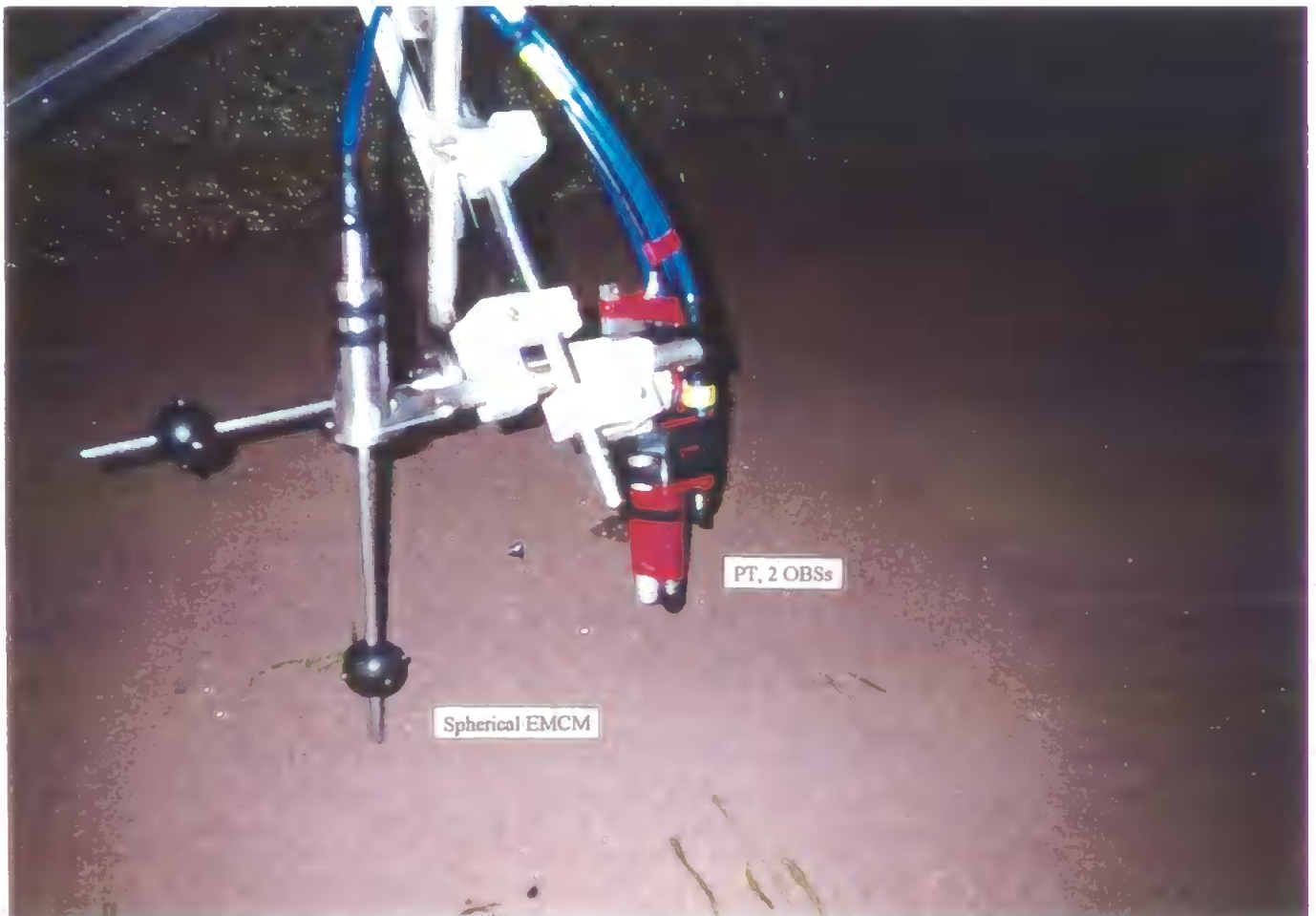


plate 3.1: Instruments on beach rig (upper) and wall rig (lower).



plate 3.2: Wall rig in action.

4. The rig was designed to present as little obstruction to the water flow as possible, and thus wave reflections were unaffected by its presence.
5. No evidence of scour around the base of the rig or by the instruments was found during the experiment.
6. The instrument cables were routed directly to the top of the wall and thus could not affect the sediment near the instruments.

3.3.4 Beach rig

The approach to deploying the instruments on the beach was a more conventional one. In this case the instruments were attached to a large frame which was buried into the beach. Like the wall rig, the frame work of the beach rig was built using 50×50×5mm zinc coated angle iron. The cables were routed from the instrument rig to the head of the beach, buried in a trench 0.5m deep. It was necessary to bury the EMCM electronics case with the base of the rig in a watertight housing attached to the rig.

During the experiment the rig remained buried and invisible to local wave activity. The beach rig layout is shown in plate 3.1. This arrangement gave the following advantages:

1. The instruments were placed at similar heights above the bed to those on the wall rig.
2. The instruments were located on a similar contour to the wall rig, and thus experienced the same incident hydrodynamic conditions.
3. No obstruction to the flow was offered by the rig as it was buried beneath the sand.
4. No scour was evident around the instruments during the experiment.

End effects of the wall were not observed to reach the beach rig - it thus remained a valid control site.

3.3.5 Data collection

Between leaving the instruments and being stored on the computer hard disk, the signals were routed along cables, filtered and sampled (figure 3.3.5.1). This process was slightly different for each instrument and this section briefly explains the method of data collection. Data was collected for 8 consecutive tides between the 12th and 16th of June, 1995.

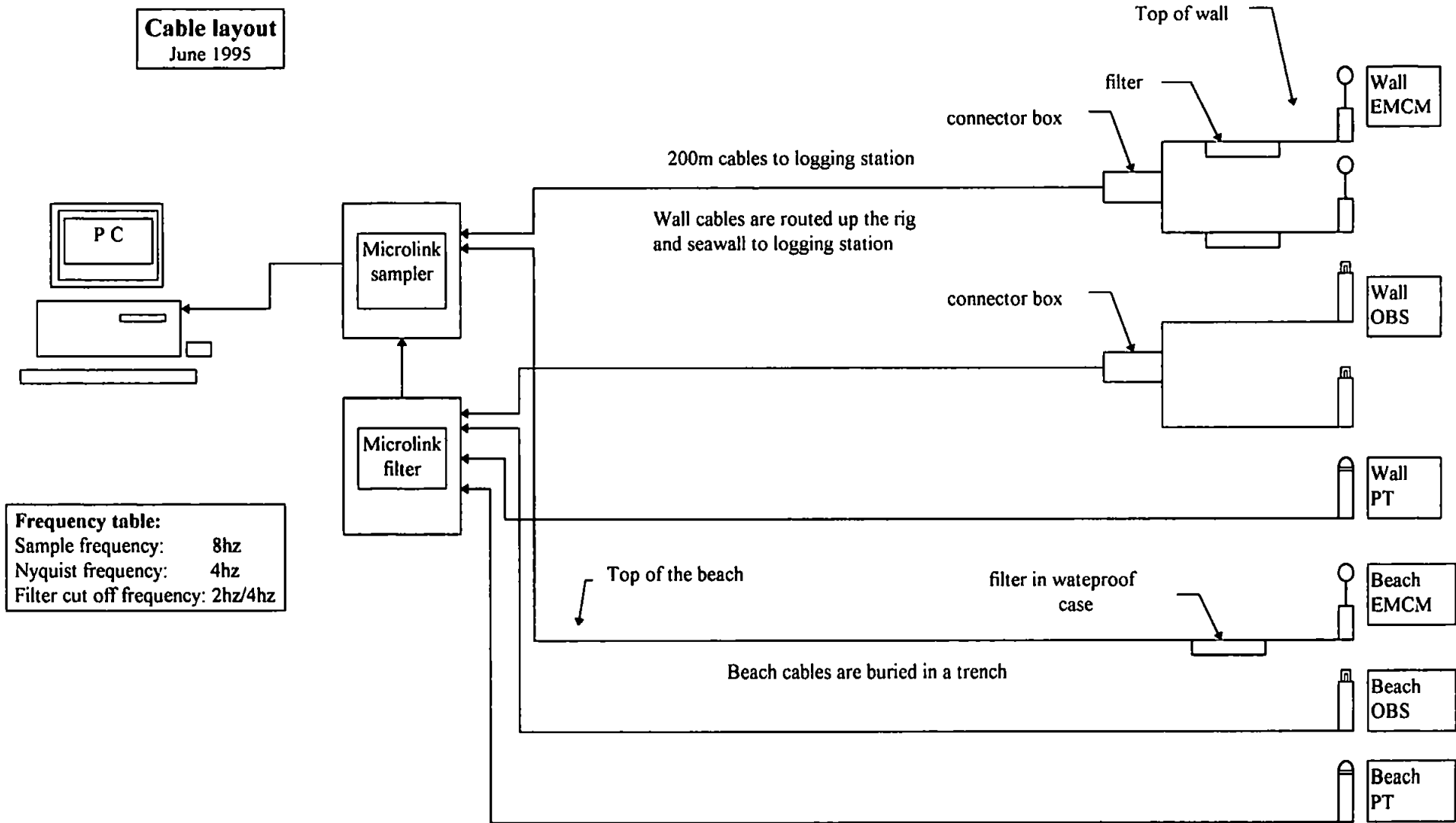
Data path for OBS and PT

The PT and OBS signals were carried directly from the instruments to the logging station in waterproof cables. Instrument cables on the wall rig were routed up the rig itself, while cables from the beach instruments were buried in a trench. The wall OBSs shared one cable from the top of the wall to the logging station having been joined in a junction box. The signals from the instruments were analogue entering the logging station, where they were anti-alias filtered immediately prior to sampling. A single ended measurement of the voltage output from the instrument was made, and this results in an output voltage relative to earth (ground), which is then subtracted from the output voltage. A single channel of data per instrument results, and this was stored on a PC.

Data path for EMCM

The current meters attached to the wall had 20m of cable between them and their electronics pod containing the filters. This was sufficient to reach the top of the wall, from where cables carried the signal to the logging station. The only difference for the beach EMCM was that the electronics pod was a waterproof one, and this was buried by the rig. The cable from the beach EMCM electronics pod to the logging station was buried with the OBS and PT cables.

The EMCM signals leaving the instruments were analogue, and were anti-alias filtered in the instruments' electronics pods. They remained analogue until sampled in the logging station. To minimise the effect of noise pick-up in the cable, between the filter pod and the logging station, a differential measurement was necessary instead of a single ended one. This means that the ground (zero) for the instrument is wired inside the cable with the signal. Noise pick-up which acts on the signal carrying wire also acts on the ground wire, and this is removed at the top of the beach when the ground is subtracted from the signal. This was not necessary in the case of the PT and OBS sensors as it was possible to put the anti-alias filters at the head of the beach, enabling a single ended measurement to be made relative to the local earth. The Microlink unit was driven by a PC and the data was transferred to the hard disk as multiplexed data.



Frequency table:

Sample frequency:	8hz
Nyquist frequency:	4hz
Filter cut off frequency:	2hz/4hz

figure 3.3.5.1: Data acquisition in the field: cable layout.

Collection frequency

There were a variety of frequencies to consider when determining the collection frequency.

They were as follows:

1. Natural frequencies of interest
2. Nyquist frequency
3. Filter cut off frequency
4. Intrinsic sampling frequency of instruments
5. Sampling frequency

Kinsman (1965) defined the incident wave band as 0.033-1 Hz and the infragravity wave band as 0.033-0.0033 Hz. Incident waves have been previously observed at Teignmouth to lie within this range and have frequencies of 0.15 to 0.2 Hz (Davidson *et al.* 1991), the roll off to turbulence occurring at frequencies higher than this. During the June 1995 experiment higher frequency wind waves were experienced, typical frequencies being in the range 0.2 to 0.3 Hz.

Sampling

Sampling took place at 8Hz, a frequency which was below the intrinsic sampling frequencies for the all the instruments, yet high enough for suitable wave reflection and sediment transport analysis to be carried out (the intrinsic sampling frequencies for the various instruments were as follows: EMCMs 10Hz; OBSs 10Hz; PT.s continuous). Such analysis of the time series requires that a spectrum is obtained.

The maximum frequency to which the spectral analysis can be carried out is given by the Nyquist frequency. With a sampling interval of Δt , the nyquist frequency is given by:

$$N_y = 1 / 2\Delta t \quad 3.3.5.1$$

A sampling frequency of 8Hz gives $\Delta t = 0.125s$ and hence $N_y = 4Hz$.

Prior to sampling it was necessary to filter the data. If frequencies above the Nyquist frequency are present in the sample, a serious form of distortion results known as aliasing, in which the higher frequency components are folded back into the spectrum below the Nyquist frequency. By filtering out the frequencies above the Nyquist frequency, this problem is avoided.

The effect of filters on the signal

The filter cut off is defined as the frequency at which a signal is reduced to half power. In the case of a normalised signal, with 1db defined as $1\text{db}=10\times\log_{10}(\text{normalised amplitude})$, the cut off for half normal amplitude is -3db. In the case of the current meters, the filters were set up by the manufacturers. The annular EMCM (beach rig) had a cut off at 4Hz while the spherical EMCMs (wall rig) had a cut off at 2Hz. The PTs and OBSs were filtered with a cut off of 4Hz using the analogue filters in the logging station (Microlink). The effect of the 2Hz and 4Hz filters on the gain can be seen in figure 3.3.5.2.

A side effect of the filters is that they introduce a small time delay into the signal, and consequently the measurements from each of the instruments can be slightly out of phase. For longer period motions this is not a problem, however for higher frequency turbulence such a time step can shift the trace significantly out of phase. The phase ϕ is related to the time delay dt by the equation $\phi = -dt \times 2\pi \cdot f$, where f is the frequency concerned.

Testing the filters using artificially generated signals showed that the phase change resulting from the time delay responded linearly with frequency as expected (figure 3.3.5.2). The time delay introduced by the filter is deduced from the slope of this line. As reflection analysis relies on the relative phase angle between the current meter and the pressure transducer, this side effect of the anti-alias filter must be taken into consideration in the analysis. To resolve this problem, the time delays for the instrument filters were measured and the pressure transducer signal was then brought into line with the current meter signal. This was done in the frequency domain prior to reflection analysis being carried out.

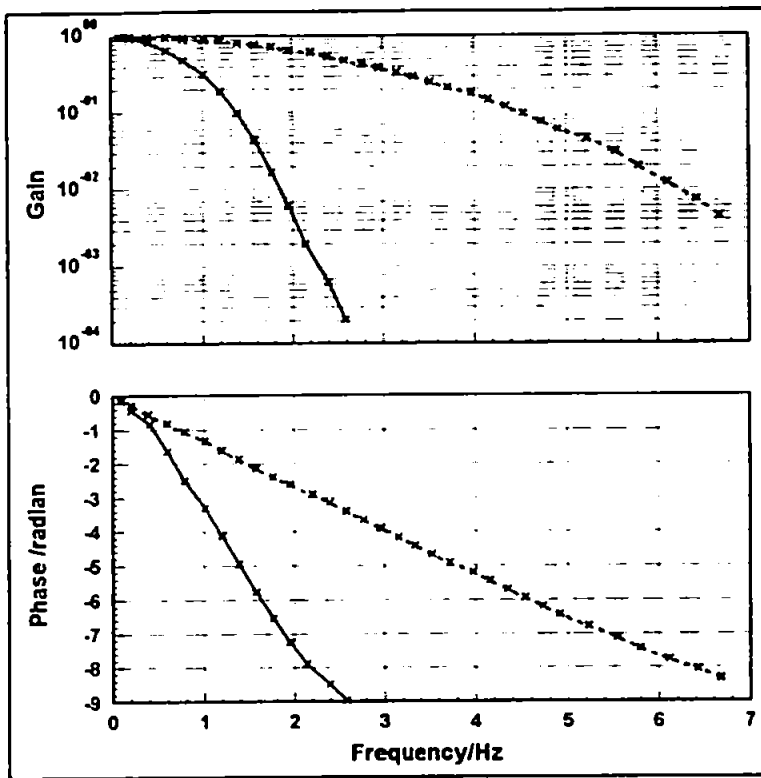


figure 3.3.5.2: Filter gain and phase characteristics for nominal 2Hz cut-off (solid line) and nominal 4Hz (dashed line).

Data collection details

Data was collected in runs of approximately 17 minutes. This length was chosen because processes would not change significantly during a single run due to tidal or meteorological effects. The instruments could therefore be considered stationary relative to the movements of tides, waves and sediment around them for the period of the run.

Each run lasted 1024 seconds and during that period 8192 data points were collected for each of the 11 channels (sampling at 8Hz). On average, 21 runs were collected on each tide. Logging started on each tide just before the instruments were first wetted, and logging ended after the tide had passed them. A sufficiently long period was allowed for the instruments to warm up (10-15 minutes) and for the field offsets to be taken before each tide. The instruments were not turned off again until further field offsets had been taken. Instrument usage is summarised in table 3.3.5.2 (overleaf). Instrument heights above the bed were taken before and after each tide using a ruler. These heights are displayed in table 3.3.5.1. Note that instrument heights were often changed between data runs.

Instrument heights above the bed for field experiment 12-16th June 1995								
measurements in cm, S = start, E = end, L = lower, U = upper								
	Beach			Wall				
	PT	EMCM	OBS	PT	EM 9170	EM 9171	OBS (L)	OBS (U)
S 12PM	32	41	35.5	12	12	N/A	9	18.5
E 12PM	33	42	36.5	9.5	9.75	N/A	6.5	16
S 13AM	17	27	21.5	9.5	9.75	N/A	6.5	16
E 13AM	17	27	21.5	9.5	10.5	N/A	6.5	16
S 13PM	17	27	21.5	9.5	10.5	10.5	6.5	16.5
E 13PM	18.75	27.5	23	9	10.5	10.5	6.5	16.5
S 14AM	18.75	27.5	23	9	N/A	10.5	6.5	16.5
E 14AM	20.1	28.4	24.8	8.6	N/A	8	5.4	15.2
S 14PM	11.7	19.6	24	8.6	28.9	8.8	5.4	15.2
E 14PM	11.7	16.2	20.8	7.7	28.05	7.9	4.5	14.3
S 15AM	11.7	21.0	16.2	7.3	20.0	7.5	4.5	14.3
E 15AM	11.9	20.8	16	7.1	19.8	7.3	4.3	14
S 15PM	7.6	20.8	16	22.4	23.4	7.3	3.6	12.5
E 15PM	8.3	21.5	16.5	21.4	22.4	6.3	2.6	11.5
S 16AM	8.3	21.5	16.5	21.4	22.4	6.3	2.6	11.5
E 16AM	8.5	22.5	17.5	22	24.5	7	3.5	12.3

table 3.3.5.1: Instrument heights above the bed before and after each tide, June 1995 deployment.

Instrument usage over period 12th - 16th June 1995								
Reference	Channel	Instrument	Instrument details	Location	Date	Direction of positive flow	Date	Direction of positive flow
1	1300	EMCM	Annular	Beach	12PM-16AM	North		
2	1301	EMCM				Onshore		
3	1302	EMCM	Spherical	Wall	12PM-13PM	Onshore	14PM-16AM	Down
4	1303	EMCM	9170			South		South
5	1304	EMCM	Spherical	Wall	13PM-16AM	South		
6	1305	EMCM	9171			Onshore		
7	1400	OBS 1	Lower	Wall	12PM-16AM			
8	1401	OBS2	Upper	Wall	12PM-16AM			
9	1402	OBS3		Beach	12PM-16AM			
10	1403	PT		Wall	12PM-16AM			
11	1404	PT		Beach	12PM-16AM			

table 3.3.5.2: Instrument channels and deployment details.

Results in chapter 5 are presented from 4 sequential tides. While the instruments are logging data, the tide rises and falls over the rigs. The slight difference in elevation of the rigs from the mean water level means that there may be different water depth over the two rigs at any time. In order to compare hydrodynamic and sediment-dynamic conditions at the wall and beach rigs, runs were compared when similar water depths covered each of the rigs. Mean water depths above the beach and wall rigs calculated from the pressure transducer signals are presented in table 3.3.5.3.

Run averaged water depths (m)								
Run	T126PM		T136AM		T136PM		T146AM	
	Wall	Beach	Wall	Beach	Wall	Beach	Wall	Beach
1	0.00	0.00	0.14	0.14	0.00	0.00	0.00	0.00
2	0.00	0.00	0.45	0.14	0.13	0.20	0.00	0.00
3	0.57	0.37	0.76	0.25	0.33	0.20	0.40	0.20
4	0.85	0.38	1.07	0.55	0.63	0.22	0.72	0.26
5	1.17	0.59	0.00	0.00	0.95	0.46	1.03	0.55
6	1.44	0.86	0.00	0.00	1.24	0.75	1.31	0.83
7	1.71	1.14	1.58	1.06	1.53	1.04	1.57	1.09
8	1.89	1.32	1.78	1.25	1.77	1.28	1.78	1.30
9	2.03	1.45	1.89	1.36	1.96	1.47	1.91	1.43
10	2.10	1.53	1.93	1.41	2.09	1.60	1.98	1.49
11	2.13	1.56	1.95	1.43	2.16	1.66	2.02	1.54
12	2.14	1.56	1.95	1.43	2.20	1.70	2.03	1.55
13	2.09	1.52	1.90	1.38	2.20	1.70	2.00	1.52
14	2.00	1.43	1.82	1.29	2.17	1.67	1.94	1.45
15	1.90	1.33	1.72	1.19	2.10	1.60	1.85	1.36
16	1.75	1.18	1.56	1.04	1.99	1.49	1.73	1.25
17	1.55	0.98	1.39	0.86	1.85	1.35	1.57	1.08
18	1.25	0.68	1.16	0.63	1.66	1.17	0.00	0.00
19	0.96	0.44	0.88	0.36	1.36	0.87	1.34	0.86
20	0.63	0.41	0.48	0.17	1.08	0.58	1.07	0.59
21	0.00	0.00	0.16	0.18	0.74	0.27	0.71	0.26
22	0.00	0.00	0.00	0.00	0.29	0.19	0.36	0.21
23	0.00	0.00	0.00	0.00	0.10	0.19	0.00	0.00

table 3.3.5.3: Mean water depths at beach and wall rigs for each run in four tides of data.

3.3.6 Environmental information

Other methods of obtaining information on the hydrodynamics and sediment dynamics of the region were employed during the experiment. They are as follows:

1. Surveying. The area was surveyed daily at low tide using a Leica TC1600 total station and prism target. This information is useful as it indicates the net movement of sediment in the region and provides the beach slope. A selection of survey data is plotted in the discussion (e.g. figure 6.4.1).
2. Sediment sampling. Samples of sediment were taken daily at the same time as the survey. The sediment was found to have a D_{50} of 0.24mm.
3. Weather charts. Weather charts for the region were obtained from the Meteorological Office using the Marinecall Metfax service. Local weather systems were monitored throughout the experiment. A typical chart is shown in figure 3.3.6.1.
4. Wind speeds were measured using an anemometer and visual observations of wave conditions were made throughout the experiment. Longshore current directions were identified at various times using neutrally buoyant floats. This information provides a useful cross reference for the pressure transducer and current meter data and is contained in the table below (table 3.3.6.1).

Summary of environmental observations made during field deployment								
Tide reference*	H.W. (BST)	Wind dir ^a	Wind speed	$H_{1/3b}$	T (secs)	Wave dir ^{a **}	Break type	Longshore Current dir ^a
T126PM	18:37	NNE	1-2 (Bft)	0.3 (m)	4	-20°	Plnge/Spill	South
T136AM	07:03	NNE	1-3	0.2 - 0.3	4 - 5	-20°	Plnge/Spill	South
T136PM	19:28	E	1	0.2	4 - 5	-10°	Plunge	South/none
T146AM	07:55		0	0.1	3 - 5	-10°	Plunge	South
T146PM	20:18	SE-NNE	1-3	0.2	4 - 5	0°	Plunge	
T156AM	08:48	SSW	<1	0.05	3	10°	Plnge/Srge	North
T156PM	21:08	SW	<1	0.1	4 - 5	10°	Plunge	North
T166AM	09:41	SW	1-2	0.1	4	10°	Plunge	North

* Protocol: T126PM stands for Teignmouth, 12 / 6 (i.e.12th June), PM tide.

** Wave direction angle given relative to shore normal (0°), positive angle indicates waves from South.

table 3.3.6.1: Environmental information.

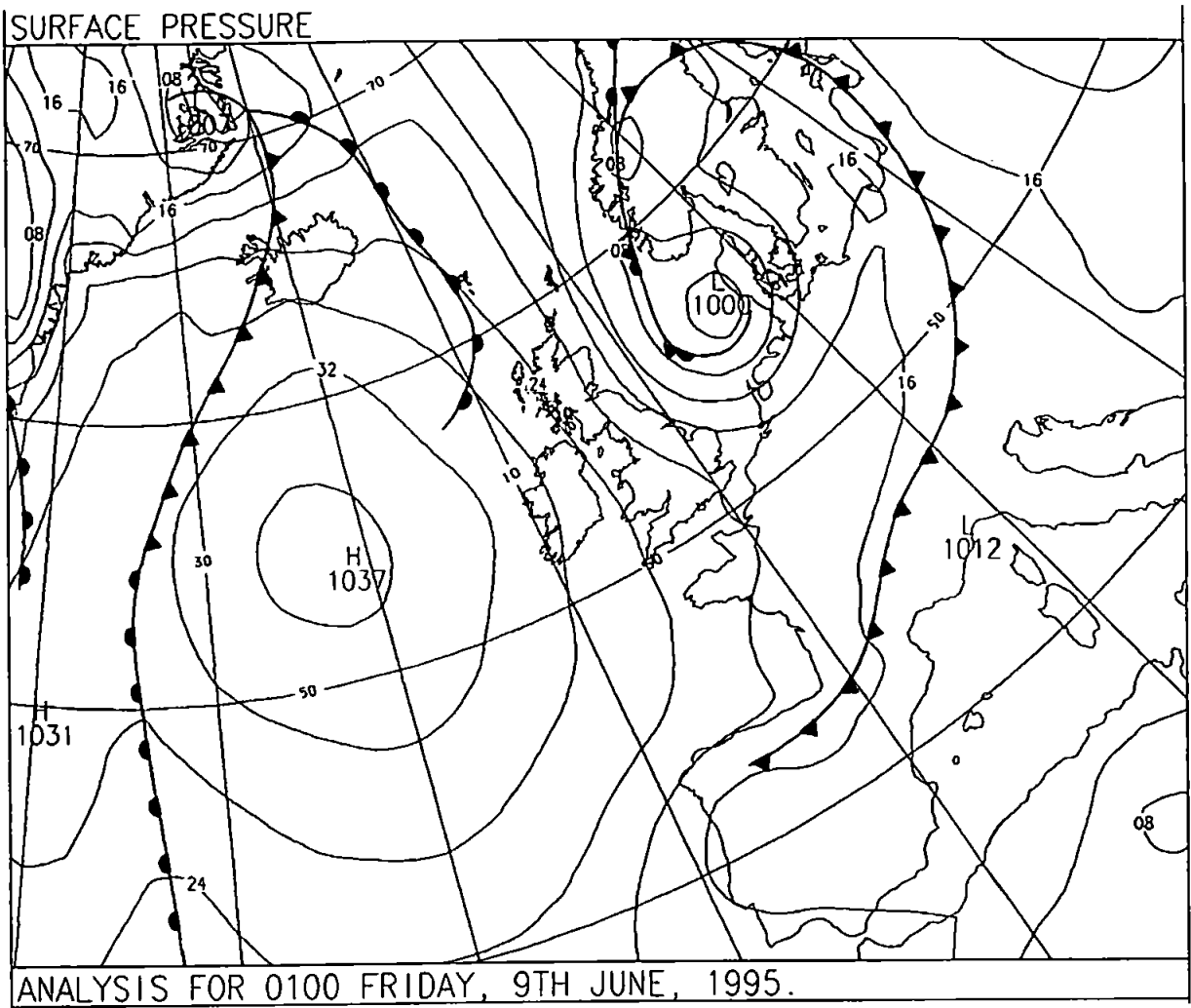


figure 3.3.6.1: Weather chart obtained immediately prior to the experiment.

3.3.7 Data processing

This section summarises the processing of the data from multiplex data to calibrated ASCII data, ready for analysis using programs written in Matlab (see also figure 3.3.7.1). Matlab is a powerful data manipulation program by Mathworks inc. which can be run on a 486 PC with sufficient memory. It is ideal for the type of data processing and analysis which is required, and is therefore used wherever possible to carry out these tasks.

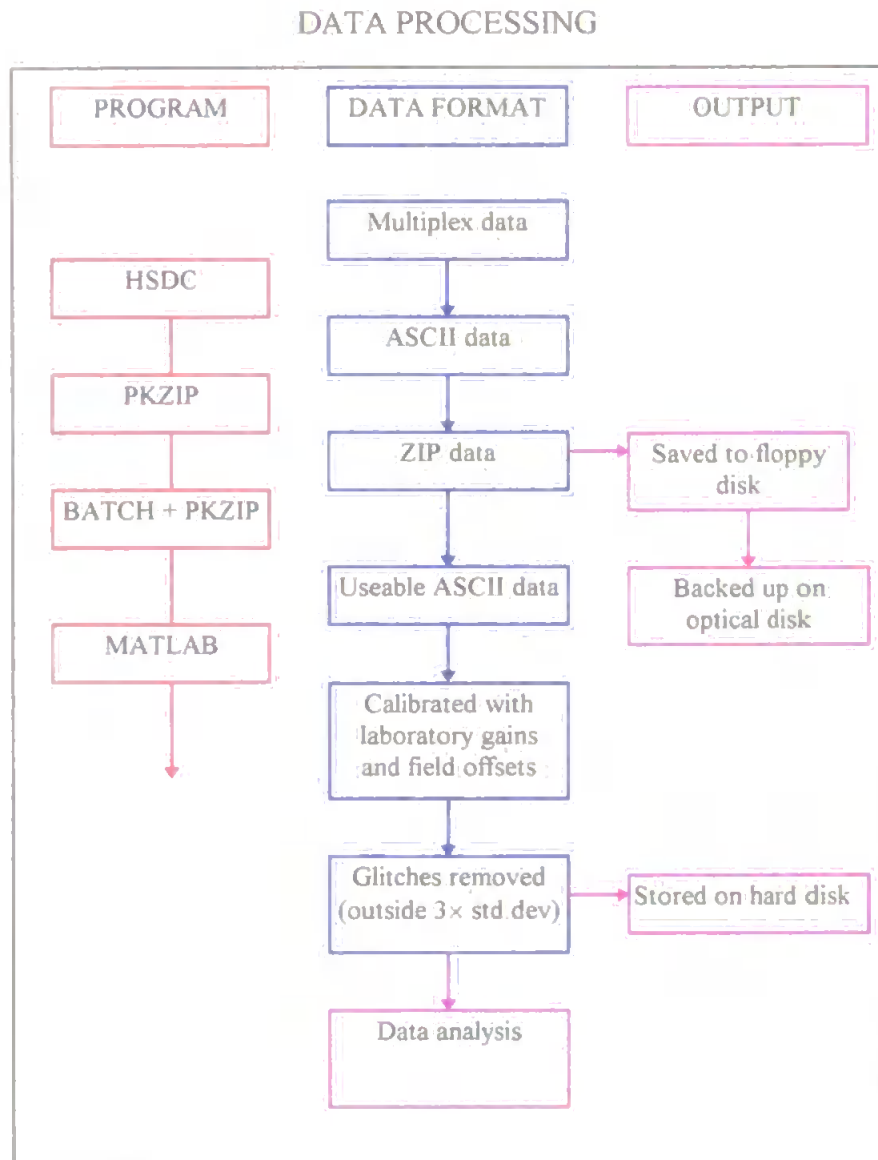


figure 3.3.7.1: Data processing path.

The electronics which filter and sample the data that comes up from the instruments were built by Microlink™. This unit was driven by PC using the program HSDC (High Speed Data Collection). HSDC outputs data in a multiplex format. This means that when data from the instruments is sampled, the 11 data points (one for each instrument channel) are listed sequentially. The 11 subsequent data points contain the data for the next sample

time, taken 0.125 seconds later. In this format the data is not user friendly and needs rearranging. This was done by HSDC, and the output consisted of a file for each individual channel of data in ASCII format. However the complete data set was large, and it was necessary to 'ZIP' the data using PKZIP. This compacted the file size by up to 60%, making it more efficient to store. This data was stored on a University of Plymouth optical disk as a backup.

To further the data processing it was necessary to 'UNZIP' the data. Individual runs, series of runs, individual channels or series of channels can be unzipped using PKZIP. This was achieved using a series of batch routines for efficiency. The result of the batch routines was that ASCII data, of the required form, arrived in the correct directory to be loaded into Matlab.

The next stage in the processing was to prepare the data for analysis. The ASCII data was loaded into Matlab, the calibrations and field offsets were applied and filter corrections made. With sufficient data in this form, Matlab was then used to carry out the data analysis contained in the next chapter.

3.4 Summary

This chapter has described a field experiment to measure and observe the hydrodynamic and sediment dynamic processes in front of a seawall. Pressure transducers, electromagnetic current meters and optical backscatter sensors were used to measure wave elevations, currents and the resulting sediment in suspension in front of a seawall at Teignmouth in South Devon in June 1995.

Two adjacent sites were chosen to make these measurements; one site consisted of an intermediate beach backed by a seawall (Sprey Point), the other was a natural beach receiving the same incident wave conditions as the seawall (south of Sprey Point). This set up was chosen so that suitable comparisons could be made between beach sediment dynamics and the dynamics associated with a more reflective structure. A specially designed rig was required to hold the instruments in place in front of the seawall at Sprey Point. A second rig was built to hold instruments in position on the beach to the south.

Instruments were co-located at the two sites so that the frequency dependent sediment transport could be ascertained and considered in relation to the effect of wave reflection from both the beach and the seawall. Similar instrument arrays were deployed at comparable heights on each of the two rigs so that valid comparisons could be made.

During the June 1995 experiment data was collected for 8 consecutive tides. Instrument heights and offsets were taken before and after each tide. A detailed survey of the local beach topography was carried out each day, and sediment samples were taken to gain an overall picture of the sediment movement during the experiment.

The data obtained from the instruments logging at high frequency was later processed so that frequency dependent wave reflection and sediment transport analysis could be carried out. This analysis will provide information on the effect that the wave reflection from the seawall has on the local sediment dynamics in front of the wall.

CHAPTER 4: Data analysis techniques

4.1 Introduction

Having collected raw data and performed calibrations as described in the previous chapter, it was necessary to build a theoretical basis for analysing the data. The calculation of means and variances is routinely carried out on wave data and these procedures are omitted from this chapter. Frequency dependent wave reflection and sediment transport analyses are less straightforward however, and the use and extension of the existing techniques requires a firm understanding of the basic principles employed by these techniques. The purpose of this chapter is therefore to build suitable procedures for analysing the hydrodynamic and sediment dynamic data.

Time varying components of the signal are first demeaned and then Fourier transformed into the frequency domain. Autospectra (power spectra) and cross spectra can then be obtained from the transforms of the data to reveal the relative contributions of the various frequency components to the process. Combining hydrodynamic features of the data allows the frequency dependent reflection coefficient to be obtained. Incorporating the sediment into the analysis leads to a better understanding of the sediment response to wave reflection. The structure of this chapter thus follows the outline: spectral analysis, reflection analysis, analysis of suspended sediment response to wave reflection.

4.2 Spectral analysis

Introduction to the Fourier Transform

In order to transform a time series of data into the frequency domain it is necessary to use a Fourier transform. A computationally efficient method of doing this is to employ the Fast Fourier Transform (FFT) algorithm. When the number of points sampled is a power of two, a further enhancement can be made by employing the Cooley-Tukey procedure which increases computational speed (Cooley and Tukey, 1965). Information on the mechanics of the FFT is contained in Bendat and Piersol (1986). Matlab's FFT uses a fast Radix-2 FFT which also requires that the number of sample points is a power of two. Matlab's spectral analysis programme is based on a procedure in Oppenheim and Schaffer (1975) to which reference can be made for further information.

The FFT of an N point stationary data series returns N-1 complex numbers which are anti-symmetrical about zero frequency. The first half of the raw FFT estimate can thus be discarded, and the remaining N/2 values represent the magnitude and phase of the sine waves which make up the signal.

Considering an N point time series $x(t)$ which is FFT'd, the second half of the output from the FFT is complex. This can be represented as:

$$x(t) \xrightarrow{\text{FFT}} X(f) = \sum_{n=1}^{N/2} (a + ib) \quad 4.2.1$$

The magnitude and phase of each raw Fourier estimate is given by:

$$|X| = \sqrt{a^2 + b^2} \quad 4.2.2$$

$$\theta = \tan^{-1} \frac{b}{a} \quad 4.2.3$$

The maximum frequency covered by the FFT, the Nyquist frequency, is given by:

$$N_y = \frac{1}{2 \cdot \Delta t} \quad 4.2.4$$

where Δt is the sampling frequency between data points. With N/2 raw Fourier estimates between zero and the Nyquist frequency, the frequency f_n of the nth component can be calculated using the equation

$$f_n = 2 \frac{N_y}{N} n. \quad 4.2.5$$

As it stands the Fourier transform of the time series is not as useful as it may first appear. In order to obtain a stable estimate of the variance within a certain frequency band it is

necessary to take several estimates of what is occurring at each frequency. This is accomplished using spectral analysis.

The Spectrum

The spectrum is, in effect, an accumulation of Fourier transforms which have had their magnitude squared and have been normalised to a unit frequency band. By increasing the number of estimates of the Fourier transform at a certain frequency, so the confidence in the spectrum increases. The Welch method of power spectral estimation is a generally accepted method for carrying this out, and this is the procedure used by Matlab's spectral analysis routine.

It is first necessary to remove the mean of the signal to ensure that no anomalous low frequency peaks occur in the spectrum. Spikes and trends must also be removed from the data. In this case, spikes which were outside three times the standard deviation of the signal were removed and replaced with the average of the points either side. Next, the data is divided into sections of m points, which are fast Fourier transformed. Prior to being FFT'd however it is necessary to window the data. This ensures that the end points of each section are zero. A window with tapered edges (e.g. Hanning or Welch) reduces leakage to other frequencies, however it results in some information being lost or damped where the window is applied. By taking further windowed sections of data which overlap the windowed parts the problem is reduced, and the total variance of the signal can be more accurately maintained.

Each of the sections, including the overlapped sections, is then Fourier transformed. Obviously there will now be $m/2$ raw Fourier estimates between zero and the Nyquist frequency for each section taken. It is from here that the power spectra, cross spectra, phase and coherence spectra are obtained, prior to being accumulated (i.e. averaged). This averaging results in stable estimates of these parameters. Frequency dependent reflection analysis takes place after the accumulation of the data so that the most accurate phase information is obtained. The phase information is preserved in the cross spectra.

Power spectrum

The power spectrum represents the variance in the signal, as it gives the square of the amplitude. Prior to being accumulated, the Fourier estimate is multiplied by its complex

conjugate. In terms of the Fourier components, this can easily be shown to be equal to the square of the magnitude (given above).

At any frequency within each section, the contribution to the power spectrum is calculated from the raw Fourier estimate:

$$\begin{aligned} P_{xx} &= (a + ib) \times (a - ib) \\ P_{xx} &= a^2 + b^2 \end{aligned} \tag{4.2.6}$$

These contributions are then accumulated according to frequency and are representative of the total variance of the signal. This is in fact a 'periodogram'. The power spectrum is obtained by dividing the periodogram by the band width. The band width, denoted Δf hereafter, is obtained simply by dividing the Nyquist frequency by the number of estimates being made through frequency up to the Nyquist frequency. When this analysis is applied to wave records, the result can be used to determine the dominant frequencies of the wave action, the amount of energy present, and also such parameters as the significant wave height and velocity.

Cross spectrum

The cross spectrum provides a measure of the frequency dependence of the co-variance of two signals. It is obtained by multiplying the Fourier estimate of one signal by the complex conjugate of the Fourier estimate of the second signal. The contribution at any frequency can be expressed in terms of the Fourier constituents as:

$$\begin{aligned} P_{xy} &= (a + ib) \times (c - id) \\ P_{xy} &= (ac + bd) + i(bc - ad) \end{aligned} \tag{4.2.7}$$

The real part represents the in-phase oscillations and is termed the *co-spectrum*. The imaginary part represents the oscillations which occur in quadrature, and is termed the *quadrature spectrum*.

Huntley and Hanes (1987) argued that sediment which was repeatedly suspended at either a crest or trough of velocity would be moved in that direction, resulting in a net transport due to a purely oscillatory flow. They used the co-spectrum to illustrate this, as it is the in phase oscillations which result in a net sediment transport. The quadrature spectrum would thus represent suspension events occurring when the oscillatory component of velocity is zero, there being no net transport in any direction.

Phase spectrum

The phase spectrum arises from the complex Fourier estimates and can be expressed as:

$$\theta = \tan^{-1}\left(\frac{bc - ad}{ac + bd}\right) \quad 4.2.8$$

at any frequency. Phases of zero and 2π between velocity and sediment mean that the peaks and troughs occur at the same time, thus indicating transport in the direction of wave travel. However, peaks in the time series which are π or $-\pi$ radians out of phase represent transport which is in the direction opposite to that of wave travel.

Coherence

The coherence between two components at any frequency is given by:

$$C_{xy} = \frac{|(P_{xy})^2|}{P_{xx} \times P_{yy}} \quad (0 < C_{xy} < 1) \quad 4.2.9$$

It is essentially a 'goodness of fit' measurement representing to what degree the signals x and y are correlated at any frequency. For measurements of velocity and elevation of uni-directional waves in shallow water one might expect a high coherence between the signals, but the non-linear nature of sediment response to the velocity field (which results in the characteristic spiky time series) means that estimates of coherence between the velocity and sediment will be lower than those obtained with the elevation and velocity time series. Where there is a spread in the wave direction spectra, there will also be de-correlation between elevation and velocity, and this will give rise to a decrease in coherence also.

Confidence

A statistical approach to evaluating the likelihood of each individual peak in the spectrum being real can be adopted, and this depends on how many sections the data is split into prior to being FFT'd and averaged. The number of degrees of freedom of the estimate where 50% overlapping is applied is given by Nuttal (1971) as:

$$ndf = 3.82 Nd - 3.24 \quad 4.2.10$$

where Nd is the number of non-overlapping sections. Multiplication factors for error bars on each spectral peak can then be obtained using figure 4.2.1 for the required level of confidence (usually 95%). As the number of non-overlapping sections increases, so does the number of degrees of freedom. The resulting decrease in spectral resolution is thus accompanied by a narrowing of the confidence interval for the spectral peak. It is thus necessary to produce spectra which have sufficient frequency resolution to identify the processes of concern while retaining enough confidence in the peaks observed.

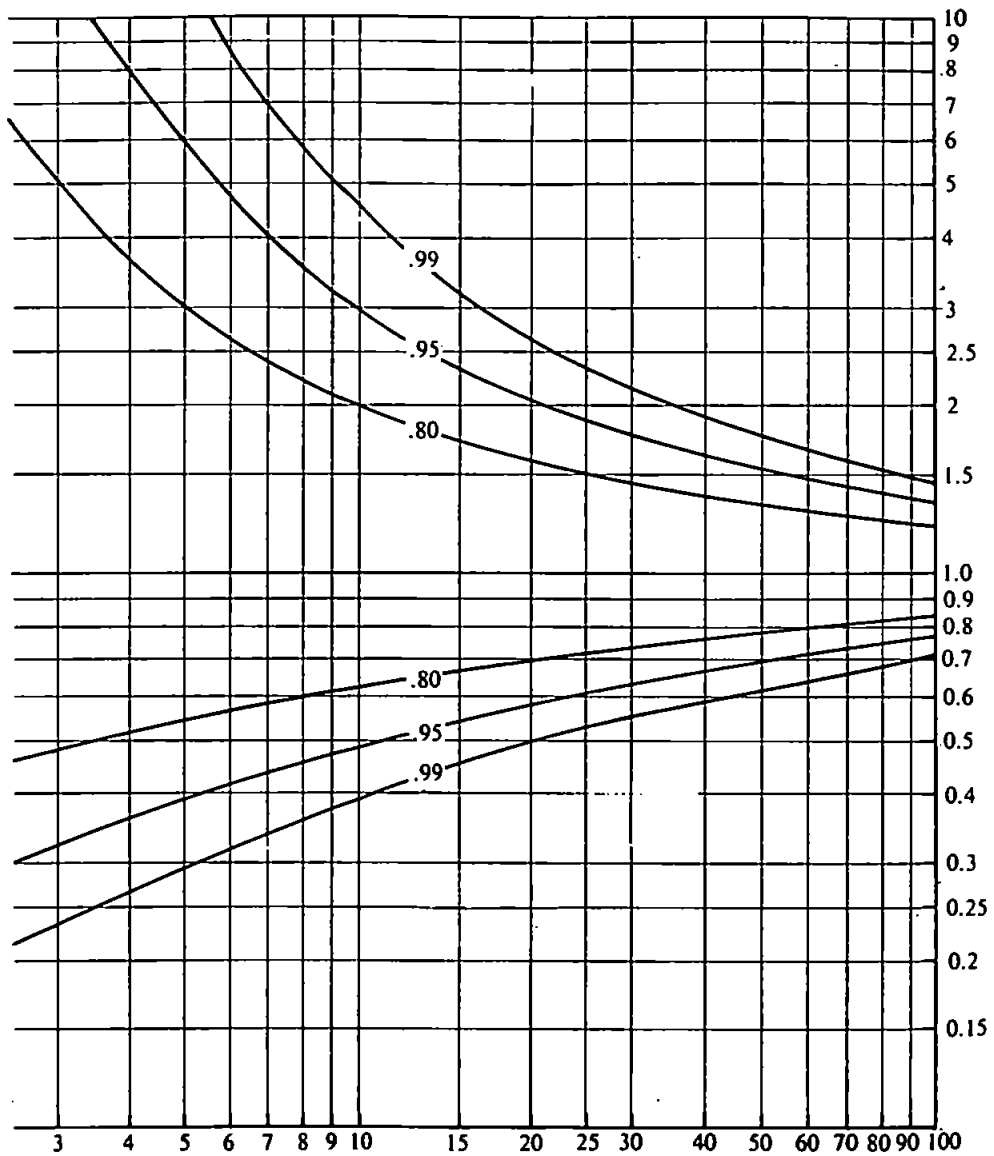


figure 4.2.1: Spectral peak multiplication factor for confidence interval (y axis) against number of degrees of freedom (x axis) for 80, 95 and 99 percent confidence from Jenkins and Watts (1968).

The Spectral Density Function and the Periodogram

By definition, the sum of the values given in a periodogram is equal to the variance in the time series. As mentioned earlier, the power spectrum or spectral density function (S.D.F., denoted S_{xx}) is obtained by dividing the periodogram by the bandwidth (Δf). This normalised form of the spectrum is useful as it allows the comparison of spectra with those obtained by other workers. The variance of the signal, the sum of the values in the periodogram and the S.D.F. are therefore related by the equation:

$$\sigma^2 = \sum_1^N \text{periodogram} = \sum_1^N S_{xx} \times \Delta f \quad 4.2.11$$

where N is the number of estimates between zero and the Nyquist frequency.

This relationship is useful in determining the variance in certain frequency bands from the spectrum. It can also be used to determine the wave height. In the version of Matlab used, the S.D.F. is related to the output S_{xx_Matlab} by the equation:

$$S_{xx} = \frac{S_{xx_Matlab}}{N_y} \quad 4.2.12$$

In order to obtain wave heights from the S.D.F., first note that the R.M.S. of the signal is equal to the square root of the variance. Therefore

$$\text{RMS} = \sqrt{\sum_1^N S_{xx} \times \Delta f} \quad 4.2.13$$

from which a statistical relationship is used to reveal an expression for $H_{1/3}$ as follows:

A sine wave of amplitude a has an RMS of $a/\sqrt{2}$, i.e. $a = \text{RMS} \times \sqrt{2}$. The wave height H is actually $2 \times a$, and so $H = 2\sqrt{2} \cdot \text{RMS}$. With $H_{1/3} = \sqrt{2} H$, the equation for $H_{1/3}$ becomes:

$$H_{1/3} = 4 \times \sqrt{\sum_1^N S_{\eta\eta} \times \Delta f} \quad 4.2.14$$

When determining the wave height in different frequency bands (e.g. if the infragravity wave height is required) it is important that energy from an unrelated frequency does not contribute to the estimate. It is thus necessary to identify the frequency band contributing to the waves of particular interest and sum over that band. In effect this is equivalent to summing the values of the periodogram within the frequency band of interest to obtain the variance within that frequency band, and applying the same statistical relationships for the significant wave height as above.

Interestingly, this analysis, when combined with a small amount of linear wave theory to estimate wave elevation from velocity, means that in the case of a unidirectional wave field it is possible to estimate the wave height from a current meter time series, provided the current meter is correctly aligned and the water depth is known.

Sediment flux

The oscillatory flux for the complete record, calculated in the time domain is simply:

$$\overline{u'c'_s} = \frac{1}{N} \sum_{n=1}^N (u - \bar{u}) \times (c_s - \bar{c}_s) \quad 4.2.15$$

This includes oscillations due to both incident waves and turbulence. The oscillatory flux can be calculated in the frequency domain, and is equivalent to the area under the co-spectrum:

$$\overline{u'c'_s} = \sum_1^N \text{Suc}_s \times \Delta f \quad 4.2.16$$

By summing within a particular frequency band, the sediment flux within that frequency band can be calculated.

Errors for this calculation were found to be small, an example being run 6 of T136PM where the value of $\overline{u'c'_s}$ calculated from the time series was 0.0020 kg/m²/s while the area under the co-spectrum gives a mean flux of 0.0019 kg/m²/s. This small difference results from the windowing of data within the spectral analysis procedure.

Units

The units of the S.D.F. for an input signal in metres, are in metres² / hz, while for both Matlab's output ($S_{xx_{\text{Matlab}}}$) and a periodogram the units are m².

Further units of interest are as follows:

	S.D.F. (normalised spectrum)	Periodogram, Matlab output
elevation power spectrum $S_{\eta\eta}$	m ² / hz	m ²
velocity power spectrum S_{uu}	m ² / s ² / hz	m ² / s ²
sediment power spectrum $S_{c_s c_s}$	(kg / m ³) ² / hz	(kg / m ³) ²
velocity-sediment cross spectrum S_{uc_s} (Co-spectrum)	kg / m ² / s / hz	kg / m ² / s
phase spectrum	radians	radians

table 4.2.1: Units of various forms of spectra.

Worked example

In this experiment, data was collected at 8Hz for 17.0667 minutes giving 8192 data points for each channel in each run. This is suitable for the Radix-2 FFT, as the solution for n of $2^n = 8192$ gives $n=13$. This length of time relative to the complete tidal cycle is considered short enough for the signals to remain stationary (c.f. Russell *et al.*, 1991; Davidson *et al.*, 1993), and spectral analysis is thus suitable. Signals were routinely de-measured and de-trended and typically split into sections of 512 points prior to being Hanning windowed (this window was found to give the smoothest spectra with the most accurate estimate of variance). The sections of the time series were then FFT'd, crossed (either with themselves to obtain autospectra, or with other series to obtain cross spectra) and accumulated. This leads to 256 estimates through frequency up to the Nyquist frequency of 4Hz. The band width in this case would be 1.5625×10^{-2} Hz.

The 16 non-overlapping sections result in 57.88 degrees of freedom, and the 95% error bars on spectral peaks are thus provided by multiplying the peak values by 0.71 (lower) and 1.49 (upper) (Jenkins and Watts, 1968). Where cross spectra were obtained, further confidence in the peaks of interest was gained by examining the coherence between the two signals.

Spectral analysis of the calibrated raw data reveals information on the wave period and the distribution of energy through frequency. Cross spectral analysis gives insight into the way in which two variables such as sediment suspension and current velocity interact. More complicated analysis procedures are required to obtain the frequency dependent reflection coefficient. Wave reflection analysis techniques can be extended to analyse the sediment transport associated with incident and reflected waves. These techniques use many of the basic principles discussed in this section, and are investigated further in the remaining sections.

4.3 Wave reflection analysis

4.3.1 Introduction

This section describes the methods available for the analysis of wave reflection using co-located current meters and elevation sensors. Testing the hypothesis that the reflection of wave energy over the foreshore increases the energy available for sediment suspension in that area requires that the process of wave reflection is measured. Whilst it is not possible to measure the reflection coefficient and its dependence on frequency directly, it is possible to calculate it from the time series of elevation and current meter data.

With a proper understanding of the workings and drawbacks of the methods for calculating the reflection, the analysis can be extended to include the sediment response. This section focuses on three methods suitable for analysis of the frequency dependent reflection coefficient. They are: the time domain method (Guza *et al.*, 1984), a frequency domain method (Tatavarti *et al.*, 1988) and the principal component analysis (PCA) applied to the frequency domain method.

4.3.2 Time domain analysis

Guza *et al.* (1984) give 'Plus Characteristic' (PC) and 'Minus Characteristic' (MC) equations for determining the incoming and outgoing surface elevation time series of shallow waves on a beach. They give:

$$\begin{aligned} \text{PC}(t) &= (\eta(t) + \sqrt{\frac{h}{g}}u(t)) / 2 \\ \text{MC}(t) &= (\eta(t) - \sqrt{\frac{h}{g}}u(t)) / 2 \end{aligned} \tag{4.3.2.1}$$

The characteristics are the time series of the incoming and outgoing waves' elevation, calculated directly from the time series of elevation and velocity. These equations arise from linear theory as follows:

The velocity potential derived from the boundary conditions associated with linear theory is:

$$\phi = \frac{-a \cdot g}{\sigma} \cdot \frac{\cosh k(z+h)}{\cosh kh} \sin(kx - \sigma t) \tag{4.3.2.2}$$

Surface elevation is given by:

$$\eta = \frac{1}{g} \left[\frac{\partial \phi}{\partial t} \right]_{z=0} \quad 4.3.2.3$$

hence

$$\eta = a \cos(kx - \sigma t) \quad 4.3.2.4$$

Horizontal particle velocity is given by:

$$u = - \frac{\partial \phi}{\partial x} \quad 4.3.2.5$$

hence

$$u = \frac{g a k \cosh k(z+h)}{\sigma \cosh kh} \cos(kx - \sigma t) \quad 4.3.2.6$$

At the surface and in shallow water (where $h/\lambda < 0.05$),

$$\frac{\cosh k(z+h)}{\cosh kh} \approx 1 \quad 4.3.2.7$$

So

$$u = \frac{g a k}{\sigma} \cos(kx - \sigma t) \quad 4.3.2.8$$

The velocity and elevation time series for progressive waves are thus in phase. Using the equations for elevation and velocity above it is possible to arrive at an expression for surface elevation from the velocity by dividing 4.3.2.4 by 4.3.2.8, and this is:

$$\eta(t) = \frac{\sigma}{gk} u(t) \quad 4.3.2.9$$

Since the celerity can be expressed as $c = \sigma / k$

$$\eta(t) = \frac{c}{g} u(t) \quad 4.3.2.10$$

For incoming waves, u is +ve maximum (+ve implies onshore in this case) when η is maximum, while for outgoing waves, u is -ve maximum when η is maximum. The time series of waves which are incoming can thus be expressed as:

$$\eta_{in}(t) = \left(\eta(t) + \frac{c}{g} u(t) \right) / 2 \quad 4.3.2.11$$

Similarly the time series of outgoing waves is given by:

$$\eta_{out}(t) = \left(\eta(t) - \frac{c}{g} u(t) \right) / 2 \quad 4.3.2.12$$

In this equation the celerity, c depends on the wave frequency which in turn depends on water depth and wavelength. In shallow water, celerity is independent of frequency and wavelength provided the depth remains constant.

As $c = \sqrt{gh}$ in shallow water, the equations become:

$$\eta_{in}(t) = \left(\eta(t) + \sqrt{\frac{h}{g}}u(t) \right) / 2 \quad 4.3.2.13$$

$$\eta_{out}(t) = \left(\eta(t) - \sqrt{\frac{h}{g}}u(t) \right) / 2 \quad 4.3.2.14$$

It is thus possible to arrive at the time series of the incoming and outgoing wave elevations in shallow water.

It would be possible at this point to calculate a bulk reflection coefficient by comparing the square root of the ratios of the energies in the signals as follows:

$$K_r = \sqrt{\frac{E_{in}}{E_{out}}} \quad 4.3.2.15$$

However, more information can be obtained about the hydrodynamics by comparing the spectra of the incoming and outgoing time series. As the spectrum provides a measure of the variance in different frequency bands (which is proportional to the amount of energy), the frequency dependent reflection coefficient is simply the square root of the ratio of the spectral estimates in each frequency bin. If S_{ii} is the spectrum of incoming waves and S_{oo} is the spectrum of outgoing waves the frequency dependent reflection coefficient $R(f)$ is given by:

$$R(f) = \sqrt{\frac{S_{ii}}{S_{oo}}} \quad 4.3.2.16$$

This time domain method for investigating the incoming and outgoing wave energies has a major advantage over its counterparts, and that is its simplicity. It does however have disadvantages. The first is that it can only work where the sensors are not at a node or antinode in elevation or velocity. When this occurs, values of zero velocity or elevation send the reflection coefficient to unity. It is possible however to guard against this by checking the coherence between the elevation and velocity signals. Coherence drops at nodes and antinodes and the reflection can only be studied when the coherence is sufficiently high. Huntley *et al.* (1995) examined the problem of the effect of high noise to signal ratios (i.e. small signals or large amounts of noise) by adding noise to a simulated signal, and comparing the calculated reflection coefficient with the true reflection coefficient for different amounts of coherence between the signals. Their results suggest that for high and low reflection coefficients ($R > 0.8$ and $R < 0.3$ respectively), the bias towards unity is less than 10% provided the coherence is greater than 0.4.

The second disadvantage of the time domain technique is that shallow water wave theory is required to formulate the solution. For the study of long waves on natural beaches this is not a great problem, however in the study of incident waves reflecting on a seawall at high water, the condition for intermediate water is often met. By carrying out a similar analysis in the frequency domain it is possible to eliminate this problem, and this is covered in the second method.

4.3.3 Frequency domain method

Huntley *et al.* (1995) point out that the reflection coefficient can be written as follows:

$$R1^2(f) = \frac{S_{\eta\eta}(f) + S_{uu}(f) - 2 \times \text{re}(S_{\eta u}(f))}{S_{\eta\eta}(f) + S_{uu}(f) + 2 \times \text{re}(S_{\eta u}(f))} \quad 4.3.3.1$$

where $S_{\eta\eta}$ is the spectrum of elevation, S_{uu} is the spectrum of velocity transformed to elevation units and $\text{re}(S_{\eta u})$ is the co-spectrum between η and u . This arises from the time domain method and can be proven in terms of the Fourier coefficients which make up the spectra. This becomes useful when attempting to examine the response of the sediment to the wave reflection.

Consider the Fourier constituents of the elevation and velocity transforms:

$$\begin{aligned} \eta(t) &\xrightarrow{\text{FFT}} \sum a + ib \\ \hat{u}(t) &\xrightarrow{\text{FFT}} \sum c + id \end{aligned} \quad 4.3.3.2$$

where $\hat{u}(t) = \frac{c}{g}u(t)$.

The incoming and outgoing waves of Guza's method are given by:

$$\begin{aligned} \eta_{\text{in}} &= (\eta + \hat{u}) / 2 \\ \eta_{\text{out}} &= (\eta - \hat{u}) / 2 \end{aligned} \quad 4.3.3.3$$

The incoming and outgoing components can be expressed in terms of the Fourier constituents at each frequency as follows:

$$\begin{aligned} \eta_{\text{in}} &= (a + ib) + (c + id) \\ \eta_{\text{out}} &= (a + ib) - (c + id) \end{aligned} \quad 4.3.3.4$$

The factor of 0.5 divides out in the reflection analysis, and can therefore be omitted.

The spectrum is given by the square of the amplitudes, hence spectrally:

$$S_{in} = \eta_{in} \eta_{in}^*$$

$$S_{out} = \eta_{out} \eta_{out}^*$$

i.e.

4.3.3.5

$$S_{in} = a^2 + b^2 + c^2 + d^2 + 2(ac + bd)$$

$$S_{out} = a^2 + b^2 + c^2 + d^2 - 2(ac + bd)$$

By noting that the autospectra of the elevation and current and the co-spectrum of elevation and current are, in terms of their Fourier constituents:

$$S_{\eta\eta} = a^2 + b^2$$

$$S_{uu} = c^2 + d^2$$

4.3.3.6

$$\text{re}(S_{\eta u}) = ac + bd$$

where $\text{re}(S_{\eta u})$ is the real part of the cross spectrum (i.e. the co-spectrum), it is possible to re-write Guza *et al.*'s (1984) method in terms of the spectral estimates of elevation and velocity:

$$Rl^2(f) = \frac{S_{\eta\eta}(f) + S_{uu}(f) - 2 \times \text{re}(S_{\eta u}(f))}{S_{\eta\eta}(f) + S_{uu}(f) + 2 \times \text{re}(S_{\eta u}(f))}$$

4.3.3.7

as required.

The co-spectrum gives the in phase oscillations, and can be replaced with a term for the phase between the elevation and velocity spectra. The benefit of doing this is explained after the derivation. To examine how the phase term can be introduced it is necessary to examine exactly what information is contained in the phase spectrum.

In an imaginary axis system $x+iy$,

$$\cos\theta = \frac{x}{\sqrt{x^2 + y^2}}$$

4.3.3.8

where θ is the angle between x and y . In this case the angle θ is the phase between η and u which arises from the cross spectrum as follows:

$$S_{\eta u} = (a + ib) \times (c - id)$$

$$S_{\eta u} = ac + bd + i(bc - ad)$$

4.3.3.9

The phase $\theta_{\eta u}$ can be expressed as the arctangent of the ratio of the imaginary to real parts, but is more usefully expressed as:

$$\cos\theta_{\eta u} = \frac{ac + bd}{\sqrt{(bc - ad)^2 + (ac + bd)^2}} \quad 4.3.3.10$$

$$\therefore \cos\theta_{\eta u} = \frac{ac + bd}{\sqrt{(bc)^2 + (ad)^2 + (ac)^2 + (bd)^2}}$$

The denominator of this equation can be written in terms of the spectra as $\sqrt{S_{\eta\eta}S_{uu}}$ while the numerator is simply $\text{re}(S_{\eta u})$ (i.e. the real part of the cross spectrum). Hence

$$\cos\theta_{\eta u} = \frac{\text{re}(S_{\eta u})}{\sqrt{S_{\eta\eta}S_{uu}}}$$

$$\therefore \text{re}(S_{\eta u}) = \sqrt{S_{\eta\eta}S_{uu}} \cos\theta_{\eta u} \quad 4.3.3.11$$

$$\therefore R1^2(f) = \frac{S_{\eta\eta} + S_{uu} - 2\sqrt{S_{\eta\eta}S_{uu}} \cos\theta_{\eta u}}{S_{\eta\eta} + S_{uu} + 2\sqrt{S_{\eta\eta}S_{uu}} \cos\theta_{\eta u}}$$

Defining a suitable gain function $G(f)$, it is possible to rewrite this equation as follows:

$$G(f) = \sqrt{\frac{S_{\eta\eta}}{S_{uu}}} \quad 4.3.3.12$$

$$R2^2(f) = \frac{1 + G^2(f) - 2G(f)\cos\theta_{\eta u}(f)}{1 + G^2(f) + 2G(f)\cos\theta_{\eta u}(f)}$$

This can easily be shown to be equivalent to $R1^2(f)$ by substituting the equation for $G(f)$ into the $R2^2(f)$ equation and multiplying the top and bottom of the RHS of the equation by S_{uu} .

Huntley *et al.* (1995) term this equation the frequency domain approach, pointing out that in the absence of spectral smoothing this equation is identical to the previous equations. However, with the smoothing which is necessary to obtain a stable spectral estimate, the $\sqrt{S_{\eta\eta}S_{uu}} \cos\theta_{\eta u}$ term is always larger than the co-spectrum. This is because replacing the magnitude of $S_{\eta u}$ by $\sqrt{S_{\eta\eta}S_{uu}}$ implies perfect coherence between the elevation and velocity time series (see equation 4.2.9). The result is that the estimation of the reflection coefficient using this method gives rise to smaller values of the frequency dependent reflection coefficient than Guza's time domain method.

Huntley *et al.* (1995) go further into this topic to investigate the effect of noise on the two sorts of analysis and find that while Guza's method consistently overestimates the reflection coefficient if noise is present in the data, the frequency domain method underestimates it, a result of the implication of perfect coherence.

Huntley *et al.* (1995) go on to discuss a third method, the principal component analysis (PCA), which they suggest is better at reducing the effect of noise in the signal than the previous two.

The frequency domain method thus has advantages over Guza's method. Firstly the full linear theory can be applied i.e. the transform of u to \hat{u} can take place in the frequency domain prior to the cross spectrum being taken and the phase obtained. Secondly the frequency domain method has a different response to noise than the time domain method - a response which results in a slight underestimation of the reflection coefficient. Having said this, the method is slightly less straightforward to apply, and the results show only a marginal difference to Guza's method for typical signals. The reader is referred to Huntley *et al.* (1995) for simulated tests on the effect of noise on the two methods.

4.3.4 Principal component analysis

The third technique which has been used in the calculation of reflection coefficients using co-located gauges is the principal component analysis (PCA hereafter). The analysis uses a similar equation to $R^2(f)$ but uses a modified gain and phase. Tatavarti *et al.* (1988) and Tatavarti (1989) argued that by taking the eigenvectors of the cross-spectral matrices at each frequency estimate, the first eigenvector would tend to extract the correlated part of the signals, while the second eigenvector would extract uncorrelated parts of the signal - i.e. noise.

The cross-spectral matrix comprises:

$$A = \begin{bmatrix} S_{\eta\eta} & S_{\eta u} \\ S_{\eta u}^* & S_{uu} \end{bmatrix} \quad 4.3.4.1$$

at each frequency, where $S_{\eta u}^*$ is the complex conjugate of the cross spectrum between elevation and velocity.

The resulting eigenvector matrix comprises of a 2×2 matrix of complex numbers representing the following:

$$V = \begin{bmatrix} H e^{i\theta_H} & N_H e^{i\theta_{NH}} \\ U e^{i\theta_U} & N_U e^{i\theta_{NU}} \end{bmatrix} \quad 4.3.4.2$$

where $He^{i\theta_H}$ gives the amplitude and phase of the correlated part of the elevation signal, $Ue^{i\theta_U}$ gives the amplitude and phase of the correlated part of the velocity signal while the N terms contain the uncorrelated (noise) parts of the signal.

A new gain function is defined as $G'(f) = \frac{H(f)}{U(f)}$ and a new phase angle as $\theta'_{Hu} = (\theta_H - \theta_U)$. These values replace $G(f)$ and $\theta_{\eta u}$ in the equation for $R2^2(f)$.

The eigenvalues which arise from the characteristic equation are proportional to the amount of noise which is rejected, and thus serve as an indicator of the noise rejection of the PCA method.

The validity of this approach has been tested on simulated data and field measurements and compared against the other two methods by Huntley *et al.* (1995) and found to be essentially bias free, except for very low values of coherence and for reflection coefficients very close to one. It thus appears that for the case of waves reflecting from natural beaches the PCA method provides the most useful method of wave reflection analysis, however for the case of waves interacting with a seawall, the reflection coefficient tends to unity at both incident and infragravity frequencies, and the method may not be as applicable.

Despite its advantage of providing a bias free reflection coefficient, the PCA method presents problems when attempting to re-create the original time series, a result of the eigenvector analysis itself.

4.4 Wave reflection and sediment transport analysis

4.4.1 Time domain method

In order to understand the effect of shoreline wave reflection on the incoming and outgoing wave field, authors such as Guza *et al.* (1984), Tatavarti *et al.* (1988) and Tatavarti (1989) have derived methods to split up the incoming and outgoing time series of wave elevation and velocity. In fact it is the effect of the combined wave fields which drives the sediment suspension, but there is much to be gained from looking at the individual components on the sediment transport.

Jaffe *et al.* (1984) was interested in the relative contributions of the mean flow and the oscillatory flow in the surf zone on the sediment flux. Although the suspension of sediment is non-linear and depends on the combination of mean and oscillatory flows, the two components have different effects on the net sediment transport. Jaffe *et al.* (1984) split the velocity time series (U) into a mean (\bar{u}) and time varying component (u') which includes both wave and turbulent oscillations. They did the same for the total sediment concentration, arriving at a term for mean sediment flux and a term for flux as a result of in phase oscillations about the mean.

In the following derivation ' c_s ' denotes 'sediment concentration' as opposed to ' c ' which is used to denote wave celerity or a Fourier constituent (depending on the context of the equation).

$$\text{If } U = \bar{u} + u' \quad 4.4.1.1$$

$$\text{and } C_s = \bar{c}_s + c'_s \quad 4.4.1.2$$

then

$$\begin{aligned} \overline{UC_s} &= \overline{(\bar{u} + u') \times (\bar{c}_s + c'_s)} \\ \therefore \overline{UC_s} &= \bar{u} \bar{c}_s + \overline{u' c'_s} + \overline{u c'_s} + \overline{u' c_s} \end{aligned} \quad 4.4.1.3$$

Since the time averaged flux of an oscillation about zero is zero, the second and third terms in the above equation are zero, and the terms contributing to the sediment flux are the first and fourth. i.e.:

$$\overline{UC_s} = \bar{u} \bar{c}_s + \overline{u' c'_s} \quad 4.4.1.4$$

Jaffe *et al.* (1984) calls the $u' c'_s$ term the 'flux coupling'. It is also frequently referred to as the oscillatory flux. The components of $u' c'_s$ can be further decomposed by looking at the cross spectrum of u' and c'_s . The in phase oscillations will result in net sediment transport, and this is given by the co-spectrum. Effectively, the co-spectrum splits u' and

c'_s into each of the frequency components of the spectrum, whereas Jaffe's analysis just looked at mean and oscillatory flows.

The argument can be further extended to wave reflection - by further separating the velocity field into incoming and outgoing components, the contributions of these components to the transport of the sediment can be examined. In this case:

$$u' = u'_{in} + u'_{out} \quad 4.4.1.5$$

The equation for the oscillatory part of the flux thus becomes

$$\overline{u'c'_s} = \overline{u'_{in}c'_s} + \overline{u'_{out}c'_s} \quad 4.4.1.6$$

These components can be most easily calculated in the time domain using a modification of Guza's method.

The elevation estimates from Guza's method are:

$$\eta_{in} = (\eta + \frac{c}{g}u) / 2 \quad 4.4.1.7$$

$$\eta_{out} = (\eta - \frac{c}{g}u) / 2$$

where c is the celerity.

By applying the relationship between elevation and velocity (equation 4.3.2.10) back to the time series, it is possible to obtain the incoming and outgoing velocity time series:

$$u_{in} = \frac{g}{c} \eta_{in} \quad 4.4.1.8$$

$$u_{out} = -\frac{g}{c} \eta_{out}$$

giving:

$$u_{in} = \frac{1}{2}(u + \frac{g}{c}\eta) \quad 4.4.1.9$$

$$u_{out} = \frac{1}{2}(u - \frac{g}{c}\eta)$$

The time series of incoming and outgoing oscillatory sediment flux are therefore given by:

$$u_{in}c_s = \frac{c_s}{2}(u + \frac{g}{c}\eta) \quad 4.4.1.10$$

$$u_{out}c_s = \frac{c_s}{2}(u - \frac{g}{c}\eta)$$

In the above equations u and η are in phase in the direction of wave travel and positive u is in the direction of positive x , which is in this case 'incoming' or onshore. The method is most easily applied in shallow water where phase velocity depends only on water depth

and not frequency ($c = \sqrt{gh}$). This allows incoming and outgoing fluxes to be calculated in the time domain.

By taking the co-spectrum between the incoming or outgoing velocity time series with the sediment time series, the relative importance of the reflected wave component on the sediment transport can be investigated. The draw back to the method is that if a time domain analysis is required, it is only possible in shallow water where the wave frequency does not affect the celerity. However, the analysis can be carried out in the frequency domain if the waves are in intermediate water.

4.4.2 Frequency domain method

In intermediate water, the shallow water approximation for celerity does not apply, i.e.

$$c \neq \sqrt{gh}. \quad 4.4.2.1$$

This leads us to examine the solution for the incoming and outgoing wave velocities further, so that the full dispersion solution can be included.

It is first necessary to arrive at a new estimation for velocity from elevation at some depth z , as the velocity signal may attenuate with depth. The difference in the velocity term is that the attenuation of velocity with depth is not cancelled out, thus

$$u = \frac{g a k}{\sigma} \frac{\cosh k(z+h)}{\cosh kh} \cos(kx - \sigma t) \quad 4.4.2.2$$

In this expression, the $\cosh k(z+h)/\cosh(kh)$ term is in fact the attenuation with depth. Whilst in shallow water this expression tends to unity, in intermediate water it deviates from one as the particle orbits get smaller with depth. This attenuation is dependent on frequency, and it is thus not possible to apply this term directly to the time series - it must be applied in the frequency domain. As before, an estimation of velocity is required from elevation and this is simply derived as:

$$\hat{u} = \frac{g k}{\sigma} \frac{\cosh k(z+h)}{\cosh kh} \eta \quad 4.4.2.3$$

The frequency of a wave of some wave number k in some depth z is given by the dispersion equation:

$$\sigma^2 = g k \tanh kh \quad 4.4.2.4$$

This can be applied to the above equation to give

$$\hat{u} = \sqrt{\frac{gk}{\tanh kh}} \frac{\cosh k(z+h)}{\cosh kh} \eta \quad 4.4.2.5$$

We now have an expression for u in terms of η , z , h and k . Obviously z and h are constant while k depends on the wave frequency and water depth and is found by solving the dispersion equation iteratively. It is therefore possible to carry out a spectral analysis of η in which each Fourier constituent is multiplied by a value as given by the equation above, a value which will depend on the frequency of the constituent, the water depth and the height of the instrument. The elevation is thus transformed to the units of velocity in the frequency domain. The argument for incoming and outgoing velocities then follows a similar line to the shallow water case.

$$\text{If } A = \sqrt{\frac{gk}{\tanh kh}} \frac{\cosh k(z+h)}{\cosh kh} \quad 4.4.2.6$$

$$\text{then } \hat{u} = A\eta \quad 4.4.2.7$$

For each frequency bin, the Fourier constituents of η , u and c_s can be written as:

$$\eta \rightarrow a + ib$$

$$u \rightarrow c + id \quad 4.4.2.8$$

$$c_s \rightarrow e + if$$

In a certain frequency bin, for a known wave depth it is possible to solve the dispersion equation for the wave number k , and the value of A can then be found. This value is applied to the Fourier constituents of elevation to give the Fourier representation of the estimation of velocity from elevation

$$\hat{u} = A\eta \rightarrow A(a + ib) \quad 4.4.2.9$$

A is constant within a given frequency band, and it is convenient to denote $A(a+ib)$ as just $(a+ib)$ in the following argument. The multiplication of the complex number by a real scalar results in no loss of phase information.

Guza's phase argument for plus and minus characteristics still applies in the frequency domain, and the Fourier constituents of the separated velocity field can be expressed in terms of the Fourier constituents of elevation and velocity as follows:

$$\begin{aligned} u_{\text{in}} &= \frac{(\hat{u} + u)}{2} \rightarrow \frac{(a + ib) + (c + id)}{2} = \frac{(a + c) + i(b + d)}{2} \\ u_{\text{out}} &= \frac{-(\hat{u} - u)}{2} \rightarrow \frac{-((a + ib) - (c + id))}{2} = \frac{-((a - c) + i(b - d))}{2} \end{aligned} \quad 4.4.2.10$$

The real part of the cross spectrum of these incoming and outgoing velocity Fourier constituents with the sediment's Fourier constituents gives the co-spectrum. In terms of the Fourier constituents, crossing the velocity with the sediment at any frequency gives:

$$u_{in} \times c_s = \frac{((a + c) + i(b + d)) \times (e - if)}{2} \quad 4.4.2.11$$

$$u_{out} \times c_s = \frac{-((a - c) + i(b - d)) \times (e - if)}{2}$$

The co-spectrum is given by the real part of the above equations, and it is this that gives the in-phase oscillations of velocity and sediment which results in sediment transport. The equations for the co-spectra for the incoming and outgoing oscillatory fluxes at each frequency in terms of the Fourier constituents are thus:

$$u_{in} c_s = \frac{(a + c)e + (b + d)f}{2} \quad 4.4.2.12$$

$$u_{out} c_s = -\frac{(a - c)e + (b - d)f}{2}$$

The stable co-spectral estimate for the flux is obtained after the windowed data is transformed to the frequency domain using an FFT, the above calculation is carried out and the bins from each section accumulated and normalised. The units of co-spectral amplitude remain as before.

This method represents the first of the frequency domain methods - while improving on the time domain in terms of the effect of intermediate water on celerity, it does not have superior noise rejection qualities. To improve the noise rejection, the principal component analysis could be applied. In practice, this frequency domain approach gives a greater confidence in the result for intermediate water, but in shallow water there is little difference between it and the time domain method.

4.5 Data simulation

Introduction

So far, this chapter has dealt with the mathematical development of analysis tools to unravel the complex processes of wave reflection and sediment transport. It is useful to apply these analysis tools to simulated data so that an indication of their performance can be gained. The aim of this section therefore is to describe the application of some of these analysis tools to a simple model. Those techniques of particular interest are the ones which will be used to analyse the field data gathered at Teignmouth. It is thus sensible to use similar parameters to those observed at Teignmouth (i.e. assume similar wave heights, periods, water depths and instrument positions.)

Conceptual model

A conceptual model was used which generated time series of data similar to that which was gathered in the field. Comparisons between input parameters and the results of the data analysis tools were therefore possible. Calculations made directly from the time series were also compared with their frequency domain counterparts. The model is not intended as a representation of the physics which drive the sediment transport. It is purely a testing ground for the analysis techniques.

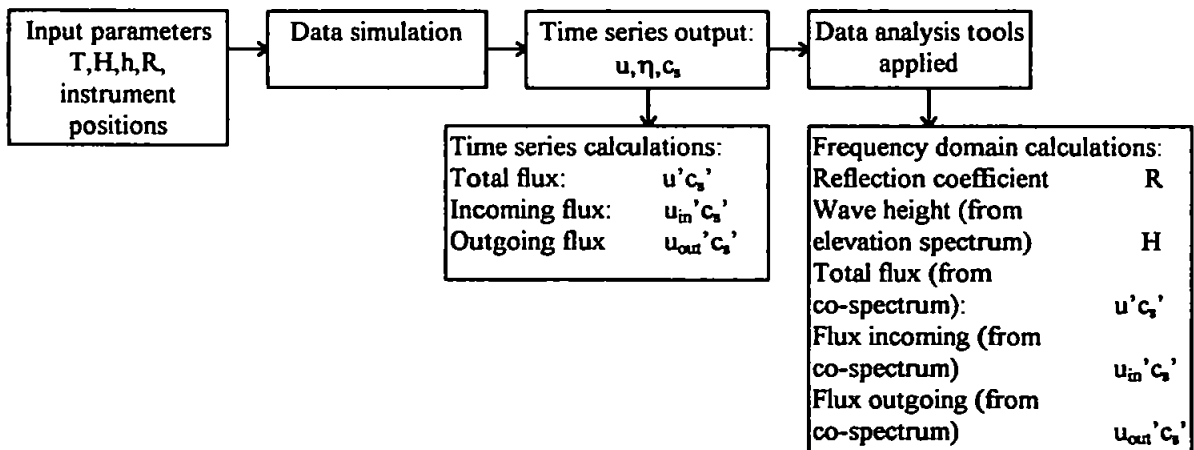


figure 4.5.1: Simulated data was used to check analysis techniques prior to their application to field data.

Input parameters

Sufficient input parameters were decided as: wave period, wave height of incident waves, water depth, instrument positions and reflection coefficient. The maximum sediment concentration was also set.

Hydrodynamics

Hydrodynamics were modelled using linear wave theory for velocity and elevation. Incoming and outgoing components of the velocity field were calculated and added. Sample points were calculated at 8Hz for a duration of 1024 model seconds (i.e. recreating a run as gathered in the field). Values of the majority of input parameters were kept constant, while the reflection coefficient was varied for different runs. The combinations of parameters used are shown at the top of the results table (table 4.5.1).

Sediment dynamics

The suspension of sediment was assumed to be a function of the velocity of the incident and reflected waves. The cube of the velocity in the direction of each component of the wave field was scaled to observed levels of sediment concentration in the field, and the incoming and outgoing components added. In the field the suspension of sediment is likely to be controlled by shearing resulting from the total velocity field. The model requires that sediment is suspended and transported in both a shoreward direction by the incoming waves and in a seaward direction by the outgoing waves. It is in this way that incoming and outgoing sediment fluxes inside the model can be calculated and compared to the results of the analysis techniques.

Application discussion

The non-linear nature of the sediment response to the velocity field means that such an approach may not correctly model the sediment suspension processes, but in certain cases may be more applicable than in others. One such suitable case may be when solitary waves are present which advect material past the instruments, reflect off the wall, and pass the instruments again, travelling in a seaward direction. This phenomenon may occur when the wall is present in the inner surf zone, where each bore could be considered as a solitary wave. It may also occur at various times in a more random sea, when sufficient time may pass between waves for an individual wave to complete the cycle without interference¹. For the purposes of this section, this model is used solely as a check of the analysis techniques and theory - to ensure that calculations of wave height and sediment transport from the spectra and cross spectra are correctly made.

¹ A second data simulation using solitary wave theory and suspension resulting from the total velocity is used in the discussion to examine the mechanism of sediment suspension.

Model Results

The model was run with reflection coefficients of 1, 0.8, 0.5, 0.3 and 0. A typical time series is shown in figure 4.5.2. Results are tabulated below (table 4.5.1):

Sediment Transport And Wave Reflection model - REFCHECK					
Input parameters: Wave frequency: 0.25hz, Water depth: 0.7m, Incident wave amplitude: 0.2m					
Instrument positions: Distance from wall: 1.2m Distance from bed: 0.2m					
Units: Flux: kg/m ² /s H: meters +ve onshore					
	Model runs: each column gives data for a run of the model				
Model R	1	0.8	0.5	0.3	0
Calculated R	1	0.7987	0.4976	0.2978	0.0392
Model H	0.4	0.4	0.4	0.4	0.4
Calculated H	0.4001	0.4001	0.4001	0.4001	0.4001
Model Flux: In	0.5224	0.5224	0.5224	0.5224	0.5224
Calc. Flux: In	0.4902	0.5139	0.5364	0.5434	0.5463
Model Flx:Out	-0.5224	-0.2138	-0.0326	-0.0042	0
Calc. Flx: Out	-0.4902	-0.1852	-0.0204	-0.0060	-0.0236
Model Tot Flux	0	0.3285	0.5157	0.5370	0.5224
Calc Tot Flux	0	0.3287	0.5160	0.5373	0.5227

table 4.5.1: Data simulation inputs and outputs.

Reflection coefficients were calculated from the model output using the time domain method (Guza *et al.*, 1984). Wave heights were calculated using the elevation spectrum. The incoming and outgoing sediment fluxes were calculated by separating the elevation and velocity time series into incoming and outgoing velocity time series before taking the co-spectrum with the time series of the total sediment concentration. The integral of the normalised co-spectrum gives the sediment flux. Mean fluxes inside the model were calculated by multiplying the component of velocity of interest by the sediment suspended as part of that phase. The total flux was calculated in the case of the model by multiplying the total velocity by the sediment and taking the mean for the run, while the observations used the co-spectrum between the total velocity and the sediment. All the flux estimates represent mean values for that run.

While errors in the calculation of the sediment transport are greater than the errors in calculating the reflection coefficient and wave height, percentage errors are still small ($\approx 12\%$) and predict the correct direction of sediment transport. These errors are attributed to the windowing of data within the cross-spectral analysis routine.

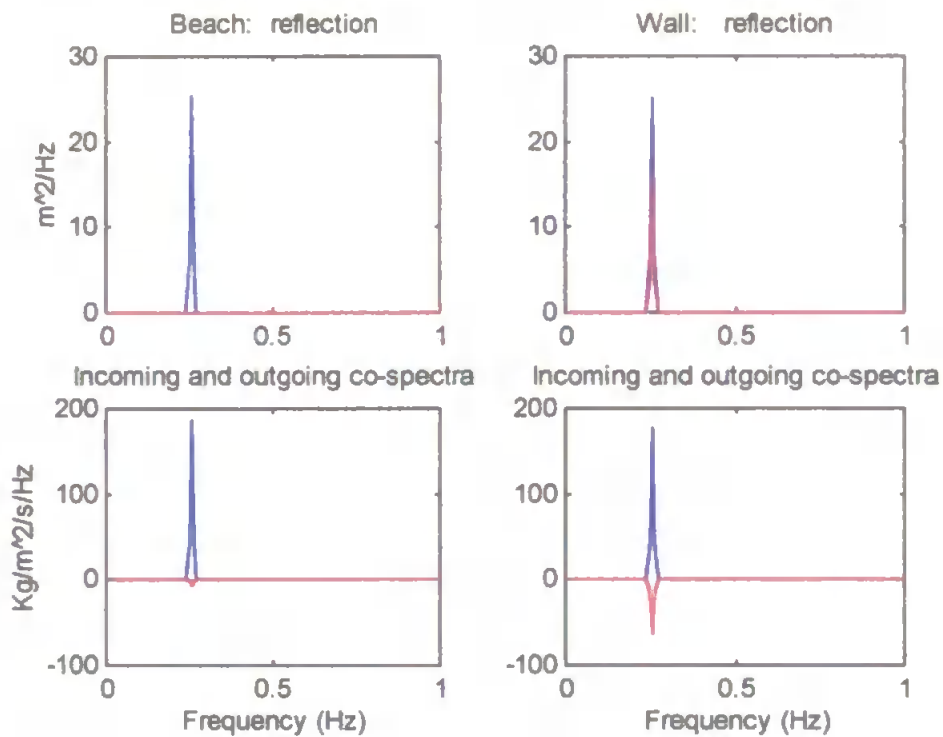
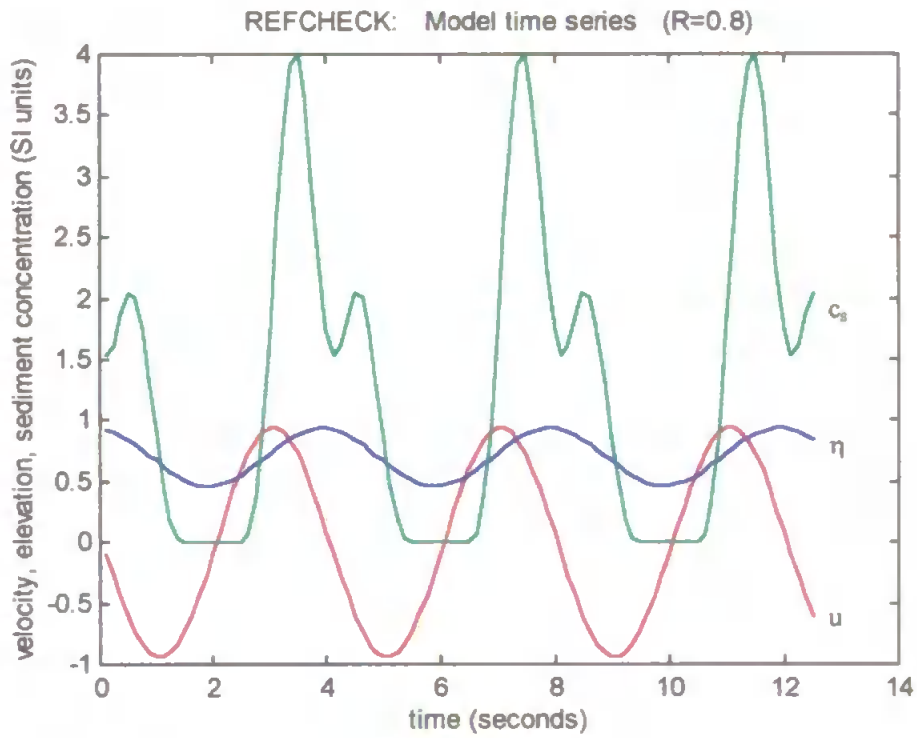


figure 4.5.2: Simulation and analysis of data using REFHECK model. The model uses simple theory to create a data set in which parameters such as the wave period, amplitude, reflection coefficient and sediment flux are known. Analysis techniques can then be tested on this data set for their accuracy. In the above spectra, blue represents energy or flux onshore, while red represents offshore directed energy or flux.

The results of the conceptual model suggest that:

1. The elevation spectrum can be used to determine the wave height - this is useful when using Iribarren type numbers to parameterise frequency dependent wave reflection.

2. In shallow water, the time domain method provides a good estimate for reflection coefficient.
3. Sediment transport rates associated with incident and reflected waves can be obtained reasonably successfully by splitting the elevation and velocity time series into incoming and outgoing velocity components and integrating the normalised co-spectrum between these components and the total sediment concentration time series.

Discussion

While it is not acceptable to infer hydrodynamic or sediment dynamic phenomena from the model, it is useful to examine the spectra of the incoming and outgoing time series and the incoming and outgoing co-spectra while understanding fully the nature of the input data so that correct analysis of the field data can be made should a similar picture arise.

The spectra in figure 4.5.2 show energy spectra for incoming and outgoing waves on a beach (zero reflection coefficient assumed) and at a wall (reflection coefficient = 0.8) (Blue: incoming, red: outgoing). The co-spectra for the beach shows onshore sediment transport (onshore is positive) associated with the incoming (blue) waves at incident wave frequency with little offshore transport. The co-spectra for the wall show onshore sediment transport associated with the incoming waves, and offshore transport associated with the outgoing waves, resulting in a net decrease in sediment transport. The logical extension of the observation is to say that if the waves incident on a beach transport sand up the beach, an increase in wave reflection will provide a mechanism for the offshore transport of the sediment at the frequency of the incident waves, resulting in a net decrease in the shoreward sediment transport. This suggests that the positioning of a seawall at the head of the beach may inhibit beach recovery.

However, if this is the case, erosion must be a non-linear process - as it is not possible for the reflection coefficient to exceed unity over any length of time. The transport of sediment offshore by the reflected waves cannot be solely responsible for beach erosion in the absence of any processes other than incident and reflected waves. Contributions to offshore sediment transport from in front of the wall must be made by other frequencies of waves (e.g. long waves) or by mean currents in the cross-shore or longshore direction. The reflection of the wave energy over the model beach does increase the mean sediment concentration however, and a result of this would be that the wall will enhance the erosion of the beach by ensuring there is more sediment in suspension to be transported away.

Physical interpretations of the model results are limited however as the model was designed solely as a test bed for the analysis techniques. A more complex model using more accurate relationships between the velocity field and the suspension of sediment would be more suitable for the physical interpretation of the effect of wave reflection on sediment transport.

4.6 Summary

The aim of this chapter has been to introduce the fundamental techniques of spectral analysis and describe the method of application of these techniques to the data, to describe three of the suitable methods for wave reflection analysis and to combine the techniques already used for oscillatory sediment transport analysis with the techniques for wave reflection analysis so that the sediment transport associated with wave reflection can be further investigated.

The chapter initially discussed how a time series signal becomes a spectrum, using the Fast Fourier Transform, and how the cross spectrum is obtained. The spectrum gives information on the frequencies of energies present, and this is especially useful for determining wave height and period from the pressure transducer trace. The real part of the cross spectrum between velocity and sediment concentration provides information on the oscillatory sediment transport. The phase was discussed in terms of the Fourier coefficients, and the coherence and confidence identified as methods of identifying the quality of the result. The technique for obtaining wave height from the elevation or velocity trace was discussed as was the technique for obtaining the oscillatory sediment flux from the co-spectrum. Units of each of the spectra were identified and an example of the basic calculations necessary during the analysis given.

The next section was devoted to the analysis of wave reflection using co-located gauges. Techniques for obtaining incoming and outgoing waves were discussed alongside techniques for obtaining the frequency dependent reflection coefficient. The time domain method was identified as the simplest of these to apply, although it requires shallow water wave theory and is more susceptible to noise than the two frequency domain methods. The first frequency domain method discussed uses the phase between the elevation and velocity traces to establish the reflection coefficient and uses full linear theory, thereby eliminating noise and the problem of intermediate water. The principal component analysis can be applied to this method as a further technique for noise reduction.

The third section described a new technique whereby the sediment is incorporated into the reflection analysis. By converting the incoming and outgoing elevation time series into velocity time series, and taking the co-spectrum between each of these components and the sediment time series, the contributions of the incoming and outgoing waves to the total transport can be established. This method, which is based on the time domain method of

separating incoming and outgoing waves, uses shallow water wave theory, and is thus not suitable for intermediate water. A second approach is derived which uses the full linear theory in the frequency domain which is more suitable for intermediate water, but is more difficult to implement.

Finally, it was necessary to check that the wave heights predicted using the spectra were as expected and that the sediment fluxes derived from the incoming and outgoing co-spectra were correct. A simple model was constructed to do this which consisted of waves travelling past virtual sensors towards a reflector. The waves suspend and transport a known quantity of sediment, and the sediment flux in the model for both incoming and outgoing waves is thus known. By constructing time series as they would occur in the field, it was possible to apply the analysis techniques to this model to investigate the accuracy of the techniques in calculating wave height and sediment transport. The results show the techniques to be correctly applied.

Overall, this chapter has developed suitable techniques for analysing time series of wave elevation, velocity and sediment concentration so that information can be gained into the nature of the sediment response to wave reflection from the seawall. Other analysis techniques which are used in this thesis, but not included here, are either suitably referenced or discussed at the point of their usage.

CHAPTER 5: Results

5.1 Introduction

In the introduction and literature review, the varied views on the effect of a seawall on the beach were presented. By taking high frequency measurements of the processes driving sediment suspension and transport in front of a seawall, further light can be shed on this complex problem. The question which has been considered in presenting the results outlined below is: ‘What is the effect of the seawall on the hydro- and sediment dynamics?’. More specifically, does an increase in the reflection coefficient of the shoreline lead to an increase in sediment transport, as suggested by Kraus (1988).

The conceptual approach to considering this problem is as follows: An initial morphology modifies oscillatory currents driven by incident waves. The waves give rise to sediment suspension, and the sediment is then available for transport by currents and waves. Sediment transport leads to a change in morphology and a feedback loop is therefore created. It is well established that wave reflection modifies the hydrodynamic environment, and it is therefore likely to modify the nature of the sediment suspension and transport in the nearshore. Evidence for this change and its implications are presented below.

The structure of the results chapter follows the conceptual approach described above. First, the nature of the hydrodynamics is identified for the beach and wall cases by examining the incoming and outgoing wave spectra and the resulting reflection coefficients for the wall and beach. Chapter 4 described three different methods of calculating reflection coefficients and all three methods are used and compared in this section.

Next, it is necessary to examine the effect of the increase in wave reflection on the sediment suspension dynamics, and this is done using time series of sediment concentrations. Mean sediment concentrations at the wall are examined and compared to those obtained on the natural beach. The analysis of the effect of the incoming and outgoing waves on sediment transport is applied to the data (as outlined in chapter 4). The transport of sediment by mean currents is examined and beach and wall cases are compared.

Most of the data presented to this point was obtained during the tide of T136PM. In order to illustrate the consistency of the sediment dynamic results, three more tides of data were analysed. The results from these different tides are presented in the final section of the chapter.

The results demonstrate for the first time how an increase in the reflection coefficient at the shoreline leads to an increase in sediment concentrations in front of the wall. This suspended sediment is then available for transport by mean currents and wave driven flows.

5.2 Wave reflection analysis at the beach and wall

Analysis of wave reflection was carried out for both the wall and beach sites. Three methods were used, and these were the time domain method of Guza *et al.* (1984) and two frequency domain methods, one of which included the principal component analysis to reduce the bias resulting from noise in the signal. The operation of these methods is discussed in detail in chapter 4. The time domain method was used to obtain incoming and outgoing wave spectra. These spectra indicate which frequencies of wave motions were most important, and this allows correct consideration of the frequency dependent reflection coefficient.

Results of analysis carried out on data from the beach rig are shown in figure 5.2.1 below:

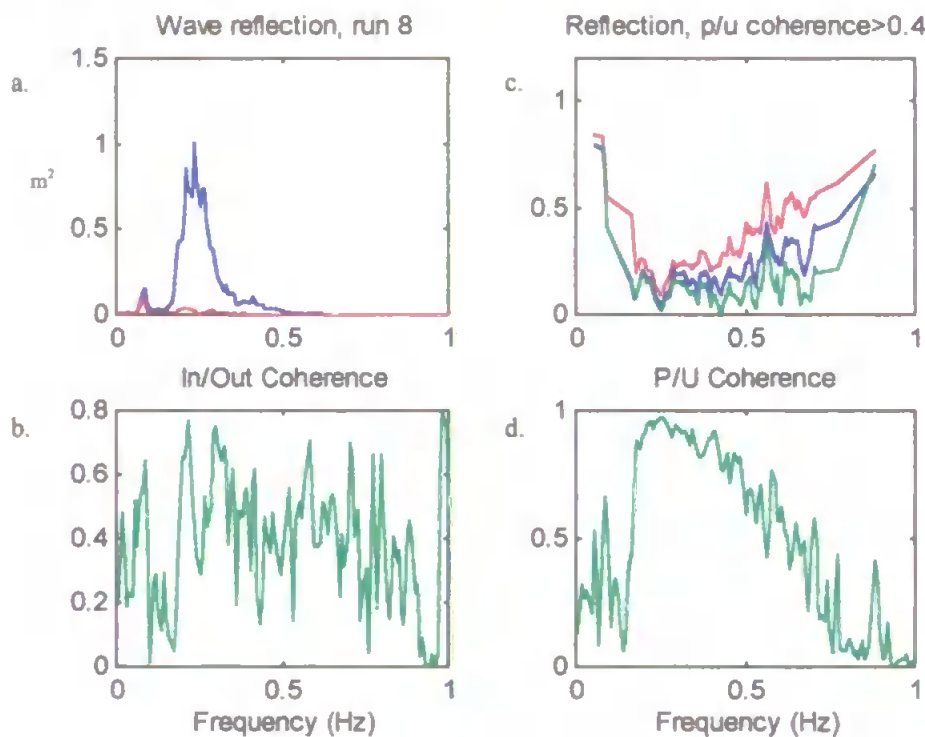


figure 5.2.1: Frequency dependent wave reflection at the beach. a: Incoming and outgoing wave spectra calculated using the time domain method. b: Coherence between calculated incoming and outgoing time series. c: Frequency dependent reflection coefficient calculated using time domain (red), frequency domain (blue) and principal component analysis (green) methods. d: Coherence between elevation (denoted 'P') and velocity. Water depth is 1.28m.

The spectra in figure 5.2.1a show incoming wave energy in blue and outgoing wave energy in red at the different frequencies. Gravity band energy incident on the beach is clearly dissipated and not reflected ($0.125 < f < 0.36$ Hz). Energy at lower frequencies than this ($0.04 < f < 0.125$ Hz) is clearly present as incident and reflected waves. Coherence between the elevation and velocity (5.2.1d) is high in the incident wave band, and this is to be expected in the case of the progressive waves. The coherence between the incoming

and outgoing waves calculated from the elevation and velocity time series also has peaks of high coherence in the incident wave band, even though there is little energy in the outgoing time series (5.2.1b). The frequency dependent wave reflection coefficient is presented in figure 5.2.1c. The results of the time domain method are shown in red, the frequency domain method in blue and the PCA method in green. Results are only presented for frequencies which have values of coherence between elevation and velocity greater than 0.4 to minimise the bias on the reflection coefficient estimate (Huntley *et al.*, 1995). For reflection coefficients less than 0.3 and greater than 0.8, Huntley *et al.* (1995) show that a coherence greater than 0.4 gives a bias in the time domain estimation of R of less than 10%. In the range $0.3 < R < 0.8$, a coherence of greater than 0.4 gives a bias of up to approximately 12%, although this bias decreases with increasing coherence.

At incident wave frequencies and frequencies lower than the incident waves, the time domain method (red) clearly gives estimates of reflection coefficient which are slightly larger than the frequency domain methods (blue and green). However the bias is small, and the overall shape of the graphs is very similar. At frequencies larger than those of the incident waves, the reflection coefficient may be expected to rise back towards unity (energy in = energy out $\Rightarrow R=1$), although this does not represent true wave reflection at the shoreline as the elevation and velocity may not be well correlated. The PCA method, applied to the frequency dependent method (green) tends to extract well correlated parts of the elevation and velocity signals, and hence shows the lowest reflection coefficients at high frequencies, as the turbulence at these frequencies is not well correlated and does not have high coherence. The time domain method is less able to detect uncorrelated parts of the signal and hence shows an increase in reflection coefficient as frequencies increase. The frequency domain method which does not include the PCA lies between the two.

The general shape of the frequency dependent reflection coefficient shown by all three methods is very much as expected - high reflection coefficients for low frequency waves indicate that they are reflected rather than dissipated by the beach while incident waves are almost completely dissipated. As energy levels drop at higher frequencies, the reflection coefficient rises again towards unity. Results similar to this were consistently found for measurements taken outside the surf zone of the natural beach.

An identical analysis was carried out on data collected at the wall in an equivalent water depth while wave conditions were still similar. The results of this analysis are presented in figure 5.2.2, which is derived from run 6, T136PM.

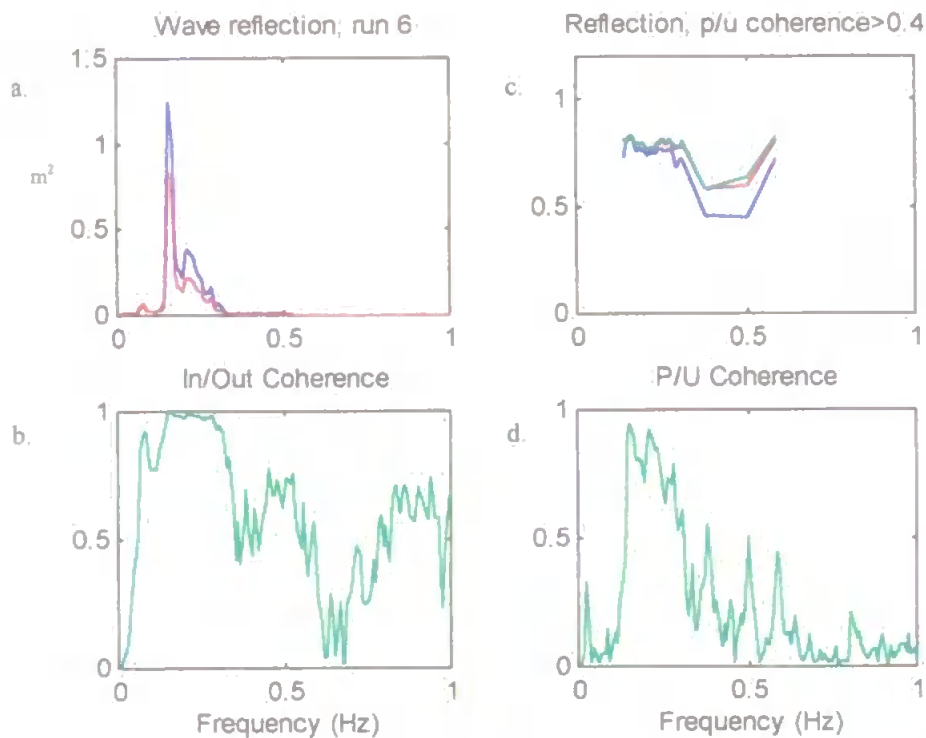


figure 5.2.2 : Frequency dependent wave reflection at the wall. a: Incoming and outgoing wave spectra calculated using the time domain method. b: Coherence between calculated incoming and outgoing time series. c: Frequency dependent reflection coefficient calculated using time domain (red), frequency domain (blue) and principal component analysis (green) methods. d: Coherence between elevation and velocity. Water depth is 1.30m.

In this case the incoming and outgoing wave energies are of similar magnitudes (5.2.2a) at all frequencies. There are slight differences however through frequency. While at low frequency reflection is almost complete, at incident wave frequency some dissipation of energy has occurred, possibly due to the effects of shoaling. In this case, the coherence between the elevation and velocity is high within the incident wave band, and is lower in other frequencies. Even in the incident wave band the elevation / velocity (P/U) coherence is not as high as for the beach case, and this is likely to be a result of the proximity of the instruments to the elevation antinode at the wall. The reflection coefficients, plotted for P/U coherence greater than 0.4, show the reflection coefficient to be larger than at the beach, as expected. The time domain method and PCA method provide remarkably similar estimates for the reflection coefficient in this case, while the frequency domain method provides a lower estimate. The similarity of the time domain method to the PCA method in this case is encouraging as the PCA method has been documented as the most accurate method for estimation of the frequency dependent reflection coefficient (Huntley *et al.* 1995). The time domain method's advantage is that it is far simpler to work with when incorporating the sediment into incoming and outgoing sediment budgets.

Deeper water at the wall gives rise to less dissipation and this results in a higher reflection coefficient. The spectra shown in figure 5.2.3 below are taken from a run when the water depth was 2.3m.

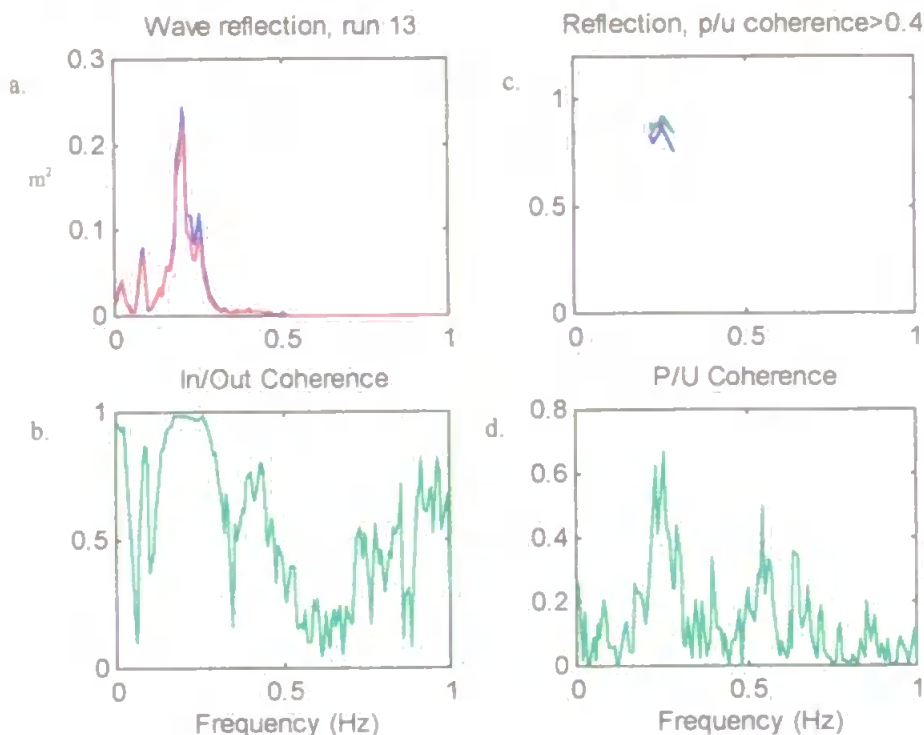


figure 5.2.3 : Frequency dependent wave reflection at the wall. a: Incoming and outgoing wave spectra calculated using the time domain method. b: Coherence between calculated incoming and outgoing time series. c: Frequency dependent reflection coefficient calculated using time domain (red), frequency domain (blue) and principal component analysis (green) methods. d: Coherence between elevation and velocity. Water depth is 2.27m.

The reflection coefficient at the incident wave frequency is in this case 0.9, compared to the previous example where a water depth of 1.3m gave rise to a reflection coefficient of 0.8 again at the incident wave frequency. While the increase in depth allows the reflection coefficient to increase, there is less interaction between the waves and the bed, and larger water depths are therefore likely to lead to less sediment suspension and transport. Results which substantiate this are presented later in this chapter.

5.3 The nature of sediment suspension

Major differences in the hydrodynamics of the natural beach and seawall environments result in different sediment dynamic conditions for these two cases. In order to illustrate the major differences several sections of data are presented. The first two examples (figures 5.3.1 and 5.3.2) demonstrate that more sediment is suspended in front of the wall than on the natural beach in similar incoming wave conditions.

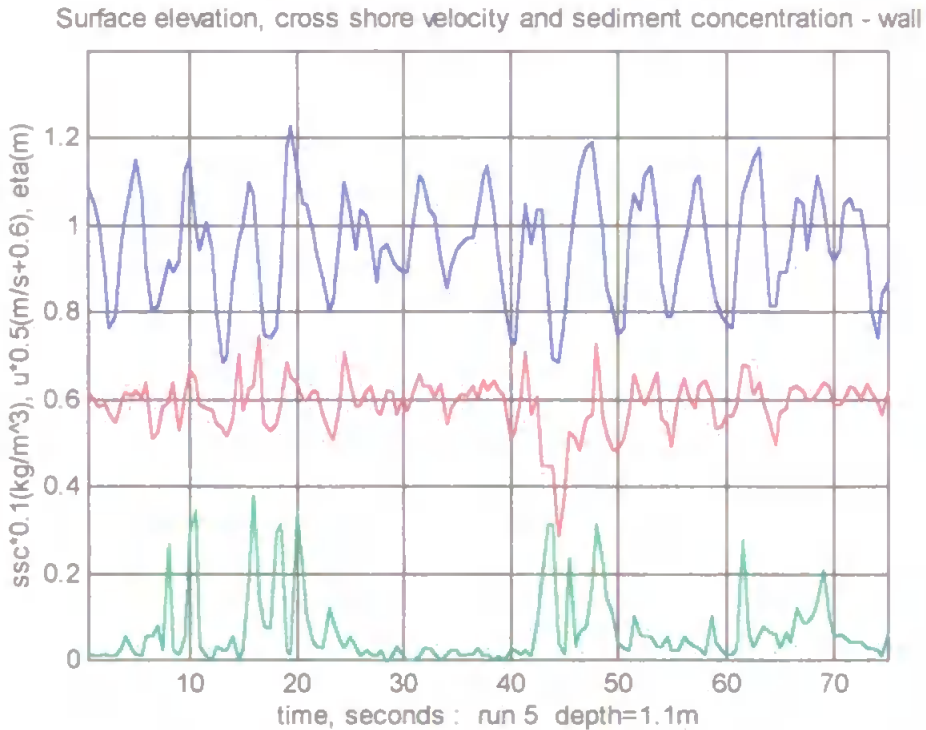


figure 5.3.1: Time series of surface elevation (blue), velocity (red) scaled by 0.5 and offset by 0.6m/s, sediment concentration (green) scaled by 0.1 at wall.

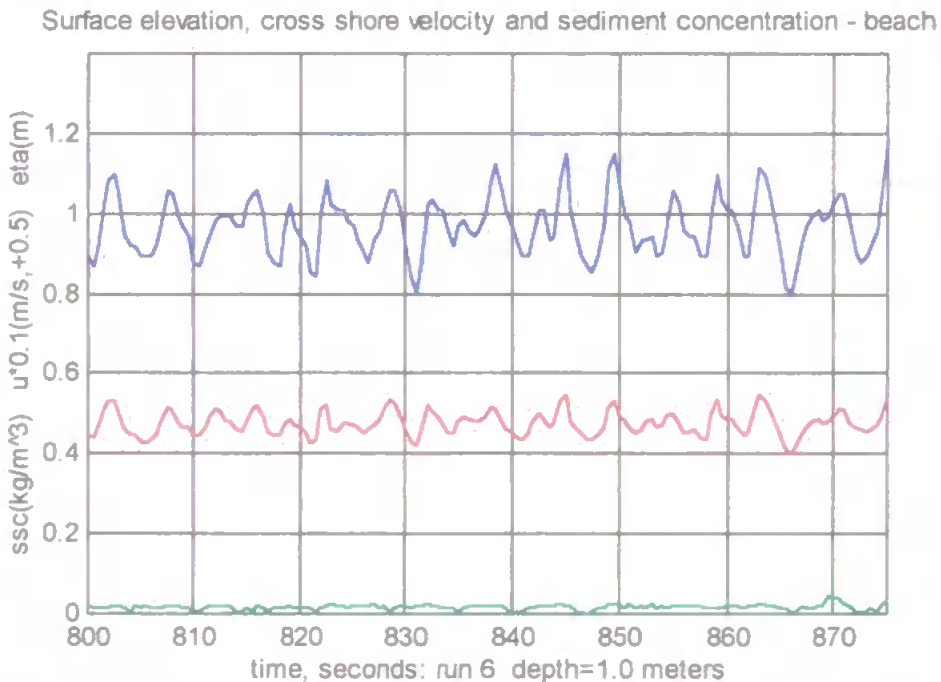


figure 5.3.2: Time series of surface elevation (blue), velocity (red) scaled by 0.1 and offset by 0.5m/s, sediment concentration (green) at beach.

In both cases the water depth is approximately 1m. Maximum wave elevations are greater at the wall rig than at the beach rig, while the beach rig measured greater cross-shore orbital velocities (note scale of axes used). This is a result of the wall rigs proximity to the elevation antinode at the wall. Traditional models of sediment suspension suggest that velocity gradients in the boundary layer lead to a shear stress which is responsible for suspending sediment (Bagnold, 1946). Despite smaller velocities at the wall rig, suspension events resulted in a considerably larger amount of suspension than was observed at the beach rig. In the examples shown, water depths are very similar, the instruments were at equivalent heights, and incident wave conditions were identical. Even so, maximum concentrations at the wall reach 3.9kg/m^3 , while at the beach rig suspension events are not present, and the concentration fails to rise above 0.07kg/m^3 .

Wave heights at the break point during this tide were approximately 0.3m. Consider the situation at the beach rig. The relationship $H_b/h=0.78$ indicates the water depth at the breakpoint should therefore be approximately 0.4m. The closest the instruments were able to get to the surf zone before becoming intermittently dry was during run 5, while the water depth was 0.48m. Measurements made at this time are shown in figure 5.3.3.

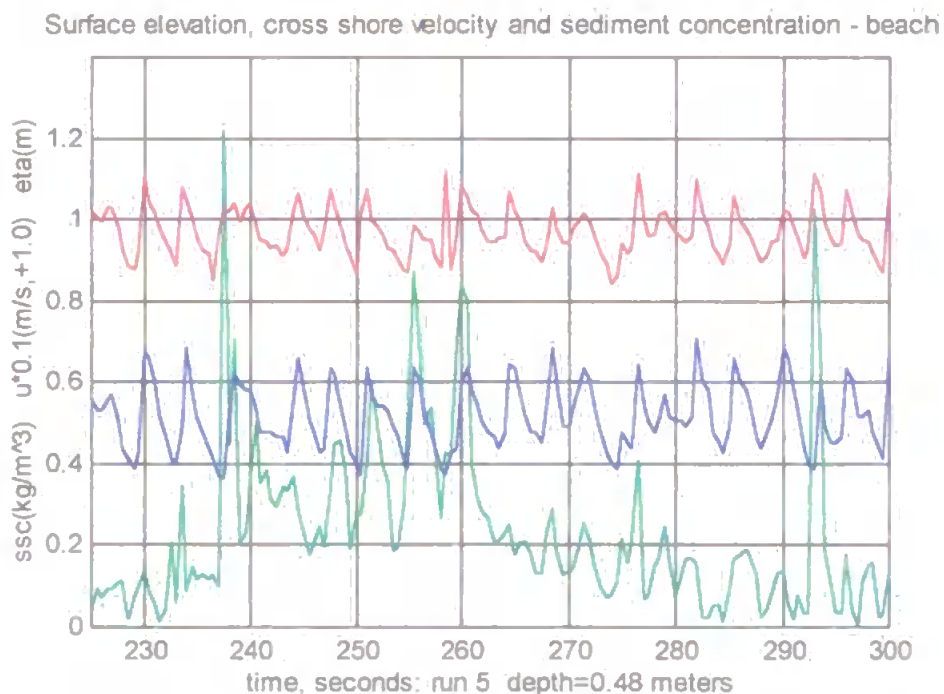


figure 5.3.3: Time series of surface elevation (blue), velocity (red) scaled by 0.1 and offset by 1.0m/s, sediment concentration (green) at beach.

Wave elevation and velocity traces exhibit noticeable skewness as the waves are shoaling and are about to break. Suspension events recorded during this run reached a maximum of

1.2kg/m^3 . In a similar water depth at the seawall, with identical incident wave conditions, maximum concentrations were recorded of just over 9kg/m^3 (figure 5.3.4).

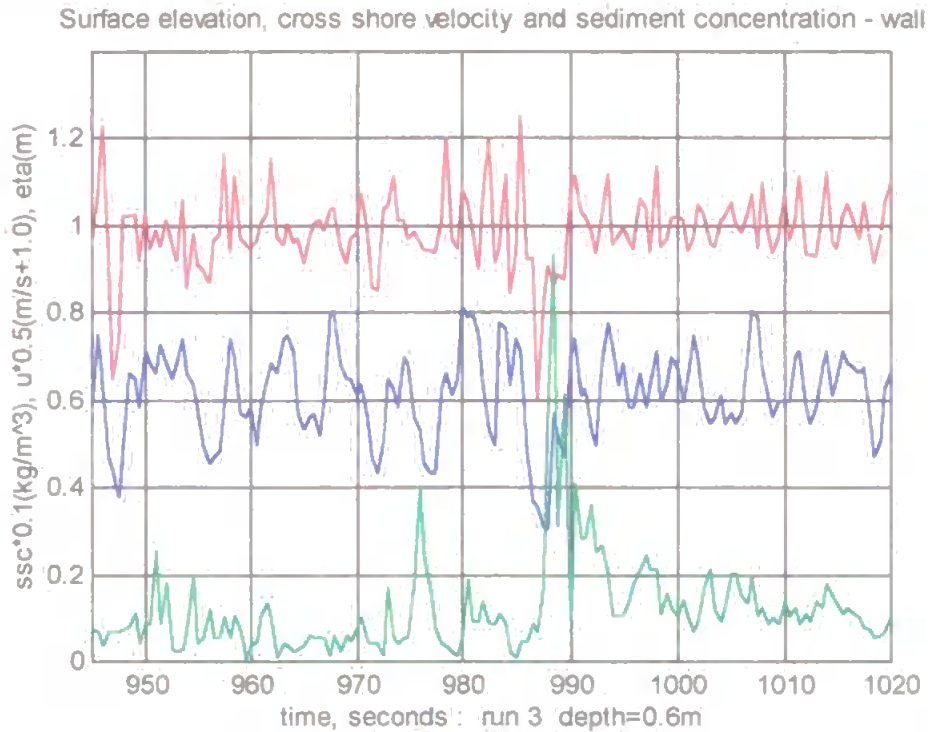


figure 5.3.4: Time series of surface elevation (blue), velocity (red) scaled by 0.5 and offset by 1.0m/s, sediment concentration (green) scaled by 0.1 at wall.

The complicated elevation and velocity traces in the signals were typical of runs where the water was shallow and waves passed the sensors as both incoming and outgoing 'solitary' waves. The resulting sediment suspension traces are complex and it is difficult to establish patterns by eye. It is for this reason that the use of spectral techniques to separate the incoming and outgoing waves and their associated sediment peaks was employed. The first main result is clear however. Regardless of the water depth, greater amounts of sediment are maintained in suspension in front of the wall than on the natural beach, given similar incident wave conditions.

This result is evident in the mean of the suspended sediment concentrations, and the mean SSC was found to be closely related to the degree of reflectivity of the shoreline. The sediment concentration was also found to be dependent on the water depth at the instruments with more sediment being suspended in shallower water (figure 5.3.5).

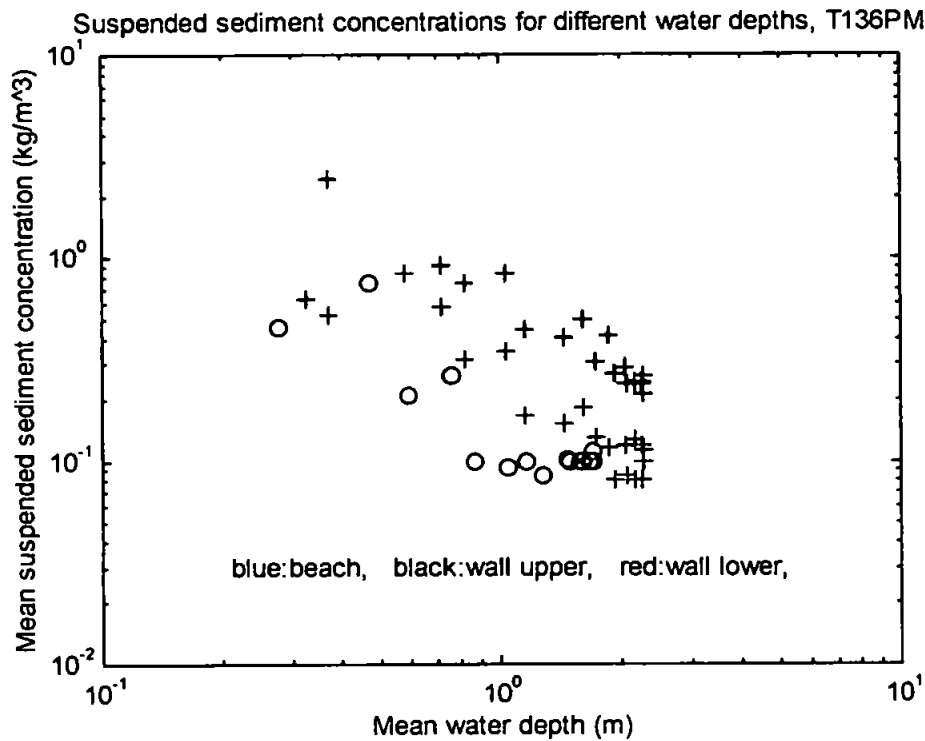


figure 5.3.5: Mean sediment concentrations at wall and beach. 'Upper' and 'lower' refer to the instrument positions on the rig.

A minimum suspension level is visible in the above plot at approximately 0.1kg/m^3 . Above this it is clear that at any particular depth, the mean sediment concentration is greater at the seawall than at the beach. There also appears to be a relationship between water depth and concentration at the height of the instruments on the wall rig. The coarse averaging over a run may result in lost information in the case of the beach rig, although a similar trend is in evidence. Data from sites with different reflection coefficients may indicate whether a different reflection coefficient alters the slope of this line, its intercept or both. With these factors understood, a parameterisation linking reflection coefficient, water depth, wave height and mean suspended sediment concentration at some depth is likely to be possible. An appropriate normalisation may also remove the hysteresis which is evident in the graph.

The next result concerns the phase of suspension events. Figure 5.3.3 displayed a typical suspension sequence which occurs outside the surf zone on a natural beach. Sediment is suspended as the crest of the wave passes the instrument and is moved onshore by the onshore velocity associated with that phase of the wave. Suspension events therefore coincide with the velocity (and shear stress) maximum associated with each wave. At the seawall however, the phase of suspension is less clear. Suspension events are observed to occur most frequently with the maximum elevation. However, the complicated nature of

the velocity field means that this may be at times of maximum velocity or at times of flow reversal. When the velocity is maximum, a plausible explanation is that the sediment peaks are driven by the velocity shear in the boundary layer (e.g. figure 5.3.6, peak at 910 seconds). However at times of flow reversal, the velocity (and shear stress) is 90° out of phase with the elevation (standing wave case), and the suspension events which occur at this time are therefore occurring at times of minimum shear stress (e.g. figure 5.3.6, peak at 955 seconds).

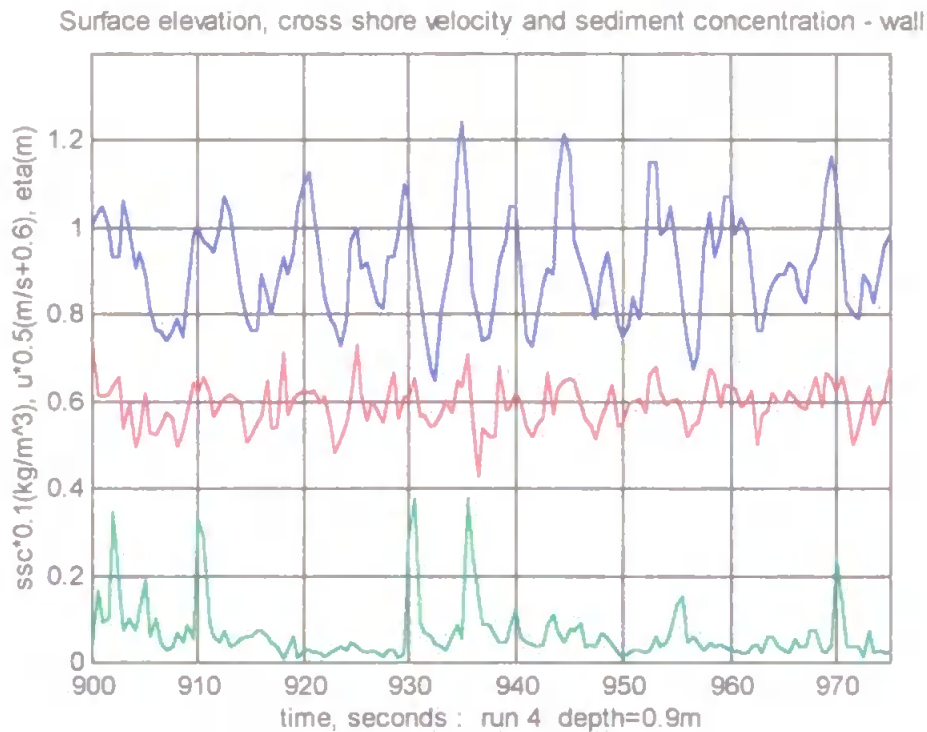


figure 5.3.6: Suspension events at the wall occurring in phase with velocity and elevation. This contrasts figure 5.3.4 where the phase of suspension is less clear.

When the water is sufficiently shallow, the phase relationship between elevation and velocity in the standing wave case is complicated, as solitary waves interact individually with the wall. The mechanism driving suspension events when the water is shallow is not clear from the time series (e.g. figure 5.3.4). Spectral analysis provides some insight into the transport of sediment, and this is covered in the next section. An attempt to identify how the wave reflection at the wall drives the suspension of sediment using a data simulation is presented in the discussion.

The result which has persistently been evident during the analysis is that the reflection of wave energy over the beach in front of the wall leads to an increase in sediment concentration.

5.4 The relationship between reflection and cross-shore sediment transport

The presence of a seawall at the head of the beach has been shown to increase the reflection of wave energy over the bed. Measurements in front of the seawall have shown this increases the amount of sediment in suspension, and affects the phase at which this suspension takes place. This section examines the effect of the incoming and outgoing waves on the sediment transport by looking at the way in which the hydrodynamics and suspension events interact at each frequency. The technique usually used to examine the frequency dependent sediment transport on natural beaches is the co-spectrum (Huntley and Hanes, 1987). The co-spectrum between incoming or outgoing waves and the sediment show how these components contribute to the on-offshore transport of sediment on the beach. The development and proof of the technique is covered in chapter 4.

The spectral techniques are applied to individual runs of data. The result is an average of processes for that run. Reflection analysis indicates the amount of energy which is incoming to the beach (or wall) and outgoing from it at different frequencies. The co-spectral technique for incoming and outgoing sediment transport indicates the magnitude and direction (on or offshore) of transport which occurs at each frequency. The results for the beach and wall are directly comparable as identical techniques are applied to each data set. Runs that are compared have similar water depths wherever possible. A typical result obtained is shown in figure 5.4.1.

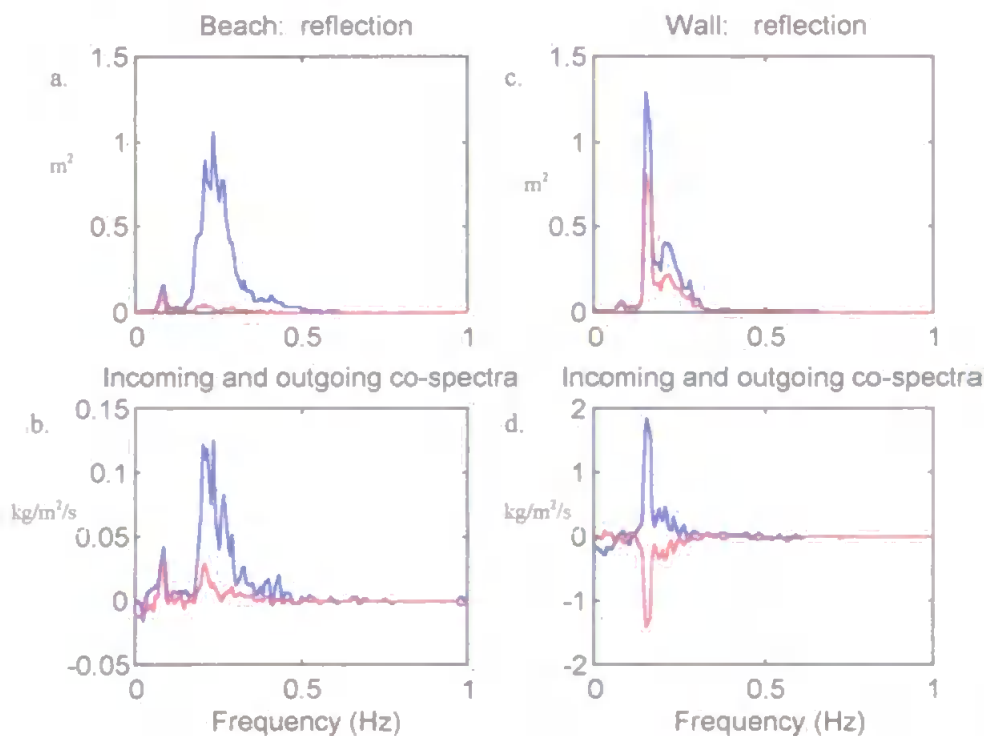


figure 5.4.1: Run 8 on the beach, run 6 at the wall, water depth = 1.4m. The colour protocol is: blue incoming, red: outgoing.

First consider the case of the beach (figure 5.4.1a). Spectral analysis of the calculated incoming and outgoing time series shows that the incoming waves exist at a frequency of 0.25Hz, and there is a lower frequency peak at 0.08Hz. While energy at the incident wave frequency is dissipated, the lower frequency energy is reflected. The phase of suspension events within the run mean that the net sediment transport associated with the incident waves is onshore (5.4.1b), while there is little transport associated with the offshore travelling waves. This result is as expected.

At the seawall, there is an increase in the offshore travelling energy at the incident wave frequency as this has not been dissipated by the shoreline but is reflected back over the beach (5.4.1c). The transport associated with the incoming waves is onshore (5.4.1d), while the transport associated with the offshore travelling waves is offshore. Physically, there is a net onshore transport on the natural beach resulting from onshore transport by the incident waves. At the seawall, however, this onshore transport is balanced by an offshore transport by the offshore travelling waves. The net transport is decreased, and the onshore transport is halted by the wave reflections. The gross transport has increased, however, and more sediment is being kept in suspension in front of the wall by the reflected waves than is present on the natural beach. This sediment is available for transport by longshore currents and thereby enhances the sediment transport in front of the seawall.

The separation of the incoming and outgoing transports is considered valid in the same way that splitting the transport to examine the different contributions of various frequencies to the sediment transport. It does not, however, indicate that suspension results from the processes separately. It must be recognised that the suspension occurs as a result of the total hydrodynamic (velocity / pressure) field. The suspension of sediment appears highly non-linear in that a re-doubling of the wave field over itself causes a disproportionate response in the sediment as was seen in the time series. However, the separation of the components of the transport provides information on the relative importance of the incoming and outgoing waves and illustrates that while sediment is maintained in suspension in front of the wall, it is prevented from being moved onshore with the incoming waves by the outgoing waves. This description is particularly applicable in shallow water, where waves traverse the shoreline as solitary waves. When moving onshore they move sediment in their direction of travel. Having been reflected, they travel offshore, and sediment suspended as the wave crest passes over is then moved offshore.

The result is found to occur throughout the tide while sufficient suspension occurs for there to be any transport (see figure 5.4.2). In deeper water the processes are similar, although the magnitudes of the transport decrease as the waves interact less with the bed (figure 5.4.3). There is little difference to the processes observed on the ebb tide (figure 5.4.4), although the magnitude of the transport has decreased in this example. This is a result of the decrease in wave activity in the latter part of this tide.

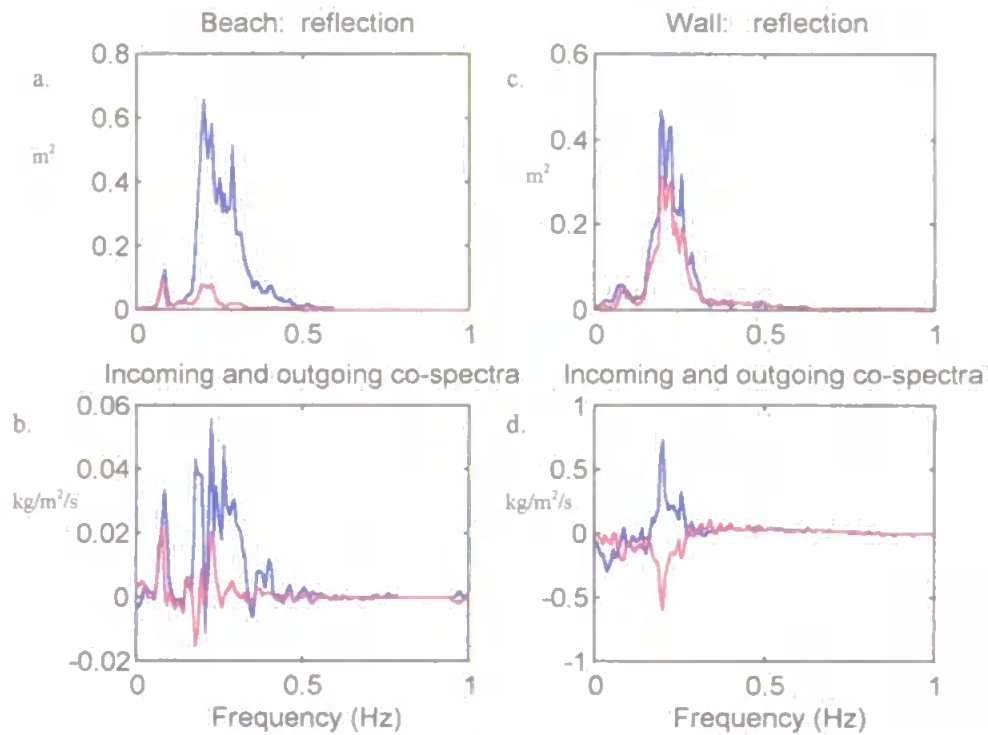


figure 5.4.2: Run 9 on the beach, run 7 at the wall. water depth=1.6m.

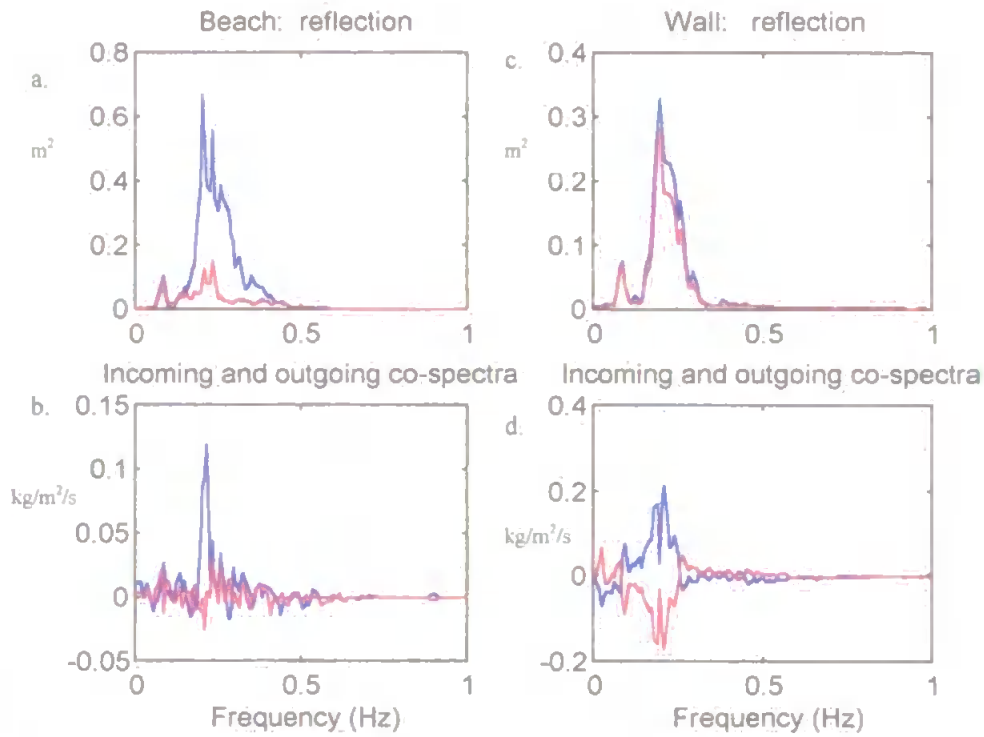


figure 5.4.3: Run 12 on the beach, run 9 at the wall, water depth =1.9m

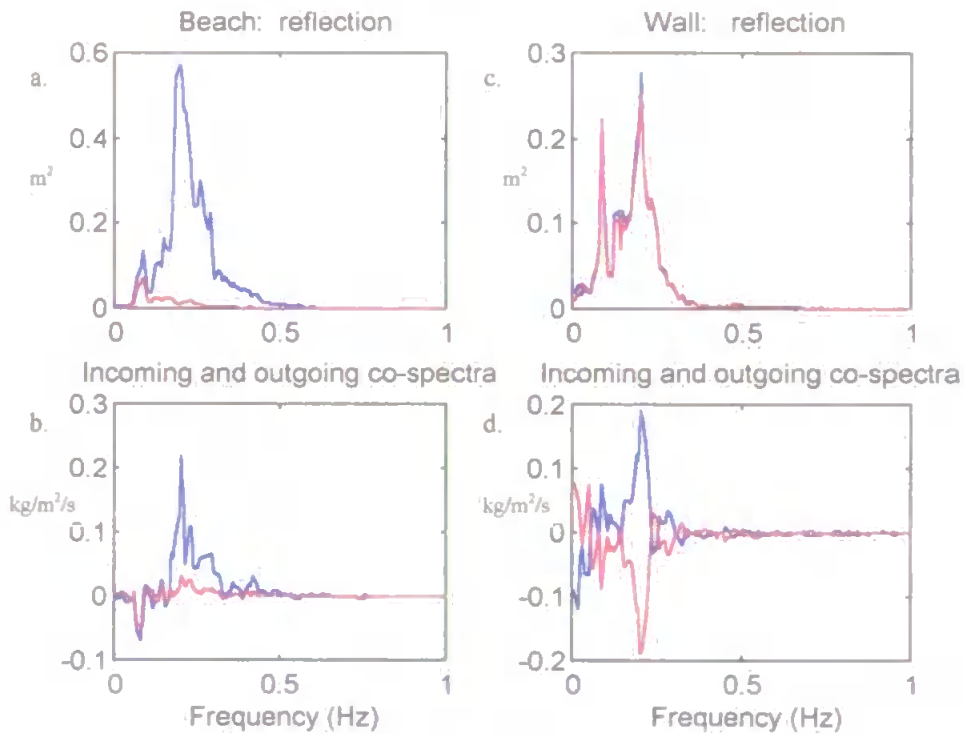


figure 5.4.4: Run 19 on the beach, run 21 at the wall, water depth =0.9m.

The important points that this analysis draws out are that:

1. Incident waves are reflected by the seawall and their energy is re-applied to the bed in front of the wall.
2. Incoming waves in both wall and beach cases transport sediment onshore.
3. Outgoing waves reflected by the seawall transport sediment offshore.

4. The offshore transport balances the onshore transport and inhibits accretion at the head of the beach.
5. There is an increase in sediment suspension in front of the wall resulting from the reflection of the energy over the bed.
6. The extra sediment in suspension is available for longshore transport.

There is however a limitation of the result. In beach experiments instruments record data from a variety of water depths. As the tide floods over an instrument array, the surf zone moves shorewards and the instruments are therefore able to make measurements of the dynamics at any cross-shore distance from the shore, provided the instruments are covered, the beach slope is linear, runs are sufficiently short for stationarity to be observed, and conditions do not change during the tide. In the wall case the cross-shore distance from the shore is fixed by the seawall, and it was therefore not possible to obtain a set of measurements from different positions within the nodal structure in front of the wall. This would require a considerably larger array of instruments. Despite this limitation, high frequency measurements of sediment suspension and transport processes directly in front of a seawall have never been successfully been made before. The results are therefore unique. Armed with the knowledge gained by the present experiment, it will be possible to carry out further experiments to examine how the suspension processes vary with cross-shore distance from the wall.

5.5 Sediment transport by mean currents

Jaffe *et al.* (1984) split sediment transport components into mean and oscillatory components. Sediment is transported by mean currents both along the coast and across a beach. In order to examine the nature of the mean sediment transport it is first necessary to examine the mean currents.

Figure 5.5.1 shows the mean currents calculated for a representative example tide of data. Cross-shore currents were found to be onshore at the wall rig for most of this tide. The reason for this is as follows. The EMCM is located at 10cm above the bed, and instruments were logging from run 4 when the water depth was $\cong 0.6\text{m}$. The instrument was therefore in the lower part of the water column, but above the boundary layer. There is known to be a circulatory cell inside the standing waves, and in this part of the standing wave the flow is onshore (Longuet Higgins, 1953). The gradual decrease in velocity is a result of the gradual decrease in wave activity throughout the tide. It would therefore be reasonable to expect a weak onshore transport of sediment by the mean currents in this part of the standing wave. This onshore transport ($\leq 0.05\text{kg/m}^2/\text{s}$) decreases dramatically as the water deepens to high water and the wave activity decreases (figure 5.5.2).

Cross-shore currents at the beach rig are directed offshore, a result which may be attributable to Longuet Higgins (1953) solution for the profile of mass transport within a standing wave. However, other workers have found mean transports to be onshore in this region (c.f. Russell *et al.*, 1991), and as the values lie inside the 10% error bar, the observed offshore mean current past the beach rig is not conclusive.

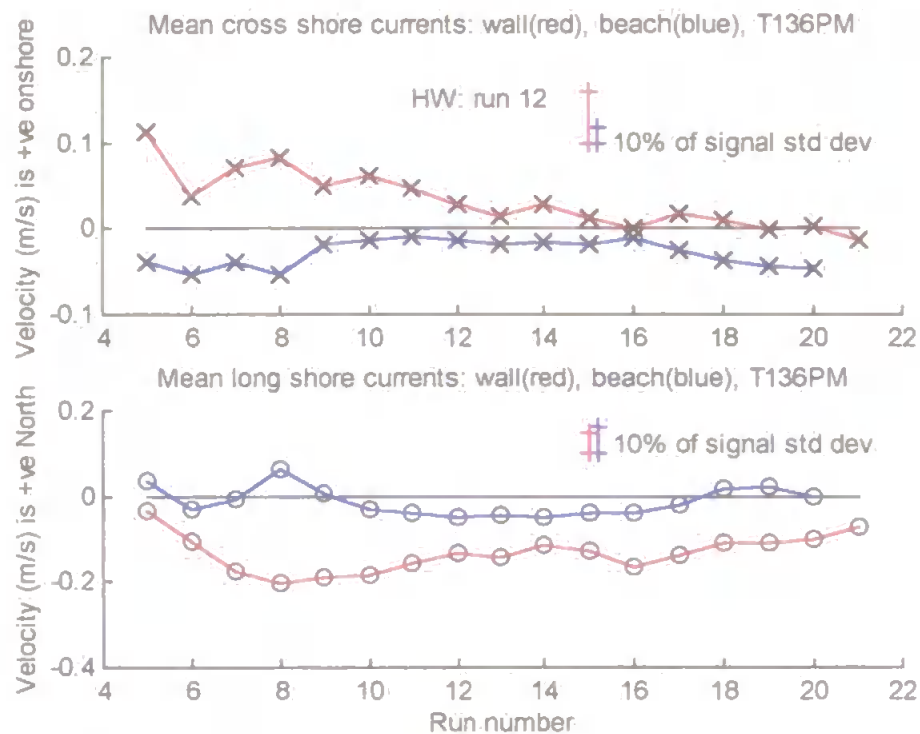


figure 5.5.1: Mean velocities at wall and beach rigs.

The main interesting result which has arisen from the mean currents is the strong longshore flow which is observed to flow along the wall to the south. This current is significantly smaller on the beach. The result is a persistent longshore sediment flux at the wall which is greater than that observed at the beach.

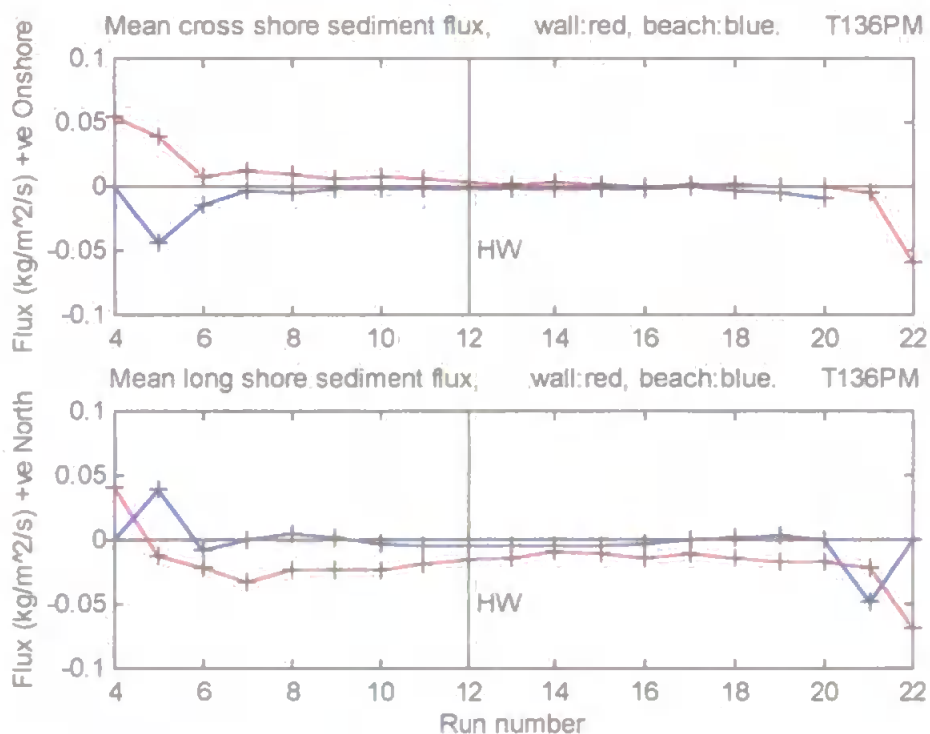


figure 5.5.2: Mean sediment fluxes at beach and wall rigs.

Waves are responsible for stirring the sediment and wave reflection in front of the wall increases the amount of sediment in suspension. This sediment in suspension is then available for transport by the mean longshore current, a current which has itself been accelerated by the presence of the wall. Contributions to the total transport are made by the oscillatory flux coupling ($u'c'$), the cross-shore transport by the mean cross-shore current ($\bar{u} \bar{c}$) and the longshore sediment transport by the mean longshore current ($\bar{v} \bar{c}$). The relative magnitudes of these components for tide T136PM are illustrated in the table below:

Wall					
h	$u'c'$	$u_{in}'c'$	$u_{out}'c'$	$\bar{u} \bar{c}$	$\bar{v} \bar{c}$
1.7727	0.0001	0.0011	-0.0010	0.0095	-0.0238
1.5346	-0.0002	0.0048	-0.0050	0.0131	-0.0321
1.2438	0.0021	0.0138	-0.0118	0.0078	-0.0215

Beach					
h	$u'c'$	$u_{in}'c'$	$u_{out}'c'$	$\bar{u} \bar{c}$	$\bar{v} \bar{c}$
1.7017	0.0014	0.0013	0.0001	-0.0014	0.0052
1.4681	0.0016	0.0015	0.0001	0.0019	-0.001
1.2791	0.0029	0.0026	0.0003	-0.0045	0.0053

table 5.5.1. Values of the run-averaged oscillatory flux coupling ($u'c'$), incoming and outgoing flux coupling components ($u_{in}'c'$ and $u_{out}'c'$), sediment transport by mean cross-shore currents ($\bar{u} \bar{c}$) and by mean longshore currents ($\bar{v} \bar{c}$) for different water depths at each rig, T136PM. Positive values imply onshore flux or northerly fluxes in the longshore case. Units of water depth (h) are meters, and flux are $kg/m^2/s$.

In the wall case, the total oscillatory transport (i.e. the flux coupling $u'c'$) is close to zero, as the offshore sediment flux by the outgoing waves ($u_{out}'c'$) is sufficient to balance that by the incoming waves ($u_{in}'c'$). Both the onshore transport by the incoming waves and the outgoing transport by the outgoing waves increase with decreasing water depth. While the waves are responsible for suspending a considerable amount of sediment in front of the wall, the balance between incoming and outgoing oscillatory sediment fluxes means that the mean cross-shore sediment flux component ($\bar{u} \bar{c}$) is large compared to the flux coupling ($u'c'$). At the height of the instruments, this mean flux is onshore, although the direction and magnitude of the mean flux will vary with height above the bed. The mean longshore transport is directed to the south at the wall rig.

At the beach rig, the flux coupling is dominated by the onshore component and is directed onshore. The mean cross-shore flux is of similar magnitude to the oscillatory flux, although both are generally smaller than at the wall rig. Mean longshore fluxes are also considerably smaller than at the wall rig.

5.6 Sediment transport: results from other days

5.6.1. Introduction

In previous sections of this chapter a detailed analysis of the PM tide of the 13th June was presented. This section gives results of analyses which were carried out on data from the tides of the 12th, 13th and 14th of June.

Similar analysis procedures to those applied to the T136PM were applied to data from the other tides. Mean sediment concentrations were analysed first as these indicate the fundamental difference between the reflective and non-reflective environment. Frequency dependent wave reflection and sediment transport analysis was carried out next. Mean sediment fluxes were obtained in cross-shore and longshore directions.

During the period of observation, the waves gradually decreased in size, leading to a variety of observational conditions (figure 5.6.1.1). Despite this, the observations of processes made of tides T126PM, T136AM and T146AM were found to be consistent with the results from tide T136PM.

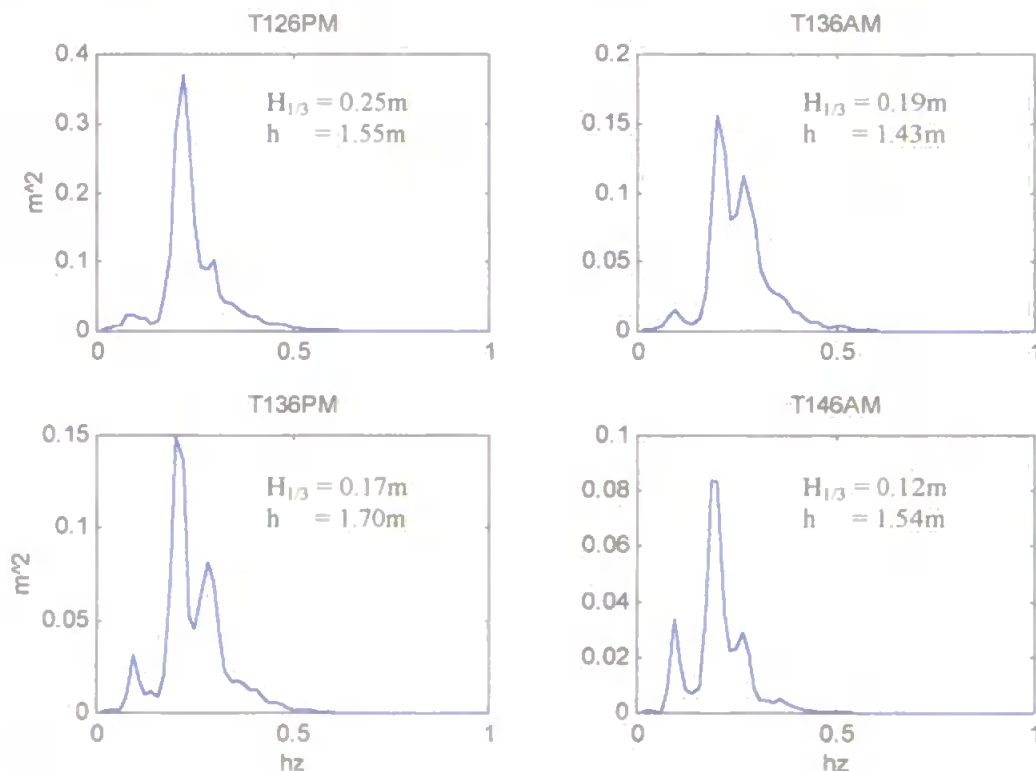


figure 5.6.1.1. Wave elevation spectra from the beach rig at high tide for the tides analysed showing the gradual decrease in wave activity. Wave heights are calculated directly from the spectra.

5.6.2 June 12th, PM tide analysis

Waves during the tide of 12th of June were typically 30cm high at the breakpoint with a period of 4 seconds (see table 3.3.6.1). These were the largest waves experienced during the experiment. Mean sediment concentrations for this tide are shown in figure 5.6.2.1.

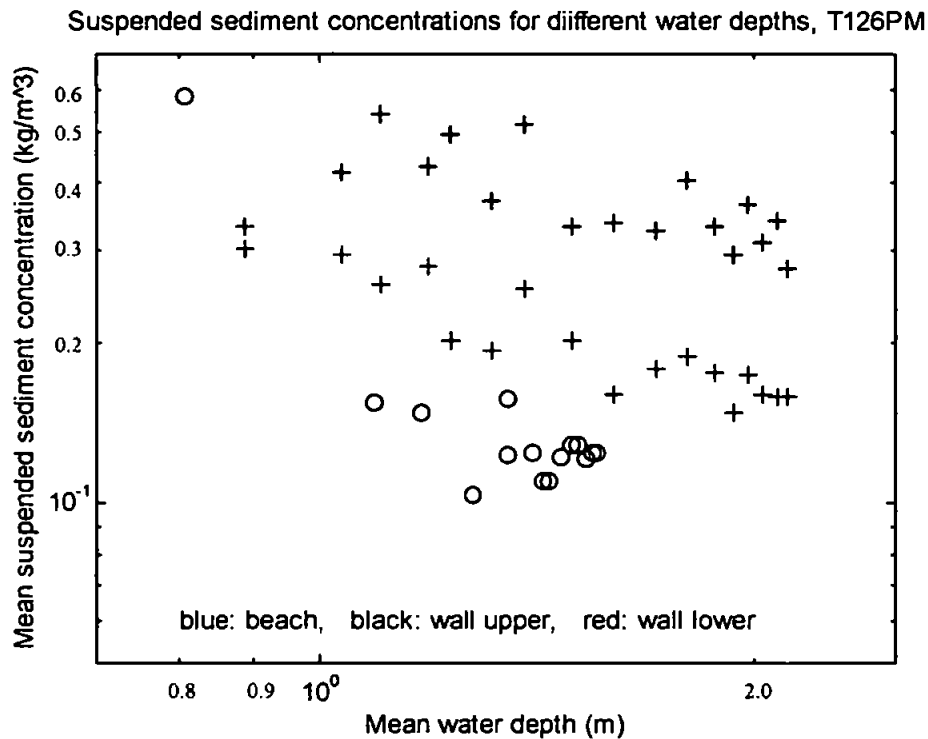


figure 5.6.2.1.

The beach OBS and wall upper OBS were at similar heights above the bed during all runs. Each point represents the mean concentration of sediment at that instrument during a run. When water depths were similar at the beach and wall rigs, there was consistently more sediment in suspension in front of the wall. Generally, in shallower water, more sediment was suspended at both wall and beach rigs.

The wall rig results also indicate that mean concentrations increase towards the bed. This broadly agrees with the results of Nielsen (1979), who found an exponential increase in sediment concentration towards the bed depending on the bed roughness. This was given as:

$$c_s(z) = C_0 \exp(-z/L_s) \tag{5.6.2.1}$$

where C_0 is the reference concentration at the bed ($C_0 = \bar{c}_s$ at the bed) and L_s is a vertical length scale (Nielsen, 1984). The L_s term represents the balance between vertical diffusivity and settling.

An estimation of L_s can be obtained for each run where the mean concentration is known at each of the two instrument heights using a re-arranged form of 5.6.2.1:

$$L_s = -\frac{z_1 - z_2}{\ln \bar{c}_{s1} - \ln \bar{c}_{s2}} \quad 5.6.2.2$$

where the subscripts 1 and 2 refer to the two different instruments.

Values of L_s were obtained throughout the tide, and the average for the whole tide obtained. In the case of T126PM the average value of L_s was found to be 0.153m. Maximum and minimum values obtained were 0.26m and 0.11m respectively.

Black and Rosenberg (1991) used a similar technique to examine values of L_s from the surf zone. They found smaller values outside the surf zone and near the breakpoint (0.055-0.071m), and larger values inside the surf zone (0.252-0.308m). They attributed the higher L_s values inside the surf zone to greater time averaged turbulence intensity beneath broken waves. Sediment sizes at Black and Rosenberg's site (Apollo bay, southern Australia) were similar to Teignmouth - see Black and Rosenberg (1994). Black and Rosenberg (1991) gave typical orbital velocities of the incident waves as 1.5m/s.

At Teignmouth, incident wave orbital velocities were approximately 1m/s or less (c.f. figures 5.3.3, 5.3.2), and the estimates of L_s were made for periods when the water depth was greater than 1m (wave height=0.3m), indicating that waves would not have been breaking at the instruments. Despite the lower values of incident wave orbital velocities than those observed by Black and Rosenberg, values of L_s in non breaking conditions were higher in front of the wall than found by Black and Rosenberg on a natural beach. This indicates a greater vertical diffusivity in front of the Teignmouth wall than on the natural beach where Black and Rosenberg took their measurements.

The reference concentration was also calculated for runs where L_s was calculated. This was done using the equation:

$$C_0 = \exp \frac{z_2 \ln \bar{c}_{s1} - z_1 \ln \bar{c}_{s2}}{z_2 - z_1} \quad 5.6.2.3$$

Values of C_0 varied typically between 0.41 and 0.91kg/m³, the average for the tide being 0.6kg/m³. This value is similar to that obtained by Black and Rosenberg who gave a value of C_0 of 0.662kg/m³ outside the surf zone. Near the breakpoint however, Black and

Rosenburg found C_0 increased considerably, to a maximum of 38.9kg/m^3 , while in the surf zone these values dropped to 2.6kg/m^3 .

At the Teignmouth seawall, both L_s and C_0 showed a tendency to increase in shallower water, where greater amounts of suspension took place (figure 5.6.2.2). A certain amount of hysteresis is again evident in these plots (c.f. figure 5.3.5), indicating the importance of both wave height and water depth on these parameters.

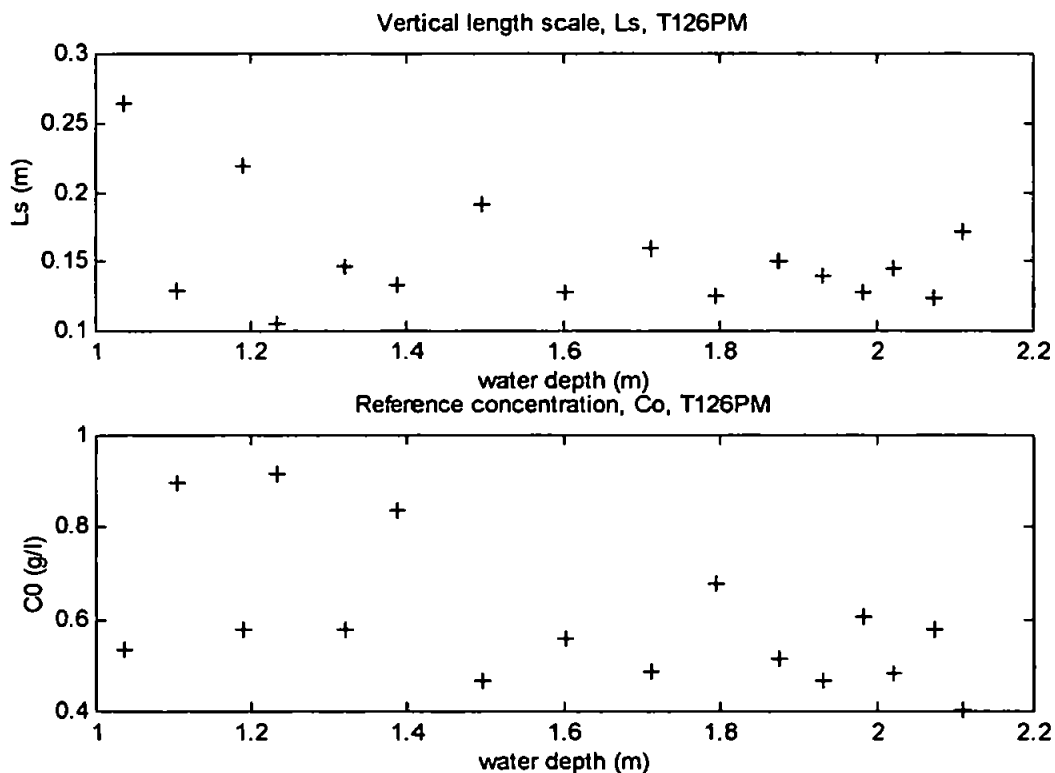


figure 5.6.2.2: Variation in vertical length scale L_s with depth (top) and variation in reference concentration C_0 with depth (bottom) for tide T126PM.

Detailed quantitative comparison with Nielsen's equation is limited however, as only two data points are available in the vertical plane for each run, and a comparable data set was not obtained at the beach rig. Furthermore, information on bed features was not obtained during the runs. Information on bedform scales is especially difficult to obtain in the field as the swash zone flattens such features as the tide ebbs, leaving a flat, consolidated beach. Also of interest in future deployments is the cross-shore variation in the parameters L_s and C_0 . Close to the wall larger values of L_s may be expected due to increased vertical velocities, while at the elevation node, greater orbital velocities leading to increased skin friction may be expected to result in enhanced reference concentration values. Both these effects would lead to enhanced sediment suspension in front of the wall, and both require further research.

The main conclusions that can be obtained from the mean sediment concentration plots in this study are therefore that:

- a) Mean sediment concentration are greater in front of the wall than on the natural beach.
- b) Mean sediment concentrations are a function of incident wave conditions, water depth and shoreline reflectivity.

The increase in mean suspended sediment concentrations in front of the wall reinforce the observations made by Dorland (1940), Silvester (1977) and Kraus (1988). It would be logical to expect that this enhancement of sediment suspension in front of the wall would lead to a difference in the morphodynamics between the wall and beach. However this idea is disputed by Kraus and McDougal (1996) and Moody (1996) who found no difference between wall and beach profiles. In this experiment, the wall did have a significant effect on the beach morphology, and this is discussed later in the next chapter.

Frequency dependent wave reflection and sediment transport analysis was carried out on data from tide T126PM. Figure 5.6.2.3 shows analysis carried out for runs 7 at the beach and run 5 at the wall. In this case the water depth at both wall and beach was 1.14m. Waves are effectively dissipated at the beach, while there is less dissipation at the wall. This results in onshore transport at the beach and wall by the incoming waves and offshore transport at the wall by the outgoing waves at incident wave frequencies.

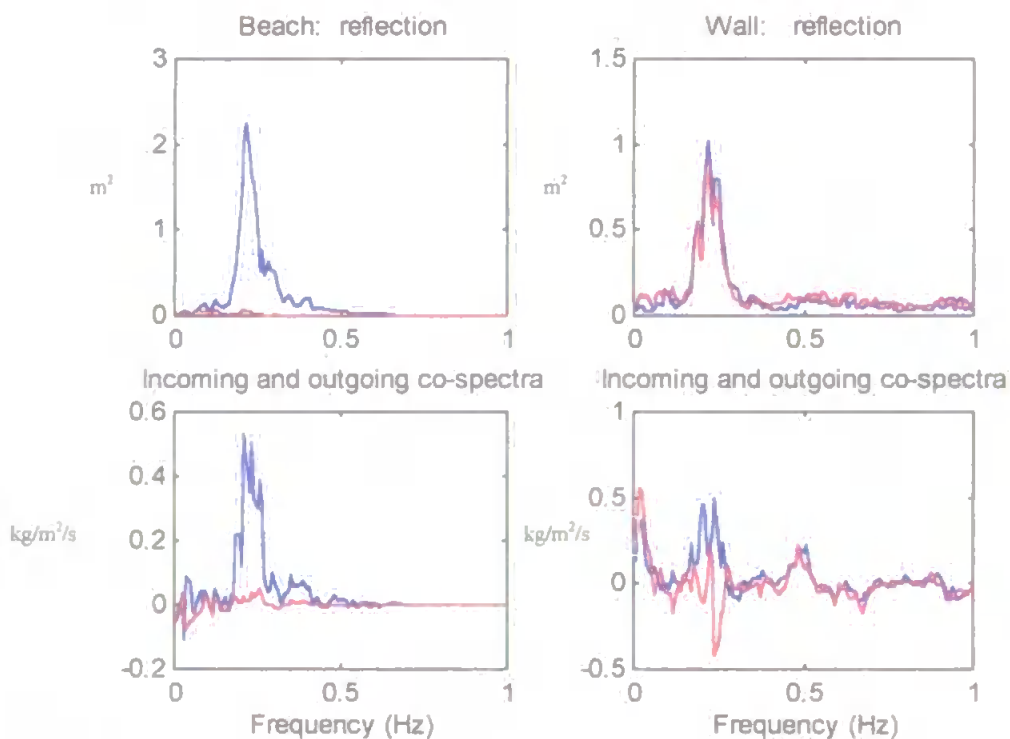


figure 5.6.2.3: Runs 7 (beach) and 5 (wall). Water depth: 1.135m.

At high water there is a greater amount of wave reflection at both the wall and the beach (figure 5.6.2.4). The wave reflection at the beach results from interactions with a small wall at the back of the beach. Interestingly, there is evidence in the co-spectra that the offshore directed waves may be responsible for transporting sediment offshore at this large distance from the reflector (negative peak in offshore directed co-spectra (beach co-spectra, red) at approximately 0.2hz). However, the relationship is not clear throughout the wind wave frequency band. Incoming and outgoing waves at the wall transport sediment largely as expected, although the offshore transport in this case appears to be slightly larger than the incoming transport.

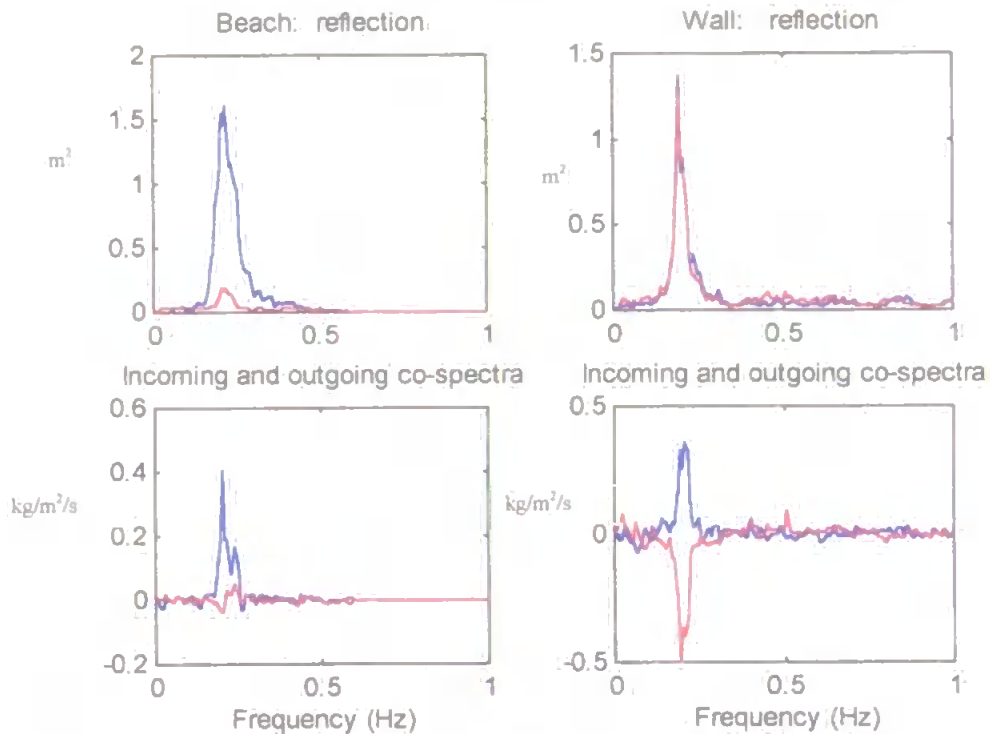


figure 5.6.2.4: Runs 13 (beach) and 17 (wall). Water depth: 1.55m.

The results on the ebb tide for this run show the same pattern of reflection and transport which has been shown earlier (figure 5.6.2.5). In this case the water depth is approximately 1m.

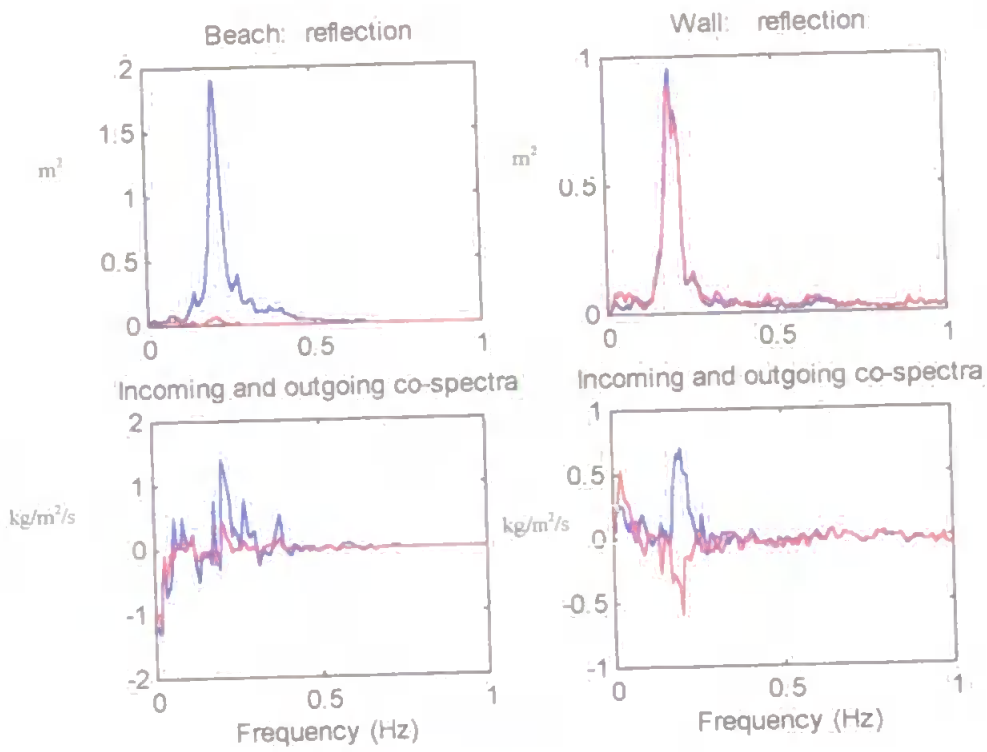


figure 5.6.2.5: Runs 17 (beach) and 19 (wall). Water depth 0.98m.

Mean sediment fluxes were found to be onshore at the wall rig, an observation which agrees with that found on the T136PM tide (presented earlier in this chapter). Mean sediment fluxes are presented in figure 5.6.2.6.

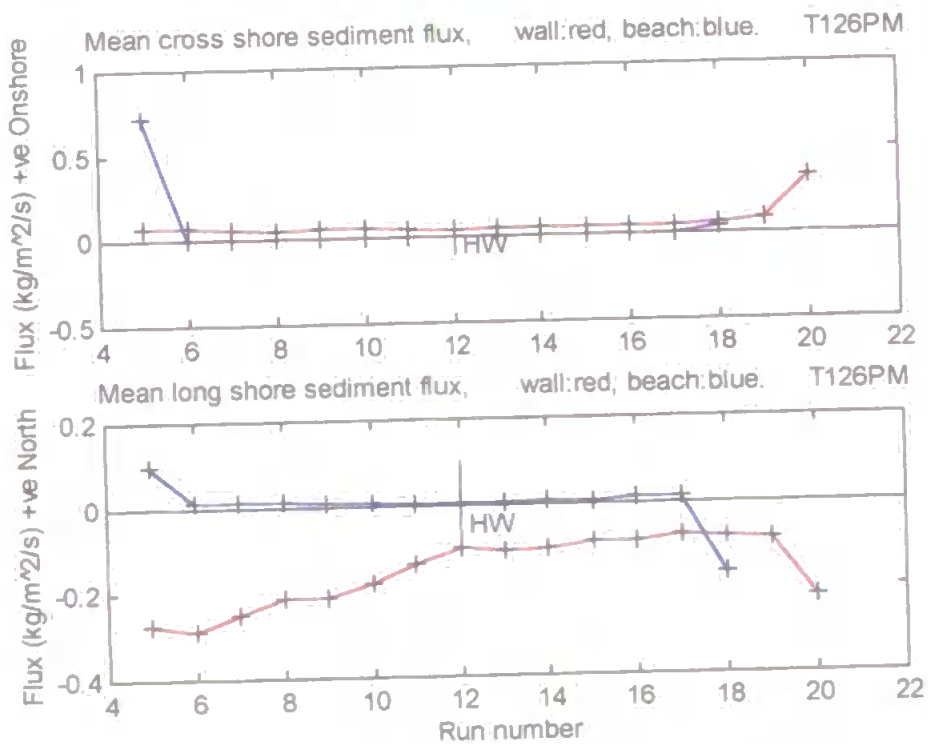


figure 5.6.2.6: Mean cross-shore and longshore sediment transport rates at the beach and wall, T126PM.

Mean cross-shore fluxes at the beach rig were weak compared to the wall cross-shore fluxes. Longshore sediment transport rates at the wall rig were considerably larger than at the beach rig and were directed to the south. It is likely that the longshore current was wave driven, resulting from a slight angle of wave incidence. Increased levels of sediment suspension in front of the wall led to an enhanced sediment transport in the longshore direction.

Values of the components of the total flux are given in table 5.6.2.1 below.

Wall					
h	$u'c'$	$u_{in}'c'$	$u_{out}'c'$	$\bar{u} \bar{c}$	$\bar{v} \bar{c}$
1.5503	0.0005	0.0138	-0.0132	0.0493	-0.0776
1.2545	0.0000	0.0047	-0.0046	0.0640	-0.0812
0.9618	-0.0001	0.0110	-0.0111	0.0815	-0.0845

Beach					
h	$u'c'$	$u_{in}'c'$	$u_{out}'c'$	$\bar{u} \bar{c}$	$\bar{v} \bar{c}$
1.5164	0.0051	0.0048	0.0002	0.0037	0.0033
1.1807	0.0078	0.0108	-0.0030	0.0027	0.0142
0.9799	0.0093	0.0143	-0.0050	0.0028	0.0132

table 5.6.2.1. Values of: run-averaged oscillatory flux coupling ($u'c'$), incoming and outgoing flux coupling components ($u_{in}'c'$ and $u_{out}'c'$), sediment transport by mean cross-shore currents ($\bar{u} \bar{c}$) and by mean longshore currents ($\bar{v} \bar{c}$) for different water depths at each rig, T126PM. Positive values imply onshore flux or Northerly in the longshore case. Units of water depth (h) are meters, and flux are $kg/m^2/s$.

As in the T136PM tide, incoming oscillatory sediment fluxes are balanced by outgoing sediment fluxes at the wall. At the beach, the flux coupling associated with the incoming waves is not balanced by offshore travelling waves, and the total oscillatory transport at the beach is therefore onshore. Mean cross-shore sediment fluxes at the wall are large compared to the oscillatory fluxes, a result of the large amount of sediment in suspension there. Mean cross-shore sediment fluxes at the beach are generally less than the oscillatory component, as expected.

Longshore transport at the wall is again directed towards the south, and is considerably larger than the transport observed at the beach rig. In both cases, sediment fluxes decrease as the water depth increases.

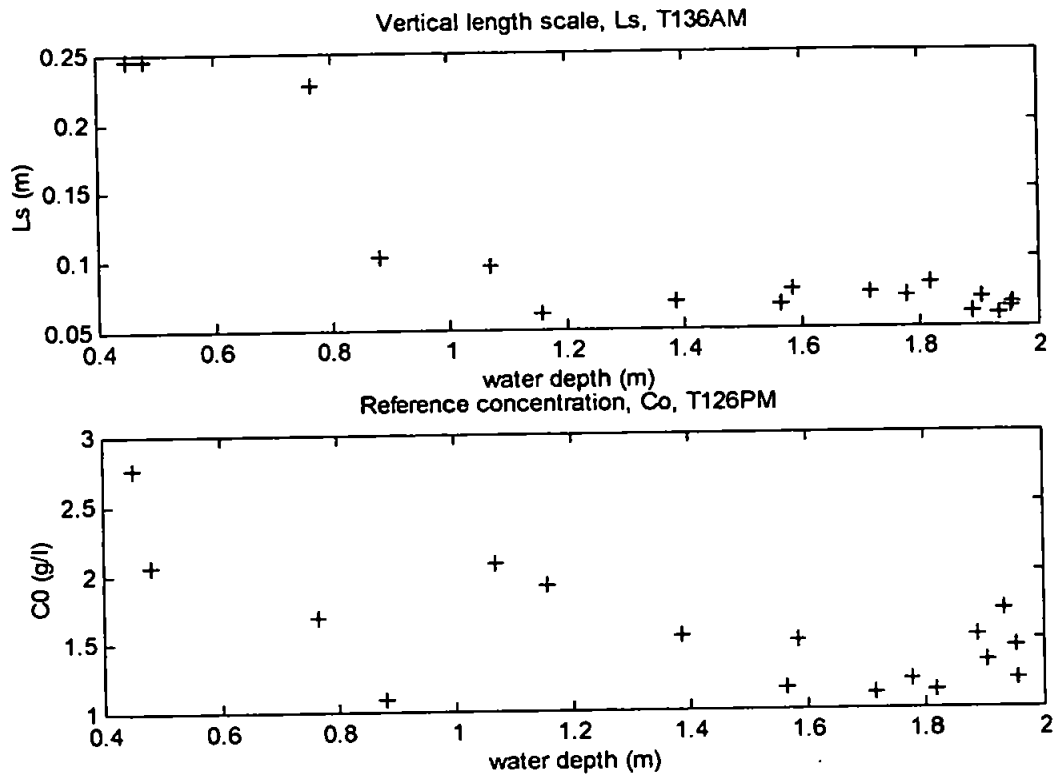


figure 5.6.3.2: Variation in vertical length scale L_s with depth (top) and variation in reference concentration C_o with depth (bottom) for tide T136AM.

Like June the 12th, data collected during this tide also conformed to the expected frequency dependent reflection and sediment transport picture, the only deviation being the reflection coefficient which is slightly larger than unity in the case shown (figure 5.6.3.3). This is likely to be a result of a small amount of noise in the data put through the time domain analysis procedure, and the error is not considered significant.

Data for this run were collected while the water depth at each rig was approximately 1.5m. At the wall rig, the transport directions associated with the incoming and outgoing gravity frequency waves again display the onshore transport associated with the incoming waves and offshore transport associated with the offshore travelling waves at the wall rig. There is some uncertainty that the low frequency sediment transport peak showing onshore transport by offshore travelling waves is real, as coherence between the outgoing wave velocity and sediment concentration was low at this frequency.

At the beach rig only the incoming waves transport a significant amount of sediment, and this is an onshore direction.

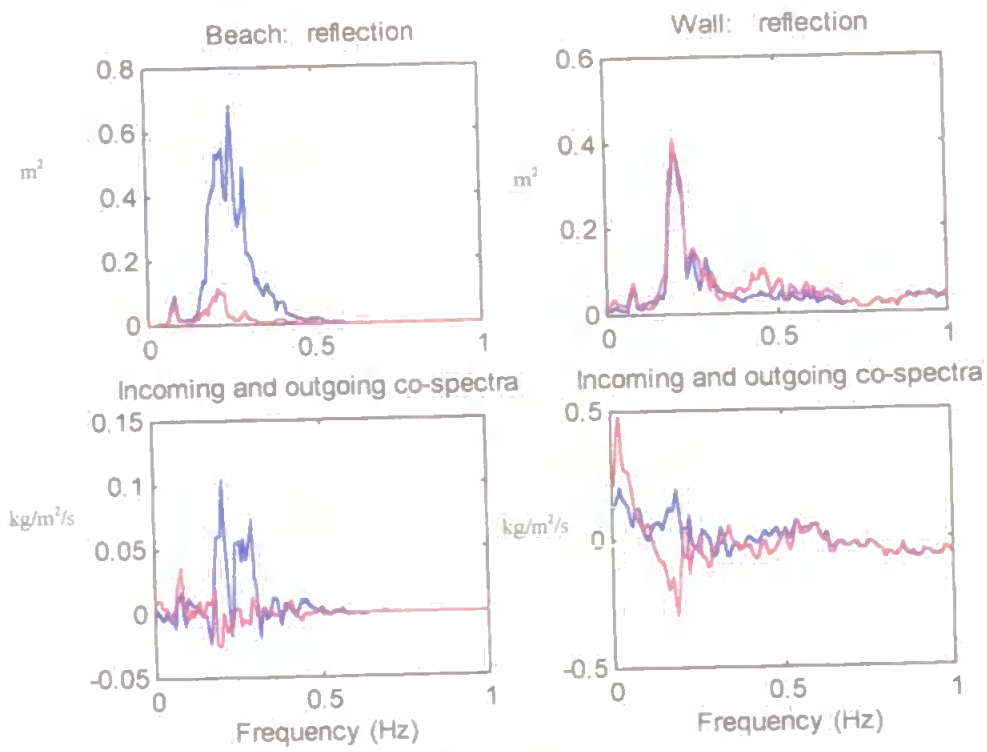


figure 5.6.3.3: Beach run 11, $h=1.4258$ Wall run 7, $h=1.5839$.

Similar results were obtained for slightly shallower water than this (see figure 5.6.3.4).

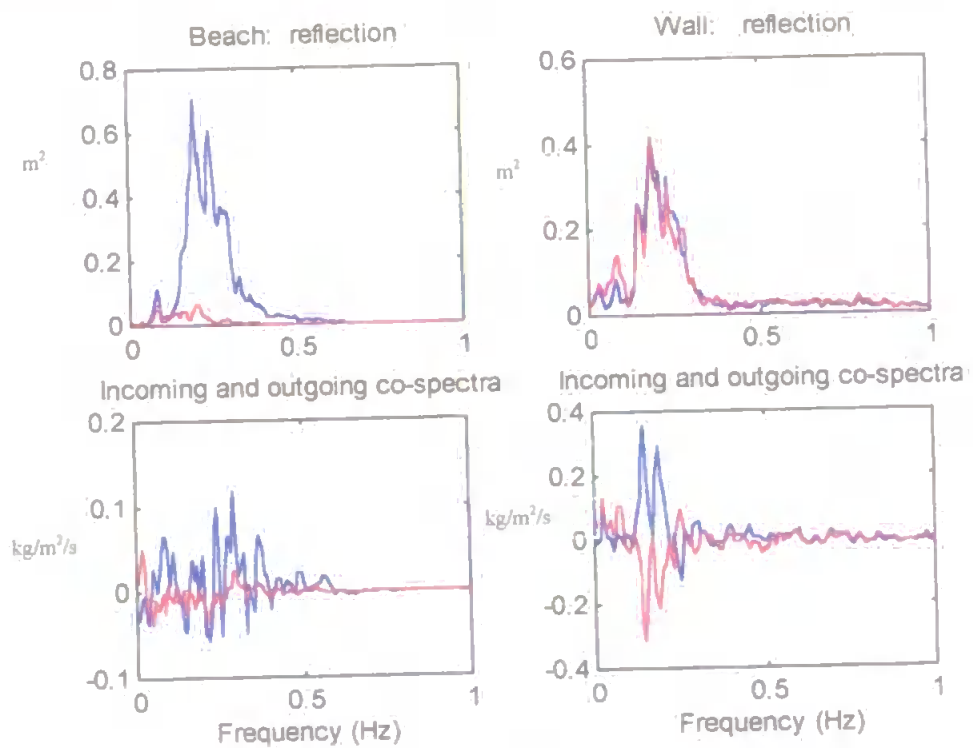


figure 5.6.3.4: Beach run 15, $h=1.1913$. Wall run 18, $h=1.1582$.

In both cases the magnitude of the co-spectral peaks for wall and beach co-spectra were considerably smaller than those found in similar water depths during the previous tide (see figures 5.6.2.3, 5.6.2.4, 5.6.2.5). This is a result of the decrease in wave activity between the two tides.

An interesting variation to this was evident during the ebb tide, where the sediment transport over the beach associated with the incoming gravity waves switched direction, and became an offshore transport (figure 5.6.3.5b). A similar result to this has been found by Davidson *et al.* (1993b) who associated the offshore transport observed at incident wave frequency with the presence of ripples outside the surf zone. This was the only example where this phenomenon was observed in this data set.

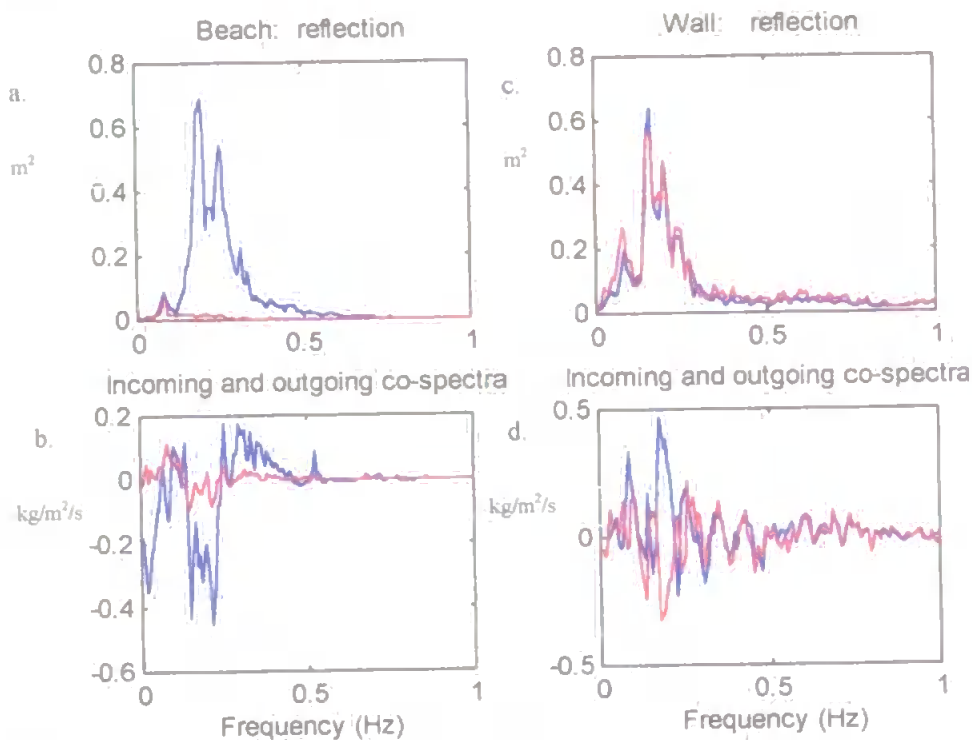


figure 5.6.3.5: Beach run 17, $h=0.8624$, Wall run 19, $h=0.8832$.

Unfortunately, field offsets for the current meters were incorrectly recorded after this tide and inferences about mean sediment transport magnitudes and directions are difficult. Application of the laboratory obtained offsets in place of the field offsets give the results shown in figure 5.6.3.6. Mean cross-shore sediment transport at the beach rig is small, a result which agrees with previous observations. Mean cross-shore sediment transport at the wall rig is offshore, a result which is unlikely to be correct - indicating an error in the offsets. Longshore sediment transport past the beach rig was small, as observed during other tides. Longshore transport at the wall is to the south, and is similar in magnitude to that observed during other days.

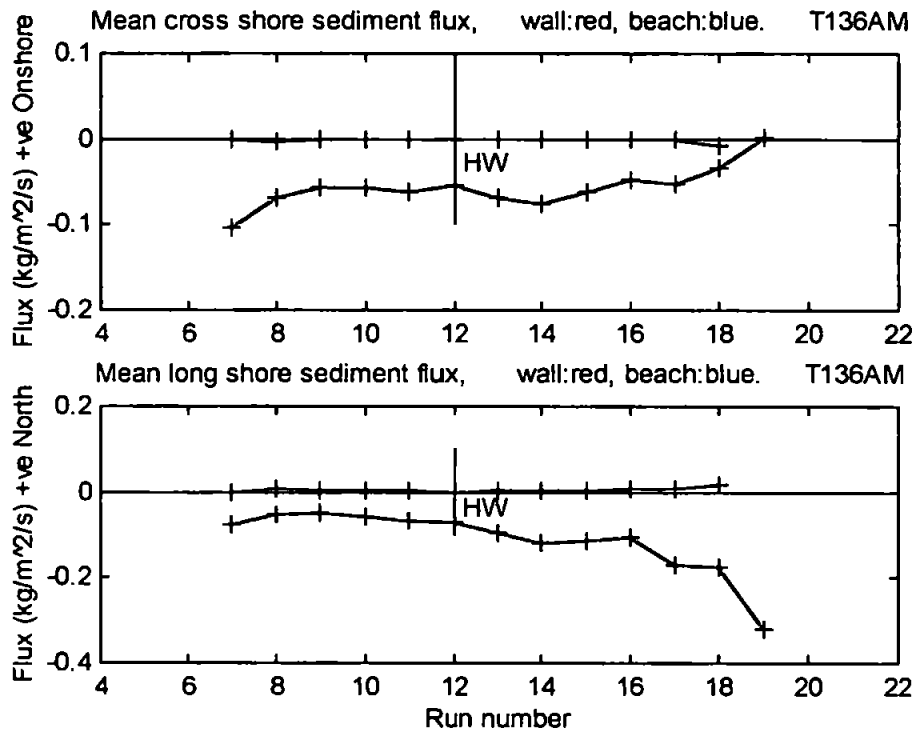


figure 5.6.3.6: Mean sediment transport rates in front of the wall and at the beach: T136AM.

The relative contributions made to the transport by the mean and oscillatory components are summarised in the table below (table 5.6.3.1).

Wall					
h	$u'c'$	$u_{in}'c'$	$u_{out}'c'$	$\bar{u} \bar{c}$	$\bar{v} \bar{c}$
1.3851	0.0025	0.0048	-0.0023	-0.0520	-0.1724
1.1582	0.0004	0.0035	-0.0031	-0.0342	-0.1762
0.8832	0.0014	0.0056	-0.0042	0.0009	-0.3200
Beach					
h	$u'c'$	$u_{in}'c'$	$u_{out}'c'$	$\bar{u} \bar{c}$	$\bar{v} \bar{c}$
1.3763	0.0020	0.0019	0.0001	-0.0017	0.0021
1.1913	0.0014	0.0017	-0.0003	-0.0011	0.0030
0.8624	-0.0030	-0.0035	0.0006	-0.0012	0.0061

table 5.6.3.1. Values of the run-averaged oscillatory flux coupling ($u'c'$), incoming and outgoing flux coupling components ($u_{in}'c'$ and $u_{out}'c'$), sediment transport by mean cross-shore currents ($\bar{u} \bar{c}$) and by mean longshore currents ($\bar{v} \bar{c}$) for different water depths at each rig, T136AM. Positive values imply onshore flux or Northerly in the longshore case. Units of water depth (h) are meters, and flux are $\text{kg/m}^2/\text{s}$.

The trends in the values are similar to those observed in the T126PM, with three notable exceptions. Firstly, in the last set of values for the beach data (0.86m depth) note that the oscillatory flux is offshore. This is the same run described above where the co-spectrum gave offshore transport at incident wave frequency, possibly related to the destruction of the ripple field on the ebb tide (Davidson *et al.* 1993b). Secondly, the magnitudes of onshore transport by the waves ($u_{in}'c'$) has decreased in the T136AM tide compared to the T126PM tide (beach and wall data). This is attributed to the decrease in wave activity. Finally, the cross-shore flux by the mean flow is offshore at the wall in this run.

5.6.4. June 14th AM tide analysis

By the 14th of June, wave activity had decreased considerably, wave heights on the beach being typically 0.1m at the breakpoint. Mean suspended sediment concentrations obtained for the tide of T146AM are shown in figure 5.6.4.1.

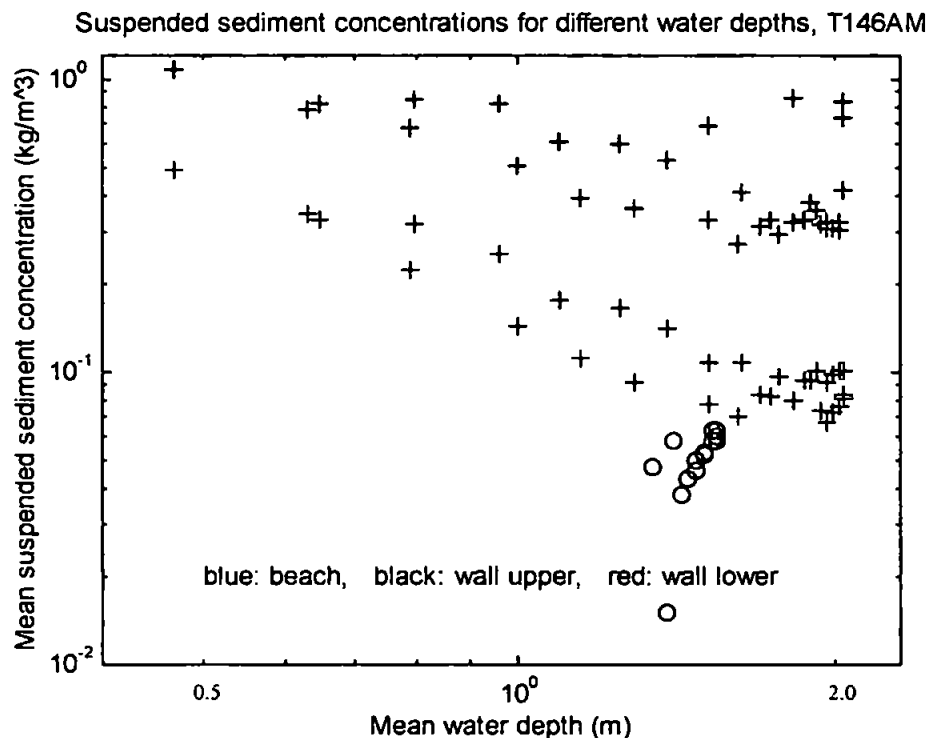


figure 5.6.4.1.

For this tide, mean concentrations were taken for half of each run, and are plotted above. This gave a clearer picture of the mean sediment concentration variation with water depth. Wall sediment concentrations vary as expected, with shallow water leading to higher sediment concentrations. As before, the lower OBS read higher levels of suspended sediment concentrations than the upper OBS. Furthermore the way in which the position of the crosses evolve through the tide indicates that there may be tidal asymmetry in the sediment concentration (note the apparent 'loop' in the data points for the wall rig). To examine this further, a detailed analysis of the wave height variation through the tide would be necessary. If wave heights do remain constant, the asymmetry may result from the development and subsequent destruction of bedforms as described by Davidson *et al.* (1993b). It is also possible that the water table variation through the tide affects the sediment concentrations and may lead to asymmetry. In order to investigate these processes fully, further research would be necessary, and this is not included here.

The beach OBS data provides less information on natural physical phenomena. While the mean concentrations are, as expected, less than the wall concentrations, the trend is

reversed. However, at these low concentrations, the instrument is operating at bit-level. The minimum concentration difference measurable by the OBSs in this experiment was 0.05kg/m^3 , and variations in sediment concentration below 0.05kg/m^3 are therefore indistinguishable in the data.

Analysis of the data for L_s gives a mean value of 0.077, while the mean value of C_0 is 0.99. The fact that these values are both lower than observed in previous tides reflects the decrease in wave activity. The trend of L_s increasing in shallow water is again visible, although the relationship between C_0 and depth is less clear (figure 5.6.4.2).

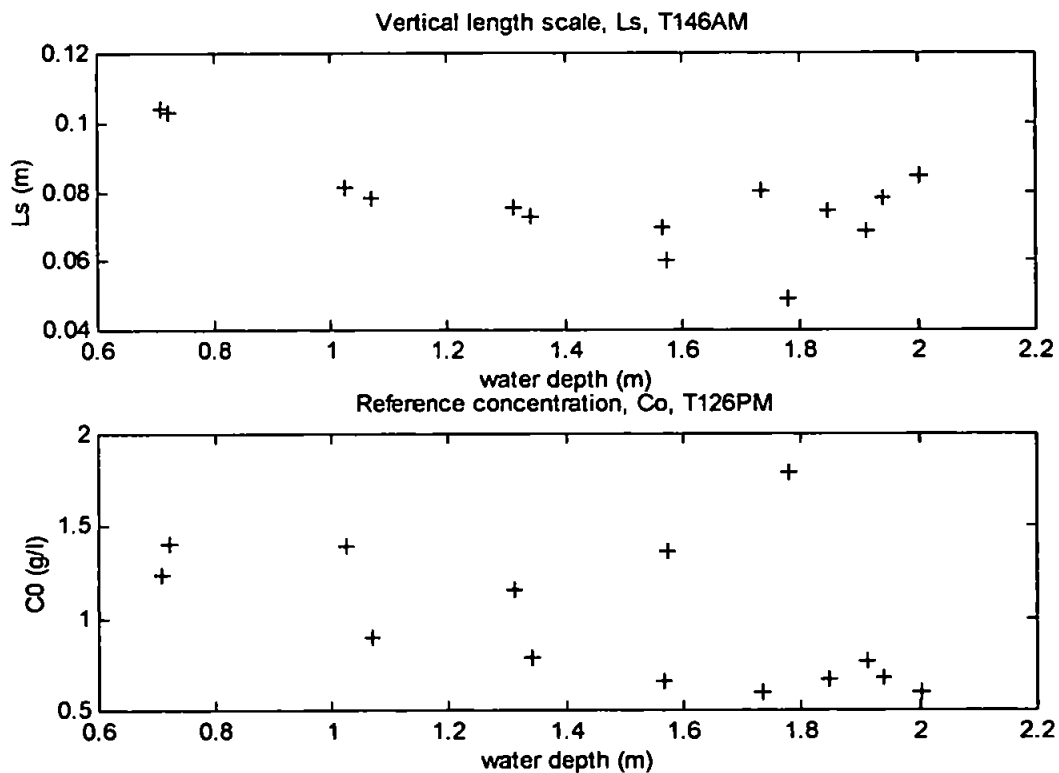


figure 5.6.4.2: Variation in vertical length scale L_s with depth (top) and variation in reference concentration C_0 with depth (bottom) for tide T146AM.

Incoming and outgoing sediment transport analysis provided some interesting results (figure 5.6.4.3). Firstly, runs 5 (beach) and 4 (wall) show that a subharmonic is well developed at a frequency of 0.1Hz, and the analysis shows this to be reflected by both wall and beach. It is possible that this is a subharmonic edge wave. The development of a prominent subharmonic is most likely in the conditions of the 14th of June, when the waves were small and reasonably linear. Non-linear interactions of incident waves with the shoreline lead to the development of the subharmonic, which may travel seaward as a leaky mode or become trapped by refraction at the shoreline to become an edge wave (Huntley, 1975; Huntley and Bowen, 1975).

Incident waves are dissipated by the natural beach but reflected by the wall. The sediment transport direction in the wall case was unfortunately not clear for run 4 at the wall.

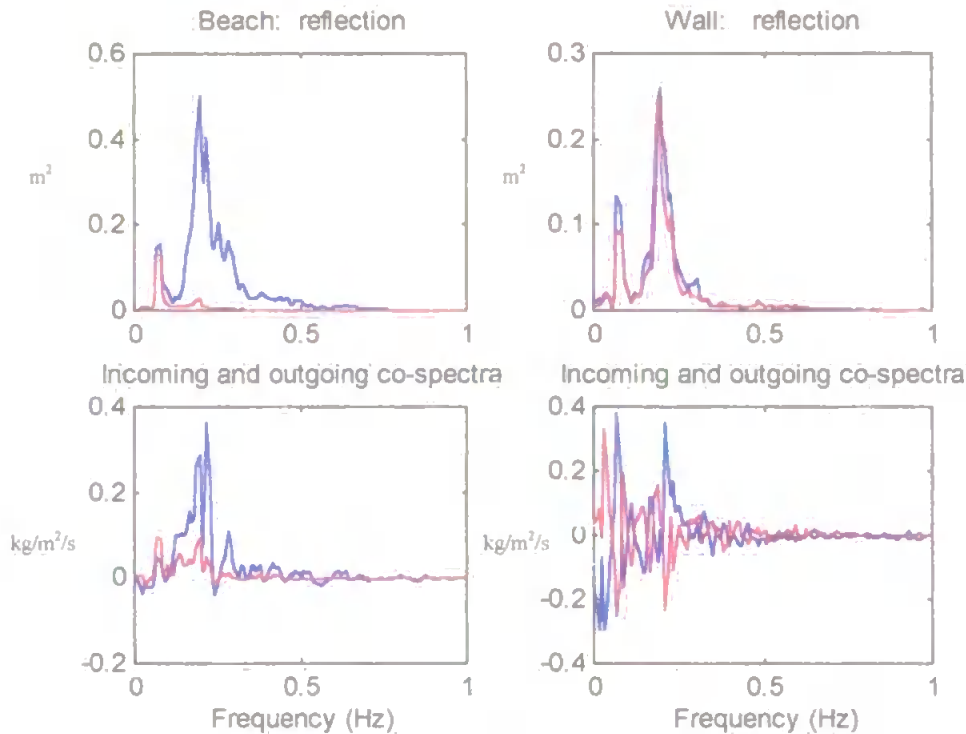


figure 5.6.4.3: Beach run 5, $h=0.5460$; Wall run 4, $h=0.7222$.

Although the direction of transport at the wall rig is unclear in the above example, it becomes clearer in the subsequent runs (figure 5.6.4.4). In the co-spectra of runs 7 (beach) and 5 (wall), the direction of transport is, as expected, onshore with the incoming waves and offshore with the outgoing waves. Of further interest is the dominance of the subharmonic peak in the wall case. This was however, an isolated event, and the subharmonic did not persist in the sediment transport co-spectra. The magnitudes of sediment transport are also indicated in the co-spectra. There is clearly a considerably larger amount of sediment in suspension in front of the wall than on the beach, a result also evident in the mean suspended sediment concentration plots.

The magnitudes of the co-spectral peaks in both wall and beach cases are noticeably smaller than earlier in the experiment when waves were larger. This can be seen by comparing figure 5.6.4.3 where the incoming incident wave co-spectral peak at the wall (blue) just reaches $0.4 kg/m^2/s$ with the corresponding spectral peaks in figures 5.6.3.4 (T136AM) and 5.6.2.4 (T126PM). In the two latter cases, the spectral peaks reach 0.4 in deeper water, and the peaks are broader, indicating that a greater amount of sediment is being transported by this phase of the wave field in earlier tides. As wave activity decreases, the amount of sediment suspended decreases, and so the amount available for transport by both oscillatory currents and mean flows decreases.

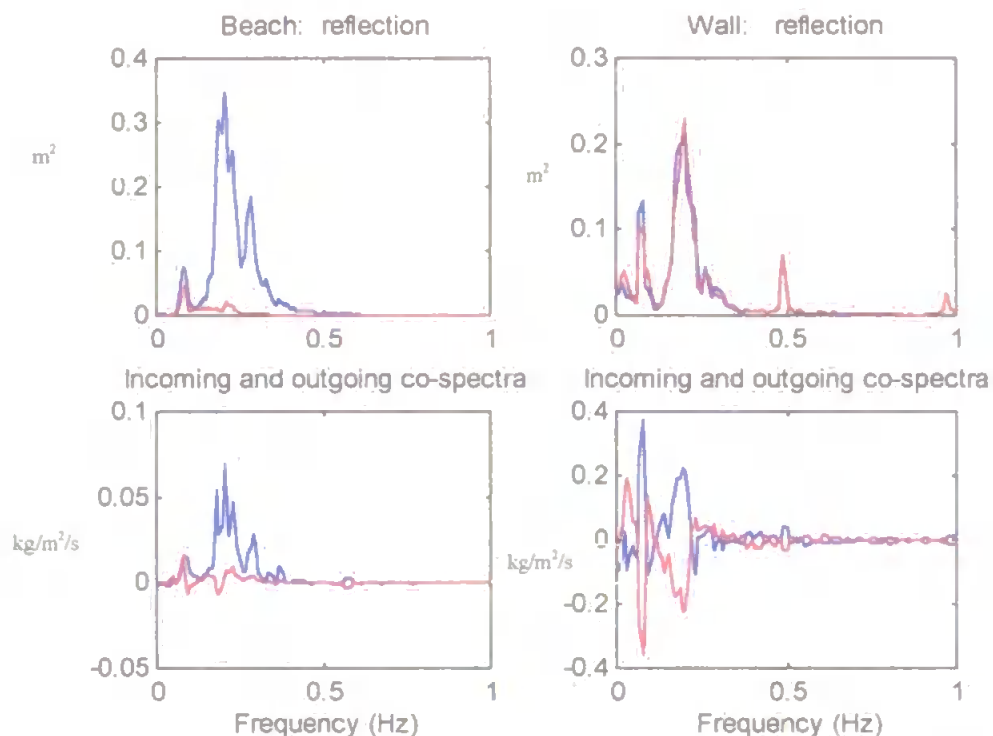


figure 5.6.4.4: Beach run 7, $h=1.0916$. Wall run 5, $h=1.026$.

The amount of dissipation by the natural beach is high when the water is shallow over the rig. However, when the water becomes deeper, the waves interact with a wall at the back of the natural beach and are reflected seaward by this vertical structure. This is evident in run 12 of this tide. In this case the depth is 1.5454m, and the wall at the back of the natural beach would therefore have approximately 40cm of water at it's base. Reflections from this, however, were not large enough to affect the sediment transport regime significantly, and the beach co-spectra remained unchanged at high tide in most cases (figure 5.6.4.5).

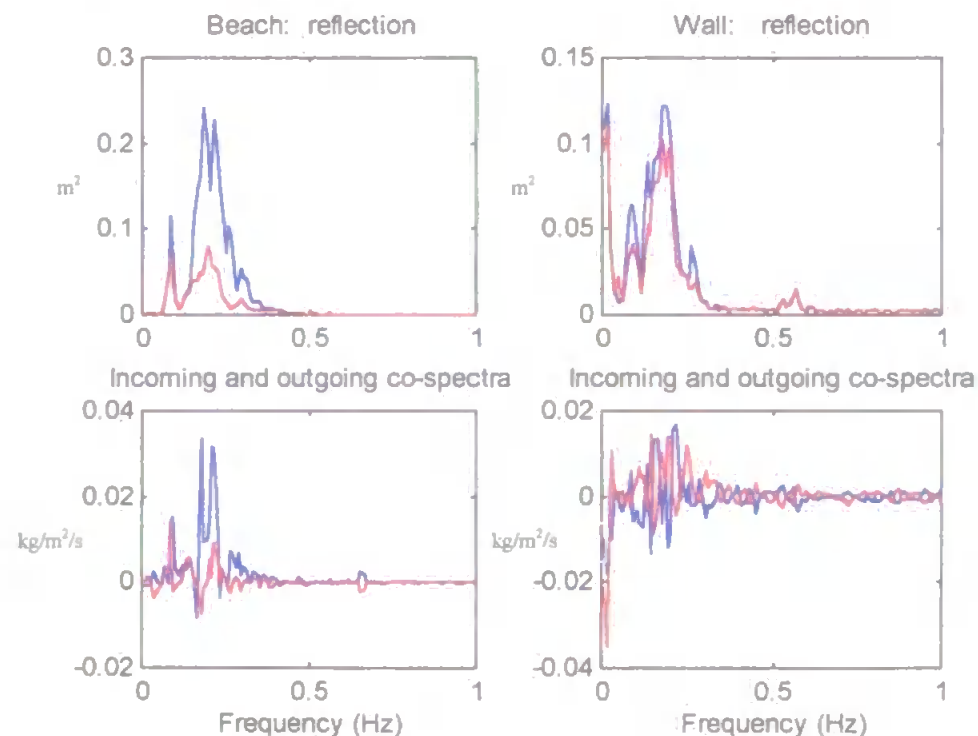


figure 5.6.4.5: Beach run 12, $h=1.5454$; Wall run 17, $h=1.5652$.

Typical values of sediment flux obtained for T146AM are given in table 5.6.4.1:

Wall					
h	$u'c'$	$u_{in}'c'$	$u_{out}'c'$	$\bar{u} \bar{c}$	$\bar{v} \bar{c}$
1.5652	0.0018	0.0011	0.0007	0.0374	-0.0167
1.3437	0.0018	0.0012	0.0006	0.0154	-0.0573
1.0260	0.0001	0.0026	-0.0025	0.0005	-0.1399

Beach					
h	$u'c'$	$u_{in}'c'$	$u_{out}'c'$	$\bar{u} \bar{c}$	$\bar{v} \bar{c}$
1.5454	0.0005	0.0005	0.0000	-0.0014	0.0008
1.3617	0.0008	0.0007	0.0001	-0.0002	0.0001
1.0916	0.0014	0.0013	0.0001	0.0006	0.0008

table 5.6.4.1. Values of the run-averaged oscillatory flux coupling ($u'c'$), incoming and outgoing flux coupling components ($u_{in}'c'$ and $u_{out}'c'$), sediment transport by mean cross-shore currents ($\bar{u} \bar{c}$) and by mean longshore currents ($\bar{v} \bar{c}$) for different water depths at each rig, T146AM. Positive values imply onshore flux or Northerly in the longshore case. Units of water depth (h) are meters, and flux are $kg/m^2/s$.

By the 14th of June, wave activity had decreased considerably, wave heights at the beach rig at high tide had decreased to 0.12m from 0.25m on the 12th of June. The amount of sediment suspended and transported was therefore considerably less at the beach rig. For example in 1m of water the oscillatory flux at the beach rig on the T126AM tide was $0.0093kg/m^2/s$, on the T146AM tide this had dropped to $0.0014kg/m^2/s$. The corresponding values of cross-shore and longshore transport by the mean flows had also dropped. At the wall, the decrease in stirring has also resulted in a decrease in mean sediment fluxes, both in the cross-shore and longshore directions, although the directions of the transport by the mean currents remain onshore and to the south, as before. In deeper water (1.5m) the lack of regular clear sediment suspension events results in an unclear relationship between the incoming and outgoing sediment flux coupling, resulting in a small net onshore transport by the waves. However in shallow water the outgoing waves re-establish themselves and the balance between incoming and outgoing sediment transport in the oscillatory part is restored.

5.7 Summary

High frequency measurements of hydrodynamic and sediment dynamic data have been made simultaneously in front of a seawall and on an adjacent natural beach. The aim was to elucidate the relationship between shoreline wave reflection and sediment suspension and transport processes. These measurements represent the first of their kind in this highly energetic environment. The aim of this chapter has been to present the results of these measurements.

Firstly, the increase in wave reflection at the shoreline was quantified and the frequency dependent reflection function determined using three different methods. The time domain method of Guza *et al.* (1984) and two frequency domain methods (Tatavarti *et al.*, 1988), one including the principal component analysis to reduce the effect of noise in the data, were applied to the data. The increase in incident wave (gravity band) reflection at the shoreline resulting from the presence of the seawall was clearly evident in all analyses. The three methods of analysis were found to give good agreement on the frequency dependent reflection coefficient, thereby validating the use of the simpler time domain method.

In order to examine the effect of the increase in wave reflection on the sediment dynamics, time series of elevation, velocity and suspended sediment concentration were examined. Two results arose from this analysis. Firstly the mean and maximum sediment concentrations were greater in front of the wall. Considerably more suspension activity was observed resulting from the wave reflection than was apparent on the natural beach. The second result concerns the phase of the suspension events relative to the velocity. On the beach, suspension took place at the time of the velocity maximum. In front of the wall however, the situation was more complex. While events generally took place during the elevation maximum, velocities were observed to be either onshore, offshore or zero at this time - depending on the way in which the incident waves and reflected waves were interacting. Suspension events at the wall therefore occurred at periods of maximum shear and at times of flow reversal. Mechanisms which may have been driving the suspension events are discussed further in the next chapter.

In order to examine the frequency dependent sediment transport associated with the incoming and outgoing waves, the time domain reflection analysis was re-applied together with a linear transformation from elevation to velocity as described in chapter 4.

A co-spectral analysis of these velocity time series crossed with the sediment suspension time series reveals the contributions of the incoming and outgoing waves to the sediment transport both in front of the wall and on the beach. While incoming waves were found to transport sediment onshore in both wall and beach cases, offshore directed waves resulting from reflection at the shoreline, transported sediment offshore in the wall case. This resulted in a decrease in net transport but an increase in the gross cross-shore transport.

Mean cross-shore currents in the case of the wall were found to be in the same direction as those predicted by Longuet Higgins' (1953) convection solution (i.e. onshore in the lower half of the water column). Longshore transport was found to be enhanced by the seawall, a direct result of the increase in suspended sediment concentrations. An increased longshore current in front of the wall also assisted this transport, which may be attributable to oblique wave reflection, or the presence of the wall acting as a constriction to the flow (see section 6.3.3 for discussion).

Results were presented from a further three separate tides in order to establish the consistency of the results. Sediment transport processes associated with wave reflection and variations from the expected pattern during the tides of T126PM, T136AM and T146PM were presented and briefly described. During these tides, wave heights decreased from 0.3m at the breakpoint to 0.1m, and this resulted in a decrease in suspended sediment concentrations and transport rates. Results from these tides were used to establish the vertical length scale L_s and the reference concentration C_0 in front of the wall, and the variation in these parameters through the tide.

An increase in shoreline wave reflection leads to an increase in sediment suspension and this leads to enhanced sediment transport in front of the seawall. In the next chapter, the processes driving suspension and transport are considered and the resultant changes in morphology are discussed.

CHAPTER 6: Discussion

6.1 Introduction

This role of this chapter is as follows: to put the results into context with the findings of other researchers both in the field and in the laboratory, to discuss aspects of the work which affect its applicability to i) other sites, ii) different instrument positioning and iii) larger wave conditions, and to use the results to discuss the morphology changes which occurred at Teignmouth during the experiment. The chapter is split into sections within three main subject areas: wave reflection dynamics (6.2), sediment dynamics (6.3), morphology change (6.4).

The calculation of the frequency dependent reflection coefficient is discussed first (section 6.2.1). This is followed by a discussion of the values of the frequency dependent reflection coefficients which were obtained when the analysis techniques were applied to the data (section 6.2.2).

The presence of the wall leads to an increase in wave reflection in front of it, and this was found to affect the sediment dynamics. Sediment suspension at both wall and beach rigs is discussed in section 6.3.1. Mean and oscillatory cross-shore sediment transport is discussed in section 6.3.2. Longshore sediment transport magnitudes and directions are discussed in section 6.3.3.

Sediment transport which was measured in front of the wall resulted in a distinct morphology change in front of the wall, and this is discussed in section 6.4. Further research is discussed in section 6.5.

6.2 Wave reflection dynamics

6.2.1 Reflection coefficient calculation

Three techniques were used to calculate the frequency dependent reflection coefficient (FDRF) from the time series of elevation and velocity. They were: the time domain method (Guza *et al.*, 1984), a frequency domain version of this method (Tatavarti *et al.*, 1988), and the principal component analysis (PCA) method of Tatavarti *et al.* (1988). Agreement between the estimations of the FDRFs for the three cases was found to be, in general, very good. This can be attributed to the low levels of noise which were present in the data, leading to good coherence between the incoming and outgoing waves. High values of coherence between the incoming and outgoing time series have been found to give low bias to the reflection coefficient estimate (Huntley *et al.*, 1995). The PCA modification to the frequency domain method was introduced by Tatavarti *et al.* (1988) to reduce the effects of noise on the signal as it extracts correlated parts of signals.

The time domain method is more susceptible to low coherence between incoming and outgoing waves, as shown by Huntley *et al.* (1995). When the in/out wave coherence is high, indicating low levels of noise, the PCA has little noise to remove, and the results therefore all give good agreement. In fact the PCA method was initially developed to eliminate the problems associated with low coherence between incoming and outgoing waves on natural beaches where the reflection coefficient is naturally low, a physical phenomenon which gives rise to weak offshore travelling wave signals. This effect is noticeable in the plots of coherence for the beach FDRF estimates, where the in/out coherence is lower than the P/U coherence (see figure 5.2.1). In the wall case, the P/U coherence is lower than the in/out coherence. This is because the instruments are located close to the surface elevation antinode at the wall, the velocity trace is therefore comparatively smaller than in the beach case, while instrument noise remains the same. Lower P/U coherence is the result, while the reflection analysis relies on the surface elevation data to create the incoming and outgoing time series and spectra (see figure 5.2.2).

The FDRF was plotted in both wall and beach cases for values of P/U coherence of greater than 0.4. At frequencies where the value of the P/U coherence was less than 0.4 considerable bias affected the reflection coefficient estimates. This occurred despite rigorous application of the principal component analysis, although the frequencies affected were generally at frequencies outside the incident wave band.

The study of reflection in the incident wave band was considered the most important as it is at this frequency which most suspension occurs in front of the seawall.

As an indicator of the reflection coefficient, the data has given good results. Further analysis would allow the implementation of the Maximum Likelihood Estimator (MLE) (Isobe and Kondo, 1984) and its modified cousin the MMLE to examine the directional wave spectra. By incorporating the sediment into this analysis a frequency dependent directional sediment transport spectrum could be obtained, although this was not attempted in this experiment. It therefore remains a possible future development in analysis procedures.

The simple derivation and application of the time domain analysis made it easy to incorporate the sediment trace, as shown in chapter 4. A slightly more complicated approach involved carrying out the analysis in the frequency domain, and this allowed full linear theory to be applied. However a satisfactory solution was not found for incorporating the PCA into the in/out velocity \times sediment cross spectrum. Had this been possible, bias resulting from noise in the data could have been reduced. However it was not possible to retain vital phase information while using the PCA method prior to carrying out the cross-spectral analysis. In calculating the reflection coefficient, this phase information is rendered un-necessary by the use of a gain function.

The versatility of the time domain method has resulted in its use for detecting the length of time it takes for a long wave on a natural beach to be reflected back out past a sensor (Masselink, 1995) and further to elucidate the relationship between standing long waves and a dissipative beach multiple bar system (Ruessink, 1995). The application of the time domain method to the sediment data will be further discussed later in this chapter.

6.2.2 Reflection estimates

Estimates of the reflection coefficient can be obtained from many parameterisations, as discussed in the literature review. Of the parameterisations available, the one presented by Hughes and Fowler (1995) is the most applicable, as this deals with waves incident on smooth slopes.

Their parameter requires the two equations below to be solved:

$$\xi = (h/g.T^2)^{1/2} / \tan \beta \quad 6.2.2.1$$

$$K_r = a / (a + \xi^b) \quad 6.2.2.2$$

where h =water depth, $g=9.81\text{m/s}^2$, T =wave period, β =structure slope, K_r =reflection coefficient, a and b are two constants. For smooth slopes, $a=0.1176$ and $b=2.6$.

Two sets of values are of interest in this case. For the wall case, typical values are: $h=1\text{m}$, $T=4\text{s}$, $\beta=53^\circ$

giving $\xi=0.06$ and $K_r=0.99$.

In the case of the beach, the only difference in input to these equations is β , for which we know that $\tan \beta \approx 0.08$. i.e. $\beta=4.57^\circ$. This gives $K_r=0.1$, assuming the beach is a 'smooth slope'.

By comparison, in the data incident wave frequency reflection coefficients at the wall were found to be approximately 0.75, while in deeper water this rose to 0.9 (see figures 5.2.2 and 5.2.3). The effect of noise in the data cannot be blamed for this difference as uncorrelated parts of the signal would result in an increase in the reflection coefficient calculated from the signal. The Hughes and Fowler (1995) parameterisation must therefore be over predicting the reflection coefficient in this case, although there is reasonable agreement. In the parameterisation, β is the slope of the wall itself. The 'structure slope' may however be an average slope of part of the beach and the wall. This would decrease β and increase K_r , and might give a result closer to the data.

In the beach case, the parameterisation approach to the prediction is remarkably accurate, the data showing that the FDRF dips to its minimum value of 0.1 at the incident wave frequency (see figure 5.2.1). At the lower frequency peak of 0.1Hz in the beach case, a reflection coefficient of 0.8 is obtained from the data, while the parameterisation offers a value of 0.56. The incompatibility of the two results may stem from the lower values of coherence obtained for this frequency, although similar high reflection coefficients for low frequency peaks have been found by Tatavarti *et al.* (1988).

However, this parameterisation approach is not aimed at the FDRF, but provides an estimate of the bulk reflection coefficient, i.e. the effect of non-linear interactions between incident waves producing lower frequency energy was not considered in the development and laboratory testing of Hughes and Fowler's parameterisation. They used monochromatic waves in a laboratory experiment. For the application of the parameterisation, the peak wave frequency was therefore used, although this is not a true representation of the complete wave field. Nonetheless, Hughes and Fowler's parameterisation appears to provide useful estimations for the bulk reflection coefficient given a linear slope, a single wave period and a known water depth.

Miche's initial hypothesis which forms the base of Hughes and Fowler's work (and most other reflection parameterisations) gives an f^{-2} dependence of reflection on frequency. The f^{-2} dependence on frequency is also implied by Carrier and Greenspan (1958), Meyer and Taylor (1972) and Guza and Bowen (1976). Interestingly Tatavarti *et al.* (1988) did not conclude a relationship similar to this, but did note that 'the reflection coefficient was high at low frequencies and usually becomes very small at high frequencies'. Elgar *et al.* (1994) found results consistent with Miche's hypothesis, using data with varying shoreface steepness as well as different frequency waves. However both Tatavarti and Huntley (1987) and Dickson *et al.* (1995) found a linear relationship between the inverse of frequency (f^{-1}) and reflection. In the present experiment a functional relationship between frequency and the reflection coefficient was not forthcoming apart from one qualitatively similar to Tatavarti *et al.*'s (1988) - lower frequency waves were reflected better by the beach than higher frequency incident waves. A larger range of data from different slopes and covering a wider range of wave frequencies would assist the development of such a parameterisation.

6.3 Sediment dynamics

6.3.1 Sediment suspension

At the beach rig, the time-series show suspension events occurring in phase with onshore velocity (see figure 5.3.3). Suspension events which occur at this phase of the wave are driven by the velocity shear in the boundary layer (Bagnold, 1946), which is maximum when the velocity outside the boundary layer is maximum. Shoaling waves become asymmetrical, and their onshore velocities become larger than the offshore velocities. When the offshore velocity fails to rise above the threshold for suspension, suspension events only occur at the wave crest. Huntley and Hanes (1987) point out that when such suspension events occur regularly in phase with the velocity, there will be a net transport in the direction of the velocity. The co-spectrum represents the in phase oscillations at all frequencies and gives the sediment flux at each frequency. The co-spectrum between the velocity and sediment concentration at the beach rig therefore gives a positive peak, indicating suspension in phase with the wave crest and transport in the direction of wave advance. By splitting up incoming and outgoing waves, correlated parts of the time series of in/out velocity can be examined in relation to suspension events. In the beach case, there is little outgoing energy, and there is therefore little sediment transport associated with outgoing waves at the incident wave frequency (see figure 5.4.1).

Conceptually, sediment suspension events at the wall which coincide with the onshore phase of an incoming wave give rise to onshore transport, while suspension events which coincide with the offshore phase of an outgoing wave give rise to offshore transport. In the time series however, the phase of the suspension events is less clear. Elevation and velocity traces are complex, resulting from the interaction of incoming and outgoing waves. The phase of suspension relative to individual velocity peaks is difficult to predict from the time-series, and the associated sediment transport is therefore difficult to ascertain. A process by which suspension may be brought about resulting from the interaction between incoming and outgoing waves is discussed later in this section. However, it is first necessary to consider why suspension is being considered over advection.

Local suspension of sediment from the bed at the instruments location is assumed, because the orbital excursions are not large enough in the region of the instruments to transport (advect) sediment from the node or antinode to the instruments. Values of the orbital amplitude are given by $A_o = U_o / \sigma$ where $\sigma = 2\pi/T$.

At the position of the instruments, typical values of U_o are 0.2m/s ($h=0.9m$), or 0.4m/s in shallower water ($h=0.6m$). These values give orbital excursions of 0.125m and 0.25m respectively, length scales which are very short when compared to the wavelength ($\lambda=12.5m$ for $T=4$ seconds in 1m of water, or $\lambda=9.7m$ for $T=4s$ and $h=0.6m$). In water of depth 1m, the distance from the elevation antinode at the wall to the first elevation node would therefore have typically been approximately 3m (1/4 of the wavelength).

The instruments were 1.2m from the wall, and it is therefore unlikely that suspension events at either the elevation node or elevation antinode were advected to and from the instruments and logged as periodic re-suspension. Rather, suspension of material directly under the instruments was logged, resulting from incident and reflected wave interaction.

Using the analysis techniques derived in chapter 4, the results section showed that incoming waves transport the sediment onshore, while outgoing waves transport the sediment offshore. An alternative, more physical way of thinking about it is that outgoing waves are capable of suspending and transporting sediment, and do so on having been reflected (plate 6.3.1.1). In shallow water where this process is most likely to occur, the incoming and outgoing transport description is likely to hold through the nodal structure, until sufficient energy is lost from the outgoing wave, or it reaches deep enough water for no more suspension to occur in phase with it. Further experimentation is required to investigate the cross-shore distribution of the sediment transport associated with the incident and reflected waves.

The development of the incoming and outgoing wave frequency dependent sediment transport analysis technique arose from the idea that the transport associated with the incident and reflected waves could be separated in the same way as the mean and oscillatory components of velocity. Means and different frequencies of waves have different roles to play in the sediment transport budget, as do incoming and outgoing waves. The total sediment transport can be considered as a linear superposition of these different components. While transport can be analysed in this way, suspension cannot. Suspension events are generally considered to result from the total velocity, not the individual components of the velocity field. In this case, the total velocity field is made up of incident waves, reflected waves, lower frequency waves and mean currents.



plate 6.3.1.1: Outgoing waves can suspend and transport considerable amounts of sediment, independently of the incoming waves, especially when broken. The results of the experiment at Teignmouth show that this offshore transport is enough to balance the onshore transport of sediment and can inhibit the recovery of the beach. The increase in reflection at the shoreline also results in an increased amount of sediment in suspension which is then available for longshore transport.

Suspension of sediment is normally assumed to result from shear stress on the bed. In a shallow water, progressive wave situation, this would occur while the elevation and velocity are maximum, as the crest of the wave passes. The difference in velocity between the top and bottom of the boundary layer generates sufficient turbulence for sediment to be entrained. In the standing wave case, it would be reasonable to expect this process to dominate at the elevation nodes. Towards the elevation antinodes in such a regular standing wave however, the cross-shore velocity decreases, and vertical velocities become more important. It is therefore plausible that Reynolds stresses may be important in the region close to the wall. However, visual observations revealed no appreciable ‘zoning’ of sediment with distance from the wall during the experiment, indicating that differences in suspending mechanisms in the cross-shore direction did not affect the sediment noticeably.

While the cross-spectral approach to sediment transport can reveal the frequency dependent nature of the sediment transport, a time series approach to the problem of sediment suspension seems more suitable than the spectral one, as it allows the non-linear interaction between incoming and outgoing waves, mean currents and turbulence to be examined. It is, however, rather more difficult to implement. In order to understand the spiky nature of the time series it is useful to conceptualise the processes which are occurring using a simple data simulation.

In the simulation, a wave is advected past some ‘instruments’, reflected from a wall 1.2m away, and the wave passes the instruments on its way out. Instrument heights in the data simulation were the same as in the field experiment. Solitary wave theory was applied because of its simplicity and similarity to waves in shallow water (Bagnold, 1947; Munk, 1949). The Boussinesq (1872) solution was applied for the surface elevation of both incoming and outgoing waves:

$$\eta = H \operatorname{sech}^2 \left(\sqrt{\frac{3}{4}} \frac{H}{h} \frac{x}{h} \right) \quad 6.3.1.1$$

The speed at which the wave progresses past the instruments to and from the instruments is given by:

$$c = \sqrt{g(h + H)} \quad 6.3.1.2$$

McCowan’s (1891) solution for the orbital velocity has been found to be the most reliable (Daily and Stephens, 1953a,b):

$$u = cN \frac{1 + \cos(Mz/h) \cosh(Mx/h)}{[\cos(Mz/h) + \cosh(Mx/h)]^2} \quad 6.3.1.3$$

where M and N are functions of H/h, calculated by Munk (1949). In the simulation, typical values of H=0.2m, h=1.0m give values of M and N as 0.65 and 0.3 respectively.

For a progressive solitary wave, the elevation is in phase with the velocity. The total elevation and velocity for the incident and reflected wave were obtained by adding the incoming and outgoing components of η and u . A mean onshore velocity was added of similar magnitude to that observed in the field ($\bar{u} = 0.1\text{m/s}$). Sediment suspension was assumed to be a function of the u_{tot}^n where $u_{\text{tot}} = u_{\text{in}} + u_{\text{out}} + \bar{u}$. Various values of n have been suggested from n=2 (Inman and Bagnold, 1963), n=3 (Owen and Thorn, 1978), to n=5 (Madsen and Grant, 1976). The magnitude of the suspension peak was considered less important than the phase at which it occurred, so for the purposes of the simulation a value of n=3 was used, and the relationship

$$c_s = u_{\text{tot}}^3 = (u_{\text{in}} + u_{\text{out}} + \bar{u})^3 \quad 6.3.1.4$$

was applied.

The results of the simulation are shown in figure 6.3.1.1.

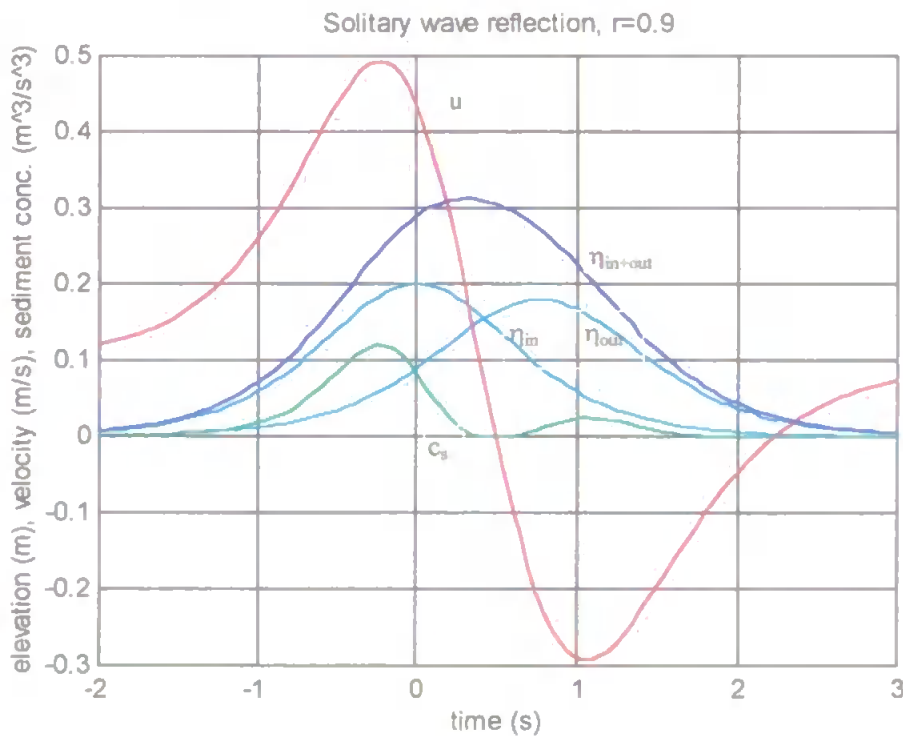


figure 6.3.1.1. Simulation of solitary wave reflection past the instruments and the associated sediment suspension. The incoming and outgoing waves are shown separately (η_{in} , η_{out}). The time lag between the peaks is the time taken to travel to the reflector and back to the instruments. The total elevation is that which would be observed by the instruments ($\eta_{\text{in+out}}$). The total velocity (u) results from incoming waves, reflected waves and a mean onshore flow which was observed at the height of the instruments during the field experiment. Suspended sediment concentrations (c_s) are assumed to be a function of the velocity cubed.

The structure in the time series of the simulation above was also found to exist in the field data. An example is given in figure 6.3.1.2. Of particular interest in this example is the suspension of sediment which occurs by both the incoming and outgoing waves, as in the simulation. Maximum suspension of sediment occurs at the same time as the velocity maximum in each case, and as in the simulation, the onshore directed sediment peak is smaller than the offshore peak.

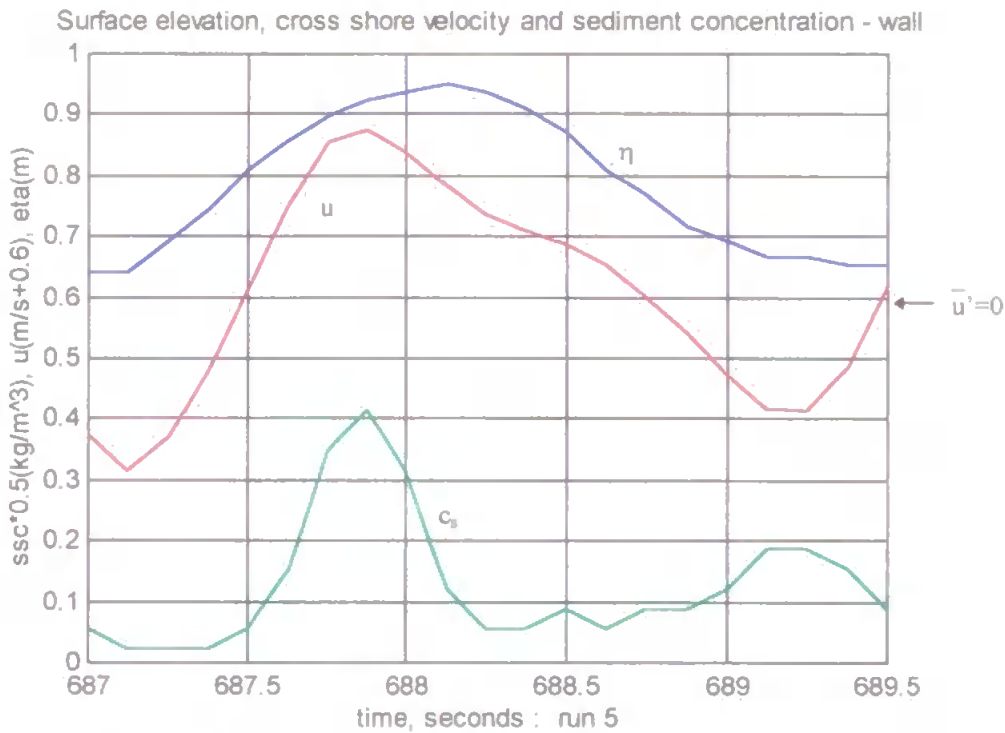


figure 6.3.1.2. Time series of elevation (η), velocity (u) and sediment concentration (c_s) at the wall rig, T136PM.

While this example supports the hypothesis that incoming waves suspend and transport sediment onshore and reflected waves suspend and transport the sediment offshore, the reality is that the velocity field is much more varied than in the simulation. The interaction between the waves and their wave troughs, turbulence and longshore flows is non-linear, and the sediment suspension which is driven by these flows is therefore correspondingly complex. When examining the time series, clear events like the one shown in the figure above only occur when individual waves are able to reflect from the wall without interference from other waves or wave groups. Nevertheless the simulation has provided a useful starting point for examining the way in which wave reflection affects sediment suspension. A detailed time series analysis is therefore probably the way forward in examining the suspension of sediment, a process which appears to be more stochastic than organised in the frequency domain.

6.3.2 Cross-shore sediment transport

It is appropriate at this point to discuss the absence of a scour trough in front of the wall. In the cross-shore direction, results from the current meter 1.2m from the wall show a mean onshore water flux at the height of the instrument throughout the logging period. The current meter was 10.5cm from the bed, while typical wave heights were approximately 30cm. For the instrument to remain submerged, and therefore give reliable results, the water depth must have been greater than 25.5cm, placing the instrument in the lower half of the water column. Mean sediment fluxes follow the direction of mean water fluxes as mean suspended sediment concentrations are always greater than zero.

Onshore water transport in the lower half of the water column outside the boundary layer was predicted by Longuet Higgins-(1953) for standing waves and partially standing waves (Allen, 1981) provided the reflection coefficient is greater than 0.41 (Carter, 1973) a value below which the mass transport follows the profile of the progressive wave. The mass transport associated with a standing or partially standing wave is shown in the literature review (figure 2.6.1).

The vertical circulatory cell in the standing wave also sets up a boundary layer circulation (see figure 2.6.1) which can affect the direction of sediment transport. Laboratory tests have shown that fine sediments are transported mainly in suspension and are eroded from the elevation node, while coarser sediment follow the boundary layer transport and accrete at the elevation node, as there is a divergence half way between the elevation node and antinode (Xie, 1981; Irie and Nadaoka, 1984). The tank tests which have given these results have generally used monochromatic waves, and it was found that it took considerable time for the scour to develop. For example, for the relatively fine material it may take up to 10,000 wave cycles for the scour to develop (Xie 1981). This corresponds to a time of 11hrs for waves of period 4 seconds, considerably longer than the length of time for which a wall at the top of a beach is generally submerged.

The wall at Sprey Point was typically interacting with the water for 6hrs during any one 12.4hr tidal period, and would hence be impacted by 5400 waves of period 4 seconds. Consider waves of wavelength 12m, impacting the wall. This case is taken as an average case for a water depth of 1m, linear theory giving $h/\lambda=0.083$. Approximately 75% of the maximum scouring depth should have been achieved in the 6hrs according to Xie's (1981)

predictions, the maximum scour in this case being 90% of the wave height. At no time during this experiment however was scour observed in front of the wall at Teignmouth.

Tests using irregular waves show that the scour troughs parallel to the wall decrease in depth with distance from the wall (Hughes and Fowler, 1991). However this feature was not evident at the Teignmouth site during the experiment.

The lack of scour may have been because the incident waves were small and low in steepness so accretionary conditions prevailed. Erosional conditions giving offshore transport from in front of the wall are believed to bring about scour in front of the wall as the sediment source from the top of the beach is effectively blocked by the wall (Dean, 1991). In this case, the net sediment transport was onshore at the wall, and the sediment supply was therefore not blocked by the wall, so a scour trough did not develop.

Cross-shore sediment transport rates

Typical values of sediment flux averaged over a run are given in table 6.3.2.1 below. Equations giving the breakdown of the total sediment flux into the components listed below are given in chapter 4. The relevant equations are 4.4.1.1 to 4.4.1.6.

Wall						Beach					
run	h (m)	Suspended sediment flux components (kg/m ² /s × 10 ⁻²)				run	h (m)	Suspended sediment flux components (kg/m ² /s × 10 ⁻²)			
		$\overline{u'c_s'}$	$\overline{u_{in}'c_s'}$	$\overline{u_{out}'c_s'}$	$\overline{u c_s}$			$\overline{u'c_s'}$	$\overline{u_{in}'c_s'}$	$\overline{u_{out}'c_s'}$	$\overline{u c_s}$
13	1.55	0.05	1.38	-1.32	4.93	17	1.52	0.51	0.48	0.02	0.37
16	1.25	0	0.47	-0.46	6.4	18	1.18	0.78	1.08	-0.30	0.27
17	0.96	-0.01	1.1	-1.11	8.15	19	0.98	0.93	1.43	-0.5	0.28

table 6.3.2.1: Run averaged sediment fluxes, T126PM. -ve values indicate offshore directed sediment transport components.

In the wall case, the values show that onshore sediment flux associated with the incoming waves ($\overline{u_{in}'c_s'}$) is balanced by offshore sediment transport associated with the outgoing waves ($\overline{u_{out}'c_s'}$). The net oscillatory sediment transport ($\overline{u'c_s'}$) is therefore small. Mean sediment transports ($\overline{u c_s}$) are an order of magnitude larger than this at the wall. This is attributed to the large value of $\overline{c_s}$ observed at the wall resulting from incident wave driven suspension, rather than larger values of \overline{u} , which would indicate a strong circulation within the nodal structure. Mean cross-shore currents observed in front of the wall at the position of the instruments were of similar magnitudes to those observed outside the surf

zone of the natural beach (see figure 5.5.1). At the beach, incoming waves are again responsible for onshore sediment transport ($u_{in}'c_s'$), and in this case, the onshore sediment transport by the waves is generally larger than the mean sediment transport. Offshore travelling waves reflected from the beach are only responsible for a small amount of offshore sediment transport. Reflected waves, when present, enhance the offshore component of the oscillatory transport.

Cross-shore sediment transport estimates have been obtained by a variety of other authors, and it is therefore possible to compare transport rates observed at Teignmouth with those obtained elsewhere.

Values of flux obtained at Teignmouth above were considerably smaller than those obtained by Jaffe *et al.* (1984). Jaffe found typical values of $u'c_s'$ to be $0.15\text{kg/m}^2/\text{s}$ outside the surf zone, rising to $0.35\text{kg/m}^2/\text{s}$ over the bar (at Duck, North Carolina, USA). Inside the bar, values of $u'c_s'$ dropped to $0.02\text{kg/m}^2/\text{s}$ as the waves lost energy. In all cases, the $u'c_s'$ flux was onshore. The reason for the larger values observed by Jaffe is simply the size of waves. Whilst at Teignmouth, the significant wave heights at the beach rig in deep water were at most 0.25m, at Duck, during the experiment being reported by Jaffe, deep water significant wave heights were 1.6m, with wave periods of 12 to 15 seconds. Jaffe's values of $\bar{u} \bar{c}_s$ varied between $-0.07\text{kg/m}^2/\text{s}$ inside the bar, increasing to $-0.2\text{kg/m}^2/\text{s}$ on the bar just landward of the bar crest. Offshore of the bar values decreased to a minimum of approximately $-0.03\text{kg/m}^2/\text{s}$. This offshore sediment flux is a result of the undertow. While offshore sediment transport by the mean cross-shore current at Teignmouth was observed outside the surf zone of the natural beach, it was not consistent, and there were several runs where the mean current at the beach rig was onshore. This result is to be expected as undertow does not generally persist far outside the surf zone. At the seawall rig cross-shore sediment fluxes by the mean cross-shore current ($\bar{u} \bar{c}_s$) were generally larger than at the beach rig but not as large as those observed by Jaffe, ranging in magnitude from $0.0005\text{kg/m}^2/\text{s}$ on T146AM to $0.08\text{kg/m}^2/\text{s}$ on T126PM.

Like Jaffe *et al.* (1984) Beach and Sternberg (1988a,b) also discussed sediment transport on a natural beach based on field observations of suspended sediment concentrations. Their measurements were taken during high energy conditions (wave heights 3-5m) and mean sediment concentrations therefore were considerably larger than those observed at

Teignmouth, reaching $20\text{--}40\text{kg/m}^3$ at elevations in excess of 26cm. Unfortunately no values of flux were presented for comparison.

Russell (1993) made measurements on a dissipative macrotidal beach on a calm day when waves were measured as up to 0.4m high. At Russell's field site (Llangennith, S. Wales) oscillatory sediment transports ($u'c_s'$) reached $-0.05\text{kg/m}^2/\text{s}$ at maximum while mean sediment fluxes ($\bar{u} \bar{c}_s$) reached $-0.07\text{kg/m}^2/\text{s}$ during these conditions. These measurements were taken just after high water in a water depth of 0.7m. Waves at this time had a significant wave height of 0.3m. Russell's OBS was 4cm from the bed, while the EMCM was 8cm from the bed. The offshore mean flux ($\bar{u} \bar{c}_s$) at Llangennith was larger than that observed on the natural beach at Teignmouth during similar incident wave conditions: on T126PM with $H_{1/3} = 0.25\text{m}$, values of $\bar{u} \bar{c}_s$ were typically $0.0037\text{kg/m}^2/\text{s}$. Values of oscillatory flux at Teignmouth's natural beach were also considerably smaller (typical values of $u'c_s'$ being $0.0051\text{kg/m}^2/\text{s}$). This is attributed to the difference in distances from the bed of the two OBSs. Of interest is the change in direction of the oscillatory transport - at Llangennith this was offshore, while at Teignmouth the transport associated with the incident waves was generally onshore.

When comparing transport rates at Teignmouth with transport rates observed at other field sites by other workers (e.g. Jaffe *et al.* 1984; Osborne and Greenwood 1982; Russell, 1993 etc.) it is apparent that the cross-shore sediment transport rates at Teignmouth were relatively small. This is generally a result of the smaller wave conditions which were observed at Teignmouth. The most important comparisons are therefore not with the results of other workers, but between the results obtained for the beach and wall rigs, as these rigs received similar incident wave conditions.

6.3.3 Longshore transport

In the results chapter, longshore sediment transport was shown to be enhanced in front of the wall (see tables 5.6.2.1, 5.6.3.1, and 5.6.4.1). Two effects are of note. First, for a given longshore current, an increase in the sediment concentration in front of the wall will lead to increased longshore transport rates. The depth dependence of the mean sediment concentration resulted in a decrease in longshore sediment transport rates in front of the wall with increasing water depth. Secondly, the longshore current velocity is increased in front of the wall. This may result from three different processes (summarised in figure 6.3.2.1):

1. The wall acting as a constriction to the flow. In this case, continuity suggests that the velocity past the obstruction should increase. Ozasa and Brampton (1980) treated the presence of a seawall protruding on the beach as an obstruction to the flow and suggested that it would, in this case, act as a groyne. In terms of the sediment transport, this means that the sediment flux past the obstacle is highly dependent on the cross-shore position of the obstruction. In shallow water, where sediment suspension is large, the increased flow may give rise to increased sediment transport. A wall protruding further into deep water may actually block the longshore drift of sediment as wave dominated suspension processes diminish in the deeper water in front of the wall.

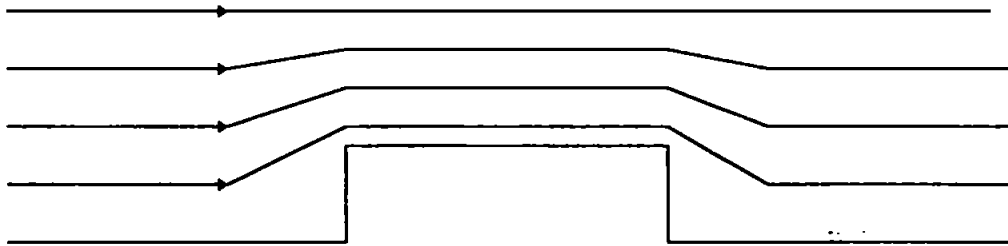
2. Waves incoming at an angle and reflected from the wall at an angle may increase the longshore current, if there is an appreciable Stokes drift in the direction of the waves. Stokes drift normally occurs in the direction of wave advance, however if waves approach the shoreline at an angle, this will have a longshore and a cross-shore component. Waves reflected from the shoreline at an angle also bring about Stokes drift. In the cross-shore direction, the incident and reflected waves act against each other, but in the longshore direction the effects are added. Silvester (1977) described the development of a short crested sea in such a situation, and suggested that it may lead to increased longshore sediment transport.

3. A final mechanism is that the longshore current is driven by dissipation at the wall. Longuet Higgins (1971) shows how the change in momentum of waves dissipating gradually in a surf zone at the shoreline forces a longshore current. In the case of a reflective environment, there is less dissipation taking place, but the dissipation that does occur happens in a very narrow band next to the wall. The rate of change of momentum in

the cross-shore direction is therefore large, and the force on the water is therefore high. In this case, the cross-shore extent of the longshore current distribution would increase with increasing eddy viscosity.

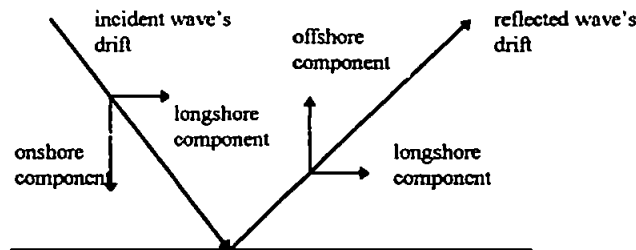
Three hypotheses for increased longshore current velocities

1. Bernoulli / continuity



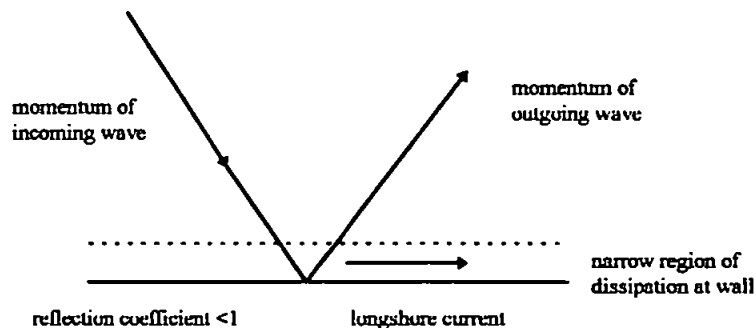
Wall protrudes into surf zone and acts as a constriction to the flow. Continuity demands that the flow must therefore accelerate past the obstruction. The increase in longshore current is therefore a function of the distance seawards that the wall protrudes.

2. Stokes drift



The drift associated with both incident and reflected waves acts in the same longshore direction, while cross-shore components cancel. The longshore current is therefore a function of $1+K_r$.

3. Radiation stress / momentum flux



A small amount of dissipation takes place at a reflective structure. The dissipation that does take place however does so over a very narrow cross-shore distance. The loss of momentum associated with the dissipation at the wall drives a longshore current in this narrow region. In Longuet-Higgins' (1971) terms, while the dissipation D is small, the cross-shore variation of D close to the wall (i.e. $\delta D/\delta x$) is large. In the Longuet Higgins derivation of the longshore current equations based on momentum exchange in the surf zone, it is the rate of change of momentum which forces the longshore current. Eddy viscosity spreads the current seawards from the narrow band in front of the wall.

figure 6.3.2.1.

The third mechanism described above is interesting as it may explain certain scour patterns in front of vertical walls. The regular, undular patterns of scour documented by workers such as Xie (1981) are rarely observed in the field (Kraus, 1996). However, the development of a single scour trough in front of the wall, undermining the wall is well documented as a mechanism which can bring about the failure of a wall (Oumeraci, 1994). A high velocity longshore jet, directly in front of the wall which is capable of stirring and transporting sediment in combination with the extra stirring effect offered by the incident and reflected wave field could result in a significant sediment deficit in front of the wall, leading to a scour trough in the immediate vicinity of the wall, but not at any multiples of wavelengths away from the wall. Where the sediment supply from upcoast is interrupted, this effect may be exacerbated. Visual observations of longshore scour troughs in front of the vertical seawalls at Teignmouth and St Ouens in Jersey during high energy conditions substantiate this hypothesis (Russell, *pers. comm.*).

In the field experiment, waves approached the coast at a slight angle from the north, and the observed direction of the longshore current was to the south. All or any of the above mechanisms may contribute to the increased longshore current in front of the wall. Having said that, even if the current were not increased, there would still be an enhanced longshore sediment transport rate in front of the wall, as the mean sediment concentrations are larger there.

6.4 Morphology changes at Teignmouth

Early in the results chapter, a feedback loop was identified whereby the waves give rise to morphology change:

morphology affects waves => drive sediment transport => changes morphology => affects waves

↑

The seawall noticeably affects the hydrodynamics of the nearshore, and is therefore likely to give rise to a different morphology than if the wall were not present. To establish the change in beach shape resulting from the local dynamics a 3-dimensional survey of the beach both in front of the seawall and to the south was carried out at each day time low tide. Contour plots of the survey data are shown in figures 6.4.1 and 6.4.2. Comparison of the 13th June profile (prior to the T136PM tide, figure 6.4.1) with the survey of the 16th of June (figure 6.4.2) reveals that there is little change in sediment height at the beach instrument rig, which remains at the contour of 500mm above mean sea level. This is substantiated by the measurements of instrument height before and after each tide, which vary only a small amount.

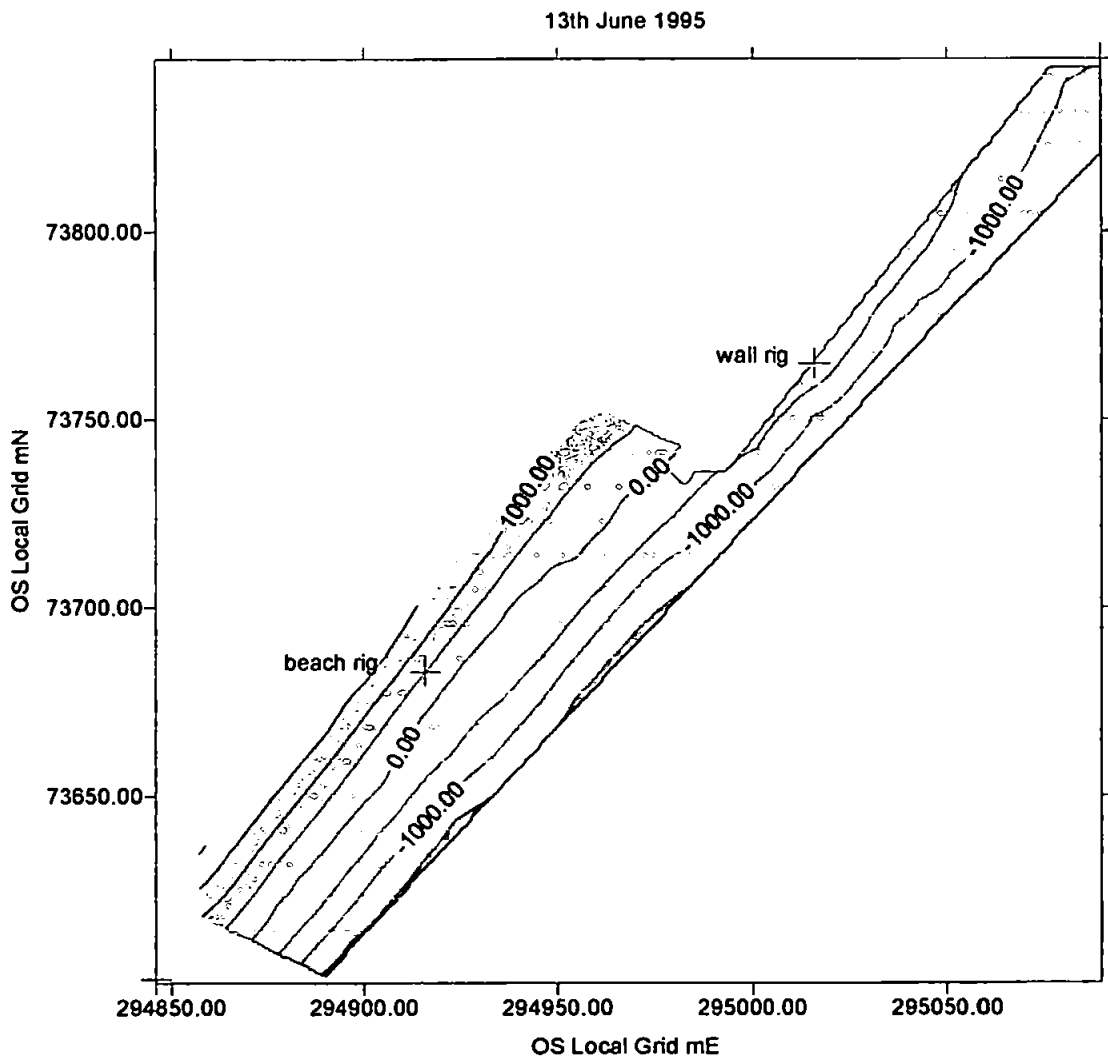


figure 6.4.1: Contour plot of beach morphology for June 13th.

16th June 1995

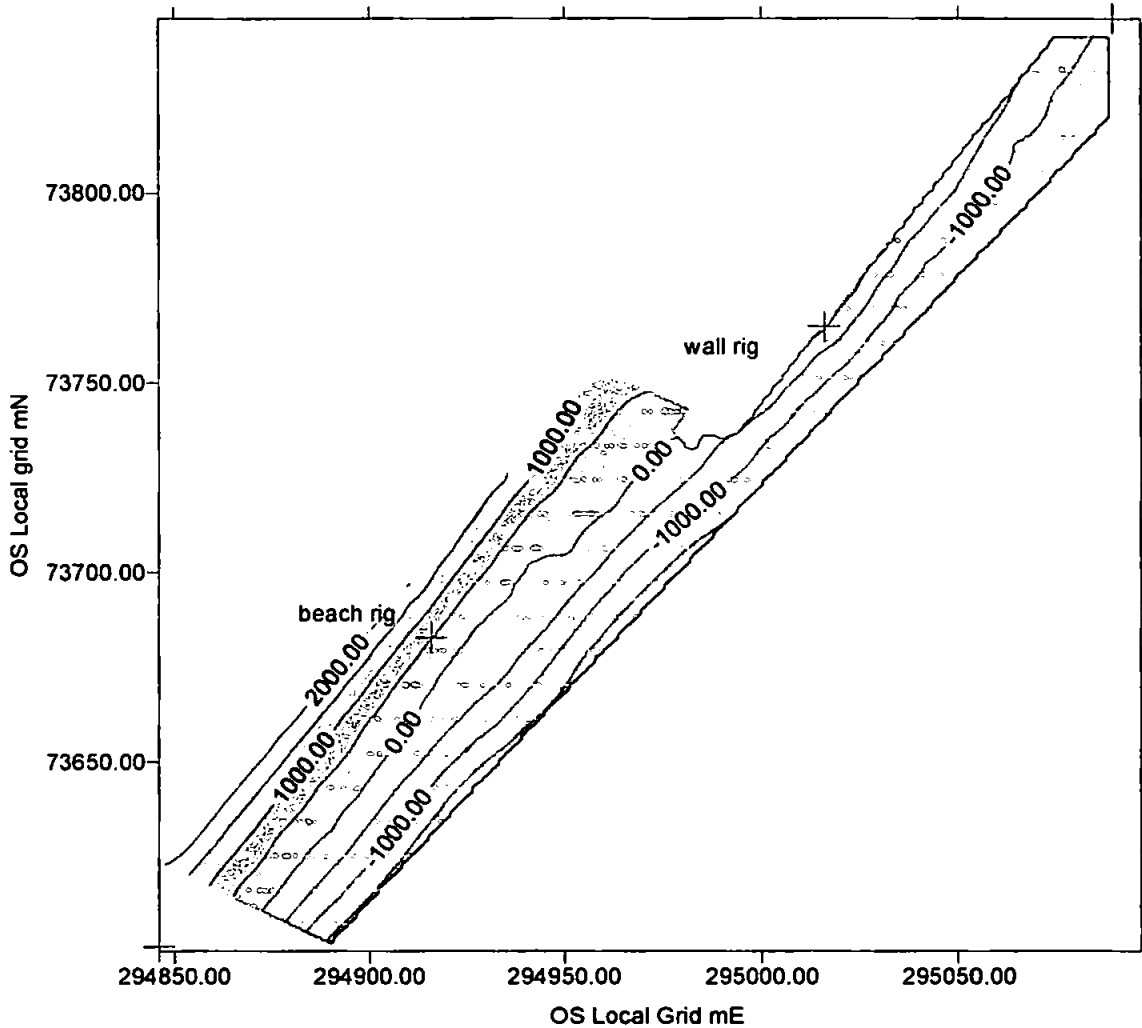


figure 6.4.2: Contour plot of beach morphology for June 16th.

Directly up-slope from the beach rig however, a pattern of accretion is in evidence - note how the 2000mm contour has crept up the coast from the south west. This raising of sand levels at the back of the beach was obvious visually during the experiment and was evident on the wall at the back of the beach. Directly down slope from the beach rig on the 13th June, the -1500mm contour dips away from the rig towards the sea, suggesting an elevated level on the lower beach compared to the 16th June. On the most seaward part of the beach, directly down-slope from the beach rig, the slope steepened between the 13th and 16th of June. (blanked areas on each plot have the same co-ordinates).

The survey was carried out using longshore transects (spaced between 10 and 20m apart in the cross-shore direction), and this has resulted in some loss of information, namely the development of a bar from the end of the seawall at GR 294980,73730 (approx.) which was clearly evident during the experiment. In future, it seems more appropriate to use cross-shore transects to establish changes in beach morphology. The bar was captured on film however, and this is shown in plate 6.4.1.



plate 6.4.1: View from Sprey Point looking south towards Teignmouth on the 15th of June. The bar developing from the south end of the wall is clearly evident in the centre foreground.

The photo was taken on the 15th of June from the top of the Sprey point wall looking South towards Teignmouth. By this time the waves were considerably smaller than earlier in the week.

At the wall rig, the accretion during the experiment resulted in an increase in the bed level of 4cm, while directly up-slope of the beach rig, at the back of the natural beach, 40cm of sand had accreted during the period of the experiment. This morphological information supports the earlier hypothesis that sediment accretion in front of the wall was minimal compared to the natural beach, even in the accretionary conditions which prevailed. The development of the bar to the south of the wall suggests that material which was held in suspension in front of the wall was no longer maintained in suspension after it passed the wall, and was able to settle out directly down stream of the end of the wall in the less energetic environment of a natural undefended beach.

Accretionary conditions at the beach and wall are to be expected given the incident wave conditions. Dean's (1973) approach that beach erosion depends on wave steepness was implemented by Baba and Thomas (1987) for a beach backed by a seawall. They found that the beach eroded for values of $H/\lambda > 0.03$. In this case the wave height of 0.3m and wavelength of 12m (linear solution to dispersion equation with waves of period 4 seconds in 1m of water) puts H/λ at 0.025, indicating waves which give accretionary conditions, as observed. While no mention of the steepness condition is made in laboratory scour test literature, Dean's 'approximate principle' requires that erosion is taking place before scour is observed at the wall. At Teignmouth, the beach was accretionary, and no toe scour was observed. Wave reflections were, however, found to alter the sediment transport dynamics by inhibiting the onshore transport of sediment which gives rise to beach recovery. Inhibited beach recovery has also been found in the presence of seawalls by Kriebel (1987), Kriebel *et al.* (1986), Sayre (1987) and Nakashima and Mossa (1991). The present study, however, remains unique in its use of high frequency field measurements of sediment dynamics in order to examine the processes associated with morphology change in the vicinity of a coastal defence structure.

6.5 Further work

Various areas requiring further work have come to light as a result of this research. The list below summarises these ideas. The first two topics arise from the analysis of the present data set. Following this is an outline of experiments which are necessary to improve understanding of the impact of coastal defences on hydro and sediment dynamics in the nearshore zone.

Longshore transport

Further analysis of the enhanced longshore current in front of the seawall: a detailed study of Longuet Higgins original work is necessary to ascertain to what extent the rapid dissipation of energy at a reflector may be responsible for increasing the longshore current. Such a longshore jet may prove to be extremely important in the development of a scour trough in front of a seawall. A cross-shore array of EMCs measuring longshore currents could show the distribution of the current away from the wall and indicate how it is affected by incident wave size and angle of approach.

Sediment suspension

Further analysis of the time series may reveal more information on the processes driving sediment suspension in front of the wall. The data simulation earlier in this chapter has shown that there is some potential in this approach to understanding the driving forces behind sediment suspension. By extending the model to include other parameters such as vertical velocity, long waves and longshore velocities, it may be possible to unravel the physical processes behind the complex patterns which can be observed in the time series.

Collection of further data in a variety of conditions

i) Repeat experiment at Teignmouth in similar wave conditions with a larger array of instruments distributed in the cross-shore direction to determine the cross-shore variability of suspension and transport processes. In particular, further information on the phase of suspension, magnitude of mean concentrations, cross and longshore sediment transport rates and their distribution. Instruments close to the wall could provide insight on suspension and transport processes in this highly energetic area, while instruments further away from the wall would provide more information on the way in which reflected waves interact with incoming ones. Instruments positioned at different distances from the wall would provide a fuller picture of the cross-shore distribution of processes through the node / antinode standing wave structure.

ii) Redeploy instruments at Teignmouth in larger wave conditions, maybe with a larger array of sensors (depending on the outcome of i) in order to determine the nature of processes at the wall during erosive events. It would also be useful to use bed level sensors during such an experiment to determine when the erosion takes place at the wall (i.e. determine the relevance of swash processes, wave breaking or deep water reflection to scour in front of the wall).

iii) Carry out similar experiments in front of less reflective structures such as rubble mound breakwaters in order to ascertain the effect of reducing the reflection coefficient on the sediment suspension and transport processes.

Further analysis of the data set as outlined above is ongoing. In order to carry out research on structures other than seawalls during a variety of incident wave conditions, an Engineering and Physical Science Research Council (EPSRC) grant is being sought. There may also be scope for carrying out these experiments at Teignmouth as part of the COAST3D programme which has recently been funded under the European Union's MAST III programme.

6.6 Summary

The calculation of the frequency dependent reflection coefficient was discussed first. The principal component analysis method (Tatavarti *et al.* 1988) was identified as the most accurate of the two frequency domain and one time domain (Guza *et al.* 1984) methods. However all three methods gave similar results. This validates the use of the simpler frequency and time domain methods in the frequency dependent reflection and sediment transport analysis.

Hughes and Fowler's (1995) parameterisation worked well for the natural beach which had a reasonably linear slope, although it over estimated the reflection coefficient at the wall. A parameterisation including both the structure slope and the beach slope in front of the wall would be more appropriate.

A reflection function with a dependence on f^2 (Miche, 1951; Carrier and Greenspan, 1958; Meyer and Taylor 1972) or f^1 (Tatavarti and Huntley, 1987; Dickson *et al.*, 1995) was not forthcoming on the natural beach. Like Tatavarti *et al.* (1988), the reflection coefficient on the natural beach was qualitatively found to be larger at low frequencies than at high frequencies.

Sediment suspension on the natural beach was identified as being in phase with the onshore velocity and elevation maxima of the incident waves. Velocity shear in the boundary layer was assumed to be the cause of sediment suspension. At the seawall, the phase of sediment suspension relative to the water motions was less clear due to the complex nature of wave reflection. A data simulation was used to suggest how both incoming and outgoing waves may be responsible for sediment suspension and transport. Sediment suspension was identified as being a function of the total velocity field.

Cross-shore sediment transport rates were examined. Large values of the mean sediment concentration in front of the wall led to the dominance of the $\bar{u} \bar{c}_s$ term over the $u'c_s'$ terms. Incident waves transported sediment onshore, and this was balanced by reflected waves transporting sediment offshore. The reflected waves thereby enhance the offshore transport of sediment, and increased the gross sediment transport rate.

Two factors resulted in an enhanced longshore transport in front of the wall. Firstly wave reflection at the wall increased stirring, and this led to an increase in the amount of

sediment in suspension in front of the wall. Secondly an enhanced longshore current was measured in front of the wall. Three mechanisms were put forward for the increase in longshore velocity, all of which would result in an enhanced longshore transport. It was suggested that the enhanced longshore transport in front of seawalls may be an important mechanism in the formation of scour troughs.

Morphology change at Teignmouth during the experiment was examined. A small amount of accretion was found at the wall rig (4cm). Ten times as much accretion was found at the back of the natural beach, directly up-slope of the beach rig. Longshore transport led to the development of a bar downcoast of the wall.

Suggestions for further research were put forward. The mechanisms driving the enhanced longshore transport need to be identified, and further work is necessary to clarify the nature of sediment suspension in front of the wall. Future field experiments could include: i) a larger array of instruments, positioned at different distances from the wall, ii) larger incident wave conditions, iii) an investigation of structures with different reflection characteristics.

Specific conclusions are given in the next chapter.

CHAPTER 7: Conclusions

A review of the literature available on sediment transport in front of seawalls has revealed that there have been no field investigations to date which have utilised high frequency measurements of suspended sediment transport rates to identify the dominant transport mechanisms which exist in front of seawalls.

This project has endeavoured to address that niche and has provided measurements of sediment dynamic and hydrodynamic processes from in front of a seawall at Teignmouth in South Devon, U.K. To accomplish this, pressure transducers, electromagnetic current meters and optical backscatter sensors were deployed in front of the seawall and on an adjacent natural beach simultaneously.

Wave heights during the experiment were typically in the range $0.1 < H < 0.3\text{m}$ in deep water outside the surf zone of the natural beach. Incident wave frequencies were typically 0.25Hz . A spectral valley was evident at 0.11Hz and there was also a lower frequency peak in the spectrum at approximately 0.07Hz . Measurements were made in water depths of between 0.5 and 2.5m . Analysis of the results has revealed some important features of the sediment transport processes in front of the wall which makes this a very different environment to that of a natural beach.

1. The most obvious difference is that there is an increase in wave reflection at the shoreline provided by the seawall. Reflection coefficients at the wall were close to unity for both incident waves and lower frequency oscillations, although incident wave reflection decreased with decreasing water depth. Typical values of the incident wave reflection coefficient at the wall were in the range $0.75 < R < 0.9$. At the beach however, the reflection coefficient was found to be much lower in the incident wave band, typically in the region $0.1 < R < 0.2$. The reflection coefficient at the beach increased for lower frequency waves to $0.7 < R < 0.9$, however the coherence between elevation and velocity was somewhat lower at these frequencies.

2. Both mean and maximum suspended sediment concentrations were found to be larger in front of the wall than on the beach for similar water depths. Mean suspended sediment concentrations measured at the wall rig varied typically between 0.08kg/m^3 and 2.8kg/m^3 . Mean sediment concentrations measured at the beach rig varied between 0.08kg/m^3 and

0.8kg/m^3 . Instantaneous maximum sediment concentrations at the wall rig reached 9kg/m^3 . In the same incident wave conditions, at the same height above the bed and in a similar water depth, instantaneous maximum concentrations at the beach rig reached 1.2kg/m^3 . Suspended sediment concentrations in front of the wall were found in all cases to increase with decreasing water depth.

Mean suspended sediment concentrations were also found to be highest close to the bed in all data runs. This is in qualitative agreement with Nielsen's (1984) equation which gives an exponential relationship between distance from the bed and sediment concentration. Values for the vertical length scale L_s were obtained and these were in the range $0.05 < L_s < 0.3\text{m}$. Values of L_s increased with decreasing water depth and decreased with decreasing wave activity. Estimates of the reference concentration C_0 were in the range $0.4 < C_0 < 2.7\text{kg/m}^3$. C_0 also showed a tendency to decrease with increasing water depth, although the relationship between C_0 and the wave height was less clear.

3. The mean cross-shore current measured by the current meters was generally onshore when the water was sufficiently deep at the wall. This qualitatively agrees with the predicted direction of mass transport in a standing wave by Longuet Higgins (1953) which shows onshore transport in the lower half of the water column above the boundary layer. Mean sediment fluxes were therefore also onshore in the lower half of the water column at the wall. Mean cross-shore velocities were of similar magnitudes at the beach and wall rigs. Typical values were in the range $-0.1 < u < 0.1\text{m/s}$.

Mean cross-shore sediment fluxes at the wall rig were larger than those observed at the beach rig. Typical values at the wall rig were $\bar{u} \bar{c}_s \text{ wall} \sim 0.05\text{kg/m}^2/\text{s}$ while at the beach rig typical values an order of magnitude less: $\bar{u} \bar{c}_s \text{ beach} \sim 0.002\text{kg/m}^2/\text{s}$. This difference was attributed to the increased amounts of sediment in suspension in front of the wall.

4. In both wall and beach cases, onshore travelling waves were found to transport sediment onshore. At the beach rig this resulted in a net onshore transport of sediment by the waves. The magnitude of the incoming oscillatory sediment flux at the wall was generally larger than at the beach, a result of the increased sediment concentrations there. Typical values of $\langle u_{in}' c_s' \rangle$ at the wall were in the range $0.0011 < u_{in}' c_s' < 0.0187\text{kg/m}^2/\text{s}$ while at the beach they were in the range $0.0005 < u_{in}' c_s' < 0.011\text{kg/m}^2/\text{s}$.

Reflected waves were found to transport an equal amount of sediment offshore from the wall as the incoming waves transported onshore, resulting in a net zero oscillatory cross-shore transport at the wall. The gross oscillatory cross-shore transport was however doubled by this process. Mean cross-shore sediment fluxes at the wall were therefore large compared to the time averaged (net) oscillatory flux ($\langle u'c_s' \rangle$).

5. Longshore current velocities were found to be greater in front of the wall than on the natural beach. Typical values of longshore current speed in front of the seawall were $0.05 < v_{\text{wall}} < 0.2 \text{ m/s}$ while at the beach rig during the same tide longshore current speeds were in the range $0 < v_{\text{beach}} < 0.05 \text{ m/s}$. Coupled with the increase in mean sediment concentrations in front of the wall, the larger longshore current led to an enhanced longshore sediment transport in front of the wall. Mean longshore sediment flux values were typically in the range $0.0167 < \bar{v} \bar{c}_s \text{ wall} < 0.320 \text{ kg/m}^2/\text{s}$ while at the beach rig typical values were considerably less: $0.0001 < \bar{v} \bar{c}_s \text{ beach} < 0.0142 \text{ kg/m}^2/\text{s}$.

6. The enhanced longshore transport is attributed to both an increased longshore current and an increase in the mean sediment concentrations in front of the wall, resulting from the presence of wave reflection. The flux of sediment in the longshore direction away from the seawall at Sprey Point prevented the build up of sediment brought onshore by the mean cross-shore flow, and reflected waves prevented onshore transport by oscillatory flows. The sediment transported down coast along the wall settled out once it had passed the wall and formed a bar which was clearly visible in the field.

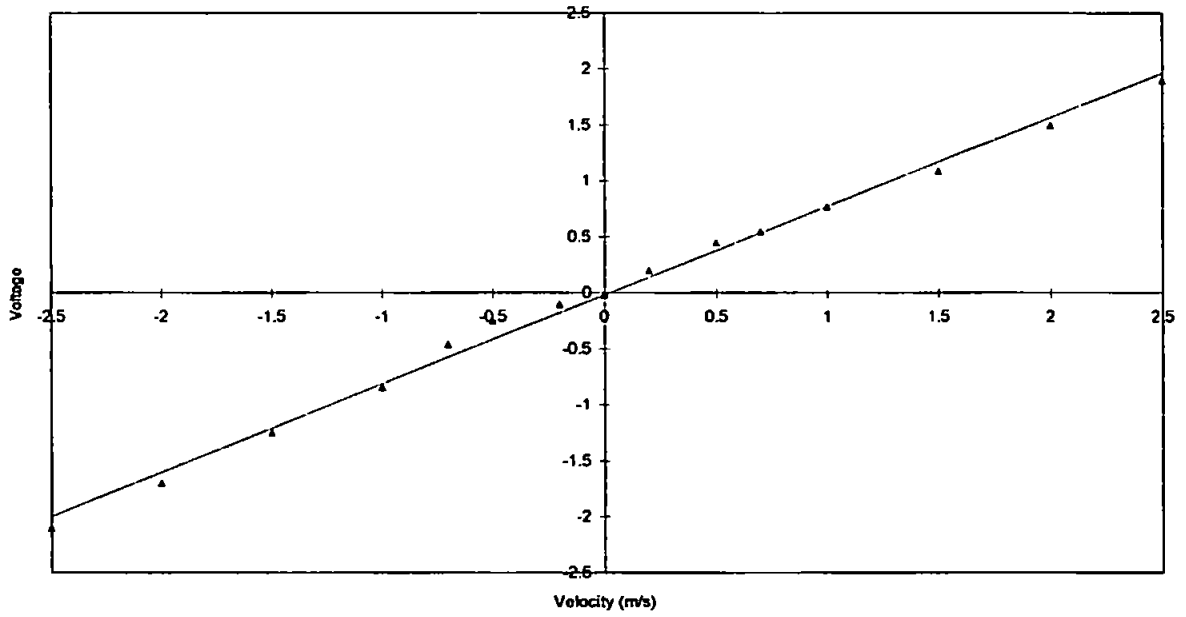
A final summary of the main processes measured during the experiment is as follows:

Incident waves are reflected back over the beach by the seawall and this results in an increase in sediment suspension. Incident waves transport the sediment onshore, while reflected waves transport the sediment offshore. While the net oscillatory sediment transport in front of the wall is reduced, the gross transport is enhanced by the offshore transport associated with the reflected waves. The recovery of the beach in front of the wall is therefore inhibited in these accretionary conditions. Longshore sediment transport is enhanced both by the increase in sediment concentrations in front of the wall and by the strong longshore currents next to the seawall.

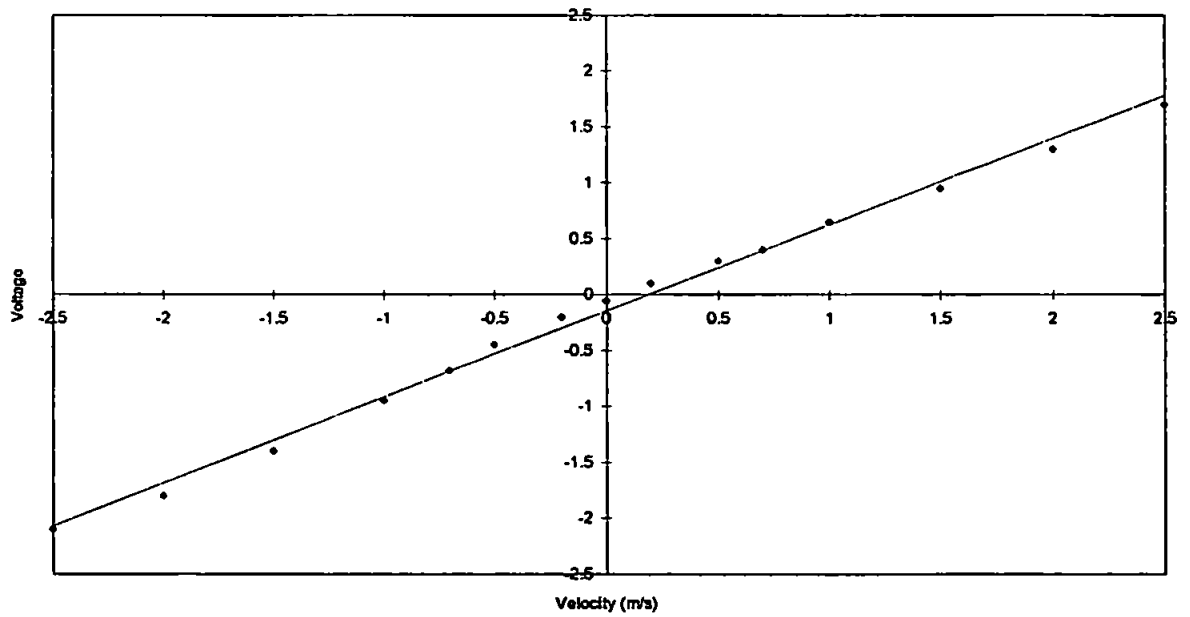
APPENDIX

Instrument calibration graphs

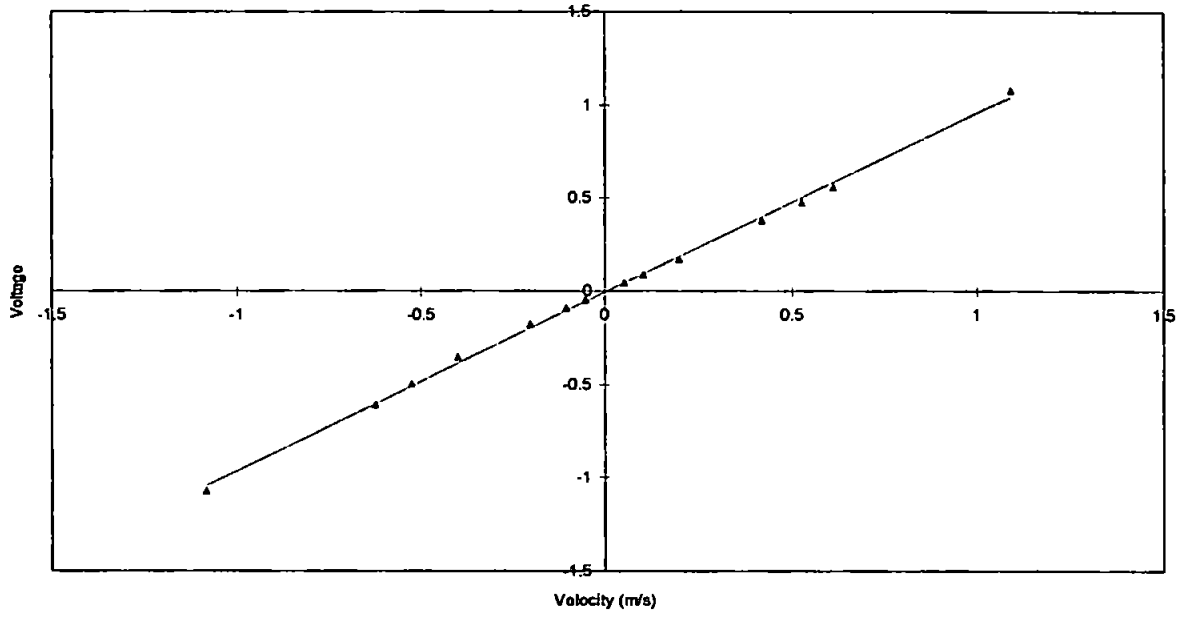
Spherical EMCM 9170 calibration, channel X



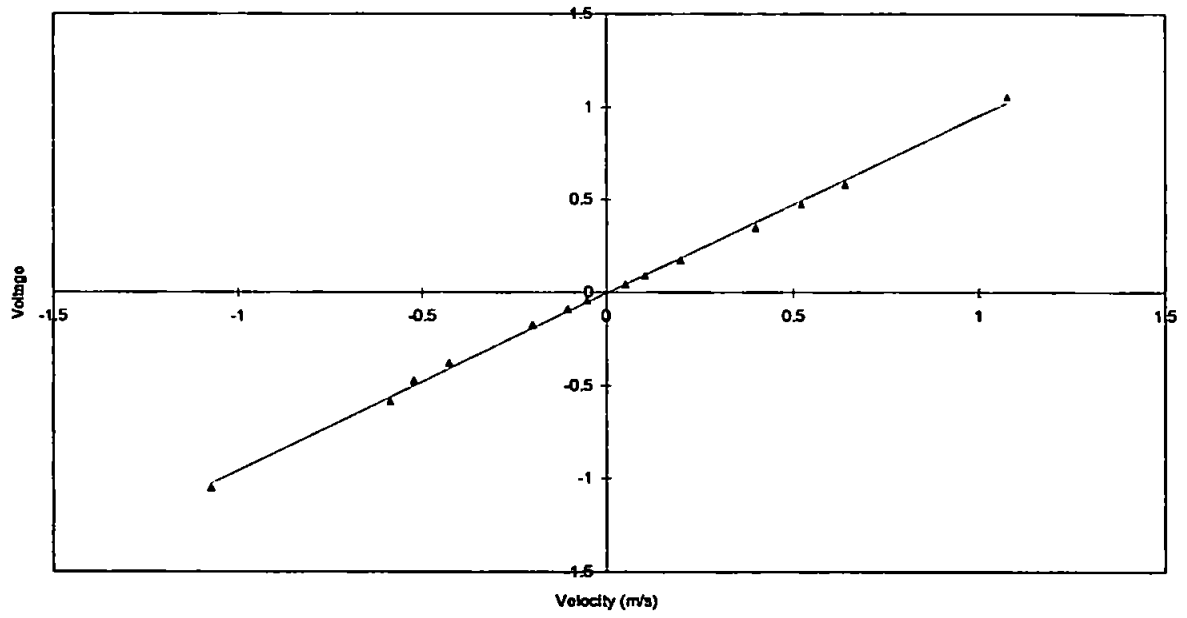
Spherical EMCM 9170 calibration, channel Y



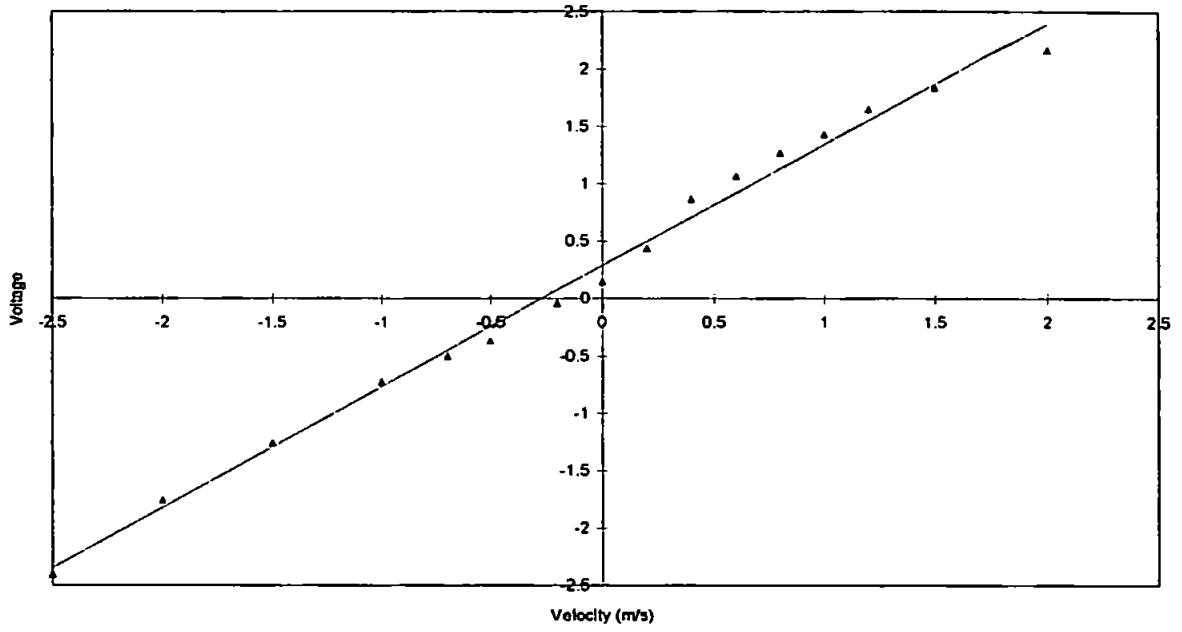
Spherical EMCM 9171 calibration, channel X



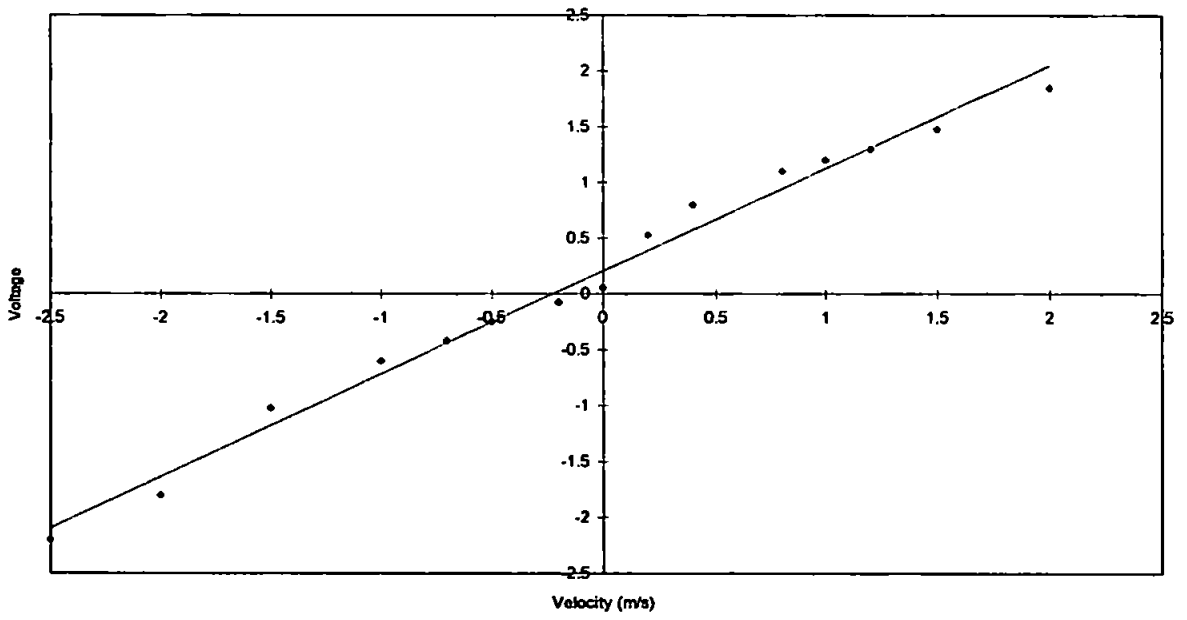
Spherical EMCM 9171 calibration, channel Y

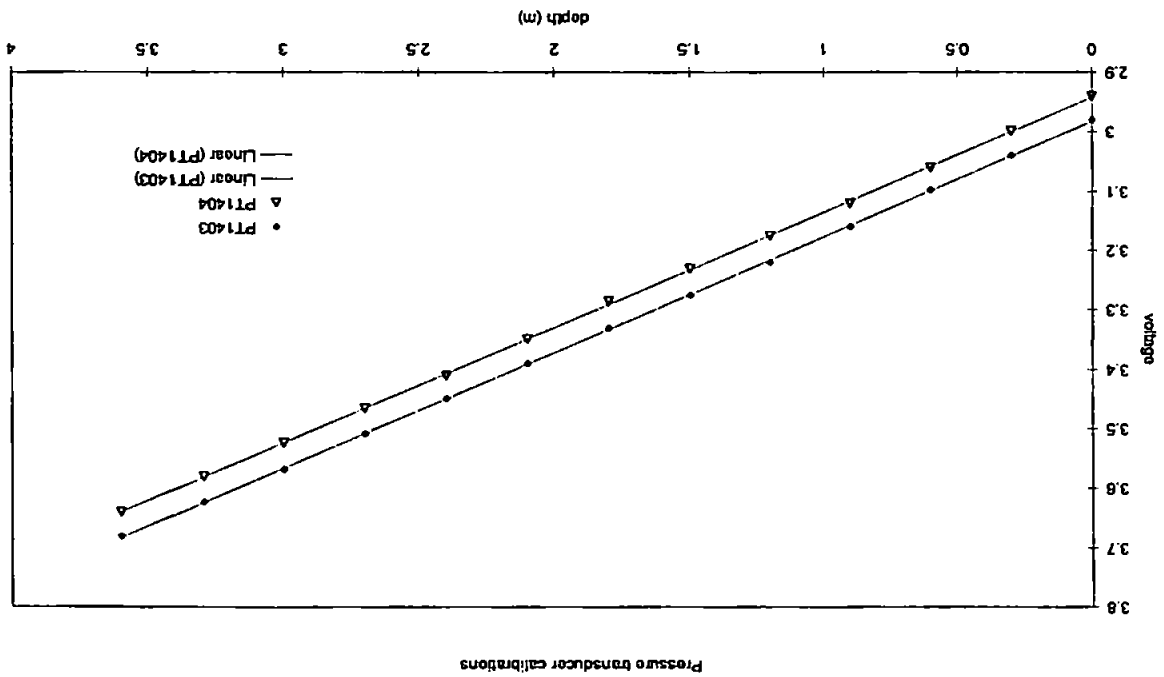
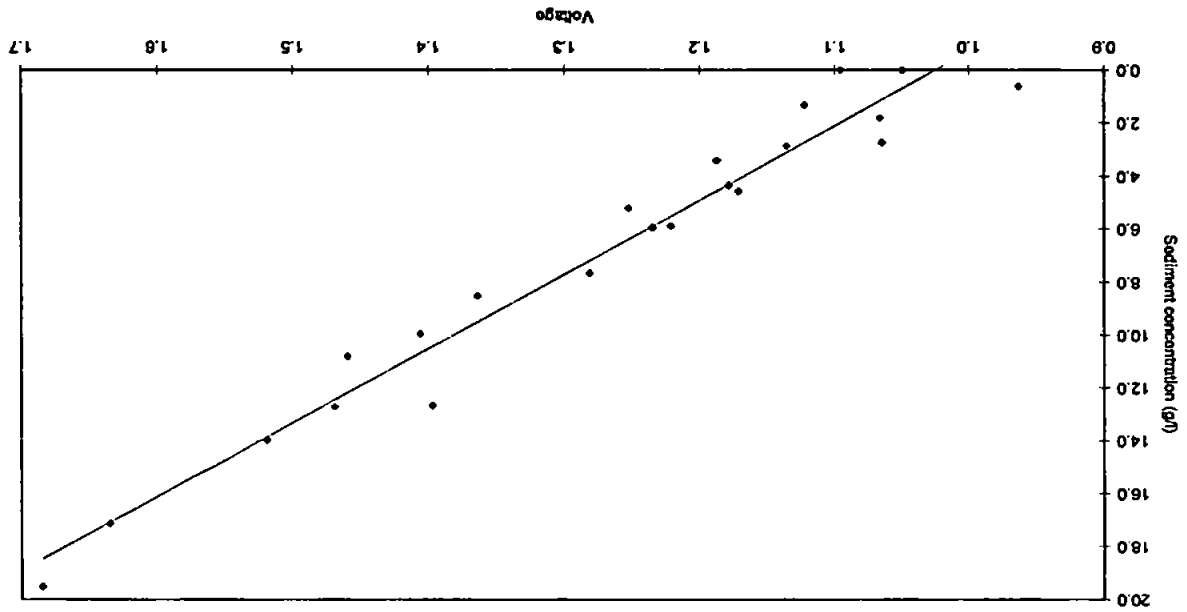


Annular EMC calibration, channel X

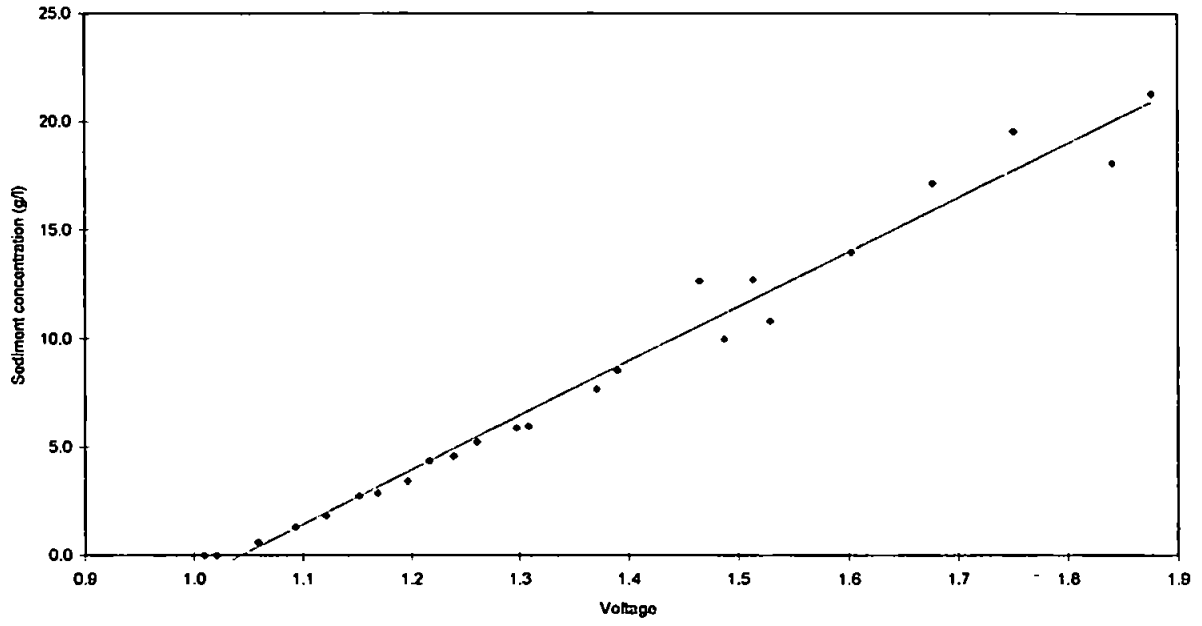


Annular EMC calibration, channel Y

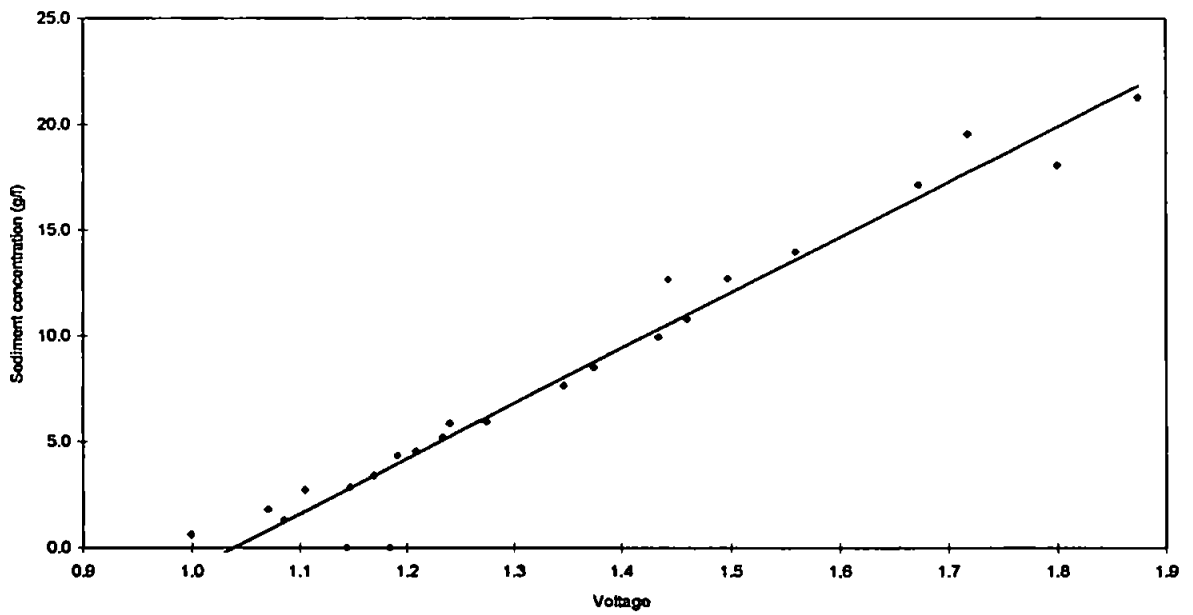




OBS 1401 calibration



OBS 1402 calibration



REFERENCES

- Aargard, T. and Greenwood B., 1994. Suspended sediment transport and the role of infragravity waves in a barred surf zone. *Marine Geology* 118, 23-48.
- Aargard, T. and Greenwood B., 1995. Longshore and cross-shore suspended sediment at far infragravity frequencies in a barred environment. *Continental Shelf Research* 15, 1235-1249.
- Airy, G.B. (Sir), 1845. 'Tides and waves'. *Encyclopedia Metropolitana*, Art. 192, 241-396.
- Allen, J.R.L., 1981. Developments in Sedimentology - Vol 1: *Sedimentary structures*. Elsevier, Amsterdam.
- Allsop, N.W.H., 1990. Reflection performance of rock armoured slopes in random waves. *Proceedings of 22nd Coastal Engineering Conference*, American Society of Civil Engineers.
- Aubrey, D.G., 1989. Measurement errors for electromagnetic current meters. In: R.J. Seymour, (Ed.) *Nearshore Sediment Transport*, Plenum Press, 67-78.
- Aubrey, D.G., Spencer, W.D. and Trowbridge, J.H., 1984. Dynamic response of electromagnetic current meters. *Tech rep.*, WHOI 84-20, 150pp, Woods Hole Oceanogr. Inst., Woods Hole, Mass.
- Aubrey, D.G. and Trowbridge, J.H., 1985. Kinematic and dynamic estimates from electromagnetic current meter data. *Journal of Geophysical Research* 93(C2), 1344-1346.
- Baba, M. and Thomas, K.V., 1987. Performance of a seawall with a frontal beach. *Proceedings of Coastal Sediments '87 - speciality conference on advances in understanding coastal sediment processes*, American Society of Civil Engineers, 1051-1061.
- Bagnold, R.A. (Major), 1940. Beach formation by waves: some model-experiments in a wave tank. *Journal of the Institution of Civil Engineers* 1, 27-52, plus figures.
- Bagnold, R.A., 1946. Motion of waves in shallow water; interactions between waves and sand bottom. *Proceedings of the Royal Society*, London, series A, 187, 1-15.
- Bagnold, R.A., 1947. Sand movement by waves: some small scale experiments with sand of very low density. *Journal of the Institution of Civil Engineers*, 27(4), 447-69.
- Barnett, M.R. and Wang, H., 1988. Effects of a vertical seawall on profile response. *Proceedings of 21st Coastal Engineering Conference*, American Society of Civil Engineers, 1493-1507.
- Basco, D.R., 1987. The effects of seawalls on coastlines and beaches (with specific application to Sandbridge Beach, Virginia). The Coastal Engineering Institute, Old Dominion University, Norfolk, Virginia. 14p, plus appendices.
- Basco, D.R., Bellomo, D.A. and Pollock, C., 1992a. Statistically significant beach profile change with and without the presence of seawalls. *Proceedings of 23rd Coastal Engineering Conference*, American Society of Civil Engineers, 1924-1937.
- Basco, D.R., Bellomo, D.A. and Pollock, C., 1992b. Sandbridge Virginia Oceanfront Seawall Hearing: Some lessons learned for coastal engineers. *Proceedings of Coastal Engineering Practice '92*, American Society of Civil Engineers, 1003-1020.
- Battjes, J.A., 1975. Surf similarity. *Proceedings of 14th Conference on Coastal Engineering*, American Society of Civil Engineers, 466-480.
- Beach, R.A. and Sternberg, R.W., 1988. Suspended sediment transport in the surf zone: response to cross-shore infragravity motion. *Marine Geology* 80, 61-79.
- Beach, R.A. and Sternberg, R.W., 1991. Infragravity driven suspended sediment transport in the swash, inner and outer surf zone. *Proceedings of Coastal Sediments '91*, 114-128.

- Beach, R.A. and Sternberg, R.W., 1992. Suspended sediment transport in the surf zone: Response to incident wave and longshore current interaction. *Marine Geology* 108, 275-294.
- Bendat, J.S. and Piersol, A.G., 1986. *Random data analysis and measurement procedures*. Second Edition, John Wiley and Sons, New York, 566pp.
- Berrigan, P.D., 1985a. The Taraval Vertical Seawall. *Shore and Beach* 53(1), 2-7.
- Berrigan, P.D., 1985b. Seasonal Changes at Taraval Seawall. *Shore and Beach* 53(2), 9-15.
- Bird, P.A., Davidson, M.A., Bullock, G.N. and Huntley, D.A., 1994. Wave measurement near reflective structures. *Proceedings of Coastal Dynamics '94*, 701-711.
- Birkemeier, W.A., 1980. The effect of structures and lake level on bluff and shore erosion in Berrigan County, Michigan, 1970-74. Coastal Engineering Research Center, Misc. Report No. 80-2, U.S. Army Corps of Engineers, 74 p.
- Birkemeier, W.A. and Thornton, E.B., 1994. The DUCK94 Nearshore field experiment. *Proceedings of Coastal Dynamics '94*, 815-821.
- Birkemeier, W.A., Bichner, E.W., Scarborough, B.L., McCarthy, M.A. and Eiser, W.C., 1991. Nearshore profile response caused by Hurricane Hugo. In: C.W. Finkl and O.H. Pilkey (Ed.s), *Impacts of Hurricane Hugo. Journal of Coastal Research, Special Issue No. 8*, 113-127.
- Black, K.P. and Rosenburg, M.A., 1991. Suspended sediment load at three time scales. *Proceedings of Coastal Sediments '91*, 313-327.
- Black, K.P. and Rosenburg, M.A., 1994. Suspended sand measurements in a turbulent environment: field comparison of optical and pump sampling techniques. *Coastal Engineering* 24, 137-150.
- Boussinesq, J. 1872. Theorie des ondes et des remous qui se propagent le long d'un canal des vitesses sensiblement paralleles de la surface au fond. *J. Math. Pures et Appliquees*, Lionvilles, France, 17, 55-108.
- Bray, M.J., Carter, D.J. and Hooke, J.M., 1992. Sea-level rise and global warming: scenarios, physical impacts and policies. Report to SCOPAC.
- Carrier, G.F. and Greenspan, H.P., 1958. Water waves of finite amplitude on a sloping beach. *Journal of Fluid Mechanics* 4, 97-109.
- Carter, R.W.G., 1988. *Coastal Environments*. Academic Press, San Diego, CA., 617pp.
- Carter, T.G., Liu, P. L-F. and Mei, C.C., 1973. Mass transport by waves and offshore sand bedforms. *Journal of Waterways, Harbors and Coastal Engineering Division*, American Society of Civil Engineers 99, No. WW2, 165-184.
- Carter, C.H., Monroe, C.B. and Guy, D.E. Jr., 1986. Lake Erie shore erosion: the effect of beach width and shore protection structures. *Journal of Coastal Research* 2(1), 17-23.
- Chestnutt, C.B. and Schiller, R.E., Jr., 1971. Scour of simulated Gulf Coast sand beaches due to wave action in front of seawalls and dune barriers. COE Report No. 139, TAMU-SG-71-207, Texas A&M University, 54pp.
- Chiu, T.Y., 1977. Beach and dune response to Hurricane Eloise of September 1975. *Proceedings of Coastal Sediments '77*, American Society of Civil Engineers, 116-134.
- Cooley, J.W. and Tukey, E.G., 1965. An algorithm for the machine calculation of complex Fourier series, *Mathematics of Computation* 19, 297.
- Cunningham, P.M., Guza, R.T. and Lowe, R.L., 1979. Dynamic calibration of electromagnetic current meters. *Proceedings of Oceans 1979*, IEEE 298-301.
- Daily, J.W., and Stephen, S.C., 1953a. The solitary wave. *Proceedings of 3rd Conference on Coastal Engineering*, 13-30.

- Daily, J.W., and Stephen, S.C., 1953b. Characteristics of the solitary wave. *Transactions of American Society of Civil Engineers.*, 118, 575-87.
- Dally, W.R., Dean, R.G. and Dalrymple, R.A., 1984. Modelling wave transformation in the surf zone. Miscellaneous paper CERC-84-8, U.S. Army Corps of Engineers, Waterways Experiment Station, Vicksburg, Mississippi.
- Dally, W.R. and Dean, G., 1984. Suspended sediment transport and beach profile evolution. *Journal of Waterway, Port, Coastal and Ocean Engineering* 110, 15-23.
- Davidson, M.A., Bird, P.A., Bullock, G.N. and Huntley, D.A., 1994. Wave reflection: Field measurements, analysis and theoretical developments. *Proceedings of Coastal Dynamics '94*, 642-655.
- Davidson, M.A., Russell, P.E., Huntley, D.A., Hardisty, J. and Cramp, A., 1993a. An overview of the British beach and nearshore dynamics programme. *Proceedings of 23rd International Conference on Coastal Engineering '92*, 1987-2000.
- Davidson, M.A., Russell, P.E., Huntley, D.A. and Hardisty, J., 1993b. Tidal asymmetry in suspended sand transport on a macrotidal intermediate beach. *Marine Geology* 110, 333-353.
- Davis, R.A., Jr. and Andronaco, M., 1987. Hurricane effects and post storm recovery, Pinellas County, Florida (1985-1986). *Proceedings of Coastal Sediments '87*, American Society of Civil Engineers, 1023-1036.
- Dean, R.G., 1973. Heuristic models of sand transport in the surf zone. *Proceedings of Conference on Engineering Dynamics in the Surf Zone*, Sydney, Australia. 208-214,
- Dean, R.G., 1987a. Coastal armoring: effects, principles and mitigation. *Proceedings of 20th Coastal Engineering Conference*, American Society of Civil Engineers, 1843-1857.
- Dean, R.G., 1987b. Coastal sediment processes: toward engineering solutions. *Proceedings of Coastal Sediments '87*, American Society of Civil Engineers, 1-24.
- Dean, R.G., 1991. Equilibrium beach profiles: Characteristics and applications. *Journal of Coastal Research* 7(1), 53-84.
- Dean, R.G. and Mauermeyer, E.M., 1983. Models for beach profile response. In: P.D. Komar (Ed.), *Handbook of Coastal Processes and Erosion*, CRC Press, Inc., Boca Raton, Florida, 151-165.
- Dean, R.G. and Yoo, C-H., 1994. Beach nourishment in presence of seawall. *Journal of Waterway, Port, Coastal, and Ocean Engineering* 120(3), 302-316.
- Detle, H.H. and Gartner, J., 1987. Time history of a seawall on the island of Sylt. *Proceedings of Coastal Sediments '87*, American Society of Civil Engineers, 1006-1022.
- De Best, A. and Bijker, E.W., 1971. Scouring of a sand bed in front of a vertical breakwater. Department of Civil Engineering, Report No. 71-1, Delft University of Technology, The Netherlands, 7p.
- De Best, A., Bijker, E.W. and Wichers, J.E.W., 1971. Scouring of a sand bed in front of a vertical breakwater. *1st International Conference on Port and Ocean Engineering Under Arctic Conditions, Vol II*, Technical University of Norway, 1077-1086.
- Dickson, W.S., Herbers, T.H.C. and Thornton, E.B., 1995. Wave reflection from breakwater. *Journal of Waterway, Port, Coastal and Ocean Engineering*, American Society of Civil Engineers 121(5), 262-268.
- Dingler, J.R. and Inman, D.L., 1976. Wave formed ripples in nearshore sands. *Proceedings of 15th Coastal Engineering Conference*, American Society of Civil Engineers, 2109-2126.
- Doering, J.C. and Bowen, A.J., 1987. Skewness in the nearshore zone: A comparison of estimates from Marsh Mc-Birney current meters and colocated pressure sensors. *Journal of Geophysical Research* 92(13), 173-183.

- Dorland, G.M., 1940. *Equilibrium sand slopes in front of seawalls*. Unpublished M.S. Thesis, Department of Civil Engineering, University of California, Berkely, California, 43p.
- Downing, J.P., Sternberg, R.W. and Lister, C.R.B., 1981. New instrumentation for the investigation of suspended sediment processes in the shallow marine environment. *Marine Geology* 42, 19-34.
- Downing, J.P., 1983. An optical instrument for monitoring suspended particulates in ocean and laboratory. *Proceedings of Oceans '83*, San Fransisco, Ca., IEEE & MTS, 199-202.
- Elgar, S., Herbers, T. H. C. and Guza, R.T., 1994. Reflection of ocean surface gravity waves from a natural beach. *Journal of Physical Oceanography* 24, 1503-1511.
- Finkl, C.W. and Pilkey, O.H. (Eds.), 1991. Impact of Hurricane Hugo: September 10-22, 1989. *Journal of Coastal Research, Special Issue No. 8*, 356 pp.
- Fitzgerald, D.M., 1980. Effects of intense storm at Winthrop beach, Massechussets. *Shore and Beach* 48(3), 6-19.
- Fitzgerald, D.M., Van Herteren, S. and Montello, T.M., 1994. Shoreline processes and damages resulting from the Halloween Eve Storm of 1991 along the north and south shores of Massachusetts Bay, U.S.A. *Journal of Coastal Research* 10(1), 113-132.
- Foster, D.L., Holman, R.A. and Beach, R.A., 1994. Sediment suspension events and shear instabilities in the bottom boundary layer. *Proceedings of Coastal Dynamics '95*, 712-726.
- Fowler, J., 1992. Scour problems and methods for prediction of maximum scour at vertical walls. Technical Report CERC-92-16, U.S. Army Engineer Waterways Experiment Station, Coastal Engineering Research Center, Vicksburg, Miss.
- Fowler, J., 1993. Coastal scour problems and methods for prediction of maximum scour. Technical Report CERC-93-8, U.S. Army Engineer Waterways Experiment Station, Coastal Engineering Research Center, Vicksburg, Miss.
- Frigaard, P. and Borsen, M., 1995. A time domain method for separating incident and reflected irregular waves. *Coastal Engineering* 24, 205-215.
- Gaillard, P., Gauthier, M. and Holly, F., 1980. Method of analysis of random wave experiments with reflecting coastal structures. *Proceedings of 17th Conference Coastal Engineering*, American Society of Civil Engineers, 204-220.
- Galvin, C.J. Jr., 1968. Breaker type classification in three laboratory beaches. *Journal of Geophysical Research* 73(12), 3651-3659.
- Giminez-Curto, L.A., 1979. *Behaviour of rubble mound breakwaters under wave action*. Unpub. Ph.D. Thesis, University of Santander, Spain (In Spanish).
- Goda, Y. and Suzuki, S., 1976. Estimation of incident and reflected waves in random wave experiments. *Proceedings of 15th Conference on Coastal Engineering, Vol II*, American Society of Civil Engineers, 828-845, Honolulu.
- Goda, Y., 1970. A synthesis of breaker indices. *Trans. Japanese Soc. Civil Engrs.* 2(2), 227-230.
- Green, T., 1986. Edge waves near a seawall. *Coastal Engineering* 10, 119-125.
- Greenwood, B., Osborne, P.D. and Bowen, A.J., 1991. Measurements of suspended sediment transport: prototype shorefaces. *Proceedings of Coastal Sediments '91*, 284-299.
- Griggs, G.B. and Tait, J.F., 1988. The effects of coastal protection structures on beaches along northern Monterey Bay, California. *Journal of Coastal Research, Special Issue No. 4*, 93-111.
- Griggs, G.B., Tait, J.F., Scott, K. and Plant, N., 1991. The interaction of seawalls and beaches: four years of field monitoring, Monterey Bay, California. *Proceedings of Coastal Sediments '91*, American Society of Civil Engineers, 1871-1885.

- Griggs, G.B., Tait, J.F. and Corona, W., 1994. The interaction of seawalls and beaches: seven years of monitoring, Monterey Bay, California. *Shore and Beach* 62(3), 21-28.
- Guza, R.T., 1988. Comment on 'Kinematic and Dynamic Estimates from Electromagnetic Current Meter Data' by D.G. Aubrey and J.H. Trowbridge. *Journal of Geophysical Research* 92(13), 1337-1343.
- Guza, R.T. and Bowen, A.J., 1975. The resonant instabilities of long waves obliquely incident on a beach. *Journal of Geophysical Research* 80, 4529-4534.
- Guza, R.T. and Bowen, A.J., 1976. Resonant interactions for waves breaking on a beach. *Proceedings of 15th Conference on Coastal Engineering, Vol. 1*, American Society of Civil Engineers, 560-579, Honolulu.
- Guza, R.T. and Inman, D.L., 1975. Edge waves and beach cusps. *Journal of Geophysical Research* 80(21), 2997-3012.
- Guza, R.T., Thornton, E.B. and Holman, R.A., 1984. Swash on steep and shallow beaches. *Proceedings of 19th Conference on Coastal Engineering*, American Society of Civil Engineers, 708-723.
- Hall, M.J. and Pilkey, O.H., 1991. Effects of hard stabilization on dry beach width for New Jersey. *Journal of Coastal Research* 7(3), 771-785.
- Hanes, D.M. and Huntley, D.A., 1986. Continuous measurements of suspended sand concentration in a wave dominated nearshore environment. *Continental Shelf Research* 6, 585-596.
- Hanson, H. and Kraus, N.C., 1985. Seawall Constraint in the Shoreline Numerical Model. *Journal of Waterway, Port, Coastal and Ocean Engineering* 111(6), 1079-1083.
- Hanson, H. and Kraus, N.C., 1989. GENESIS: Generalised Model for Simulating Shoreline Change, Report 1: Technical Reference. Technical Report CERC 89-19, U.S. Army Engineer Waterways Experiment Station, Coastal Engineering Research Center, Vicksburg, Miss.
- Hayashi, R.M., 1987. Beachwalls for beach erosion protection. *Proceedings of 20th Coastal Engineering Conference*, American Society of Civil Engineers, 1909-1914.
- Hazen, D.G., Doering, J.C. and Bowen, A.J., 1990. A note on a low cost pressure sensor for nearshore wave measurements. *Continental Shelf Research* 14, 85-90.
- Herbich, J.B. and Ko, M.S., 1969. Scour of sand beaches in front of seawalls. *Proceedings of 11th Coastal Engineering Conference*, American Society of Civil Engineers, 622-643.
- Hirinandi, M.G. and Gole, C.V., 1961. Shoreline advancement by seawall and groynes at Cochin. *Proceedings of 7th Coastal Engineering Conference*, American Society of Civil Engineers, 860-871.
- Holman, R.A., 1981. Infragravity energy in the surf zone. *Journal of Geophysical Research* 86(7), 6442-6450.
- Horikawa, K., 1987. *Nearshore dynamics and coastal processes - theory, measurement and predictive models*, Univ. of Tokyo Press, 515pp.
- Hotta, S., Miziguchi, M. and Isobe, M., 1981. Observations of long period waves in the nearshore zone. *Coastal Engineering in Japan* 24, 41-76.
- Hsu, J.R.C. and Silvester, R., 1989. Model test results of scour along breakwaters. *Journal of Waterway, Port, Coastal and Ocean Engineering* 115(1), 66-85.
- Hughes, S.A. and Fowler, J.E., 1991. Wave induced scour prediction at vertical walls. *Proceedings of Coastal Sediments '91*, 1886-1900.
- Hughes, S.A., 1992. Estimating wave induced bottom velocities at a vertical wall. *Journal of Waterway, Port, Coastal and Ocean Engineering*, 118(2), 175-192.

- Hughes, S.A., 1993. Laboratory wave reflection analysis using co-located gauges. *Coastal Engineering* 20, 223-247.
- Hughes, S.A. and Fowler, J.E., 1995. Estimating wave induced kinematics at sloping structures. *Journal of Waterway, Port, Coastal and Ocean Engineering* 121, 209-215.
- Huntley, D.A., 1979. Summary and recommendations. Workshop on instrumentation for currents and sediments in the nearshore zone. National Research Council of Canada Associate Committee for Research on Shoreline Erosion and Sedimentation, 191-194.
- Huntley, D.A., 1982. In situ sediment monitoring techniques: a survey of the state of the art in the U.S.A. *Report No. C2S2-1 for the Canadian Coastal Sediment Study*, 34pp.
- Huntley, D.A. and Bowen, A.J., 1975. Comparison of the hydrodynamics of steep and shallow beaches. In: J. Hails and A. Carr (Eds.), *Nearshore Sediment Dynamics and Sedimentation*, John Wiley and Sons Ltd., London, 69-109.
- Huntley, D.A. and Bowen, A.J., 1975. Field observations of edge waves and their effect on beach material. *Journal of the Geological Society, London*, 131, 69-81.
- Huntley, D.A. and Hanes, D.M., 1987. Direct measurement of suspended sediment transport. *Proceedings of Coastal Sediments '87*, American Society of Civil Engineers, 723-737.
- Huntley, D.A., Simmonds, D. and Davidson, M.A., 1995. Estimation of frequency-dependent reflection coefficients using current and elevation sensors. *Proceedings of Coastal Dynamics '95*, 57-68.
- Huntley, D.A., Davidson, M.A., Russell, P.E., Foote, Y. and Hardisty, J., 1993. Long waves and sediment movement on beaches: Recent observations and implications for modelling. *Journal of Coastal Research, Special Issue No. 15*, 215-229.
- Inman, D.L. and Bagnold, R.A., 1963. Beach and nearshore processes. Part II. Littoral processes. In Hill, M. N. (Ed), *The Sea: Vol. 3*, Wiley Interscience, New York, 529-553.
- Iribarren, C.R. and Nogales, C., 1949. Protection des Ports, Section II, Comm. 4, XVIIth Int. Nav. Congress, Lisbon, 9-32.
- Irie, I. and Nadaoka, K., 1984. Laboratory reproduction of seabed scour in front of breakwaters. *Proceedings of 19th Coastal Engineering Conference, Vol. II*, American Society of Civil Engineers, 1715-1731.
- Irie, I., Kuriyama, Y. and Asakura, H., 1986. Study on scour in front of breakwaters by standing waves and protection methods. *Report, Port and Harbour Res. Inst., Japan* 25(1), 4-86.
- Isobe, M. and Kondo, K., 1984. Method for estimating directional wave spectrum in incident and reflected wavefield. *Proceedings of 19th Conference on Coastal Engineering, Vol. I*, American Society of Civil Engineers, 467-483.
- Jaffe, B.E., Sternberg, R.W. and Sallenger, A.H., 1984. The role of suspended sediment in shore normal beach profile changes. *Proceedings of Coastal Engineering '84*. 1983-1996.
- Jenkins, G.M. and Watts, D.G., 1968. *Spectral Analysis and its Applications*. Holden-Day, San Fransisco, Ca., 525pp.
- Johnson, C.N., 1992. Mitigation of harbor caused shore erosion with beach nourishment delayed mitigation, St. Joseph Harbor, MI. *Proceedings of Coastal Engineering Practise '92*, American Society of Civil Engineers, 137-153.
- Kajima, R., 1969. Estimation of incident wave spectra under the influence of reflection. *Proceedings of 13th Congress IAHR*, Kyoto, Japan 5(1), 285-288.
- Kamphius, J.W., Ratchet, K.A. and Jui, J., 1992. Hydraulic model experiments on seawalls. *Proceedings of 23rd Coastal Engineering Conference*, American Society of Civil Engineers, 1272-1284.
- Kinsman, B., 1965. *Wind waves, their generation and propagation on the ocean surface*. Dover press.

- Komar, P.D. and McDougal, W.G., 1988. Coastal erosion and engineering structures: The Oregon experience. In: N.C. Kraus and O.H. Pilkey (Eds.), The effects of seawalls on the beach. *Journal of Coastal Research, Special Issue No. 4*, 77-92.
- Kondo, K., Akama, M. and Isobe, M., 1986: Measurement of reflection coefficient of a seawall in Omura bay. *Proceedings of 20th Conference on Coastal Engineering*, American Society of Civil Engineers, 1987-2001.
- Kraus, N.C., 1987. The effects of seawalls on the beach: a literature review. *Proceedings of Coastal Sediments '87*, American Society of Civil Engineers, 945-960.
- Kraus, N.C., 1988. The effects of seawalls on the beach: extended literature review. *Journal of Coastal Research, Special Issue No. 4*, 1-28.
- Kraus, N.C., Gravens, M.B. and Mark, D.J., 1988. Coastal processes at Sea Bright to Ocean Township, New Jersey, Volume 2: Appendices b - G.U.S. Army Engineer Waterways Experiment Station, Coastal Engineering Research Center.
- Kraus, N.C., Smith, J.M. and Sollitt, C.K., 1992. SUPERTANK laboratory data collection project. *Proceedings of 23rd International Conference on Coastal Engineering*, American Society of Civil Engineers, 2191-2204.
- Kraus, N.C. and Hanson, H., 1995. Discussion of: Dean, R.G. and Yoo, C-H. 1994. Beach nourishment in presence of seawall. *Journal of Waterway, Port, Coastal and Ocean Engineering*, 121(3) 272-274.
- Kraus, N.C. and McDougal, W.G., 1996. The effects of seawalls on the beach: part 1, an updated literature review. *Journal of Coastal Research* 12(3), 691-701.
- Kriebel, D.L., 1987. Beach recovery following Hurricane Elena. *Proceedings of Coastal Sediments '87*, American Society of Civil Engineers, 990-1005.
- Kriebel, D.L., Dally, W.R. and Dean, R.G., 1986. Beach profile response following severe erosion events. Coastal and Oceanographic Engineering Department, UF/COEL-86-016, University of Florida, Gainesville, FL.
- Kriebel, D.L. and Dean, R.G., 1985. Numerical simulation of time dependent beach and dune erosion. *Coastal Engineering* 9, 221-245.
- Kubota, S., Mizuguchi, M. and Takezawa, M., 1990. Reflection from swash zone on natural beaches. *Proceedings of 22nd Coastal Engineering Conference, Vol. I*, American Society of Civil Engineers, 154-172, Delft.
- Lamb, H., 1932. *Hydrodynamics*. Sixth Edition, Dover Publications, New York, 738pp.
- Larson, M. and Kraus, N.C., 1989. SBEACH: Numerical model for simulating storm induced beach change. Report 1: Theory and model foundation, CERC Technical report CERC-89-9, U.S. Army Corps of Engineers, Waterways Experiment Station, Vicksburg, Mississippi, 267pp.
- Lin, M-C., Wu, C-T., Lu, Y-C. and Liang, N-K., 1986. Effects of short crested waves scouring around the breakwater. *Proceedings of 20th Coastal Engineering Conference*, American Society of Civil Engineers, 2050-2064.
- Lippmann, T.C. and Holman, R.A., 1990. The spatial and temporal variability of sand bar morphology. *Journal of Geophysical Research* 95(7), 11575-11590.
- Longuet Higgins, M.S., 1953. Mass transport in water waves. *Phil. Trans. Royal Soc. London, Series A, Vol. 245*, No. 903, 535-581.
- Longuet Higgins, M.S., 1970. Longshore currents generated by obliquely incident sea waves. *Journal of Geophysical Research* 75(33), 6778-6801.
- MacDonald, H.V. and Patterson, D.C., 1985. Beach response to coastal works Gold Coast, Australia. *Proceedings of 19th Coastal Engineering Conference*, American Society of Civil Engineers, 1522-1538.

- Madsen, O.S. and Grant, W.D., 1976. Quantitative description of sediment transport by waves. *Proceedings of 15th Coastal Engineering Conference*, American Society of Civil Engineers, 1093-1112.
- Mansard, E.P.D. and Funke E.R., 1980. The measurement of incident and reflected spectra using a least squares method. *Proceedings of 17th International Conference on Coastal Engineering*, Vol. I, 154-172, Sydney.
- Martens, D.E. and Thornton, E.B., 1987. Nearshore zone monitoring system. *Proceedings of Coastal Hydrodynamics*, American Society of Civil Engineers, 579-588.
- Mason, C., Salenger, A.H., Holman, R.A. and Birkemeier, W.A., 1984. DUCK82 A coastal storm process experiment. *Proceedings of 19th Coastal Engineering Conference*, American Society of Civil Engineers, 1913-1928.
- Masselink, G. and Short, A.D., 1993. The effect of tide range on beach morphodynamics and morphology: A conceptual beach model. *Journal of Coastal Research* 9(3), 785-800.
- Masselink, G., 1995. Group bound long waves as a source of infragravity energy in the surf zone. *Continental Shelf Research* 15(13), 1525-1547.
- McCowan, J., 1891. On the solitary wave. *Phil. Mag., series 5*, 32, 45-58.
- McDougal, W.G., Sturtevant, M.A. and Komar, P.D., 1987. Laboratory and field investigations of the impact of shoreline stabilisation structures on adjacent properties. *Proceedings of Coastal Sediments '87*, American Society of Civil Engineers, 961-973.
- McDougal, W.G., Kraus, N.C. and Ajibowo, H., 1994. Simulation of wave and beach profile change in SUPERTANK seawall test. *Coastal Dynamics '94*, 278-295.
- McDougal, W.G., Kraus, N.C. and Ajiwibowo, H., 1996. The effects of seawalls on the beach part II, numerical modelling of SUPERTANK seawall test. *Journal of Coastal Research* 12(3), 702-713.
- Miche, M., 1951. Le pouvoir reflechissant des ouvrages maritimes exposes a l'action de la houle. *Ann. Points. Chaussees* 121, 285-319.
- Ministry of Agriculture, Fisheries and Food (MAFF), 1991. Advice on allowance for sea level rise. *MAFF Publications*.
- Moody, P.M. and Madsen, O.S., 1996. Effects of seawalls on crossshore sediment transport. *Proceedings of 25th International Conference on Coastal Engineering*, book of abstracts, 176-177, Orlando, Florida.
- Morton, R.A., 1988. Interactions of storms, seawalls and beaches of the Texas coast. *Journal of Coastal Research, Special Issue No. 4*, 113-134.
- Munk, W.H., 1949. The solitary wave theory and its application to surf problems. *N.Y. Acad. Sci. Ann.*, 51, 376-424.
- Murray, P.B., 1992. *Sediment pick up in combined wave-current flow*. Unpublished Ph.D. Thesis, University of Wales, 189pp.
- Nakashima, L.D. and Mossa, J., 1991. Responses of natural and seawall backed beaches to recent hurricanes on the Bayou Lafourche headland, Louisiana. *Z. Geomorph. N.F.* 35(2), 239-256.
- Nelson, R. C. and Gonsalves, J., 1990. A field study of reflections from an exposed dissipative beach. *Coastal Engineering* 14, 457-477.
- Nielsen, P., 1979. Some basic concepts of wave sediment transport. Series Paper 20, Institute of Hydrodynamics and Hydraulic Engineering (ISVA), Technical University of Denmark, 160pp.
- Nielsen, P., 1984. Field measurements of time averaged suspended sediment concentrations under waves. *Coastal Engineering* 8, 51-72.

- Nuttal, A.H., 1971. Spectral estimation by means of overlapped FFT processing of windowed data. Naval Underwater Systems Center Report No. 4169, New London, CT, USA (and supplement NUSC TR-4169S).
- O'Brien, M.P., 1984. Wave action at a vertical seawall. *Shore and Beach* 52(3), 31.
- Oppenheim, A.V. and Schaffer, R.W., 1975. *Digital signal processing*, Prentice Hall, New Jersey.
- Osborne, P.D. and Greenwood, B., 1992a. Frequency dependent cross shore sediment transport. 1. A non-barred shoreface. *Marine Geology* 106, 1-24.
- Osborne, P.D. and Greenwood, B., 1992b. Frequency dependent cross shore sediment transport. 2. A barred shoreface. *Marine Geology* 106, 25-51.
- Osborne, P.D. and Greenwood, B., 1993. Sediment suspension under waves and currents: time scales and vertical structure. *Sedimentology* 40, 599-622.
- Oumeraci, H., 1993. Scour in front of vertical breakwaters - *Review of scaling problems*. Mitteilungun, Heft 125, ISSN 0343 1223, 345-382.
- Oumeraci, H., 1994. Review and analysis of vertical breakwater failures - lessons learned. *Coastal Engineering* 22, 3-29.
- Owen, M.W. and Thorn, M.F.C., 1978. Effect of waves on sand transport by currents. *Proceedings of 16th Coastal Engineering Conference.*, 1675-1687.
- Ozasa, H. and Brampton, A.H., 1979. Models for predicting the shoreline evolution of beaches backed by seawalls. Rep. IT 191, HRS, Wallingford, Berks.
- Ozasa, H. and Brampton, A.H., 1980. Mathematical modelling of beaches backed by seawalls. *Coastal Engineering* 4, 47-64.
- Palmer, R. (Ed.), 1996. History of Coastal Engineering in Britain. In: *History and Heritage of Coastal Engineering*, N.C. Kraus (Ed.), 214-274.
- Pilkey, O.H. and Wright, H.L., 1988. Seawalls verses beaches. *Journal of Coastal Research, Special Issue No. 4*, 41-46.
- Plant, N.G. and Griggs, G.B., 1992. Interactions between nearshore processes and beach morphology near a seawall. *Journal of Coastal Research* 8(1), 183-200.
- Postma, G.M., 1989. *Wave reflection from rock slopes under wave attack*. Unpublished Ph.D. Thesis, Delft University of Technology, 106pp.
- Rakha, K.A. and Kamphuis, J.W., 1995. A morphology model to predict erosion near a seawall. *Proceedings of Coastal Dynamics '95*, 879-890.
- Ruessink, B.G., 1995. On the origin of infragravity waves in the surf zone of a dissipative multiple bar system. *Proceedings of Coastal Dynamics '95*, 93-104.
- Russell, P.E., 1990. *Field studies of suspended sand transport on a high energy dissipative beach*. Unpub. Ph.D. Thesis, University of Wales, 318pp.
- Russell, P.E., 1993. Mechanisms for beach erosion during storms. *Continental Shelf Research* 13(11), 1243-1265.
- Russell, P., Davidson, M., Huntley, D., Cramp, A., Hardisty, J. and Lloyd, G., 1991. The British Beach And Nearshore Dynamics (B-BAND) Programme. *Coastal Sediments '91*, 371-384.
- Russell, R.C.H. and Ingliss, C., 1953. The influence of a vertical wall on a beach in front of it. *Proceedings of the Minnesota International Hydraulics Convention*, American Society of Civil Engineers, 221-226.
- Sallenger, A.H. and Holman, R.A., 1987. Infragravity waves over a natural barred profile. *Journal of Geophysical Research* 92(9), 9531-9540.

- Sato, S., Tanaka, N. and Irie, I., 1969. Study on scouring at the foot of coastal structures. *Proceedings of 11th Coastal Engineering Conference*, American Society of Civil Engineers, 579-598.
- Sawaragi, T. and Kawasaki, Y., 1960. Experimental study on behaviours of scouring at the toe of seawalls by waves. *Proceedings of 4th Japanese Coastal Engineering Conference*, Japan Society of Civil Engineers, 1-12 (in Japanese; figure and table captions in English).
- Sayre, W.O., 1987. Coastal erosion on the barrier islands of Pinellas County, West-Central Florida. *Proceedings of Coastal Sediments '87*, American Society of Civil Engineers, 1037-1050.
- Seelig, W.N. and Ahrens, J.P., 1981. Estimation of wave reflection and energy dissipation for beaches, revetments and breakwaters. CERC Technical paper 81-1, Fort Belvoir, US Army Engineer Waterways Coastal Experiment Station, Vicksburg, Miss., 40pp.
- Seymour, R.J., 1989. *Nearshore sediment transport*, Plenum Press, New York, 450pp.
- Sexton, W.J. and Moslow, T.F., 1981. Effects of Hurricane David, 1979, on the beaches of Seabrook Island, South Carolina. *Northeastern Geology* 3(3/4), 297-305.
- Shi, N.C. and Larsen, L.H., 1984. Reverse sediment transport by amplitude modulated waves. *Marine Geology* 60, 199-218.
- Shields, A., 1936. *Anwendung der aenlichkeitsmechanik und der turbulenzforschung an die geschicebewegung*. Mitt. Preuss, Berlin.
- Shore Protection Manual, 1984. 4th edition. Coastal Engineering Research Centre, U.S. Army Corps. Eng., Washington.
- Short, A.D., 1991. Macro-Meso Tidal Beach Morphodynamics- An Overview. *Journal of Coastal Research* 7(2), 417-436.
- Silvester, R., 1972. Wave reflection at seawalls and breakwaters. *Proc. Inst. Civil. Eng.* 51, 123-131.
- Silvester, R., 1974. *Coastal Engineering. Vol I and II*, 457pp and 338pp. Elsevier.
- Silvester, R., 1977. The role of wave reflection in coastal processes. *Proceedings of Coastal Sediments '77*, American Society of Civil Engineers, 639-652.
- Simmonds, D., Voulgaris, G. and Huntley, D.A., 1995. Dynamic processes on a ridge and runnel beach. *Proceedings of Coastal Dynamics '95*, 868-878.
- Sternberg, R.W., Shi, N.C. and Downing, J.P., 1984. Field investigations of suspended sediment in the nearshore zone. *Proceedings of 19th Coastal Engineering Conference*, American Society of Civil Engineers, 1782-1798, Houston.
- Suhayda, J.N., 1974. Standing waves on beaches. *Journal of Geophysical Research* 72, 3065-3071.
- Suhayda, J.N. and Pettgrew, N.R., 1977. Observations of wave height and wave celerity in the surf zone. *Journal of Geophysical Research* 82(9), 1419-1424.
- Tanaka, N., Irie, I. and Ozasa, H., 1972. A study on the velocity distribution of mass transport caused by diagonal, partial standing waves. Report, Port and Harbour Res. Inst., Japan, 11(3), 112-140, (in Japanese).
- Tait, J.F. and Griggs, G.B., 1990. Beach response to the presence of a seawall. *Shore and Beach* 58(2), 11-28.
- Tatavarti, R.S.V.N., 1987. Decomposition of random wave energy on beaches. *Proceedings of Dock and Harbour Engineering, 355-361*, Madras, India.
- Tatavarti, R.S.V.N., 1989. *The reflection of waves on natural beaches*. Unpublished Ph.D. Thesis. Dalhousie University, Halifax, Nova Scotia, Canada, 175pp.

- Tatavarti, R.S.V.N. and Huntley, D.A., 1987. Wave reflections at beaches. *Proceedings of Canadian Coastal Conference*, 241-256, Quebec City, Canada.
- Tatavarti, R.V.S.N., Huntley, D.A. and Bowen, A.J., 1988. Incoming and outgoing wave interactions on beaches. *Proceedings of 21st Conference on Coastal Engineering*, American Society Civil Engineers, 1104-1120.
- Terchunian, A.V., 1988. Permitting coastal armoring structures: can seawalls and beaches coexist? In: N.C. Kraus and O.H. Pilkey (Eds.), *The effects of seawalls on the beach. Journal of Coastal Research, Special Issue No. 4*, 65-75.
- Toue, T. and Wang, H., 1990. Three dimensional effects of seawall on the adjacent beach. *Proceedings of 22nd Coastal Engineering Conference*, American Society of Civil Engineers, 2782-2795.
- Uda, T., 1989. Is the presence of seawalls and concrete armor blocks the cause of foreshore erosion? *Proceedings of 49th Annual Conference on Civil Engineering*, Japan Society of Civil Engineers, 42-43 (in Japanese).
- Van de Hulst, H.C., 1957. *Light scattering by small particles*. Wiley, New York, 470pp.
- Vincent, C.E., Hanes, D.M., Tamura, T. and Clarke, T.L., 1986. The acoustic measurement of suspended sand in the surf zone. *Int. Conf. Measuring Techniques of Hydraulics Phenomena in Offshore*, Coastal and Inland Waters. Br. Hydraul. Res. Assoc., London, 443-451.
- Walton, T.L., 1992. Wave reflection from natural beaches. *Ocean Engineering* 19, 239-258.
- Walton, T.L. and Sensabaugh, W., 1978. Seawall design on sandy beaches. *University of Florida Sea Grant Report*.
- Walton, T.L. and Sensabaugh, W., 1979. Seawall design on the open coast. *Florida Sea Grant College, Report No 29*, 24pp.
- Wiegel, R.L., 1964. *Oceanographical Engineering*, Prentice Hall Inc., 532pp.
- Willis, D.H., 1987. The Canadian Coastal Sediment Transport Study: An overview. *Proceedings of Coastal Sediments '87*, American Society Civil Engineers, 682-693.
- Wright, L.D., Boon, J.D., Kim, S.C. and List, J.H., 1991. Modes of cross-shore sediment transport on the shoreface of the Middle Atlantic Bight. *Marine Geology* 96, 19-51.
- Wright, D., Chappell, J., Thom, B.G., Bradshaw, M.P. and Cowell, P., 1979. Morphodynamics of reflective and dissipative beach and inshore systems: Southeastern Australia. *Marine Geology* 32, 105-140.
- Wright, D., Guza, R.T. and Short, A.D., 1982. Dynamics of a high energy dissipative surf-zone. *Marine Geology* 45, 41-62.
- Wright, L.D. and Short, A.D., 1984. Morphodynamic variability of surf zones and beaches: A synthesis. *Marine Geology* 56, 93-118.
- Xie, S.-L., 1981. Scouring patterns in front of vertical breakwaters and their influence on the stability of the foundations of the breakwaters. Department of Civil Engineering, Delft University of Technology, Delft, The Netherlands, 1-61.
- Xie, S.-L., 1985. Scouring patterns in front of vertical breakwaters. *Acta Oceanologica Sinica* 4(1), 153-164.
- Xie, S.L., 1987. The properties of irregular waves and their action on a sand bottom. *China Ocean Engineering* 1(1), 83-97.
- Zanevald, J.R.V., Spinrad, R.W. and Bartz, R., 1982. An optical settling tube for the determination of particle size distributions. *Marine Geology* 49, 357-376.
- Zimmerman, M.S. and Bokuniewicz, H.J., 1987. Multi-year beach response along the south shore of Long Island, New York. *Shore and Beach* 55(2), 3-8.

PUBLICATIONS

Papers presented at international conferences

1. Miles, J.R., Russell, P.E. and Huntley, D.A., 1996. Sediment transport and wave reflection near a seawall. *Proceedings of the 25th International Conference on Coastal Engineering*, (Orlando, Florida), ASCE. 2612-2624.
2. Miles, J.R., Russell, P.E. and Huntley, D.A., *in press*. Suspended sediment response to wave reflection. *Proceedings of Coastal Dynamics '97*, (Plymouth), ASCE.

Sediment transport and wave reflection near a seawall.

Jonathon R. Miles¹, Paul E. Russell¹, David A. Huntley¹.

Abstract

This paper describes results of a field experiment to examine the effect of wave reflection on suspended sediment transport in front of a seawall. High frequency measurements of wave elevation, velocity and suspended sediment concentrations were made simultaneously on a natural beach and in front of a seawall at Teignmouth in South Devon (U.K.) in June 1995. Wave reflection at the natural beach was found to be dependent on frequency; low frequency waves being preferentially reflected while incident waves were dissipated. At the seawall the incident wave reflection coefficient was 0.9 indicating only a small amount of dissipation. The doubling of energy over the sea bed was found to greatly increase the suspended sediment concentrations in the water column, although the amount of this increase depended on the water depth. A data analysis technique was developed which allowed the incoming and outgoing wave contributions to the sediment transport to be analysed. In these accretionary conditions incoming waves transported sediment onshore in both wall and beach cases, while in the wall case sediment transported offshore by the outgoing waves balanced the onshore transport. Sediment build up which was observed at the top of the natural beach was not observed in front of the wall. Sediment maintained in suspension in front of the wall was available for longshore transport, and this was enhanced by the presence of the wall.

Introduction

Seawalls have been used for many years as a method of coastal protection on eroding shorelines. It has been suggested that the reflection of wave energy over the beach fronting the wall actually helps to erode the beach (Silvester 1977), but the processes controlling this erosion remain poorly understood. There has been considerable debate over the effect of the seawall on the beach in recent years

¹ Institute of Marine Studies, University of Plymouth, Drake Circus, Plymouth, U.K., PL4 8AA.

(Kraus, 1988; Kraus and McDougal, 1996), with experimenters carrying out laboratory experiments with moveable beds (e.g. McDougal et al., 1996) or carrying out surveys of defended and undefended coastlines (e.g. Griggs and Tait, 1988). Researchers into beach processes have identified driving forces behind beach morphology change using high frequency point measurements of suspended sediment concentrations and water velocities (e.g. Jaffe et al., 1984). This approach has been applied to the reflective seawall environment for the first time and the method and initial results are presented in this paper.

Method

To compare similar wave conditions in a surf zone with a reflective wall environment a location was required with a wall adjacent to a natural beach. The site chosen was Sprey point at Teignmouth in South Devon, UK which has a 7m high seawall fronted by a beach of slope 1/15. The sand in front of the wall is medium quartz sand with $D_{50}=0.24\text{mm}$. The beach is macro-tidal and morphodynamically intermediate. A rig designed to minimise interference with the hydro and sediment dynamic conditions whilst providing a stable base for instrumentation was built and bolted to the wall. An extendable rod was positioned on the front of the rig, extending close to the bed, to which the instruments were attached. Two EMCMs, (Electro Magnetic Current Meters) two OBSs (Optical Backscatter Sensors) and a PT (Pressure Transducer) were attached to this rod, 1.5m from the wall in a vertical array. A rig of instruments was also dug in to the adjacent beach on a similar depth contour so that comparisons could be made. This beach site had one EMCM, one OBS and one PT.

All of the *in-situ* monitoring devices were logged at a frequency of 8Hz and were pre-filtered between 3-4Hz. EMCM and PT offsets were determined in the field at the beginning and end of each tide. Surveys were carried out daily to establish beach morphology. Sediment samples were taken for size distribution analysis. During the period of observation and recording, in June 1995, the wind was generally light and the waves were, on average, 30cm in height at the breakpoint with an average period of 4 seconds. The robust design of the rig should enable measurements to be made in waves of up to 2m. The layout of the site is shown in figure 1:

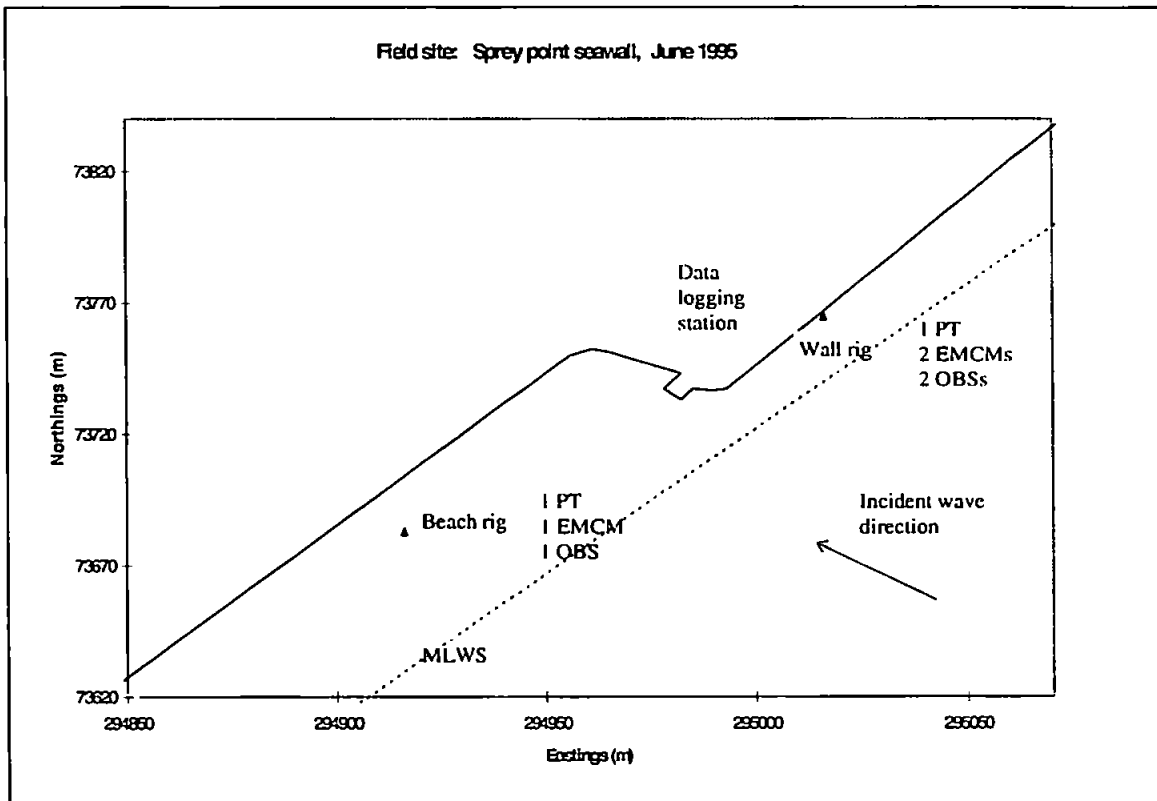


figure 1. Experiment site at Teignmouth.

Instruments were calibrated both before and after the experiment, and the calibrations were applied to the raw data. EMCs were calibrated in a tow tank at the Royal Naval Engineering College (RNEC) at Manadon, Plymouth (U.K.). Pressure transducers were calibrated for water depth in a 3m deep tank at the RNEC. OBSs were calibrated in the laboratory using sediment samples taken from the experiment site. To calibrate the OBSs a paint stirrer was used to suspend sediment in a tank while samples of the beach sediment were filtered from next to the OBS head. This calibration of the OBSs provided an excellent linear correlation between suspended sediment concentrations and voltage output.

Time series

Time series of surface elevation and suspended sediment concentration are shown in figure 2. Time series have been selected so that water depths are similar in the wall and beach examples, in this case the water depth is approximately 0.8m. Instruments suspended from the wall are 1.2m away from it. This puts them closer to the antinode at the wall than the node 2.7m away from the wall (for a wave period of 4 seconds). The maximum surface elevation deviation from the mean is therefore clearly larger than that observed at the beach rig. Suspended sediment data which is

compared in these examples is taken from OBSs at similar heights, both being approximately 18cm from the bed. The scale of the axis of the wall OBS is reduced so that the data fits the plot. In similar incident wave conditions levels of suspended sediment are clearly much larger at the wall, reaching 4 kg/m^3 at this height above the bed, while at the beach OBS sediment concentrations only reach 0.6 kg/m^3 .

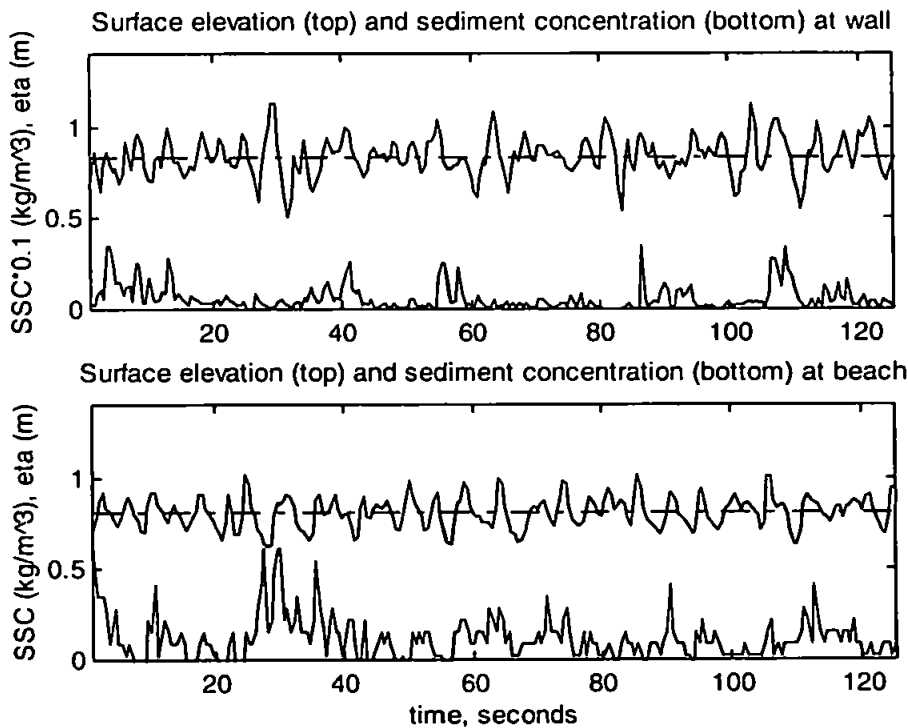


figure 2. Time series of surface elevation and suspended sediment concentrations at the wall and beach rigs. N.B. The sediment concentrations in the wall time series have been scaled down by a factor of 10.

Theory

Incoming and outgoing elevation time series were obtained from elevation and velocity time series using the method of Guza, Thornton and Holman (1984). The separation of incoming and outgoing waves forms the basis for most reflection analysis techniques which involve co-located elevation and velocity sensors. The analysis can also be extended to obtain the incoming and outgoing velocity time series. This allows the frequency dependent oscillatory sediment transport associated with the incident reflected waves to be found.

The derivation of Guza et al.'s (1984) time domain technique arises from linear shallow water theory:

The velocity potential for progressive water waves is as follows:

$$\phi = \frac{-a \cdot g}{\sigma} \cdot \frac{\cosh k(z+h)}{\cosh kh} \sin(kx - \sigma t)$$

The surface elevation can be obtained from this by differentiating with respect to time, and the attenuation term tends to 1 in shallow water.

$$\eta = \frac{1}{g} \left[\frac{\partial \phi}{\partial t} \right]_{z=0} \quad \text{giving} \quad \eta = a \cos(kx - \sigma t)$$

A similar equation for velocity is obtained by differentiating with respect to x

$$u = - \frac{\partial \phi}{\partial x} \quad \text{gives} \quad u = \frac{g a k}{\sigma} \cos(kx - \sigma t)$$

By dividing the elevation and velocity equations the following time domain transformation can be obtained relating velocity and surface elevation (provided the water is shallow).

$$\eta(t) = \frac{c}{g} u(t)$$

It is necessary to transform to the frequency domain and use full linear theory if this relationship is to be applied in intermediate or deep water.

Progressive wave surface elevation traces for waves incoming to a beach and outgoing from it can be obtained from the time series of elevation and velocity as follows:

$$\eta_{in}(t) = \left(\eta(t) + \frac{c}{g} u(t) \right) / 2$$

$$\eta_{out}(t) = \left(\eta(t) - \frac{c}{g} u(t) \right) / 2$$

In this case, a positive velocity implies an onshore flow, while a negative velocity an offshore flow. In order to obtain a frequency dependent reflection function (FDRF) it is necessary to carry out a spectral analysis of the incoming and outgoing elevation traces separately. After obtaining the power spectra of the incoming and outgoing elevation time series, $S_{ii}(f)$ and $S_{oo}(f)$ respectively, the frequency dependent reflection coefficient is simply:

$$R(f) = \sqrt{\frac{S_{ii}(f)}{S_{oo}(f)}}$$

This technique was examined for signal noise related bias by Huntley et al. (1995) who found that when the coherence between elevation and velocity was high, the bias in the FDRF was low. Two other techniques were discussed by Huntley et al. (1995). These were a frequency domain method by Tatavarti (1989) and a Principal Component Analysis method (Tatavarti et al., 1988). All three techniques were applied to the data in order that the frequency dependent reflection coefficient for the beach and wall cases could be identified. The three different methods were

found to offer similar results. This gives confidence in the time domain method which is the most simple to program and extend for incoming and outgoing sediment analysis.

In order to understand the effect of the reflected wave field on the suspended sediment transport, it is possible to carry out a cross-spectral analysis of the incoming and outgoing waves with the sediment.

It is first necessary to apply the transformation from elevation to velocity to obtain incoming and outgoing velocity time series. The appropriate transformations are:

$$u_{in} = \frac{g}{c} \eta_{in}$$

$$u_{out} = -\frac{g}{c} \eta_{out}$$

A wave crest (elevation maximum) correlated with onshore flow therefore represents a wave crest travelling onshore, while a wave peak correlated with an offshore velocity represents a wave crest travelling offshore. The equations for incoming and outgoing velocity are therefore:

$$u_{in} = \frac{1}{2} \left(u + \frac{g}{c} \eta \right)$$

$$u_{out} = \frac{1}{2} \left(u - \frac{g}{c} \eta \right)$$

It is next necessary to assume that the oscillatory sediment flux can be split into incoming and outgoing components. Jaffe et al. (1984) assumes a similar principle when considering the breakdown of the mean and oscillatory fluxes. They assume that the total velocity can be split into a mean and oscillatory component:

$$U = \bar{u} + u'$$

and that the sediment concentration is also separable into mean and oscillatory parts:

$$C_s = \bar{c}_s + c'_s$$

The time average of the flux therefore reduces to the mean flux and the flux coupling:

$$\overline{UC_s} = \overline{\bar{u} \bar{c}_s} + \overline{u' c'_s}$$

Signals are routinely de-meant, and the remaining step is to split the oscillatory velocity into incoming and outgoing components before crossing with the suspended sediment to obtain the flux:

$$u' = u'_{in} + u'_{out}$$

The time average of the incoming and outgoing oscillatory flux is therefore:

$$\overline{u' c'_s} = \overline{u'_{in} c'_{in}} + \overline{u'_{out} c'_{out}}$$

Huntley and Hanes (1987) identified that the frequency dependent sediment transport could be found by taking the co-spectrum of the oscillatory cross shore velocity with the sediment concentration time series. The frequency dependent

sediment transport associated with the incoming and outgoing waves is therefore obtained from the co-spectrum of the incoming or outgoing velocity time series with the sediment time series. The contributions of the incoming and outgoing waves to the sediment transport can therefore be identified.

Frequency dependent wave reflection

Three methods were used to determine levels of energy incoming and outgoing from the natural beach and the wall. Incoming and outgoing wave spectra were obtained from the incident and reflected time series obtained using Guza et al.'s (1984) method. The frequency dependent reflection coefficient was then determined using this method and two frequency domain methods. All three methods require that the current meter and pressure transducers are co-located and log data simultaneously. The analysis was first applied to data from the beach rig (figure 3).

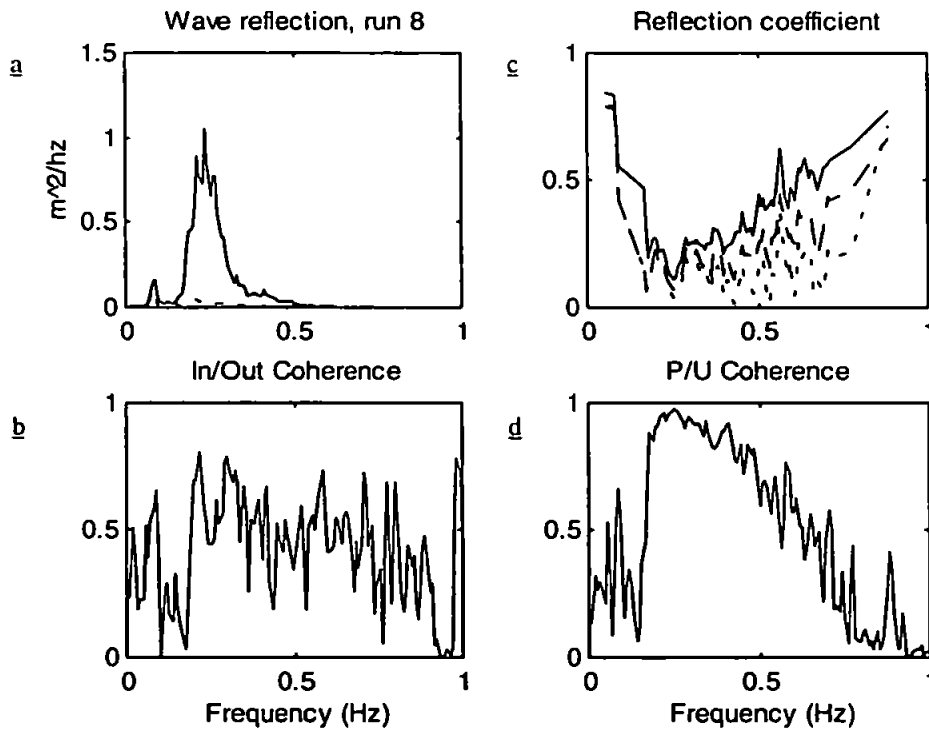


figure 3. Frequency dependent wave reflection at the beach. a: Incoming and outgoing wave spectra calculated using the time domain method. b: Coherence between calculated incoming and outgoing time series. c: Frequency dependent reflection coefficient calculated using time domain (solid), frequency domain (dashed) and principle component analysis (dotted) methods. d: Coherence between elevation and velocity. Water depth is 1.28m.

The energy spectra show clearly that the incident waves (frequency 0.25 Hz) are dissipated by the natural beach, while at a lower frequency (0.1Hz) wave reflection is taking place. By dividing the square root of the spectral estimates, the FDRF for this time domain method was obtained, and this shows a reflection coefficient of 0.1 for the incident waves on the natural beach while for the low frequency waves the reflection coefficient is 0.8. Of the three lines on the reflection coefficient figure above (top right). the lines show the methods of the time domain method (top), the frequency domain method (middle) and the Principal Component Analysis (bottom). The three methods give good agreement where there is good coherence between elevation and velocity.

A similar analysis was carried out to data from the wall rig. The results are shown in figure 4.

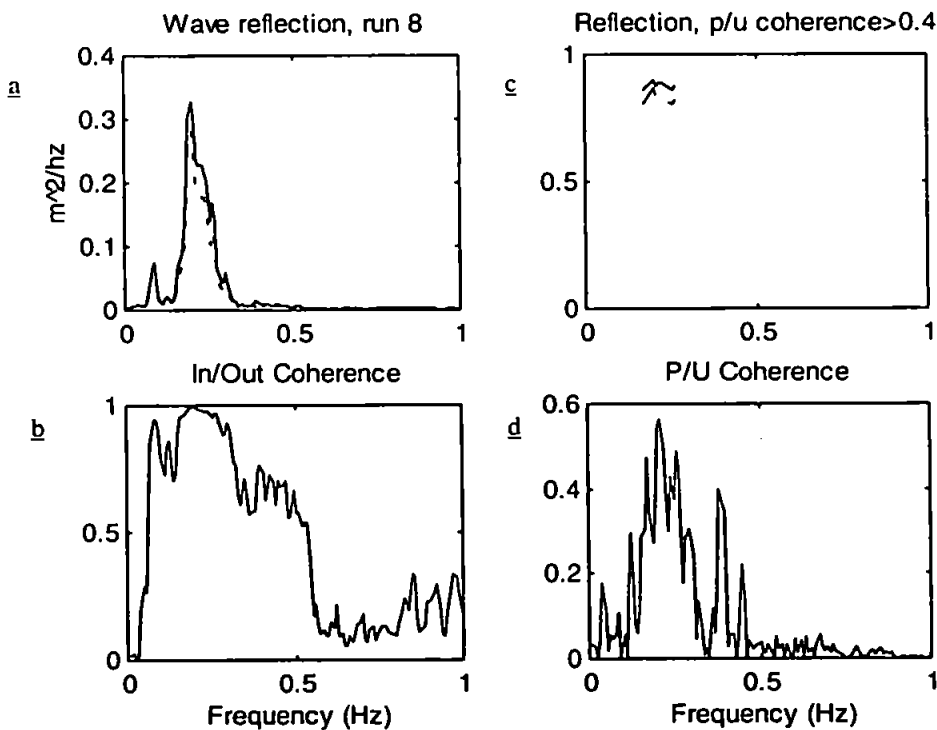


figure 4. Frequency dependent wave reflection at the wall. a: Incoming and outgoing wave spectra calculated using the time domain method. b: Coherence between calculated incoming and outgoing time series. c: Frequency dependent reflection coefficient calculated using time domain (solid), frequency domain (dashed) and principle component analysis (dotted) methods. Reflection estimates are plotted for values of P/U coherence > 0.4 so that there is 95% confidence in the coherence between P and U. This is necessary as cross spectral analysis is carried out in the determination of the FDRF using the frequency domain methods. d: Coherence between elevation and velocity. Water depth is 1.30m.

Similar amounts of energy were found in the spectra of both incoming and outgoing wave time series, indicating that reflection of the incident waves was occurring at the wall. At incident wave frequency all three methods of determining the frequency dependent reflection coefficient gave a value of 0.9 at the wall. The wall is in fact slightly sloping at the position of the rig and this may account for the reflection coefficient being less than unity.

Mean suspended sediment concentrations

The next part of the investigation was to examine the effect of the increase in reflection coefficient at the shoreline on concentrations of suspended sediment. To do this, data from OBSs on the beach and wall rig were compared. During the experiment OBSs were carefully positioned on each rig so that they were at the same height above the bed and are therefore comparable. Mean concentrations were calculated for each run. Mean water depths were also calculated and sediment concentrations in each case were then plotted against depth. The results are shown in figure 5.

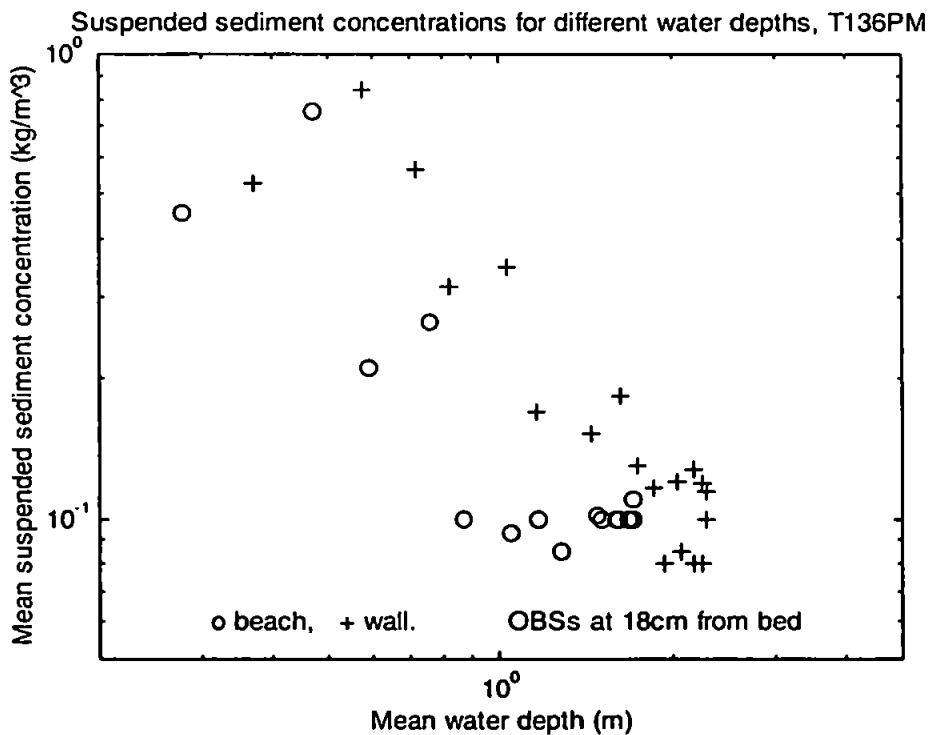


figure 5. Mean suspended sediment concentrations - comparison of data from wall and beach OBSs. Both instruments were mounted approximately 18cm from the bed. Incident waves were approximately 30cm high at the breakpoint.

The results show a greater concentration of sediment was in suspension in front of the wall than was in suspension on the natural beach when water depths were the same. Incoming wave conditions did not vary significantly during this tide, and the results therefore imply that it is the increase in wave reflection at the shoreline which must be responsible for increasing the concentrations of suspended sediment in front of the wall. The distinct linear trend in the data, especially in the wall rig data suggests that it may be possible to parameterise the mean suspended sediment concentrations in this region in terms of the reflection coefficient, water depth, height above bed and incident wave height. Further experimentation with a larger array of instruments would be necessary for this however.

Frequency dependent sediment transport

The incoming and outgoing frequency dependent sediment transport was obtained for both wall and beach rigs for each run of data logged. A clear picture emerged in all runs as to the nature of this transport and this is shown in figure 6.

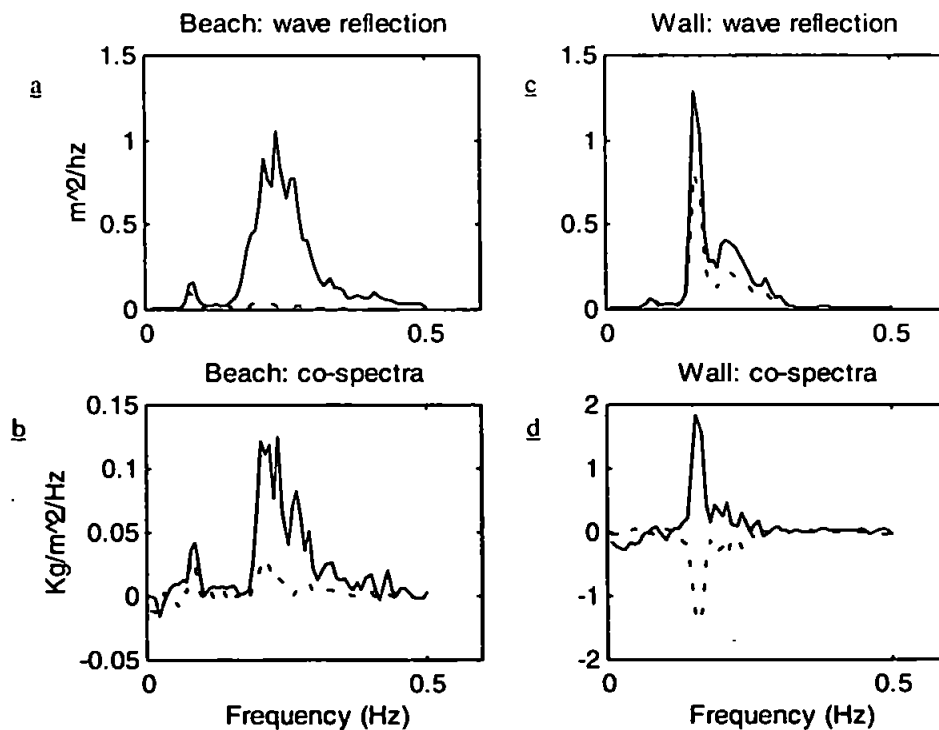


figure 6. Incoming and outgoing spectra and co-spectra in beach (a,b) and wall (c,d) cases. In the energy spectra plotted above, the solid lines represent incoming energy, the dashed lines represent outgoing energy. In the co-spectra, positive is onshore, solid lines are the cospectra between incoming waves and the sediment, dashed lines are cospectra between outgoing waves and sediment. Water depth is 1.3m

In the beach case (figure 6b), incoming waves are found to transport sediment onshore. This result is similar to that observed by Huntley and Hanes (1987). Suspension events occur at the same time as onshore directed flows, and the resultant transport is onshore. There is little energy outgoing from the beach however, and there is therefore little transport associated with the offshore directed waves.

At the wall, the situation is rather different (figure 6d). The incident waves are still responsible for onshore sediment transport, while the outgoing waves give rise to offshore transport. The onshore transport by the incoming waves is effectively halted by the outgoing waves. The net cross-shore oscillatory transport is therefore reduced. The fact that there is more sediment in suspension in front of the wall is also evident in this analysis as the magnitudes of the co-spectra are considerably larger in the wall case than in the beach case.

Longshore transport comparison

Mean longshore transport rates were calculated for both wall and beach rigs. The results are shown in figure 7.

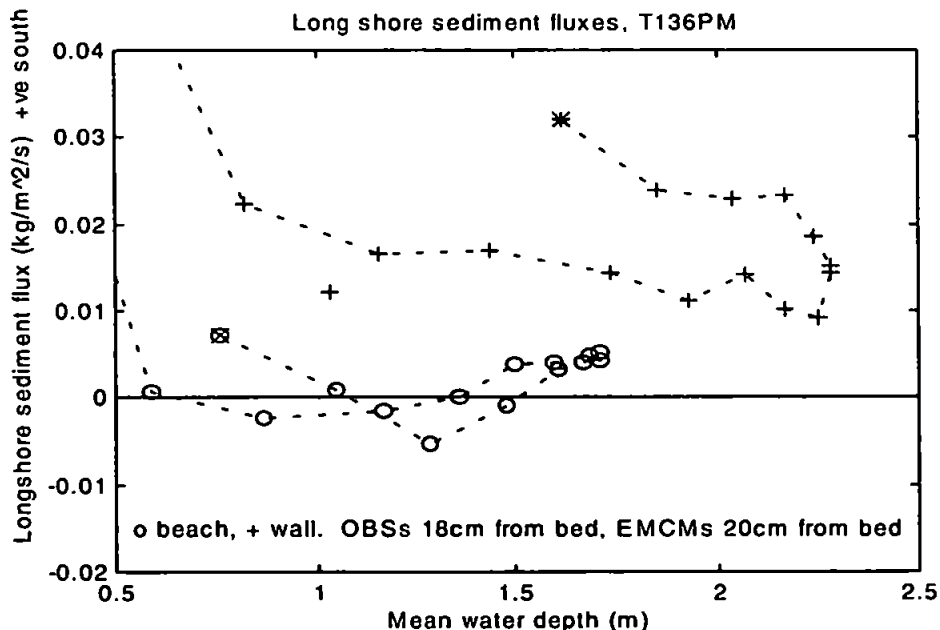


figure 7. Longshore transport rates measured at the beach and wall.

Longshore transport rates in front of the wall were found to be greater than at the beach rig at all times, and this was attributed to both the increase in suspended sediment concentrations and also an increase in the longshore current which passed

in front of the wall. The south-westward direction of longshore transport in the wall case is a result of the oblique wave approach from the east (see figure 1).

During the period of observation, morphology changes were monitored using surveying techniques. Increased levels of longshore transport along the Sprey point wall resulted in the development of a small bar to the south west of the wall. (extending SW from point 294990,73740; see figure 1). Shoreward of the beach rig, a net accretion was observed. This is likely to have resulted from the onshore transport by the incident waves. At the wall rig however there was no net accretion or erosion. The balance in transport between the incoming and outgoing waves prevented accretion taking place in this region, while increased levels of sediment in suspension led to an enhanced longshore transport of sediment in front of the wall.

Conclusions

This paper has described initial results of a field experiment to examine the effect of wave reflection on suspended sediment transport in front of a seawall. High frequency measurements of wave elevation, velocity and suspended sediment concentrations were made simultaneously on a natural beach and in front of a seawall. The doubling of energy over the sea bed was found to greatly increase the suspended sediment concentrations in the water column, although the amount of this increase depended on the water depth. A data analysis technique was developed which allowed the incoming and outgoing wave contributions to the sediment transport to be analysed. Incoming waves transported sediment onshore in both wall and beach cases, while in the wall case outgoing waves balanced the onshore transport. Sediment which was maintained in suspension in front of the wall was available for longshore transport, and this was enhanced by the presence of the wall.

Symbols

a	wave amplitude
c	wave celerity
c_s	sediment concentration
f	wave frequency
g	gravitational acceleration
h	water depth
k	wave number ($2\pi/\lambda$)
t	time
u	horizontal cross shore velocity
x	horizontal co-ordinate
z	vertical position. $z = 0$ at the surface, $z = -h$ at the bed
R(f)	frequency dependent reflection coefficient
S_{ii}	power spectrum of incoming wave time series
S_{oo}	power spectrum of outgoing wave time series
T	wave period

σ angular frequency ($2\pi/T$)
 η surface elevation
 λ wavelength
 ϕ velocity potential
in denotes incoming wave
out denotes outgoing wave

References

- Griggs, G.B. and Tait, J.F., 1988. The effects of coastal protection structures on beaches along northern Monterey Bay, California. *Journal of Coastal Research*, Special Issue No. 4, 93-111.
- Guza, R.T., Thornton, E.B. and Holman, R.A., 1984. Swash on steep and shallow beaches. *Coastal Engineering*, 708-723.
- Huntley, D.A. and Hanes, D.M., 1987. Direct measurement of suspended sediment transport. *Proceedings, Coastal Sediments '87, ASCE*, 723-737.
- Huntley, D.A., Simmonds, D. and Tatavarti, R.S.V.N., 1995. On the measurement of coastal wave reflection using co-located elevation and current sensors. *Proceedings, Coastal Dynamics*, 57-68.
- Jaffe, B.E., Sternberg, R.W. and Sallenger, A.H., 1984. The role of suspended sediment in shore normal beach profile changes. *Proceedings, Coastal Engineering, 1983-1996*.
- Kraus, N.C., 1988. The effects of seawalls on the beach: extended literature review. *Journal of Coastal Research*, Special Issue No. 4, 1-28.
- Kraus, N.C. and McDougal, W.G., 1996. The effects of seawalls on the beach: part I, an updated literature review. *Journal of Coastal Research*, 12 (3), 691-701.
- McDougal, W.G., Kraus, N.C. and Ajiwibowo, H., 1996. The effects of seawalls on the beach part II, numerical modelling of SUPERTANK seawall test. *Journal of Coastal Research*, 12 (3), 702-713.
- Silvester, R., 1977. The role of wave reflection in coastal processes. *Proceedings of Coastal Sediments '77, American Society of Civil Engineers*, 639-652.
- Tatavarti, R.S.V.N., 1989. The reflection of waves on natural beaches. Unpub. PhD thesis. Dalhousie University, Halifax, Nova Scotia, Canada. 175pp.
- Tatavarti, R.S.V.N. and Huntley, D.A., 1987. Wave reflections at beaches, *Proceedings, Canadian Coastal Conference., Quebec City, Canada*, 241-256.

Acknowledgements

The authors would like to thank Mr Peter Ganderton at the University of Plymouth for his assistance with the field-work phase of the project, and Dr Mark Davidson for helpful suggestions throughout the study.

SUSPENDED SEDIMENT RESPONSE TO WAVE REFLECTION

Jonathon R. Miles¹, Paul E. Russell¹ and David A. Huntley¹.

Abstract

A field experiment has been carried out to examine the nature of sediment suspension and transport in front of a seawall. Synchronous high frequency measurements of surface elevation (using pressure transducers), water velocity (using electromagnetic current meters) and suspended sediment concentrations (using optical backscatter sensors) have been taken from in front of the Brunel seawall at Teignmouth, South Devon, UK. Measurements were also made simultaneously on an adjacent natural beach to provide control data. Wave reflections from the seawall lead to an increase in suspended sediment concentrations, and alter the phase of sediment suspension. The results emphasise the importance of wave reflection on the dynamics of beaches backed by seawalls.

Introduction

Measurements of sediment suspension and transport processes have been made on a variety of different types of beach, from macrotidal high energy dissipative beaches (e.g. Russell, 1993) to steeper reflective beaches (Davidson *et al.*, 1993). Sediment transport processes vary depending on the incident wave conditions, the sediment characteristics and the steepness (reflectivity) of the beach. An impermeable vertical seawall at the head of the beach increases the reflection coefficient of the shoreline considerably, and would therefore be expected to alter the nature of sediment suspension and transport both in the cross-shore and longshore directions. Initial results of this field investigation of the suspended sediment response to wave reflection from a coastal structure using *in-situ* measurements were presented by Miles *et al.* (1996). In the present paper results are presented which illustrate that there are significant differences between the suspension of sediment in front of a seawall and on an adjacent natural, undefended beach.

¹ Institute of Marine Studies, University of Plymouth, Drake Circus, Plymouth, Devon, PL4 8AA

Field site

To compare sediment suspension on a natural beach with suspension in front of a wall, a location was required with a wall adjacent to a natural beach. The site chosen was Sprey Point at Teignmouth in South Devon, U.K., which has a 7m high seawall fronted by a macrotidal beach. To the south of Sprey Point is a natural beach which receives the same incident wave conditions as the Sprey Point wall.

A rig designed to minimise interference with the hydro and sediment dynamic conditions whilst providing a stable base for instrumentation was built and bolted to the wall for a period in June 1995. Two EMCs, (electromagnetic current meters) two OBSs (optical backscatter sensors) and a PT (pressure transducer) were attached to this rig and suspended 1.2m seaward of the wall in a vertical array. A similar array of instruments was dug in to the adjacent beach on approximately the same depth contour to provide an experimental control. The layout of the site is shown in Figure 1. The base of the wall at Sprey Point slopes at an angle of 53° and the average beach slope in front of the wall is approximately 3.3° . The beach to the south is of similar slope to the beach in front of the Sprey Point wall, having an average slope of 3.9° . The grain size of the sand is that of medium quartz sand with $D_{50} = 0.24\text{mm}$.

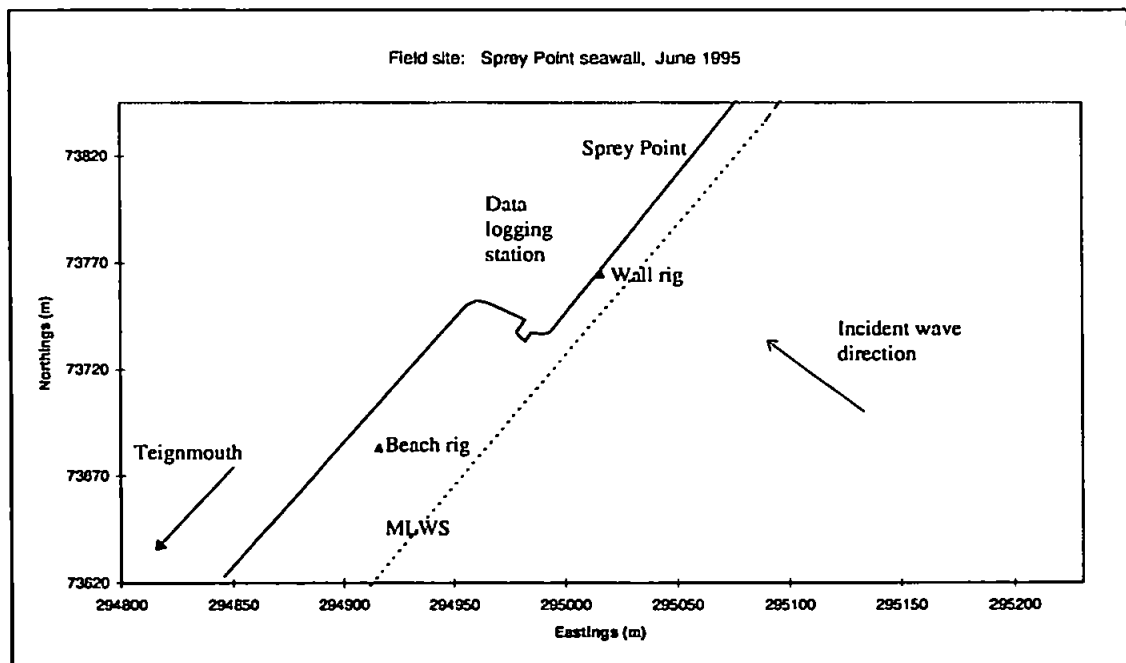


Figure 1: Field site layout.

Data was logged at 8Hz and pre-filtered at 2 or 4Hz. Surveys and sediment samples were obtained daily to establish beach morphology. The beach profiles and the position of the instruments on the beach are shown in Figure 2.

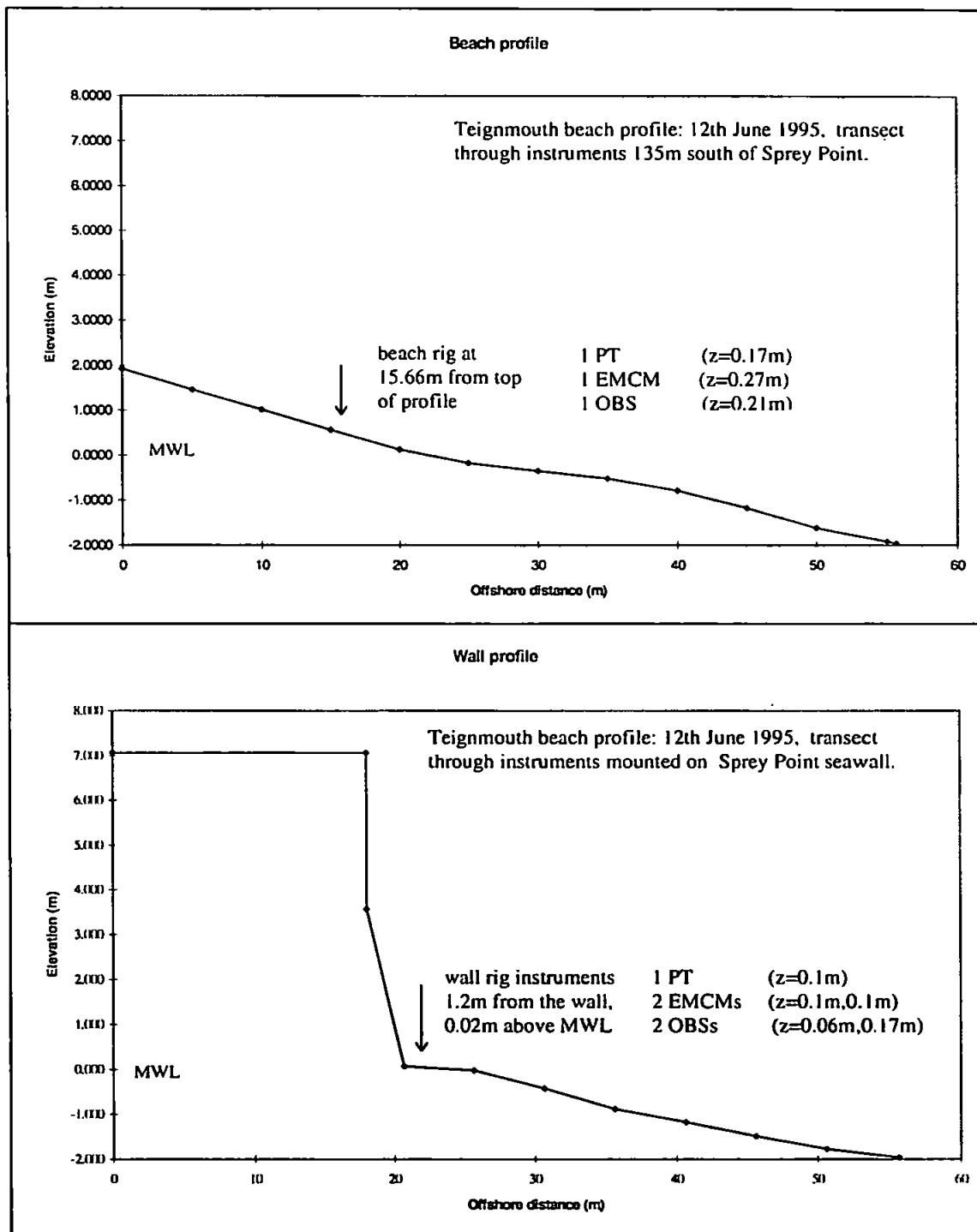


Figure 2: Beach profiles at the wall and beach sites, Teignmouth, June 1995.

Results

Data analysed in this paper were collected on the afternoon tide of 13th June, 1995. Water depth was taken as the normalising factor for the comparison of data between the two rigs, as the wave height was approximately constant between

runs when similar water depths covered the two rigs. The incident wave heights measured at the beach rig decreased gradually during the tide from 0.22m to 0.14m.

The nature of sediment suspension

Major differences in the hydrodynamics of the natural beach and seawall environments result in different sediment dynamic conditions for these two cases. In order to illustrate the major differences several sections of data are presented. The first two examples demonstrate that more sediment is suspended in front of the wall (Figure 3) than on the natural beach (Figure 4) in similar incoming wave conditions.

Surface elevation, cross shore velocity and sediment concentration - wall

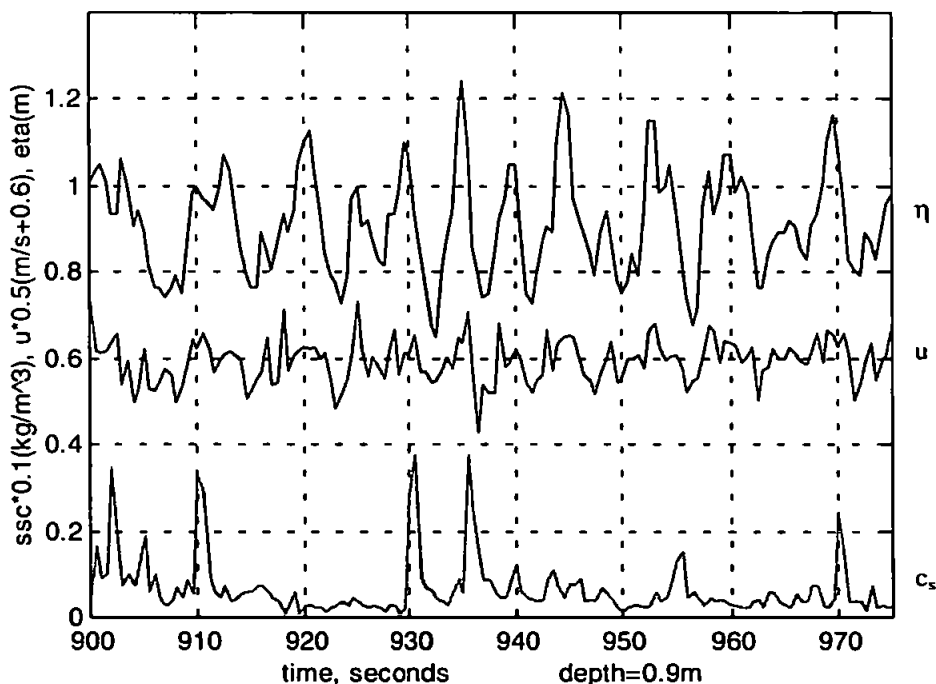


Figure 3: Time series of surface elevation, velocity (scaled by 0.5, offset by 0.6m/s), sediment concentration (scaled by 0.1) at wall.

Maximum wave elevations are greater at the wall rig (Figure 3) than at the beach rig (Figure 4), while the beach rig measured greater cross-shore orbital velocities (note scale of axes used). Typical values of wave period ($T=4s$) and water depth ($h=1m$) give a wavelength of $\lambda=12.5m$, placing the node at $\lambda/4=3.1m$ from the wall. The differences in velocities and elevations are therefore to be expected, as the instruments are closer to the elevation antinode at the wall than the node. Traditional models of sediment suspension suggest that velocity gradients in the boundary layer lead to a shear stress which is responsible for suspending sediment (Bagnold, 1946). Despite smaller velocities at the wall rig, a greater number of suspension events resulted in a considerably larger amount of entrainment at the wall than was observed at the beach rig. In the examples shown, instruments were at similar heights and incident wave conditions were identical. Even so, maximum

concentrations at the wall reach 3.9kg/m^3 , while at the beach rig suspension events are absent, and the concentration fails to rise above 0.1kg/m^3 .

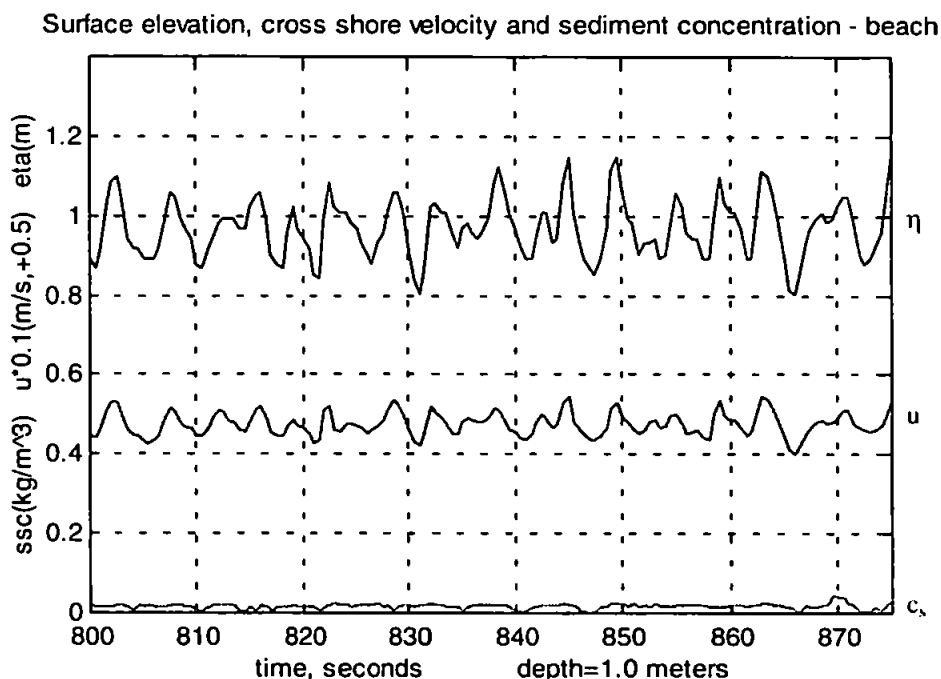


Figure 4: Time series of surface elevation, velocity (scaled by 0.1, offset by 0.5m/s), sediment concentration at beach.

Wave heights at the breakpoint during this tide were approximately 0.3m on the natural beach. The relationship $H_b/h=0.78$ indicates the breakpoint water depth should therefore be approximately 0.4m. The closest the beach rig instruments were able to get to this before becoming intermittently dry was when the water depth was 0.48m. Measurements made at this time are shown in Figure 5. They differ considerably from those made at the wall in a similar water depth (Figure 6).

In Figure 5, wave elevation and velocity traces exhibit noticeable asymmetry as the waves are shoaling and are about to break. Suspension events recorded during this run reached a maximum of 1.2kg/m^3 . In a similar water depth at the seawall, with the same incident wave conditions, maximum concentrations were recorded of just over 9kg/m^3 (Figure 6). The complicated elevation and velocity traces in the signals were typical of runs where the water was shallow and waves passed the sensors as both incoming and outgoing 'solitary' waves. The resulting sediment suspension traces are complex.

Surface elevation, cross shore velocity and sediment concentration - beach

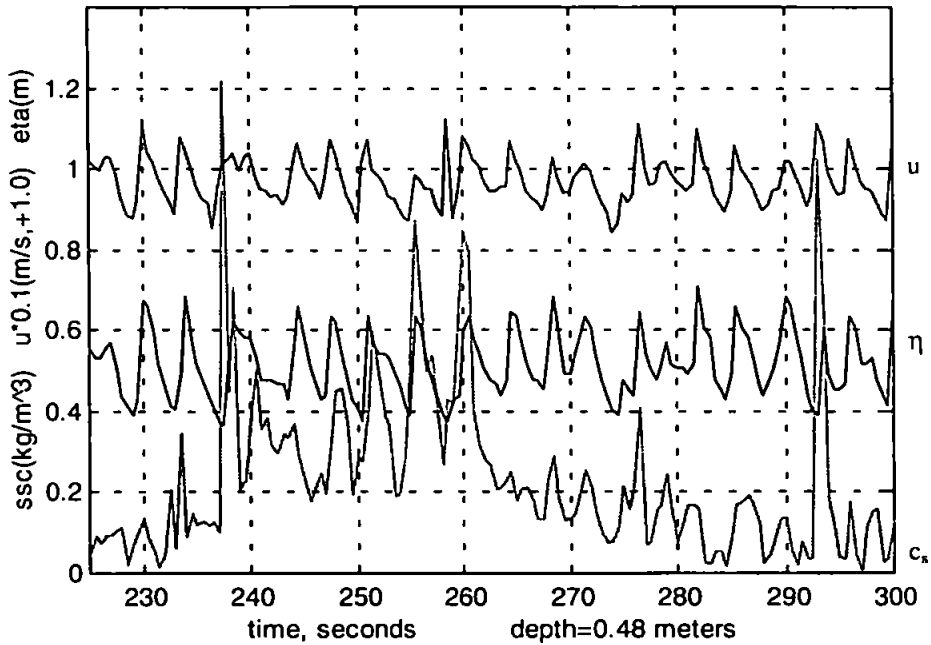


Figure 5: Time series of velocity (scaled by 0.1 and offset by 1.0m/s), surface elevation and sediment concentration at beach.

Surface elevation, cross shore velocity and sediment concentration - wall

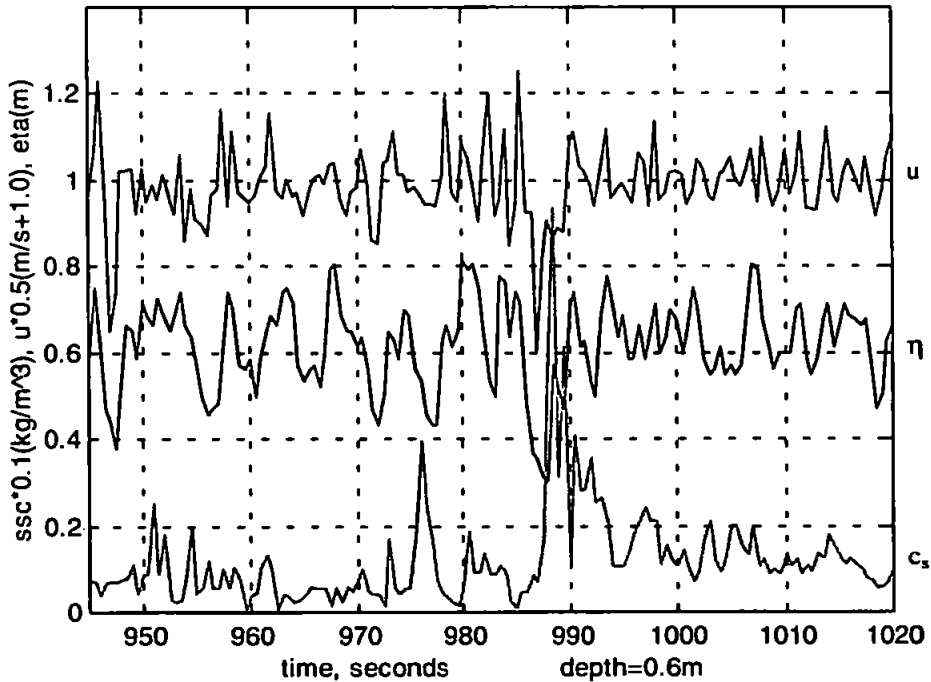


Figure 6: Time series of velocity (scaled by 0.5 and offset by 1.0m/s), surface elevation and sediment concentration (scaled by 0.1) at wall.

The phase of suspension

At the beach rig, the time-series show suspension events occurring in phase with onshore velocity (e.g. Figure 5, peak at 251 seconds). Suspension events which occur at this phase of the wave may be driven by the velocity shear in the boundary layer (Bagnold, 1946), which is maximum when the velocity outside the boundary layer is maximum. Shoaling waves become skewed, and their onshore velocities become larger than the offshore velocities. When the offshore velocity fails to rise above the threshold for suspension, suspension events only occur at the wave crest. In this case, the suspension events often appear to develop during the acceleration phase of the wave, and reach their maximum just before the crest of the wave passes (e.g. Figure 5, peak at 294 seconds). Generally however, the majority of sediment suspension peaks observed at the beach rig reach their maximum at or approaching the maximum velocity. Huntley and Hanes (1987) show that when suspension events occur in phase with onshore velocity, this gives rise to onshore sediment transport at the frequency of the waves.

At the seawall however, the phase of suspension is less clear. Suspension events are observed to occur most frequently with the maximum elevation. However, the complicated nature of the velocity field means that this may be at times of maximum velocity or at times of flow reversal. When the velocity is maximum, a plausible explanation is that the sediment peaks are driven by the velocity shear in the boundary layer (e.g. Figure 3, peak at 910 seconds). However at times of flow reversal, the velocity (and shear stress) is 90° out of phase with the elevation for the standing wave case, and the suspension events which occur at this time are therefore occurring at times of minimum shear stress (e.g. Figure 3, peak at 955 seconds).

The suspension of sediment at flow reversal has also been documented by Foster *et al.* (1994) who suggested that the mechanism may result from the release of turbulence from the bed during the reversal of the velocity. Murray (1992) also documented a flow reversal peak from a flume experiment and found that in some cases, the flow reversal peak was in fact larger than the shear peak.

Data simulation

A simple data simulation has been applied in order that the processes driving the time series results can be conceptualised. In the simulation, a wave is advected past some 'instruments', reflected from a wall 1.2m away, and the wave passes the instruments on its way out. Instrument heights in the data simulation are the same as in the field experiment. Solitary wave theory was applied because of its simplicity and similarity to waves in shallow water (Bagnold, 1947).

The equations used were as follows:

$$\eta_{in,out} = H \sec h^2 \left(\sqrt{\frac{3}{4}} \frac{H}{h} \frac{x}{h} \right) \quad \text{Boussinesq (1872)}$$

$$u = c N \frac{1 + \cos(Mz/h) \cosh(Mx/h)}{[\cos(Mz/h) + \cosh(Mx/h)]^2} \quad \text{McCowan (1891)}$$

where $c = \sqrt{g(h+H)}$, and both M and N are functions of H/h , calculated by Munk (1949). Typical values of $H=0.2\text{m}$, $h=1.0\text{m}$ give values of M and N as 0.65 and 0.3 respectively.

For a progressive solitary wave, the elevation is in phase with the velocity. The total elevation and velocity for the incident and reflected wave were obtained by adding the incoming and outgoing components of η and u . A reflection coefficient (r) of 0.9 was determined from the field data (Miles *et al.*, 1996) and this was used in the simulation to obtain the amplitude of the outgoing wave. A mean onshore velocity was added of similar magnitude to that observed in the field ($\bar{u} = 0.1\text{m/s}$) Suspension was assumed to be a function of the u_{tot}^n where $u_{tot} = u_{in} + u_{out} + \bar{u}$. Various values of n have been suggested from $n=2$ (Inman and Bagnold, 1963), $n=3$ (Owen and Thorn, 1978), to $n=5$ (Madsen and Grant, 1976). The magnitude of the suspension peak was considered less important than the phase at which it occurred, so for the purposes of the simulation a value of $n=3$ was used, and the relationship $c_s = u_{tot}^3 = (u_{in} + u_{out} + \bar{u})^3$ was applied. The simulation results are shown in Figure 7.

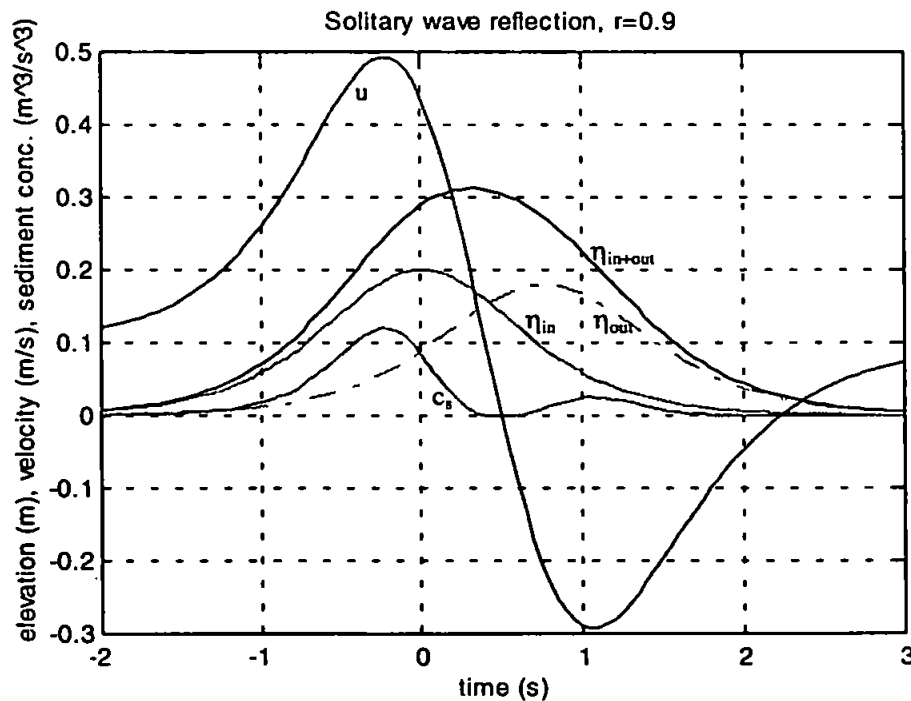


Figure 7. Simulation of solitary wave reflection past the instruments and the associated suspension.

The incoming and outgoing waves (η_{in} and η_{out}) are separated by the time it takes to travel to and from the wall. The difference in the direction of the velocity which is associated with each of these waves, combined with the lag between them results in the rapid change in cross-shore velocity (u). The reflection coefficient of 0.9 and the superimposition of the oscillatory flow on a mean onshore flow results in two sediment peaks, the second of which is smaller than the first.

The structure in the time series of the simulation above was also found to exist in the field data. An example is given in Figure 8. Of particular interest in this example is the suspension of sediment which occurs by both the incoming and outgoing waves, as in the simulation. Maximum suspension of sediment occurs at the same time as the velocity maximum in each case, and as in the simulation, the onshore directed sediment peak is smaller than the offshore peak.

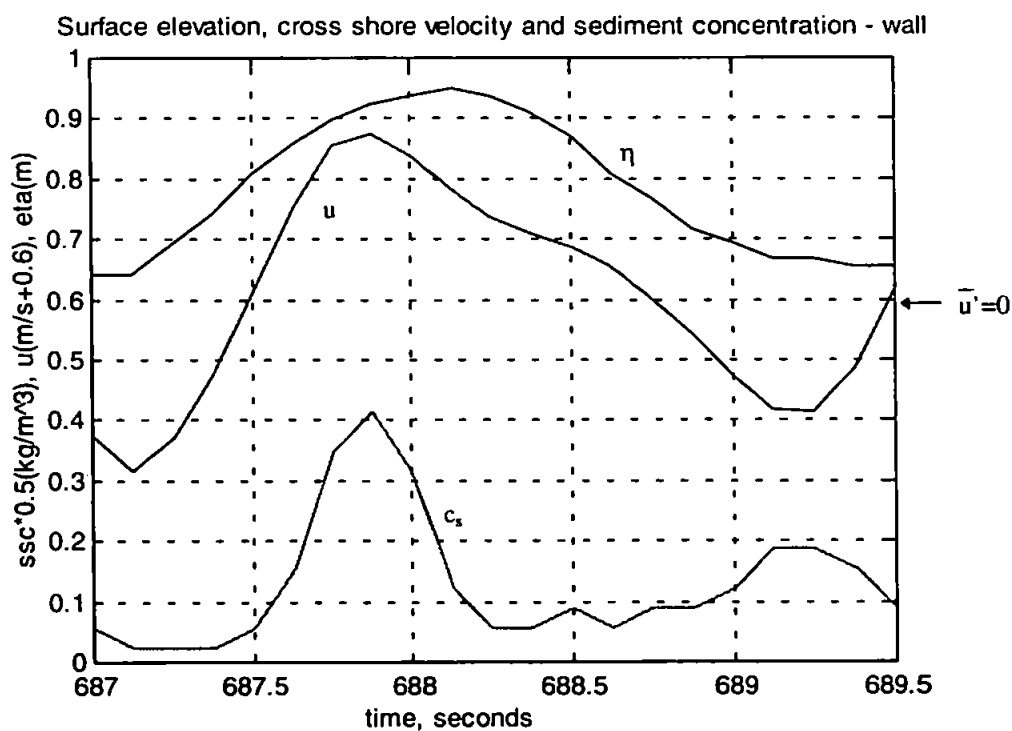


Figure 8. Time series of elevation (η), velocity (u) and sediment concentration (c_s) at the wall rig.

While the data simulation above is a gross simplification of the processes driving suspension in front of the wall, it is a useful tool in understanding the contributions of the incoming waves, the outgoing waves and the mean cross shore flow to sediment suspension. Wave reflection from a seawall radically alters the hydrodynamics in front of the wall, and this experiment has shown that this in turn affects the nature of sediment suspension considerably.

Conclusions

1. The observations have shown that near-bed suspended sediment concentrations on a beach backed by a seawall are increased by an order of magnitude relative to near-bed suspended sediment concentrations on an adjacent undefended beach.
2. The suspension of sediment in front of the wall may occur at times of maximum shear *or* at times of flow reversal.
3. Sediment suspension in front of the seawall results from the complex interaction of incoming waves, outgoing waves, mean currents and turbulence. Further work is required both in the observation and modelling of these processes.

References

- Bagnold, R.A., 1946. Motion of waves in shallow water; interactions between waves and sand bottom. *Proceedings of the Royal Society, London, series A*, 187, 1-15.
- Bagnold, R.A., 1947. Sand movement by waves: some small scale experiments with sand of very low density. *Journal of the Institution of Civil Engineers*, 27(4), 447-69.
- Boussinesq, J. 1872. Theorie des ondes et des remous qui se propagent le long d'un canal des vitesses sensiblement paralleles de la surface au fond. *J. Math. Pures et Appliquees*, Lionvilles, France, 17, 55-108.
- Davidson, M.A., Russell, P.E., Huntley, D.A., Hardisty, J. and Cramp, A., 1993a. An overview of the British beach and nearshore dynamics programme. *Proceedings of 23rd International Conference on Coastal Engineering '92*, 1987-2000.
- Foster, D.L., Holman, R.A. and Beach, R.A., 1994. Sediment suspension events and shear instabilities in the bottom boundary layer. *Proceedings of Coastal Dynamics '95*, 712-726.
- Huntley, D.A. and Hanes, D.M., 1987. Direct measurement of suspended sediment transport. *Proceedings of Coastal Sediments '87*, American Society of Civil Engineers, 723-737.
- Inman, D.L. and Bagnold, R.A., 1963. Beach and nearshore processes. Part II. Littoral processes. In Hill, M. N. (Ed), *The Sea: Vol. 3*, Wiley Interscience, New York, 529-553.
- Madsen, O.S. and Grant, W.D., 1976. Quantitative description of sediment transport by waves. *Proceedings of 15th Coastal Engineering Conference*, American Society of Civil Engineers, 1093-1112.
- McCowan, J., 1891. On the solitary wave. *Phil. Mag., series 5*, 32, 45-58.
- Miles, J.R., Russell, P.E., Huntley, D.A., Sediment transport and wave reflection near a seawall. *Proceedings of the 25th International Conference on Coastal Engineering '96*, 2612-2624.
- Murray, P.B., 1992. *Sediment pick up in combined wave-current flow*. Unpublished Ph.D. Thesis, University of Wales, 189pp.
- Owen, M.W. and Thom, M.F.C., 1978. Effect of waves on sand transport by currents. *Proceedings of 16th Coastal Engineering Conference.*, 1675-1687.
- Russell, P.E., 1993. Mechanisms for beach erosion during storms. *Continental Shelf Research* 13(11), 1243-1265.